SEISMIC VULNERABILITY OF THE ALASKAN WAY VIADUCT: WSDOT TYPICAL UNIT

by

Marc O. Eberhard
Assistant Professor
Department of Civil Engineering
University of Washington

Jaime De la Colina
Research Associate
Department of Civil Engineering
University of Washington

Stanley Ryter
Graduate Research Assistant
Department of Civil Engineering
University of Washington

TECHNICAL REPORT STANDARD TITLE PAGE

1. REPORT NO.	2. GOVERNMENT ACCESSION NO.	3. RECIPIENT'S CATALOG NO.
WA-RD 363.1		

4. TITLE AND SUBTITLE	5. REPORT DATE
SEISMIC VULNERABILITY OF THE ALASKAN WAY VIADUCT: WSDOT TYPICAL UNIT	June 1995
	6. PERFORMING ORGANIZATION CODE

7. AUTHOR(S)	8. PERFORMING ORGANIZATION REPORT NO.
Marc Eberhard, Jaime De la Colina, Stanley Ryter	

9. PERFORMING ORGANIZATION NAME AND ADDRESS	10. WORK UNIT NO.
Washington State Transportation Center (TRAC) University of Washington, Box 354802 University District Building; 1107 NE 45th Street, Suite 535 Seattle, Washington 98105-4631	
	11. CONTRACT OR GRANT NO.
	Agreement T9233, Task 41

12. SPONSORING AGENCY NAME AND ADDRESS	13. TYPE OF REPORT AND PERIOD COVERED
Washington State Department of Transportation Transportation Building, MS 7370 Olympia, Washington 98504-7370	Final technical report
	14. SPONSORING AGENCY CODE

15. SUPPLEMENTARY NOTES
This study was conducted in cooperation with the U.S. Department of Transportation, Federal Highway Administration.

16. ABSTRACT

An engineering team from the University of Washington (UW) evaluated the seismic vulnerability of the Alaskan Way Viaduct, located in Seattle, Washington. This report presents the evaluation of a typical three-bay unit that was designed by WSDOT. The evaluation team performed response-spectrum analyses and nonlinear analyses for both fixed-base and pinned-base conditions. The team considered a widely used soft-soil spectrum and worst-case, site-specific spectra. Wherever possible, the UW team evaluated the vulnerability to each failure node following two or three procedures, including those proposed by the Applied Technology Council (1983) and Priestley, Seible, and Chai (1992).

The evaluation team found that the vulnerability of the Alaskan Way Viaduct exceeds that of bridges built to current standards. The vulnerability is a result of a combination of two factors: (1) the ground motion is likely to strongly excite the viaduct; and (2) many of the WSDOT unit's structural components are likely to behave in a brittle manner. The following deficiencies were identified as the most critical.

- The first-story column-reinforcement splices are too short, they have too little confinement reinforcement, and they are located in regions likely to experience large ductility demands.

- The column/beam joints have inadequate confinement reinforcement, and during strong ground motions, they could experience a diagonal-tension failure.

- The shear strength of the first-story columns is marginal.

- If the first-story columns develop their flexural capacity during an earthquake, the pile-supported footings could fail in shear.

17. KEY WORDS	18. DISTRIBUTION STATEMENT
Bridge, earthquakes, evaluation, reinforced concrete	No restrictions. This document is available to the public through the National Technical Information Service, Springfield, VA 22616

19. SECURITY CLASSIF. (of this report)	20. SECURITY CLASSIF. (of this page)	21. NO. OF PAGES	22. PRICE
None	None	181	

DISCLAIMER

The contents of this report reflect the views of the authors, who are responsible for the facts and the accuracy of the data presented herein. The contents do not necessarily reflect the official views or policies of the Washington State Transportation Commission, Department of Transportation, or the Federal Highway Administration. This report does not constitute a standard, specification, or regulation.

TABLE OF CONTENTS

TABLE OF CONTENTS (Continued)

LIST OF FIGURES

LIST OF TABLES

SUMMARY

At the request of the Washington State Department of Transportation (WSDOT), an engineering team from the University of Washington (UW) evaluated the seismic vulnerability of the Alaskan Way Viaduct. The viaduct is a 2.2-mile long, reinforced concrete structure that runs parallel to the shore of Elliot Bay in Seattle, Washington. The viaduct was selected for detailed evaluation for the following reasons: (1) it is an important link in the region's transportation network; (2) it is underlain by loose, hydraulic fills; (3) its reinforcement details do not satisfy current code requirements; and (4) its geometry is similar to double-deck structures that were damaged during the 1989 Loma Prieta Earthquake. Kramer and Eberhard (1995) provide a summary of the seismic evaluation of the Alaskan Way Viaduct.

This report presents the evaluation of a typical three-bay unit that was designed by WSDOT. A companion report by Kramer et al. (1995) considers the viaduct's geotechnical hazards. The results of the geotechnical study provided the structural team with estimates of ground motions and liquefaction potential for various site profiles. A third report discusses the vulnerability of the typical unit that was designed by City of Seattle Engineering Department (Knaebel et al. 1995).

The evaluation team performed linear response-spectrum analyses and nonlinear static analyses for both fixed-base and pinned-base conditions. These two base conditions provided upper and lower bounds for the footing's rotational stiffnesses. In addition, the pinned-base model approximated the behavior of the typical unit if the column-base splices were to lose their flexural capacity.

The response-spectrum analyses were computed with a three-dimensional model of the typical unit. The team considered a soft-soil spectrum (ATC-6, 1981) and worst-case, site-specific spectra. Two-dimensional, nonlinear analyses were performed for typical longitudinal and transverse frames, following the recommendations of Priestley et al.

(1992). Wherever possible, the UW team evaluated the vulnerability for each failure mode following several procedures. These procedures included those proposed; by the Applied Technology Council (ATC-6-2, 1983); by Priestley et al. (1992), by Priestley et al. (1994); by Ascheim and Moehle (1992); and by Thewalt and Stojadinvic (1992).

The evaluation team found that the vulnerability of the Alaskan Way Viaduct exceeds that of bridges built to current standards. The vulnerability is a result of a combination of two factors: (1) the ground motions are likely to strongly excite the viaduct; and (2) many of the structural components are likely to behave in a brittle manner. The following deficiencies were identified as the most critical.

- The first-story column reinforcement splices are too short, they have inadequate confinement reinforcement, and they are located in regions likely to experience large ductility demands.

- The first- and second-story joints have inadequate confinement reinforcement, and during strong ground motions, they could experience a diagonal-tension failure.

- The shear strength of the first-story columns is marginal.

- If the base of the first-story columns develop their flexural capacity, the footings could fail in shear.

CHAPTER 1

INTRODUCTION

1.1 CONTEXT

As part of an ongoing seismic retrofit program, the Washington State Department of Transportation (WSDOT) has identified major bridges with unique features that require detailed evaluation. The Alaskan Way Viaduct is one such bridge. This 2.2-mile long, reinforced concrete structure serves traffic on State Route 99, one of only two north-south freeways through downtown Seattle. The viaduct carries approximately 86,000 vehicles per day.

The Alaskan Way Viaduct is a complex structure. The northern third of the viaduct (Bents 1-53) consists of two, single-deck structures that were designed by the City of Seattle Engineering Department (SED) in 1950. The viaduct then transitions to a double-deck configuration, also designed by SED, that extends from Bents 53 to 121. The southern third of the viaduct (Bents 121-183) was designed by WSDOT in 1956. Most of this portion has a double-deck configuration, but it reverts to two, single-deck structures as it approaches the southern abutment.

Concern about the viaduct's vulnerability to earthquakes stems from both structural and geotechnical considerations. Because the Alaskan Way Viaduct was constructed in the 1950s, its structural details do not provide the ductility capacity required by current design standards. Specifically, the transverse reinforcement in the columns and joints is sparse, the column splices are located in potential plastic hinging zones, the lap splices are short, the bar anchorage lengths are short, and the footings lack top reinforcing steel.

The geotechnical environment exacerbates the viaduct's structural vulnerability. This structure lies to the west of the historic shoreline of Elliot Bay, and it is underlain by loosely-placed, hydraulic fill. This fill poses two problems: (1) it may amplify long-period components of ground motion; and (2) it may liquefy during an earthquake.

3

Two preliminary investigations, one by WSDOT (Dodson et al. 1990) and one by the University of Washington (Brown et al. 1992) identified the need for a detailed investigation of the viaduct and its geotechnical context. Both evaluation teams developed three-dimensional, linear models of typical, three-bay units. They characterized the viaduct's seismic vulnerability in terms of flexural and shear capacity-to-demand ratios for typical structural members. Both studies concluded that it would be impossible to have confidence in the viaduct's seismic resistance without evaluating its structural details, and they found the information available on subsoil conditions and expected soil behavior to be inadequate. Consequently, the WSDOT commissioned this research to explore these issues.

1.2 GEOTECHNICAL AND SEISMOLOGICAL CONSIDERATIONS

To reduce the geotechnical uncertainties, the researchers and WSDOT performed a subsoil investigation, the results of which are summarized in a companion, geotechnical report. Kramer et al. (1995) present the results of a subsoil investigation; a seismic risk assessment; site-specific ground-motion studies; and an evaluation of the potential for liquefaction. The geotechnical report also considers liquefaction's potential effects on the viaduct's piles.

The evaluation team considered two types of response spectra. The first spectrum was developed using the Applied Technology Council's "Seismic Design Guidelines for Highway Bridges, ATC-6" (1981). To be consistent with the site-specific spectrum for a nearby site, the team selected an effective acceleration of 0.25g and Soil Type III. The structural evaluation also considered site-specific spectra that the geotechnical team developed (Kramer et al. 1995). These spectra were the products of a probabilistic seismic hazard analysis and were based on consideration of the dynamic response of various soil profiles. The spectra were consistent with a ground motion with a 10 percent chance of exceedence in 50 years.

4

1.3 SCOPE OF REPORT

This report evaluates the seismic vulnerability of a three-span, double-deck unit that extends from Bents 151 to 154. This unit, which was designed by WSDOT, will be referred to as the "WSDOT unit." This unit is typical of the southern third of the Alaskan Way Viaduct (Bents 121-183). Bent 121 is near the First Avenue South off-ramp next to the Kingdome, and Bent 183 corresponds to the southern abutment. Figure 1.1 shows a portion of the Alaskan Way Viaduct that was designed by WSDOT. Chapter 2 describes the WSDOT typical unit's geometry, its reinforcing steel arrangement, and its material properties. Structural drawings for the unit are presented in Appendix A.

The researchers implemented two assessment procedures. The first procedure is documented in "Seismic Retrofitting Guidelines For Highway Bridges, ATC-6-2," published by the Applied Technology Council (1983). According to the ATC-6-2 guidelines, the vulnerability of each member to each failure mode is measured in terms of the ratio between the member's capacity and its imposed demand. Member capacities are computed with equations similar to those used to design new bridges, and member flexural demands are obtained from linear, dynamic analysis. Chapter 3 discusses the three-dimensional, linear analyses of the typical unit. In particular, it presents the finite-element model, results of the gravity and dynamic analyses, and the resulting flexural capacity-to-demand ratios. The ATC-6-2 assessment procedure relies heavily on these ratios as a means of quantifying the unit's vulnerability.

The researchers also implemented a procedure advocated by Priestley, Seible and Chai (1992) at the University of California, San Diego (UCSD). This evaluation procedure relies on two-dimensional, nonlinear analysis and on the results of recent research. Chapter 4 discusses the nonlinear, finite-element models of the typical unit and the computed structural response. The two-dimensional models directly incorporate the beam's and column's nonlinear moment-curvature relationships.
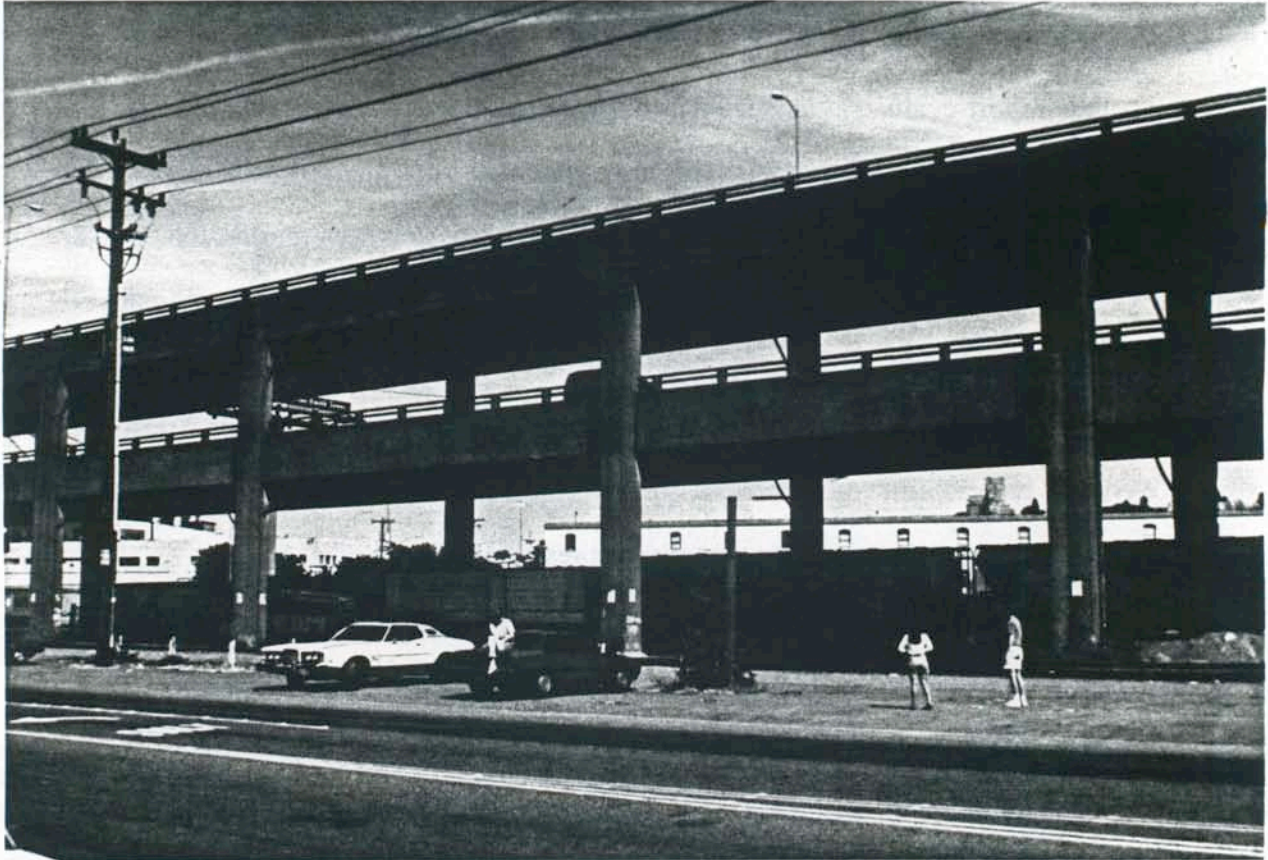
Figure 1.1. Photograph of Alaskan Way Viaduct

The unit's vulnerabilities to the various failure modes are explored in Chapters 5 through 10. Wherever possible, each chapter presents the results of implementing both the ATC-6-2 and Priestley et al. (1992) methodologies. Chapter 5 discusses the consequences of the scarcity of confinement reinforcement in the columns and beams. The shear vulnerability is addressed in Chapter 6, Chapter 7 addresses the anchorage conditions, and Chapter 8 focuses on the vulnerability of the lap splices. Chapter 9 addresses the vulnerability of the beam/column joints, an important topic not addressed by ATC-6-2. The joints are evaluated with criteria proposed by Priestley et al. (1992)

and by Thewalt and Stojadinvic (1992). Chapter 10 considers the capacity of the pile-supported footings.

Finally, to give the reader a sense of the relative significance of each potential failure mode, the likelihood of each type of failure, as well as the associated consequences, are described in Chapter 11. This discussion, combined with reference to the relative costs of suppressing the various potential failure modes, provides a basis upon which engineers can develop retrofit priorities.

1.3 COMPANION REPORTS

The evaluation of the Alaskan Way Viaduct's seismic vulnerability is documented and discussed in several reports. Knaebel et al. (1995) consider the structural vulnerability of a typical three-span unit that the City of Seattle Engineering Department (SED) designed. Kramer et al. (1995) address geotechnical aspects of the evaluation. Kramer and Eberhard (1995) summarize the results of the evaluation of the Alaskan Way Viaduct's seismic vulnerability.

CHAPTER 2

DESCRIPTION OF WSDOT TYPICAL UNIT

The WSDOT-designed section of the viaduct (Bents 121 to 183) consists primarily of three-bay units, which are separated from adjacent units by a 2-inch gap. These units are not identical. They vary to accommodate curves, superelevations, off-ramps, and a series of outrigger columns. The outrigger columns are located near the South abutment, where the viaduct changes from a double-deck to a single-deck configuration.

Despite these atypical features, this report considers the seismic vulnerability of Bents 151 to 154 only; these bents are located near South Royal Brougham Way. The researchers selected these bents for evaluation because they are typical of much of the southern third of the Alaskan Way Viaduct. Consequently, the cost of mitigating the typical unit's deficiencies is likely to make up a significant portion of the cost of retrofitting the entire viaduct. Moreover, many of the details of the typical units are repeated in the atypical units. The structural drawings for the typical unit are presented in Appendix A. The typical unit was constructed entirely of cast-in-place, reinforced concrete.

2.1 GEOMETRY OF TYPICAL UNIT

The longitudinal elevation of a typical 184-foot long unit is depicted in Figure 2.1. In the longitudinal direction, the unit has two exterior spans, which are approximately 56 feet long, and a center span, which is 25 percent longer (70.3 feet). The bottom deck is located approximately 36.3 feet above the tops of the footings, and the top deck is located approximately 58.3 feet above the tops of the footings. A consequence of these deck elevations is that the clear span of the first-story columns (29 feet) is nearly twice the

9
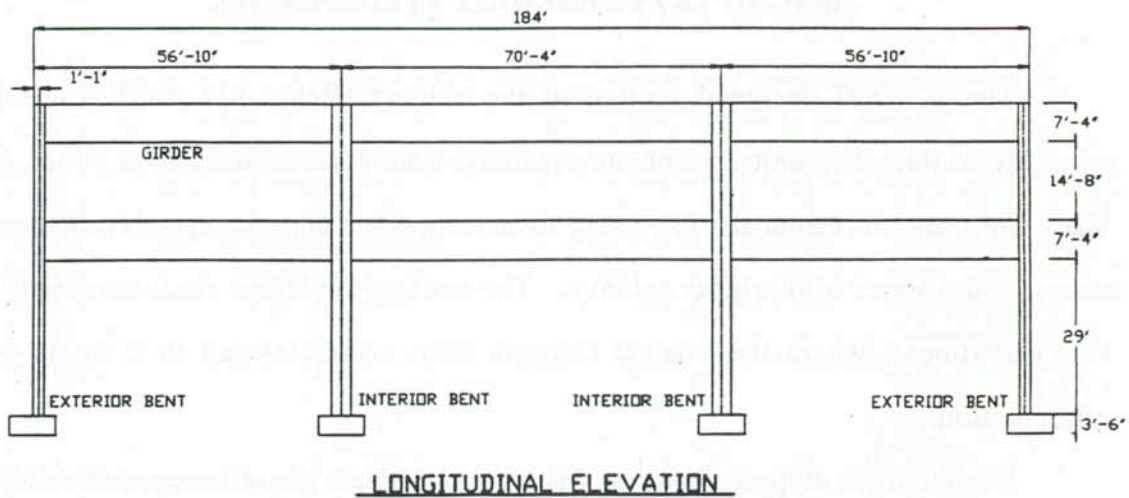
Figure 2.1 Longitudinal Elevation of Typical Unit

span of the second-story columns (14.7 feet). In the transverse direction (Figs. 2.2 and 2.3), the unit has a single span whose center-to-center column spacing is 47 feet.

The floor systems for both levels have the same geometry. The roadway surface consists of a 6.5-in. thick, reinforced concrete slab, which is supported by four longitudinal stringers. The longitudinal stringers frame into end beams (1.5 by 5.0 feet), which span between the columns (Figs. 2.2 and 2.3), and into two intermediate beams, which span between deeper girders (1.5 by 7.3 feet). These girders span in the longitudinal direction between the columns (Fig. 2.1). The exterior and interior columns have the same cross-sectional dimension in the transverse direction (4 feet), but in the longitudinal direction, the dimensions differ. The longitudinal dimension of the interior columns is almost twice as deep as the exterior columns (3.5 feet versus 2 feet).

The columns rest on pile-supported footings that are 3.5-feet thick. The interior footings support a single column, whereas each exterior footing bears the load of two exterior columns, one from each adjacent unit. As shown in Appendix A, the interior

10
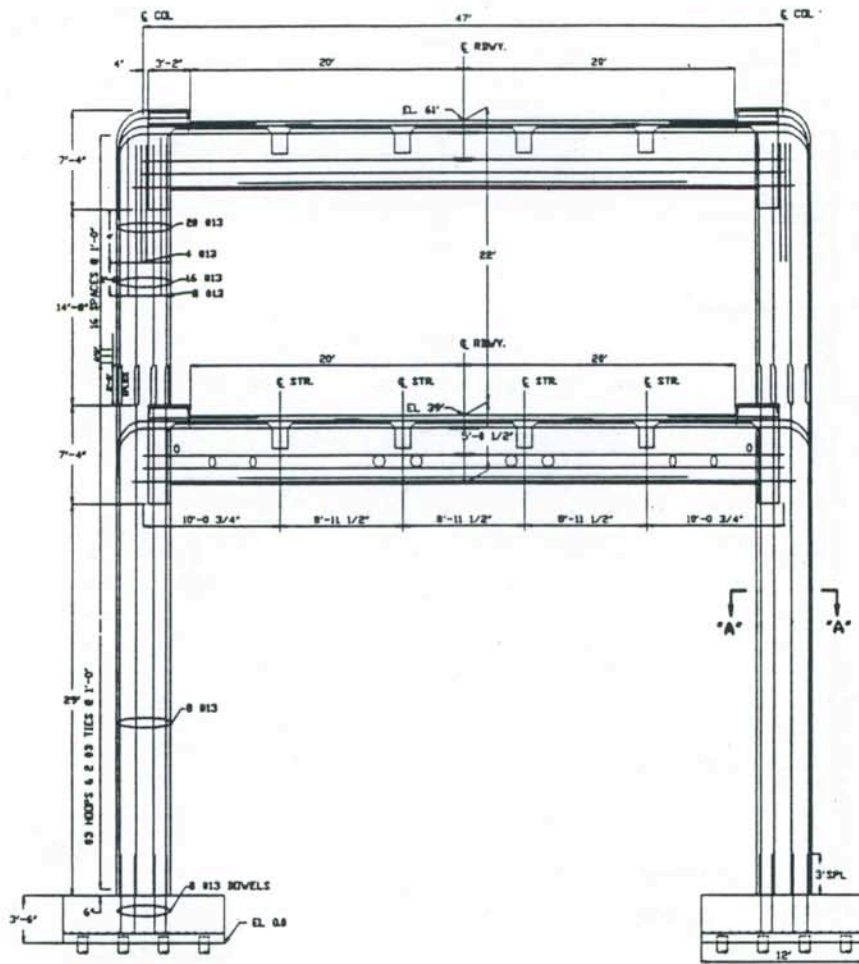
TRANSVERSE ELEVATION OF EXTERIOR BENT
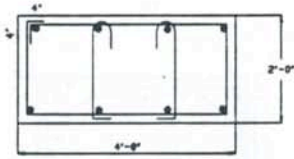
SECTION 'A-A'

Figure 2.2. Elevation of Exterior Transverse Frame

11
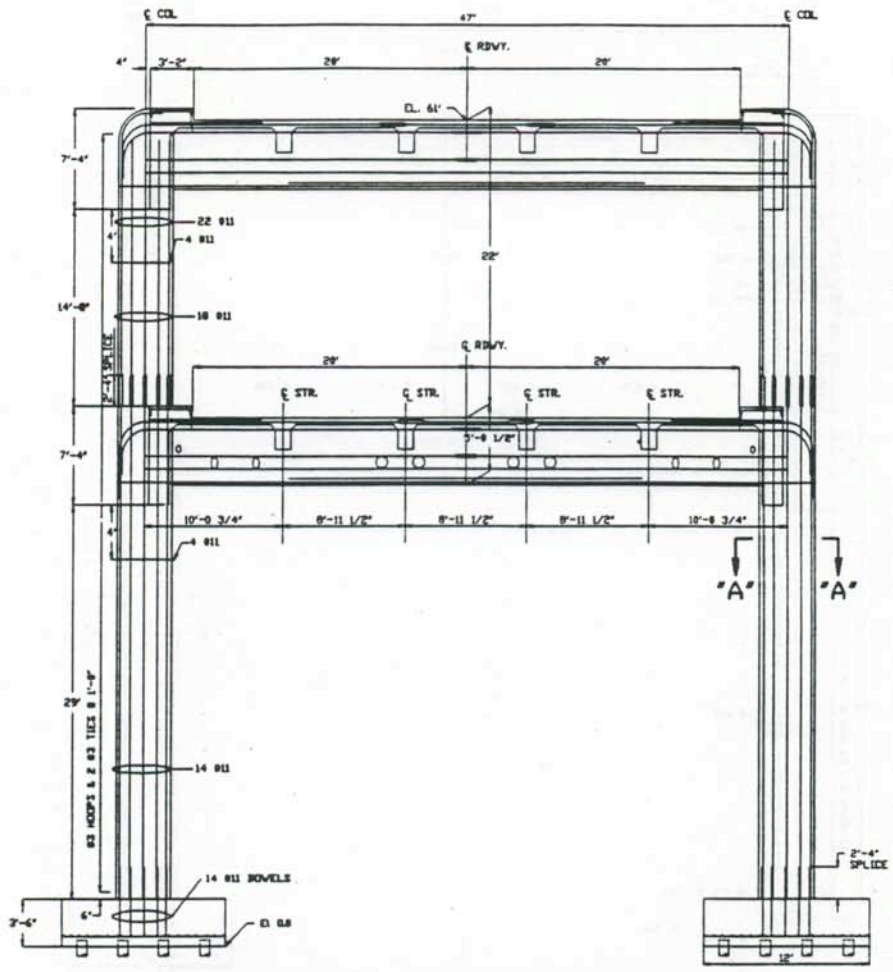
TRANSVERSE ELEVATION OF INTERIOR BENT
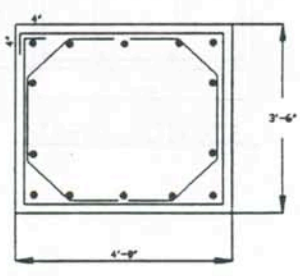
SECTION 'A-A'

Figure 2.3. Elevation of Interior Transverse Frame

12

footings are supported by 16 concrete piles, arranged in four rows of four piles each. The exterior footings are supported by 11 piles, which are staggered in three rows. These concrete piles are spliced with timber piles below the water table, approximately 15 feet below grade. The piles extend through the fill and tidal deposits, and they penetrate into the stiff, glacial till by a short distance (Kramer et al. 1995).

2.2 REINFORCEMENT

The distribution of flexural and shear reinforcement is consistent with the gravity-load moment diagrams. The reinforcement arrangement is complex. For example, although all the beams have the same geometry, the designers specified six flexural reinforcement arrangements, the choice among which was based on the beam's location. Moreover, the stirrup spacing often varies from stirrup to stirrup, and the eastern half of the beams have a slightly different spacing pattern than does the western half. The reinforcing arrangement for each member is described in the following paragraphs, and Appendix A documents the reinforcing details.

The deck is reinforced by #4 bars, top and bottom, in the longitudinal direction, and it is reinforced by #5 bars, top and bottom, in the transverse direction. The longitudinal stringers are reinforced with #9 bars, top and bottom, and #4 U-shaped stirrups. The slab and stringer reinforcement is illustrated on Sheets 4 and 5 of Appendix A.

The intermediate and end beams, shown in Sheets 6, 7, and 8 of Appendix A, are reinforced for positive moments with #13 bars and #17 bars. The top reinforcing consists of #9 bars and #13 bars. Some bars are anchored in the columns with 90-degree hooks while others merely penetrate straight into the column. Shear reinforcing is provided by #5, U-shaped stirrups with external 90-degree hooks at both ends.

The girders are reinforced primarily with #17 bars and #13 bars in two layers on the bottom and with #17 bars and #9 bars at the top of the member. Shear reinforcing

13

consists of #5 stirrups at variable spacing ranging from 6 in. to 26 in. A girder elevation and section is shown on Sheet 5 of Appendix A.

Figures 2.2 and 2.3 illustrate the reinforcing details of the columns and the footings. The exterior columns have a reinforcement ratio of about 1.4 percent at the base, as compared with 1.1 percent for the interior columns. A splice occurs just above the bottom deck, and bars were added to raise the reinforcing ratio to 4.0 percent at the top of the exterior column and 1.7 percent at the top of the interior column. All of the longitudinal bars in the exterior columns are #13, whereas bars in the interior columns are #11.

The hoops and ties are inadequately anchored and widely spaced compared to current seismic design standards. Transverse confinement in the columns consists of a #3 hoop and two #3 ties at 12-inch spacings. The hoops in both the exterior and interior columns are closed with a 4-inch, 90-degree bend at each end of the bar. The ties in the exterior column are made of two J-hooks with a 180-degree bend at one end and a 90-degree bend at the other (Fig. 2.2). In the interior column, the ties consist of two half-hexagons (Fig. 2.3), which face one another to form a full hexagon. The spacing of the hoops and ties remains constant through the longitudinal girder-transverse beam joint. The scarcity of transverse steel is of particular concern near the lap splices because they are located in regions that are likely to yield. For construction convenience, these short splices were placed directly above the footings and directly above the first-story deck.

At the base of the columns, a lap splice connects the column longitudinal reinforcement to dowels embedded in the pile-supported footings. Within the footings, these dowels hook away from the centerline of the column in the transverse direction. The footings have bottom reinforcing only, consisting of #9 bars in each direction. A bar list, indicating the length and bending diagram for each reinforcing bar, is provided in Sheet 9 of Appendix A.

2.3 MATERIAL PROPERTIES

Class A concrete was specified for the entire structure except for the pile-supported footings (for which the concrete was specified as Class B). According to the 1948 Standard Specifications for Roads and Bridges (Standard Specifications, 1948), Class A corresponds to a specified strength of 3000 psi, and Class B had a specified strength of 2200 psi. The 1948 Specifications call for Intermediate Grade (40 ksi) reinforcing steel for all structures unless otherwise specified.

Following the recommendations of Priestley, Seible, and Chai (1992), the evaluation team assumed that the actual concrete compressive strengths, f'_c, were 1.5 times those originally specified. The elastic modulus, E, was taken as $57,000 \sqrt{f'_c}$ as suggested by ACI-318, Section 8.5.1 (ACI-318-89, 1989). The steel, whose nominal yield stress was 40 ksi, was assumed to have a yield strength 44 ksi (Priestley et al. 1992). No concrete cores or steel coupons were extracted from the viaduct.

CHAPTER 3

LINEAR, DYNAMIC ANALYSIS

To study the dynamic response of the WSDOT typical unit, the evaluation team assembled linear, finite-element models, representing both fixed-base and pinned-base conditions. The fixed-base condition best represents the likely foundation stiffness, and the pinned-base condition represents a lower band on the foundation's rotational stiffness. The pinned-base analysis also provides useful information on the behavior of the WSDOT unit should the moment capacity at the base of the first-story columns be greatly reduced. This reduction might occur if the column lap splices or footings failed.

The finite-element models are described in Section 3.1; Section 3.2 reports the results of gravity-load analyses; and Section 3.3 reports the results of modal analyses. To generate force demands in the longitudinal and transverse directions, response-spectrum analyses were performed with an ATC-6-2 spectrum (Sec. 3.4) and with spectra developed specifically for various soil profiles (Sec. 3.5). Based on the results of these analyses and the computed strengths of the members, the researchers calculated flexural capacity-to-demand (C/D) ratios for the columns, girders, and beams. These ratios, reported in Section 3.6, greatly affected the results of the ATC-6-2 evaluation, which is discussed in Chapters 5 through 8. ◆

3.1 DESCRIPTION OF STRUCTURAL MODEL

The researchers modeled a typical, three-bay, 184-ft unit corresponding to Bents 151 to 154 (Figs. 2.1, 2.2, and 2.3). The three-dimensional model retained the basic geometry of the WSDOT model described in the report "Preliminary Investigation of the Seismic Vulnerability of the Alaskan Way Viaduct" (Brown et al. 1992). However, the researchers used a different finite-element program for the new analyses. The earlier model had been assembled with the SAP90 program (Wilson and Habibullah, 1988). The

17

researchers performed the new analyses with ANSYS 5.0 (ANSYS, 1993). In addition, the researchers modified some of the joint locations, constraints, and "rigid" links.

The finite-element model is shown in Figure 3.1. The footings, columns, beams, girders, and rigid links were modeled with three-dimensional beam elements (BEAM4 in ANSYS). Shear deformations were neglected. The bridge deck was modeled with shell elements (SHELL63), which include both membrane and plate-bending stiffnesses. Linear springs (COMBIN14) modeled the soil stiffness. To model the fixed-base condition, the soil springs were assigned a stiffness 100 times the column stiffness. To model the pinned-base condition, a pinned support was placed on the bottom face of the footing.

The structural components were modeled at their centerlines. Each bridge deck had three layers of nodes, whose elevations corresponded to the centerlines of the slab, the longitudinal stringers, and the longitudinal girders. Although the transverse beam centerlines are located slightly above the girder centerlines, the beams were placed on the same level as the girders. To model composite action, the researchers placed vertical, "rigid" links to connect the three levels. The actual stiffness of the rigid links was slightly greater than that of an interior column element. For convenience, the researchers did not model the superelevations and the curbs.
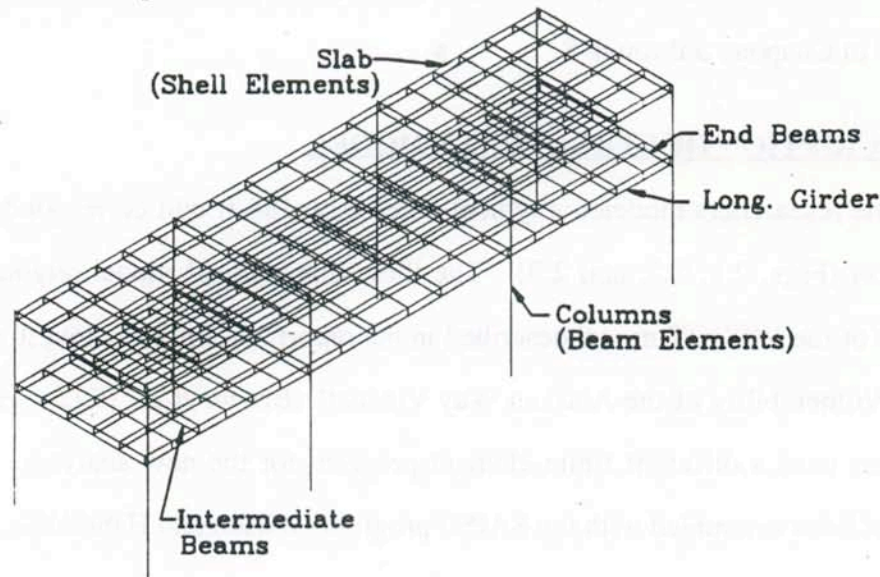
Figure 3.1. Linear, Finite-Element Model of Typical Unit

It would have been tedious to compute transformed-section moments of inertia for all the beam and column cross-sections because the reinforcing pattern in the structural elements changes frequently. Consequently, all structural elements were assigned a moment of inertia equal to half that computed on the basis of the gross-section dimensions. As suggested in a CALTRANS study of two-level viaducts, the researchers increased the column stiffness by a factor of eight in the joint regions.

3.2 GRAVITY ANALYSIS

The researchers performed gravity analyses for both fixed- and pinned-base conditions. Traffic and other live loads were neglected, and the unit weight of the concrete was assumed to be 150 pcf. No load factor was applied to the dead load.

Fixed-Base Condition

The moment and shear diagrams for the exterior transverse frame with fixed bases are shown in Figure 3.2. In the transverse direction, the moments and shears were much larger in the second story than in the first story. This difference in moment demands is consistent with the geometry of the transverse frames. The second-story columns, whose clear height is 14.7 feet, are much stiffer than the first-story columns, whose clear height is 29 feet. Therefore, the beam end moments are transferred primarily to the second story. The difference in moment demands is also consistent with the distribution of flexural reinforcement (Sec. 2.2). The second-story columns have more flexural reinforcement than do the first-story columns.

The moments and shears carried by the transverse, interior frames are reported in Figure B.1. Because their tributary area is larger, the moments and shears for the interior frames were approximately twice as large as those for the exterior frames. The magnitudes of the column moments and shears in the longitudinal frame were similar to the magnitudes of the transverse moments and shears (Fig. 3.3). In contrast, the girder

19

EXTERIOR FRAME, FIXED BASE
GRAVITY LOADS

213
253

231
256

84

57 K-FT

47
34

47
34

5

5 K
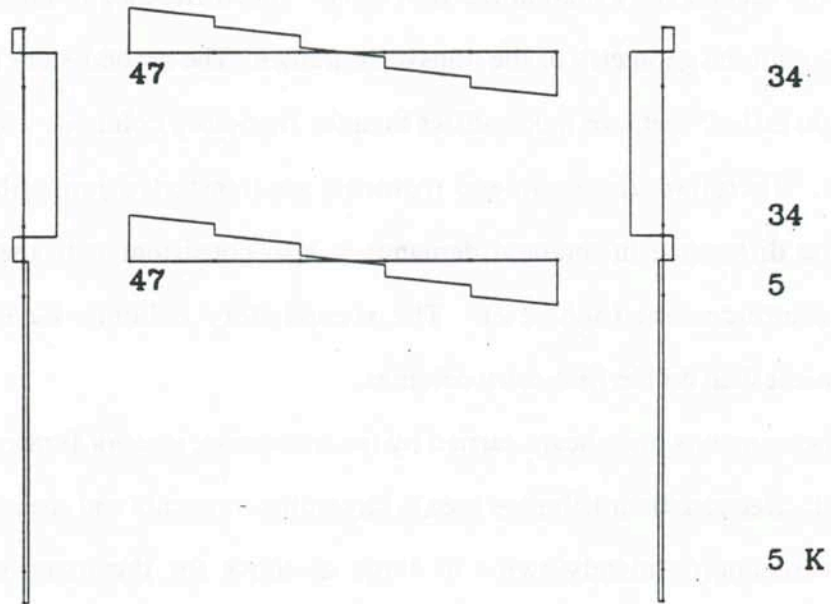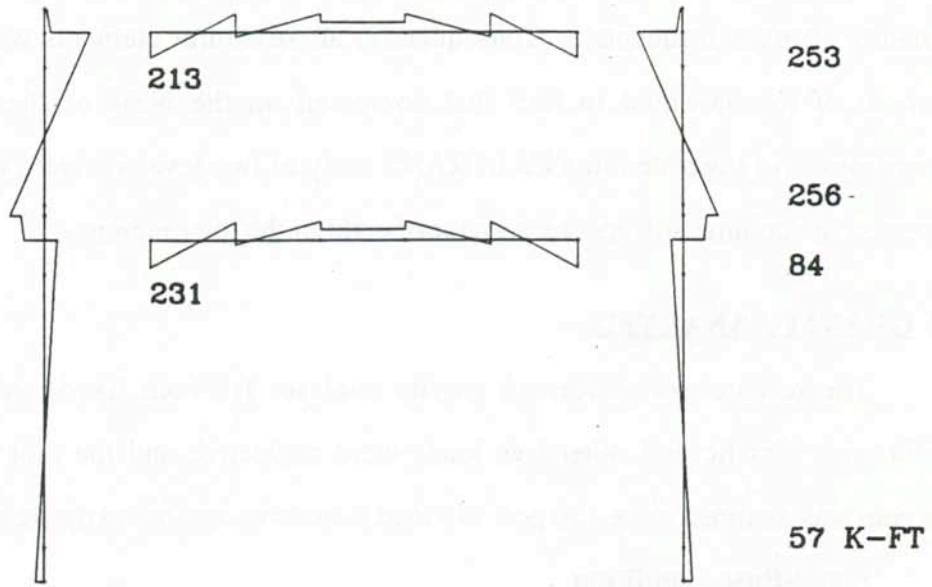
Figure 3.2. Gravity Moment and Shear Diagrams: Exterior Transverse Frame
(Fixed Bases)

LONGITUDINAL FRAME, FIXED BASE
GRAVITY LOADS
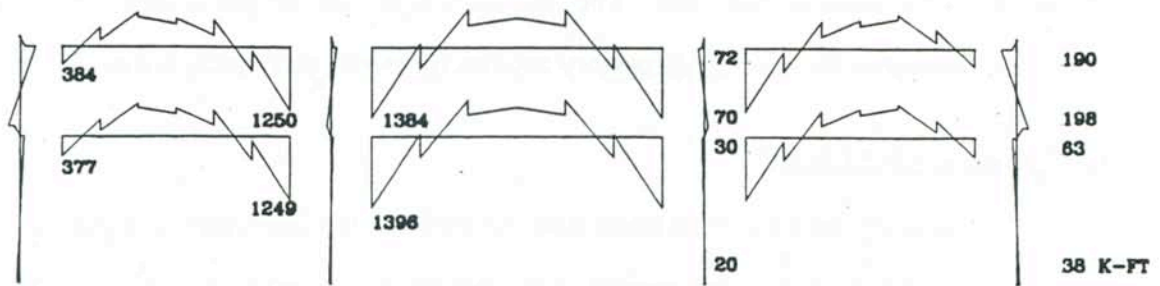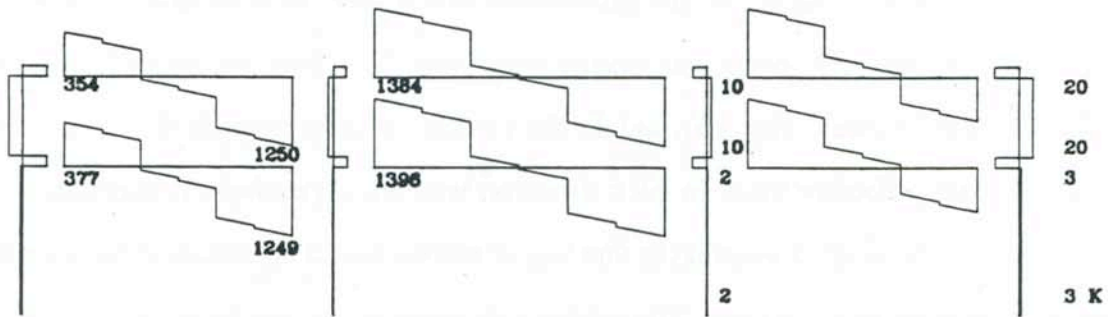
a) Moments

b) Shears

Figure 3.3. Gravity Moment and Shear Diagrams: Longitudinal Frame (Fixed Bases)

moments were much larger than the column and beam moments. The maximum girder moments occurred at the interior columns.

Pinned-Base Condition

The calculated pinned-base moments, shown in Figures B.2, B.3 and B.4, were almost identical to the fixed-base moments. For example, the moment at the end of the first-level beam in the exterior transverse frame was 231 kip-ft in the fixed-base case and 226 kip-ft in the pinned-base case. The similarity between the fixed- and pinned-base results is reasonable because the first-story column moments and shears are small.

3.3 MODAL ANALYSIS

Modal analyses were performed with ANSYS for the fixed-base and pinned-base models. The mode shapes and periods were determined through a reduced subspace analysis with 576 degrees of freedom. Then, the first 20 mode shapes were expanded from the reduced set to the full set of degrees of freedom.

The computed mode shapes and the values of the effective masses were consistent. For both the fixed- and pinned-base conditions, the principal component of movement for the first mode was longitudinal sway (Fig. 3.4); the second mode was mostly transverse sway (Fig. 3.5); and the third mode was a torsional mode. As shown in Table 3.1, the effective mass in each direction was almost entirely concentrated in a single mode. As such, it is unlikely that higher modes would contribute significantly to the structure's seismic response. The calculations indicate that, for fixed-base conditions, the modal periods of the typical unit is 0.9 seconds in the longitudinal direction and 0.8 seconds in the transverse direction. For pinned-base-conditions, the periods for the first three modes approximately doubled.
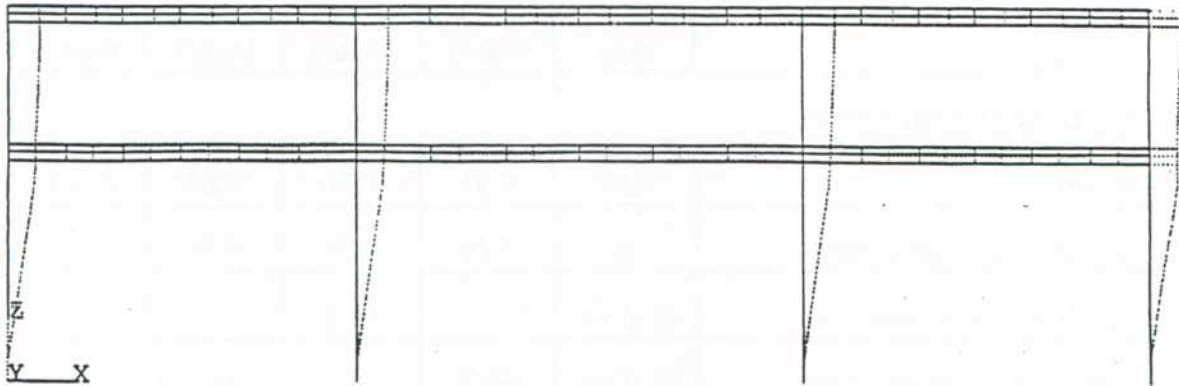
Figure 3.4. Mode 1: Longitudinal Sway
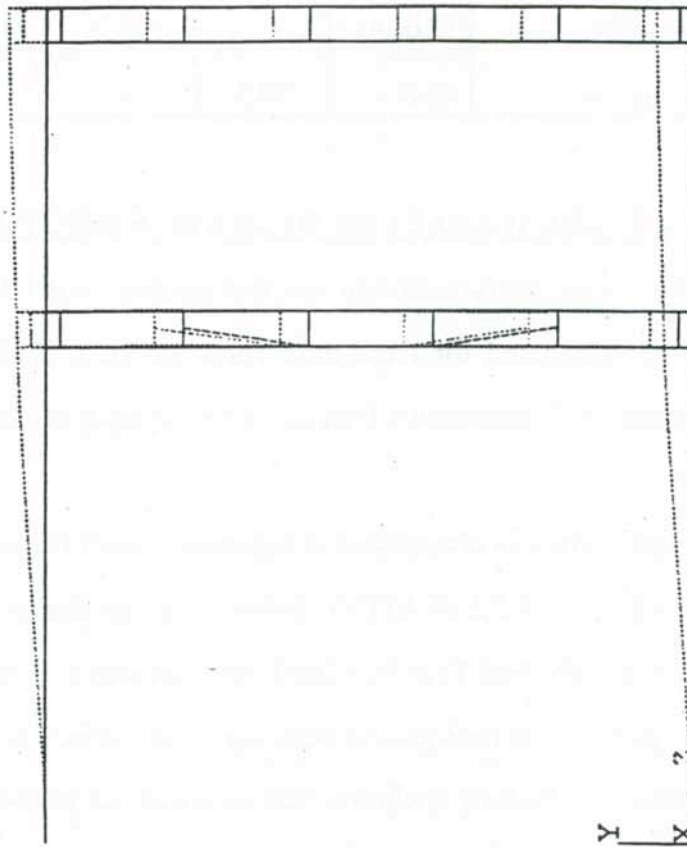
Figure 3.5. Mode 2: Transverse Sway

23

Table 3.1. Computed Modal Properties

	Units	Mode 1	Mode 2	Mode 3	Mode 4
FIXED-BASE STRUCTURE					
Period	sec	0.91	0.76	0.66	0.19
Spectral Acceleration (ATC)	g	0.46	0.54	0.59	0.39
Effective Mass (transverse)	% of wt.	-	98.5	-	-
Effective Mass (longitudinal)	% of wt.	99.1	-	0.7	-
PINNED-BASE STRUCTURE					
Period	sec	2.02	1.63	1.45	0.20
Spectral Acceleration (ATC)	g	0.28	0.32	0.35	0.40
Effective Mass (transverse)	% of wt.	-	99.0	0.1	-
Effective Mass (longitudinal)	% of wt.	99.5	-	-	0.3

3.4 RESPONSE-SPECTRUM ANALYSIS WITH ATC-6 SPECTRUM

The evaluation team performed four spectral analyses with the ATC spectrum. These analyses were conducted for fixed-base condition in both the transverse and longitudinal directions. The researchers then repeated the analyses for the pinned-base condition.

A response spectrum was constructed in accordance with the multimodal spectral method described in Section 5.2.2 of ATC-6 "Seismic Design Guidelines For Highway Bridges" [ATC-6, 1981]. For Soil Type Profile III, the least stiff soil profile, a spectral curve is shown in Figure 3.6. A peak ground acceleration of 0.25g was selected to anchor the spectrum because the resulting spectrum best matched the Hart-Crowser spectrum developed for the adjacent Seattle Transit Access Project (Dodson, Rochelle,

24

Acceleration Spectrum
ATC−6, 0.25g
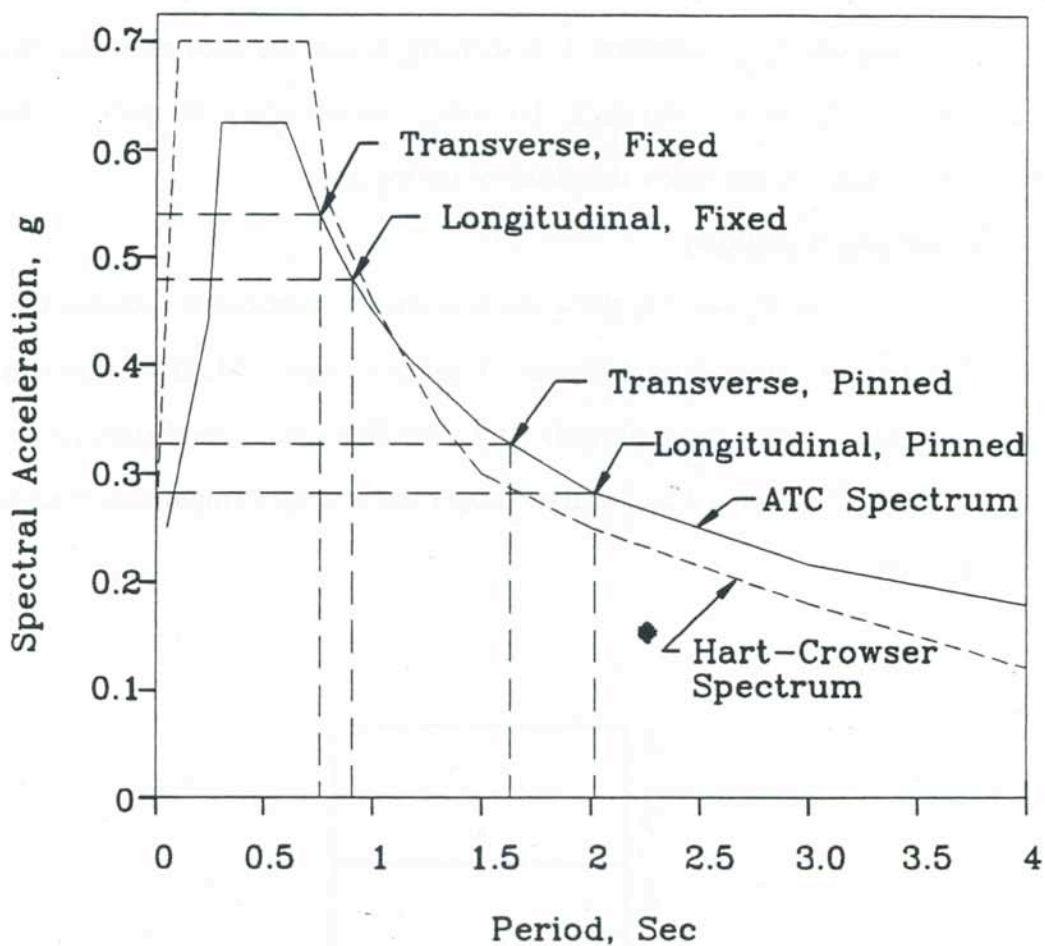
Figure 3.6. ATC-6-2 Response Spectrum: Soil Type III, 0.25g

and Stoddard, 1990). The Hart-Crowser spectrum was developed for a damping ratio of 5 percent.

The Complete Quadratic Combination (CQC) method was chosen to combine the modal responses. Because the viaduct's response in each direction was dominated by one mode, the CQC method produced results similar to those of the Square Root Sum of the Squares method (Wilson and Der Kiureghian, 1981). Five percent structural damping was included in the CQC method.

To facilitate discussion, it is convenient to define four locations on each column, as shown in Figure 3.7. Location 1 is directly above the footing. Location 2 is underneath the girder of the lower deck. Location 3 lies just above the girder of the lower deck, and Location 4 is just below the girder of the top deck.

Fixed-Base Condition

Table 3.1 and Figure 3.6 show the spectral acceleration associated with each mode. For both the longitudinal (Mode 1) and transverse (Mode 2) directions, the response acceleration was approximately 0.5g. The first- and second-story relative drift ratios and are listed in Table 3.2. For fixed-base condition, all computed drift ratios were below 1 percent.
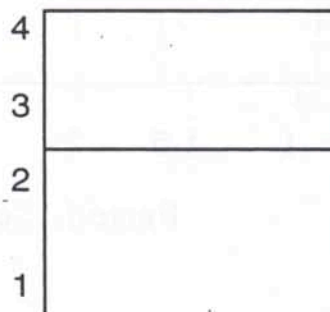
Figure 3.7. Definition of Column Locations 1 to 4

Table 3.2. Story Drifts and Drift Ratios

	Transverse Direction		Longitudinal Direction	
	Drift [ft]	Drift Ratio	Drift [ft]	Drift Ratio
FIXED-BASE STRUCTURE				
1st Story	0.23	0.6%	0.28	0.8%
2nd-Story	0.05	0.2%	0.05	0.2%
Overall	0.28	0.5%	0.33	0.6%
PINNED-BASE STRUCTURE				
1st Story	0.71	2.0%	0.94	2.6%
2nd-Story	0.05	0.2%	0.04	0.2%
Overall	0.76	1.3%	0.98	1.7%

The moments and shears for an exterior transverse frame are shown in Figure 3.8. As expected for fixed-base conditions, the maximum moments occurred at the base and at the top of the first-story columns (Locations 1 and 2). In comparison, the second-story moment demands were much smaller than those that occurred in the first-story. The moments were particularly small at Location 3, where the moment corresponded to 17 percent of moment at Location 1.

The moment and shear diagrams for the interior transverse frame are reported in Figure B.5. The moments and shear distributions for the interior frame resembled those for the exterior frames, but the magnitudes differed because the interior columns are wider. The distribution of shears among the interior and exterior frames was proportional to column stiffness. The moment of inertia of the interior-frame columns is 1.75 times that of the exterior frame columns, and the interior-frame columns carried approximately 1.5 to 1.7 times the shears of the exterior transverse frames (Figs. 3.8 and B.5).

EXTERIOR FRAME, FIXED BASE
ATC-6 SPECTRUM, .25g

798

1264

608

2131

2861

3563 K-FT

71

127

127

180

221

221 K
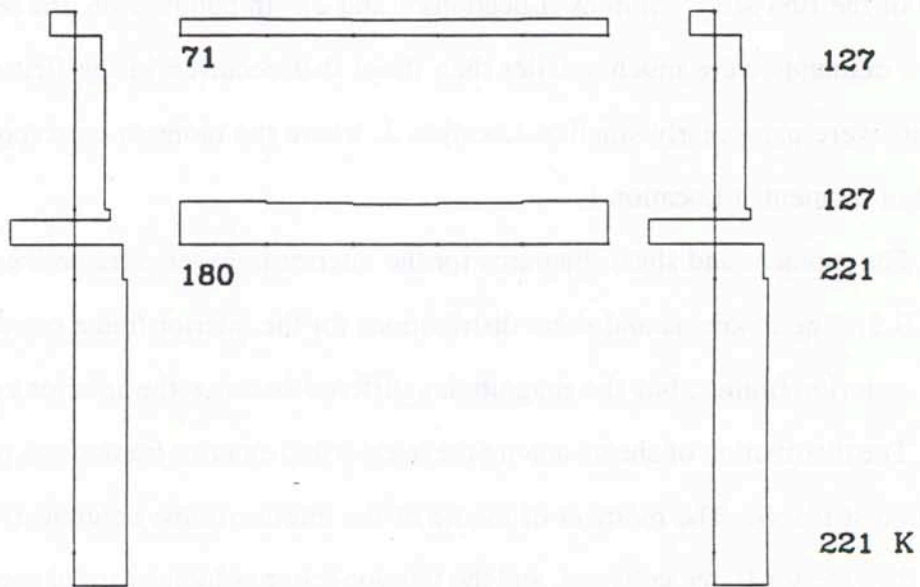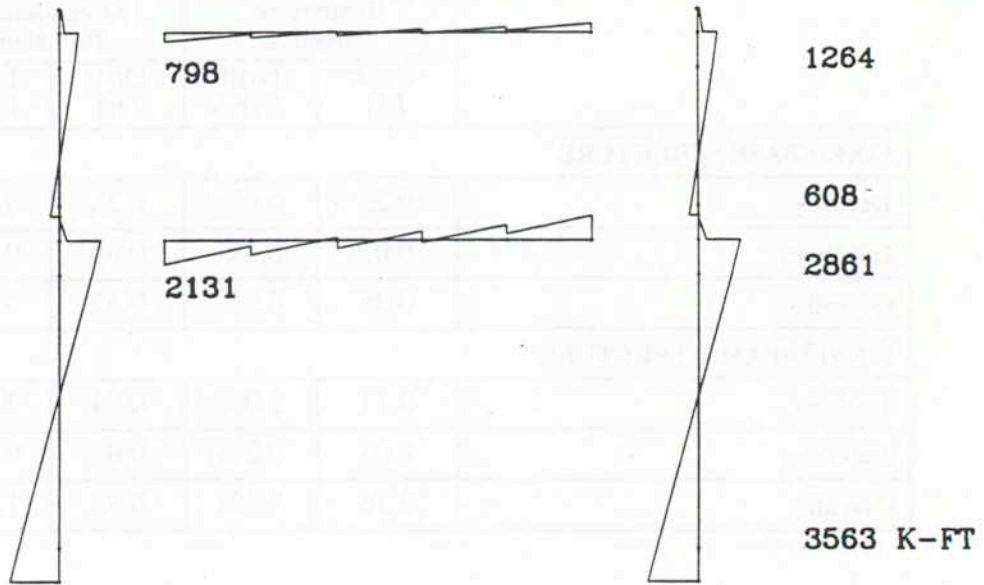
Figure 3.8. Seismic Moment and Shear Diagrams: Exterior Transverse Frame
(Fixed Bases)

Figure 3.9 shows the moment and shear diagrams for longitudinal response. The largest moments occurred at the base of the interior columns. In the longitudinal direction, the moment of inertia of the interior columns is four times that of the exterior columns. Likewise, the interior columns carried about four times the moment and shear. At the base of the interior columns, the seismic moments exceeded the gravity moments by a factor of 320. In contrast, the maximum seismic moment in the beams (Fig. 3.9) was only 2.2 times the maximum negative moment due to gravity (Fig. 3.3).

Pinned-Base Condition

The spectral ordinates for the pinned-base analyses decreased by 40 percent from the fixed-case values because the periods were longer (Table 3.1 and Fig. 3.6). Because only one mode contributed to response in each direction, the base shears also decreased by 40 percent (Figs. B.6, B.7, and B.8). In contrast, the drift ratios approximately tripled. Most of the drift occurred in the first story while the second-story displacements were almost negligible. The maximum first-story drift ratio was 2.6 percent (Table 3.2).

Figures B.6, B.7, and B.8 depict the moment diagrams for the pinned-base analyses. As in the fixed case, the second-story moments were smaller than the first-story moments, and the moment demand at Location 3 was insignificant. The largest moments developed at Location 2, just below the bottom-deck girder. Moreover, despite the lower base shears, the moment at Location 2 for the pinned-base condition exceeded the maximum moment for the fixed-base condition (Figs. 3.8, B.5, and 3.9). A consequence of this moment redistribution was that the beam and girder moments in the first story increased in comparison with the fixed case.

3.5 RESPONSE SPECTRUM ANALYSIS WITH SITE-SPECIFIC SPECTRA

To incorporate the effects of the local geotechnical conditions into the evaluation, Kramer et al. (1995) generated site-specific response spectra. The geotechnical team conducted a probabilistic seismic hazard analysis to estimate the intensity of bedrock

LONGITUDINAL FRAME, FIXED BASE
ATC-6 SPECTRUM, .25g
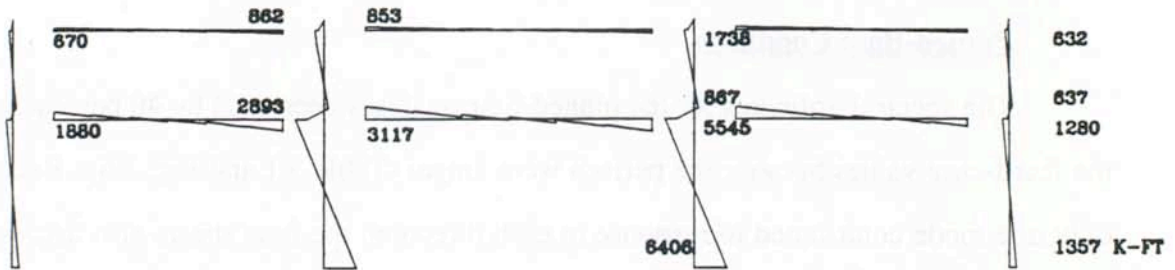
a) Moments
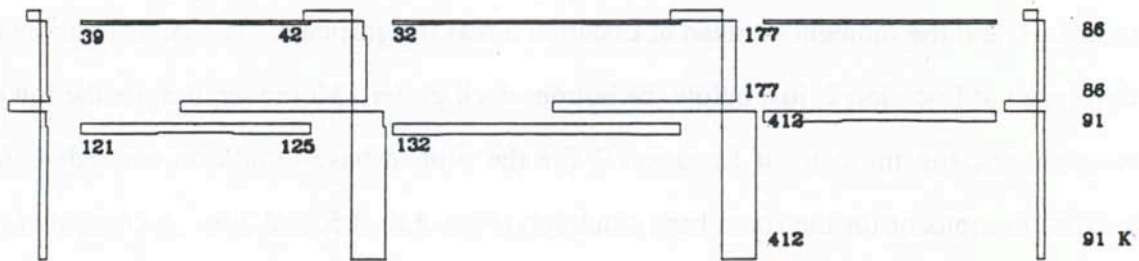
b) Shears

Figure 3.9. Seismic Moment and Shear Diagrams: Longitudinal Frame (Fixed Bases)

motion of an earthquake with a 10 percent chance of exceedence in 50 years. On the basis of bore-hole data, shear-wave velocity tests, and seismic-cone penetrometer results, the team determined the soil profile along the length of the viaduct. The team estimated the ground motion and developed response spectra for three different typical soil profiles underlying the WSDOT section. These profiles correspond to 20 feet of fill on top of 20 feet of tidal deposits, 30 feet of fill on top of 30 feet of tidal deposits, and 40 feet of fill on top of 40 feet of tidal deposits. A fourth profile characterized the soil conditions at Bents 151 to 154, which are underlain by 38 feet of fill and 26 feet of tidal soil.

The four response spectra are shown in Figure 3.10. The stiffest soil profiles, those with 40 feet of soft soil, had the highest peak ground acceleration. More importantly, these profiles had the largest spectral ordinates for periods of up to 1.5 seconds. At a period of 2.0 seconds, the response accelerations were largest for the profiles with 60 to 80 feet of soft soil. Because soil profiles vary along the viaduct, the .evaluation team performed "worst case analyses" for the fixed- and pinned-base cases.

Fixed-Base Condition

The spectrum for 20 feet of fill and 20 feet of tidal soil had the highest spectral acceleration for both the transverse and longitudinal directions. In comparison with the ATC-6 spectrum, the spectral accelerations increased by 30 percent in the transverse direction and 71 percent in the longitudinal direction. The moment and shear demands increased by the same proportion because only one mode contributed significantly to response in each direction.

Pinned-Base Condition

In the pinned case, the spectrum generated for 30 feet of fill and 30 feet of tidal soil was critical. In comparison with the ATC spectra, the response ordinates increased by 58 percent in the transverse direction and 44 percent in the longitudinal direction. The moment and shear demands increased proportionally.

Figure 3.10. Site-Specific Response Spectra
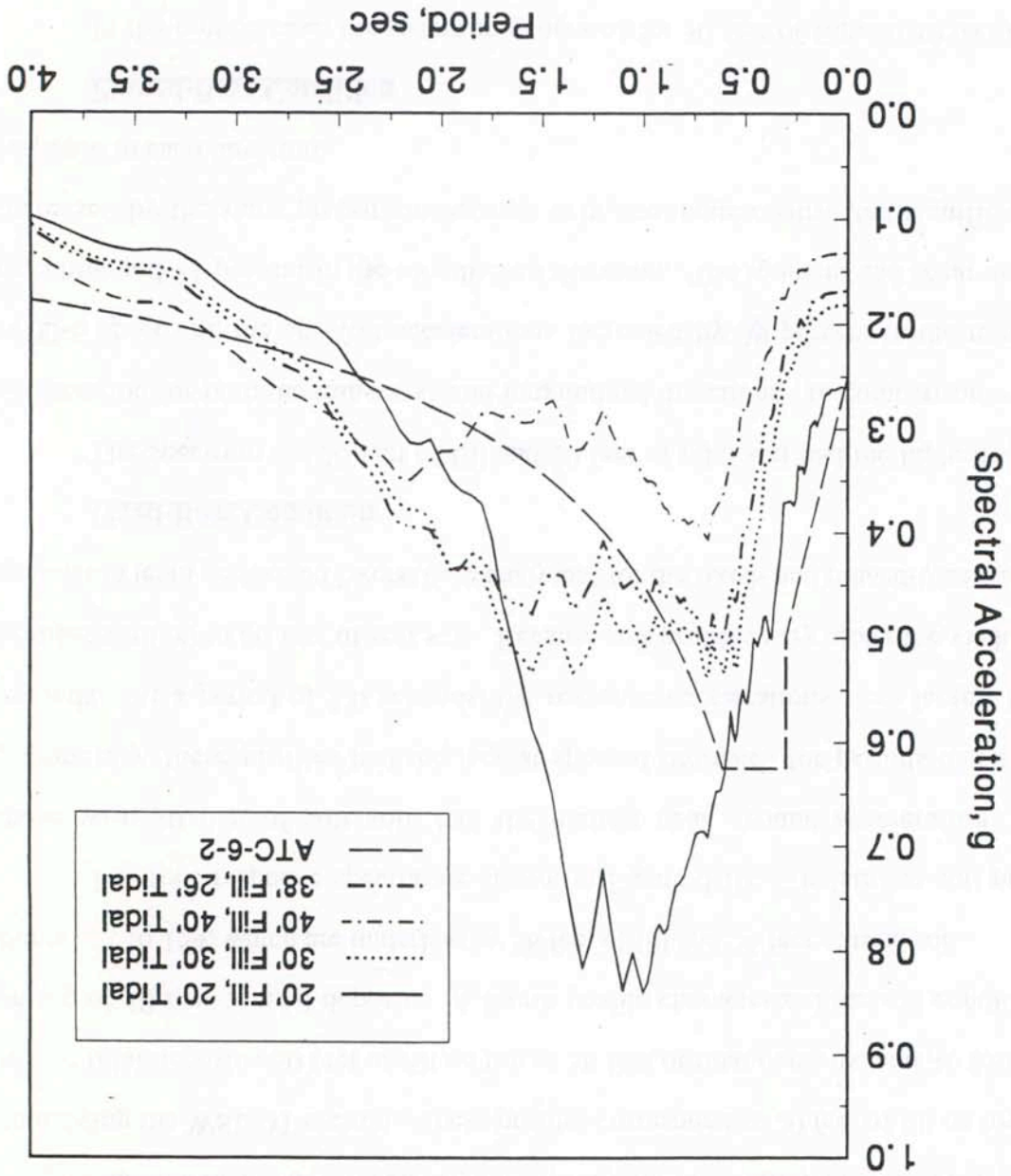
3.6 FLEXURAL C/D RATIOS FOR ATC SPECTRUM

The ATC-6-2 evaluation procedure relies heavily on the ratios of the flexural demand (as calculated with linear analysis) to the computed capacity. A flexural capacity-to-demand ratio (C/D) below 1.0 indicates that the moment demand in the member is greater than its capacity. As a first approximation, the C/D ratio can be thought of as the inverse of the ductility demand.

The demands were reported in Sections 3.4 and 3.5. Each member's moment capacity was calculated using the modified Kent and Park model for confined concrete (Park, Priestley, and Gill, 1992). The computations considered strain hardening of the longitudinal reinforcement (Table 4.1), the effect of confinement, and the contribution of the slab. The column flexural capacities were computed for the axial loads that were obtained with the nonlinear analyses described in Chapter 4. The flexural C/D ratios did not take into account the influence of limited anchorage lengths. The details of the strength computations are reported in Chapter 4. The details of the flexural C/D calculations for the columns and beams are reported in Appendix C.

Figures 3.11 and 3.12 show the computed flexural C/D ratios, r_{ec}, for the columns. The values shown on the left half of the frames were computed for the condition in which the seismic axial load acts in tension. The right half of the frame shows r_{ec} for the condition in which the seismic axial load increased the compressive axial load in the columns.

Fixed-Base Condition

The values of r_{ec} for the first story were almost identical for the interior and exterior transverse frames (Fig. 3.11). The C/D ratios were lowest in the first story (Locations 1 and 2), where r_{ec} ranged from 0.46 to 0.69. In the second story columns, r_{ec} ranged from 1.96 to 9.87, indicating that these columns did not develop their flexural capacity.

EXTERIOR FRAME
FIXED BASE

$r_{ec} = 3.12$	$r_{ec} = 2.15$
$r_{ec} = 4.35$	$r_{ec} = 1.96$
$r_{ec} = 0.62$	$r_{ec} = 0.69$
$r_{ec} = 0.49$	$r_{ec} = 0.56$

EXTERIOR FRAME
PINNED BASE

$r_{ec} = 3.99$	$r_{ec} = 2.51$
$r_{ec} = N/A$	$r_{ec} = 4.39$
$r_{ec} = 0.38$	$r_{ec} = 0.44$
$r_{ec} = 3.34$	$r_{ec} = 3.84$

INTERIOR FRAME
FIXED BASE

$r_{ec} = 1.91$	$r_{ec} = 1.17$
$r_{ec} = 9.87$	$r_{ec} = 1.88$
$r_{ec} = 0.60$	$r_{ec} = 0.67$
$r_{ec} = 0.46$	$r_{ec} = 0.53$

INTERIOR FRAME
PINNED BASE

$r_{ec} = 2.48$	$r_{ec} = 1.34$
$r_{ec} = N/A$	$r_{ec} = 3.47$
$r_{ec} = 0.36$	$r_{ec} = 0.42$
$r_{ec} = 3.14$	$r_{ec} = 3.68$

Figure 3.11. Flexural Capacity-to-Demand Ratios, r_{ec}: Transverse Frames

LONGITUDINAL FRAME
FIXED BASE

$r_{ec} =3.57$	$r_{ec} =1.70$	$r_{ec} =1.56$	$r_{ec} =1.97$
$r_{ec} =1.65$	$r_{ec} =3.18$	$r_{ec} =2.72$	$r_{ec} =0.92$
$r_{ec} =0.66$	$r_{ec} =0.50$	$r_{ec} =0.50$	$r_{ec} =0.71$
$r_{ec} =0.61$	$r_{ec} =0.43$	$r_{ec} =0.43$	$r_{ec} =0.69$

LONGITUDINAL FRAME
PINNED BASE

$r_{ec} =4.70$	$r_{ec} =2.35$	$r_{ec} =2.10$	$r_{ec} =2.26$
$r_{ec} =2.19$	$r_{ec} =N/A$	$r_{ec} =29.6$	$r_{ec} =1.05$
$r_{ec} =0.45$	$r_{ec} =0.31$	$r_{ec} =0.32$	$r_{ec} =0.52$
$r_{ec} =3.73$	$r_{ec} =2.78$	$r_{ec} =2.79$	$r_{ec} =4.29$

Figure 3.12. Flexural Capacity-to-Demand Ratios, r_{ec}: Longitudinal Frames

The results for the longitudinal direction (Fig. 3.12) were similar to those obtained for the transverse direction. Yielding was again indicated at Locations 1 and 2, where r_{ec} ranged from 0.43 to 0.71. The second story C/D ratios ranged from 0.92 to 3.57.

For almost all of the beams, the values of r_{ec} exceeded 1.0 (Table C.2). The one significant exception: the exterior column beam at the first level, where the C/D ratio was 0.50 for positive bending. Of the cross-sections listed in Table C.2, this location had the smallest flexural capacity (945 kip-feet). In the second level, r_{ec} exceeded 2.0 at all member ends. The girder moments were generally well below the flexural capacity, particularly in the second level. The lowest value of r_{ec} for the girders was 0.80, which occurred in the negative moment region of the first-level girders where they frame into the exterior frame.

Pinned-Base Condition

The results of eliminating the foundation rotational fixity were predictable (Tables C.3 and C.4). The flexural C/D ratios increased greatly at the base of the columns. At the top of the first-story columns, the values of r_{ec} decreased, ranging from 60 to 70 percent of the fixed-base values. The lowest value of r_{ec} (0.31) occurred at Location 2 of the interior column for longitudinal motion. The C/D ratios increased in the second-story columns, where the lowest value of r_{ec} was 1.05. The moment release also reduced the C/D ratios for the first-level beams. In the beams, the lowest value of r_{ec} (0.43) occurred at the exterior-column beam at the first level.

3.7 FLEXURAL C/D RATIOS FOR SITE-SPECIFIC SPECTRA

The flexural capacity-to-demand ratios for the columns are summarized in Tables C.5 and C.6 for the fixed- and pinned-base analyses. The changes in the flexural C/D ratios were not proportional to the increase in moment demands because the gravity-load component of the moments did not change. Nonetheless, the C/D ratios decreased at all locations.

36

For the fixed-base condition, r_{ec} decreased by 20 to 30 percent in the transverse direction and 40 to 50 percent in the longitudinal direction. The lowest values of r_{ec} were found at Locations 1 and 2, where they ranged from 0.25 to 0.30. In the second story, r_{ec} exceeded 1.0 or approached 1.0 at all locations except for one. At Location 3 on the exterior column, r_{ec} was equal 0.59 for motion in the longitudinal direction. For the pinned-base condition, the lowest values of r_{ec} were found at Location 2, where r_{ec} ranged from 0.22 to 0.36.

CHAPTER 4

NONLINEAR, STATIC ANALYSIS

4.1 INTRODUCTION

The dynamic analyses described in Chapter 3 were based on the assumption that member force-displacement relationships are linear. To gain further insight into the behavior of the WSDOT typical unit, this chapter presents the results of nonlinear, static analyses. The assessment procedure proposed by Priestley, Seible, and Chai (1992) incorporates the results of the nonlinear analyses into the vulnerability assessments for the various failure modes (see Chapters 5 through 10).

The researchers estimated the lateral, force-displacement response of typical, two-dimensional frames in the transverse and longitudinal directions. The analysis procedure and the structural models are described in Section 4.2. Because the soil properties vary greatly and because the lap splices are vulnerable to flexural failure, the researchers considered both fixed-base and pinned-base conditions. The nonlinear model represented material nonlinearities only; the model neglected nonlinear effects caused by large displacements. The nonlinear model also neglected the possibility of anchorage, shear, or joint failure.

In the transverse direction, two interior frames and two exterior frames provide the WSDOT unit's lateral-load resistance. The computed transverse, force-displacement responses for each frame and for the whole unit are reported in Section 4.3. In the longitudinal direction, the WSDOT unit has two identical frames, whose responses are considered in Section 4.4. The results of all these analyses are discussed in Section 4.5.

4.2 DESCRIPTION OF ANALYSIS

Analytical Models

The structure was idealized as a set of orthogonal planar frames whose columns and beams consist of a series of prismatic segments. Typical transverse and longitudinal

frame models are shown in Figures 4.1 and 4.2. Except for their weight, the stringers and intermediate beams were not considered in the analyses. Outside the joints, the nonlinear moment-curvature (M-ϕ) relationships for the segments reflected variations in longitudinal reinforcement along the length of the members. Within the joints, the segments were assumed to have a moment of inertia two orders of magnitude larger than the inertia of the other elements. To obtain a good representation of the curvature distribution along the frame members, the segments were short near the member ends, where the curvature gradients were expected to be large. The shortest element was 1-foot long, which corresponds to one third of the plastic-hinge length (Priestley and Park, 1987).

The researchers computed moment-curvature relationships for each segment on the basis of the structural plans (Appendix A) and the material properties listed in Table 4.1. The concrete's stress-strain relationship was modeled with the equations proposed by Park, Priestley, and Gill (1992). Concrete was assumed to have a compressive strength of 4500 psi, which corresponds to 1.5 times the specified concrete compressive strength (Sec. 2.3). A trilinear model represented the longitudinal steel's stress-strain relationship. The assumed reinforcement yield stress of 44 ksi corresponds to 1.1 times the nominal yield stress. The actual steel strength is likely to exceed the assumed steel strength of 55 ksi.

To reflect the slab's contribution to flexural resistance, a portion of the slab and the reinforcement contained in its width were assumed to be effective both in tension and in compression. The effective width was selected by following the provisions of the American Concrete Institute's Building Code Requirements for Reinforced Concrete (ACI 318-89, 1989). As recommended by Priestley et al. (1992), the ultimate curvature for each section was defined as the curvature at which either (1) the maximum concrete compressive strain was equal to 0.005, or (2) the maximum steel tensile strain was 0.05. Computed moment-curvature relationships were further simplified to consist of two,

40

Typical Transverse Frame

0.6V

47'

0.4V

Rigid Segments

108 Nodes

102 Prismatic Beam Elements

22'

34.75'

V = Base Shear
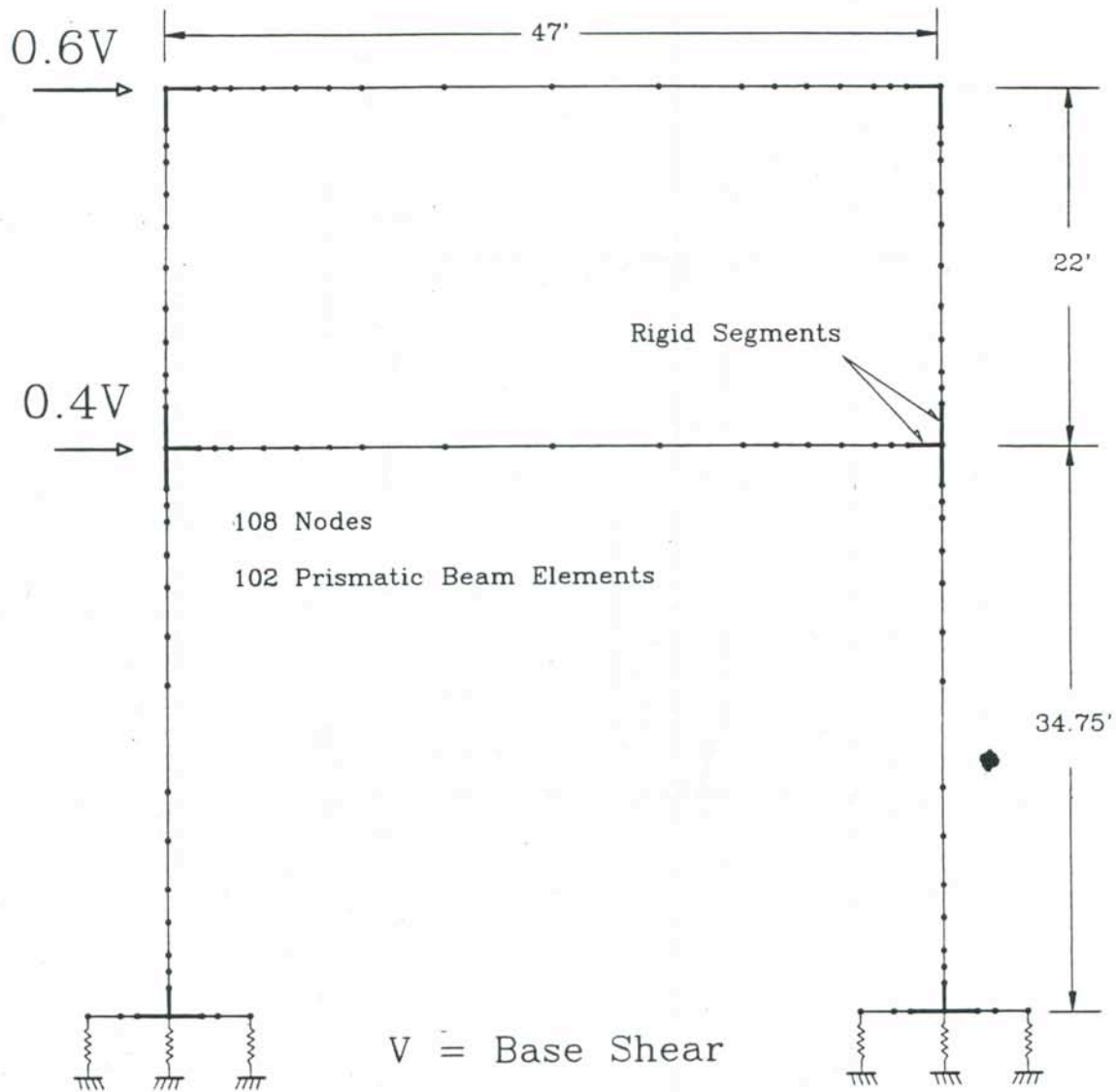
Figure 4.1. Nonlinear Model for Transverse Frames

41

Typical Longitudinal Frame
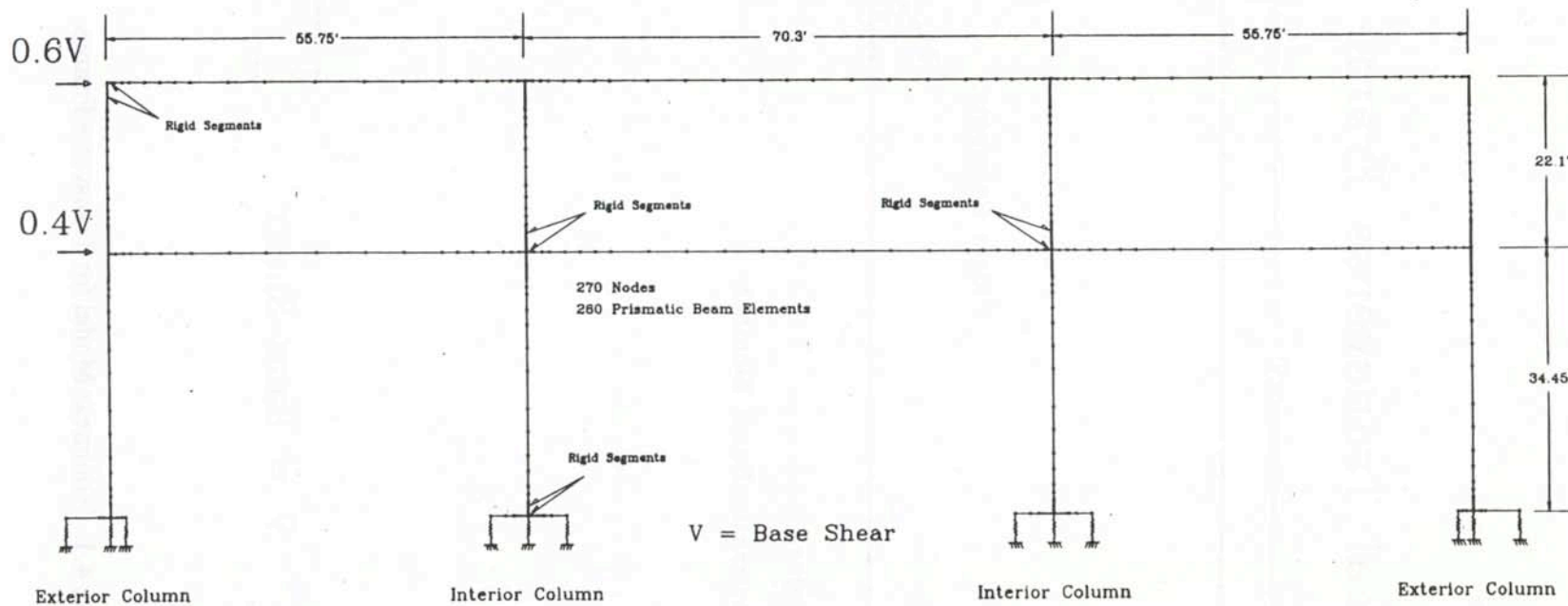
Figure 4.2. Nonlinear Model for Longitudinal Frames

Table 4.1. Assumed Material Properties

Parameter	Units	Value
Concrete Compressive Strength, f 'c	psi	4500
Strain at 0.5f 'c on Falling Unconfined Concrete's Curve		0.004
Yield Stress of Steel	ksi	44
Ultimate Stress of Steel	ksi	55
Strain at Yielding of Steel		0.0015
Strain at the Onset of Strain Hardening		0.015
Strain at Ultimate Stress		0.05
Strain-Hardening Stiffness	ksi	314

three, or four straight lines. As an example, Figure 4.3 shows typical computed and idealized moment-curvature relationships.

Gravity Loads

The researchers considered the effect of gravity loads (dead loads) on the lateral force-displacement relationships. Dead loads were caused by the weight of the structural elements of the viaduct, including the following: slabs, stringers, intermediate beams, end beams, girders, curbs, and columns. In computing the magnitude of these loads, the unit weight of the reinforced concrete was assumed to be 150 pcf. Furthermore, the researchers assumed that the gravity loads were distributed to the columns and beams on the basis of each member's tributary area. Live loads were not considered.

To model the effect of gravity loads in the two-dimensional models, concentrated and distributed loads were applied to the transverse and longitudinal frames. For the transverse frames, concentrated loads (P_1 and P_2) represented column weights and loads from the longitudinal girders (Fig. 4.4 and Table 4.2). Distributed forces on the transverse end beams modeled the weight of slab and stringers (W_1), as well as the

43
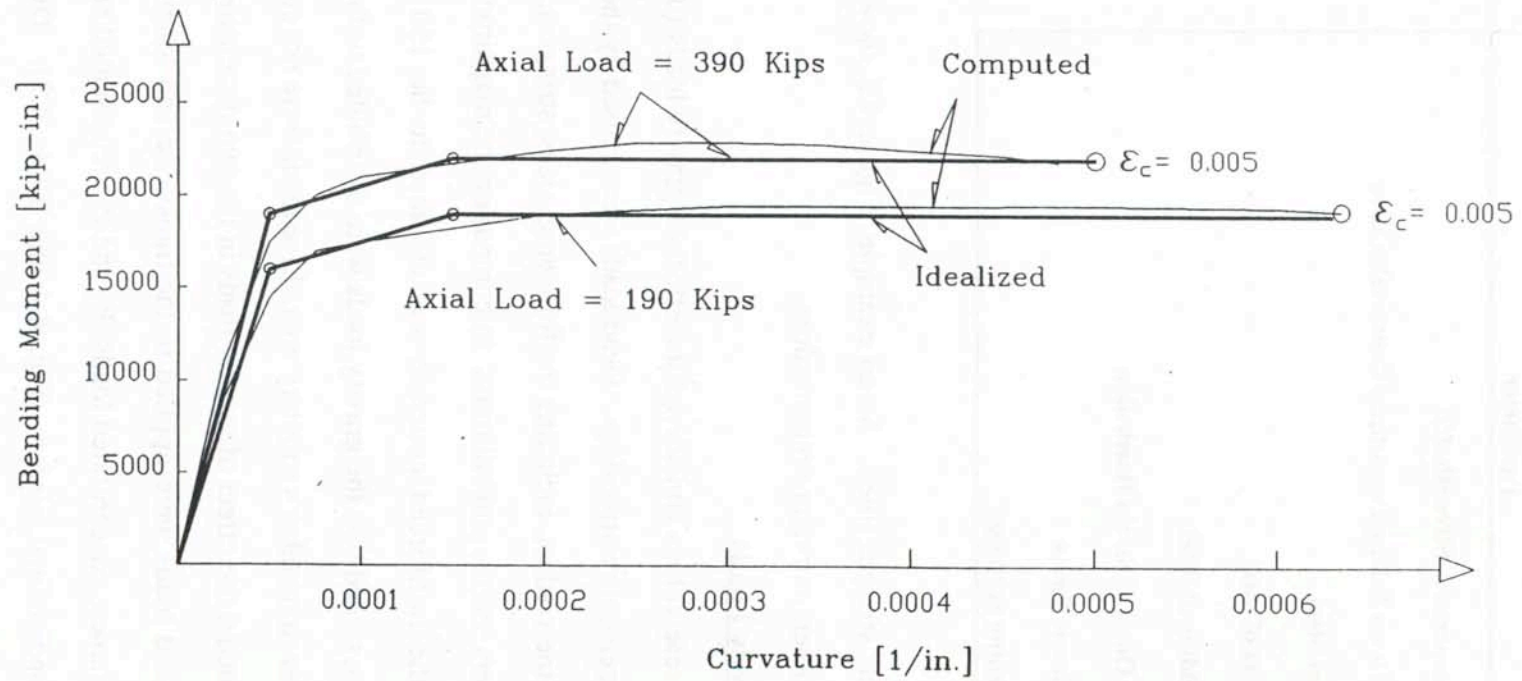
Figure 4.3. Moment-Curvature Relationships for an Interior Column Bent About its Weak Axis

Plan View

56'-10"   70'-4"   56'-10"

End Beams   Tributary Area for Interior Columns

47'

63.6'

Stringers   Intermediate Beams   Slab Tributary Area for the End Beam   Tributary Area for Exterior Column

Transverse Frame Elevation
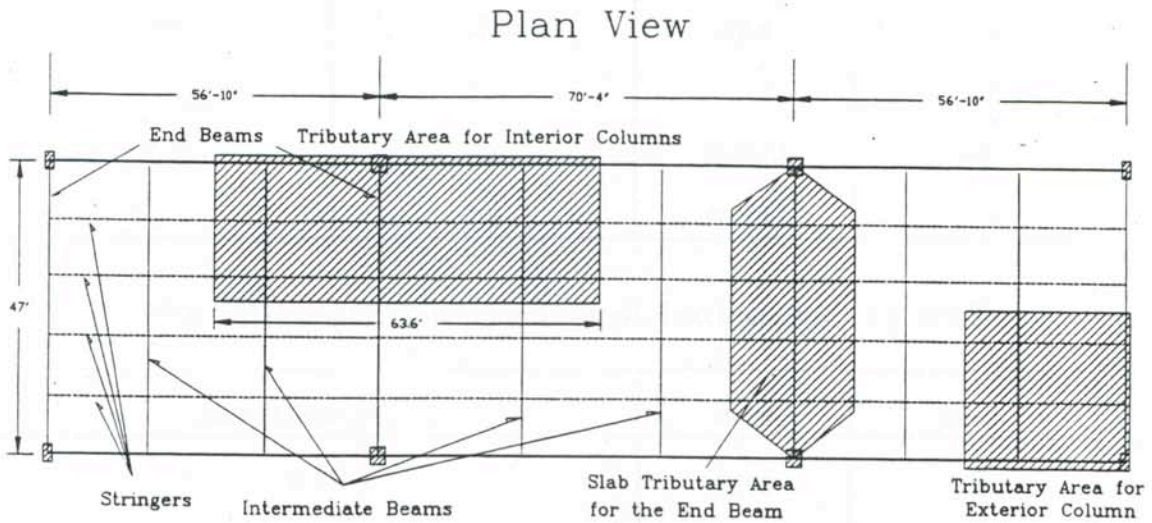
NOTE:

Loads P_1 and P_2 were obtained after substracting the contribution of W_1 and W_2 from the total axial loads of columns.

P_2 W_1 P_2 W_1

W_2 W_2

P_1 W_1 P_1

W_2
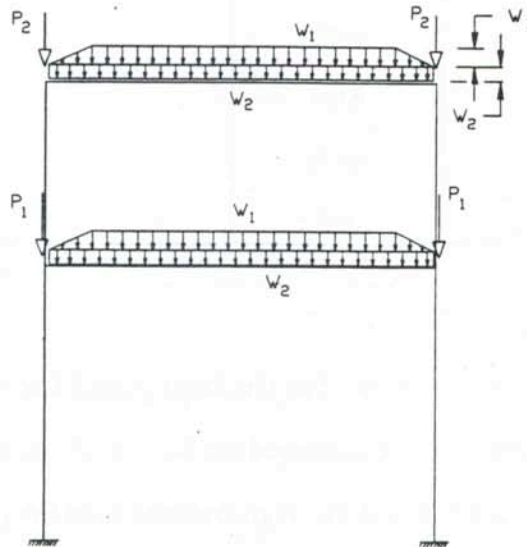
Figure 4.4. Gravity Loads on Transverse Frames

45

Table 4.2. Vertical Loads for Transverse Frames (Fig. 4.4)

Load	Units	Interior Frame	Exterior Frame
P_1	kips	332	159
P_2	kips	318	151
W_1	kips/ft	1.7	0.76
W_2	kips/ft	1.5	1.14

Table 4.3. Vertical Loads for the Longitudinal Frames (Fig. 4.5)

Load	Units	Longitudinal Frames
P_1	kips	64.4
P_2	kips	76.1
P_3	kips	84.2
P_4	kips	144.0
P_5	kips	76.2
P_6	kips	129.4
W_1	kips/ft	1.81

weight of the end beam (W_2). For the longitudinal frames, concentrated forces modeled the loads transmitted by the intermediate beams (P_1 and P_2) and end beams (P_3, P_4, P_5, and P_6) (Fig. 4.5 and Table 4.3). A distributed load (W_1) modeled the girder weight and its tributary slab load.

Tables 4.4 and 4.5 list the axial forces at the base of the first-story columns caused by the gravity loads. Overlapping material was subtracted in computing these loads. As expected, the computed axial load in the interior columns was approximately twice that computed for the exterior columns. For all of the columns, the axial stresses

Plan View
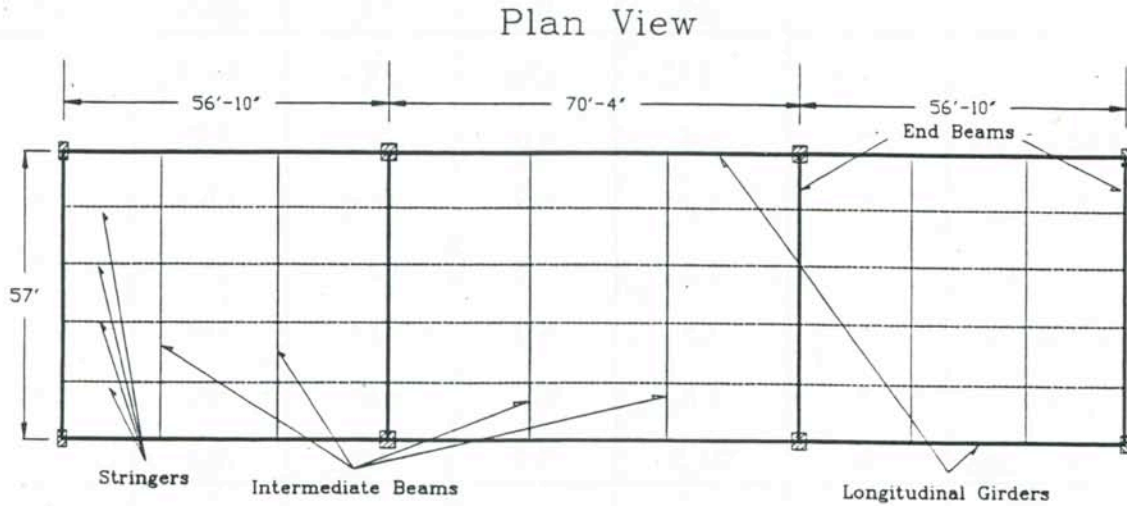
Longitudinal Frame Elevation
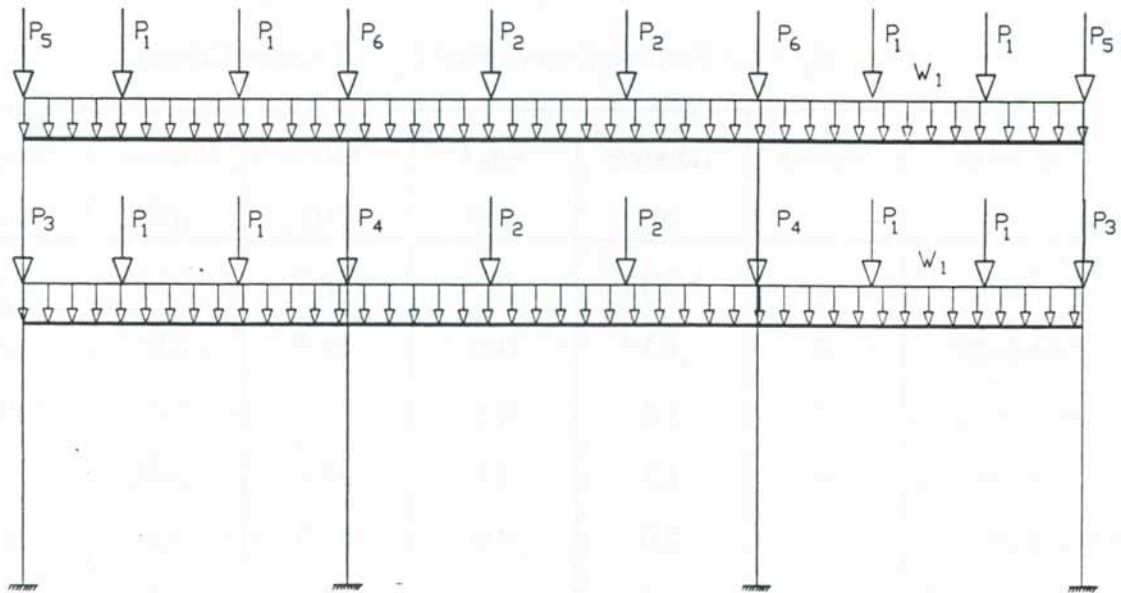
Figure 4.5. Gravity Loads on Longitudinal Frames

Table 4.4. Axial Force at Base of First-Story Interior Column

Member	Number	Thickness [ft]	Side 1 [ft]	Side 2 [ft]	Volume [ft^3]	Weight [Kips]
Slab	2	6.5/12	63.6	23.5	1619	243
End Beams	2	1.5	4.0	23.5	272	41
Ext. Girders	2	1.5	6.8	63.6	1261	189
Stringer	4	1.3	1.8	63.6	582	87
Columns	1	3.5	4.0	51.0	714	107
Curbs	2	1.8	9/12	63.6	167	25
Floor Beams	4	23.5	1.5	4.5	618	93
Total					5233	785

Table 4.5. Axial Force at Base of First-Story Exterior Column

Member	Number	Thickness [ft]	Side 1 [ft]	Side 2 [ft]	Volume [ft^3]	Weight [Kips]
Slab	2	6.5/12	28.4	23.5	724	109
End Beams	2	1.5	4.0	23.5	272	41
Ext. Girders	2	1.5	6.8	28.4	563	85
Stringer	4	1.3	1.8	28.4	260	39
Columns	1	2.0	4.0	51.0	408	61
Curbs	2	1.8	9/12	28.4	75	11
Floor Beams	4	23.5	1.5	4.5	309	46
Total					2611	392

corresponded to approximately 12 percent of the specified compressive strength. The corresponding bending moments are presented in Sections 4.3 and 4.4, along with the results of the lateral-load analyses.

Analysis Procedure

The researchers developed a computer program to calculate the frames' nonlinear lateral force-deflection relationships. The secant-stiffness algorithm considered both flexural and axial member deformations, but it neglected shear deformations. To reflect the material's nonlinear properties, the secant flexural stiffness was updated at each load step on the basis of the segment's moment-curvature relationship and average curvature. The average curvatures were calculated on the basis of the rotations and segment lengths. The segment's axial stiffness remained constant throughout the analyses.

The analysis procedure can be summarized as follows. First, vertical loads were applied to the structure to simulate the influence of gravity loads. Next, the horizontal loads were gradually increased in a series of load steps. The lateral loads were applied in a pattern resembling the first mode of vibration obtained from a linear, dynamic analysis (Sec. 3.3). For both the fixed- and pinned-base cases, the top-level force was 60 percent of the total base shear (the first-level force was 40 percent). At each lateral-load step, the initial element stiffness was obtained from the M-ϕ curves and the average curvature from the previous load step (or iteration). The program then assembled the structure's stiffness matrix and computed the displacements. If the displacements differed by less than 2.5 percent from the previous iteration, the algorithm proceeded to the next load step. However, if displacements differed by more than 2.5 percent, the element stiffnesses were updated, and another iteration was carried out.

The lateral load was increased until one member reached its ultimate curvature. Because average curvatures for each segment only approximated the curvature distribution along the members, this procedure yielded slightly larger base-shear capacities than would have been obtained with shorter segments.

49

4.3 TRANSVERSE-DIRECTION RESPONSE

Two interior frames and two exterior frames contribute to the unit's resistance to transverse loads. This section presents the results of push-over analyses for both types of frames and for the whole unit. For both fixed-base and pinned-base conditions, this section reports lateral force-displacement relationships and bending-moment distributions.

Fixed-Base Condition

Lateral force-displacement relationships for the interior and exterior frames are depicted in Figure 4.6. The total capacity in the transverse direction was calculated to be 1120 kips, which corresponds to 24 percent of the unit's weight. As expected, the computed lateral capacity of the interior frame exceeded that of the exterior frame. Each exterior frame contributed 18 percent of the forces (200 kips), and each interior frame resisted 32 percent of the forces (360 kips). The analysis stopped when the elements at the base of the columns reached their ultimate curvature, ϕ_u. At this point, the top-deck displacement was equal to 0.4 feet, corresponding to a drift ratio of 0.7 percent.

a) Interior frame

Figure 4.7 shows the flexural demands and capacities for the bottom-deck beam of an interior frame. Flexural demands were computed with the procedure described in Section 4.2, in which splice deterioration, anchorage pullout, shear failure, and joint failure were neglected. Demands are depicted for dead load (DL) alone and for several combinations of dead load plus lateral load near the frame's capacity. In this figure, the numbers accompanying the letters "DL" denote the frame base shear in kips. The capacities, denoted by dashed lines, were estimated by assuming a development length of 30-bar diameters. Figure 4.7 shows that the most likely location of yielding is the positive moment region near the beam end. At this location, the capacity was limited by the bottom-layer bars' short anchorage length. Figure 4.8 shows the corresponding

50
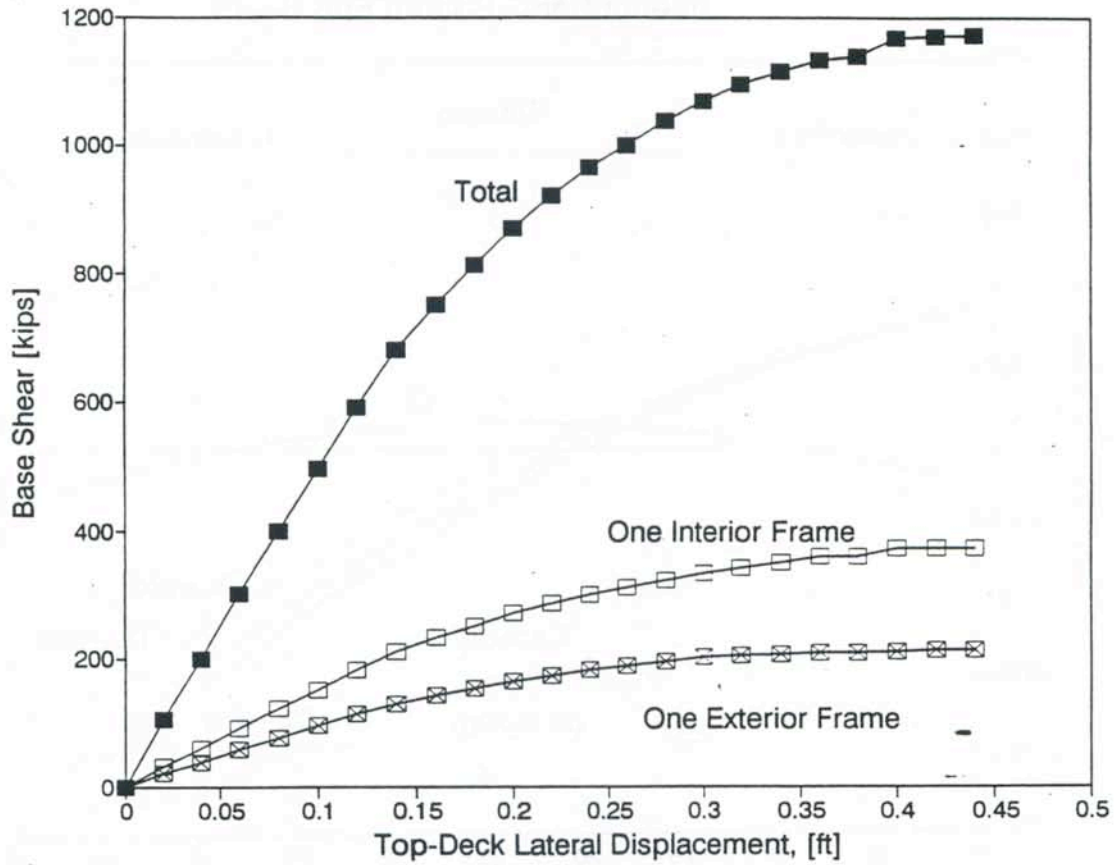
Figure 4.6. Transverse Force-Displacement Relationships (Fixed Bases)

51

Bending Moment Diagrams
Interior Bent - Bottom End Beam
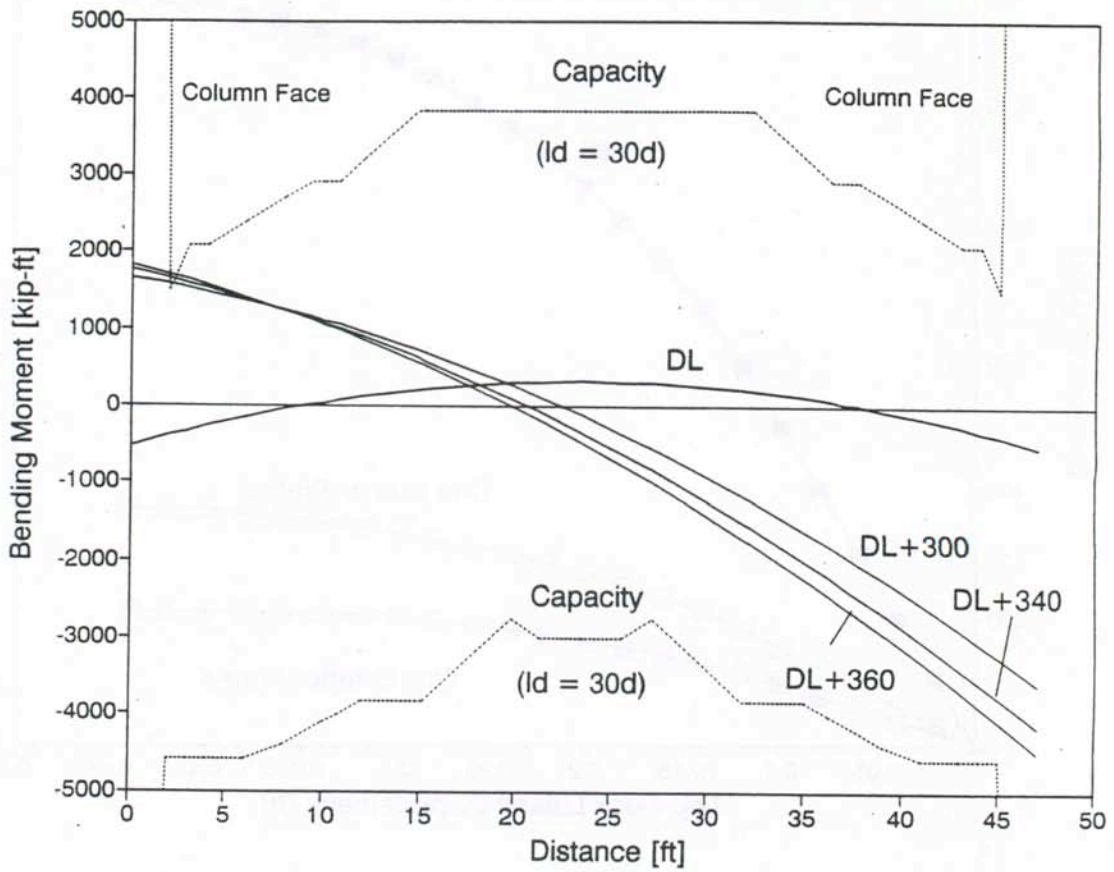
Figure 4.7. Moments in Interior-Frame, Lower-Deck Beam (Fixed Bases)

52

Bending Moment Diagrams
Interior Bent - Top End Beam
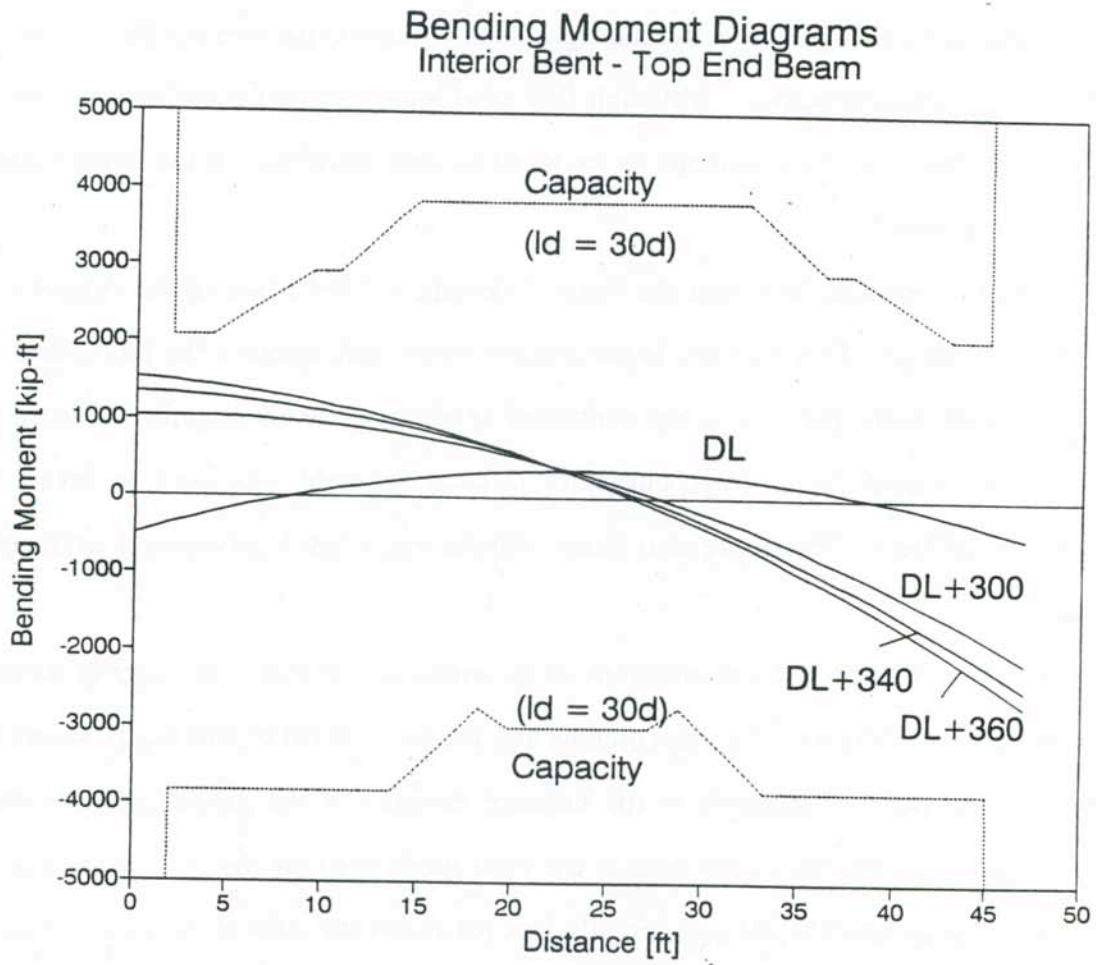
Figure 4.8. Moments in Interior-Frame, Upper-Deck Beam (Fixed Bases)

bending diagrams for the top-deck beam. Despite this beam's short anchorage length, it is unlikely to yield.

Bending-moment diagrams and capacities of interior-bent columns are shown in Figure 4.9 for three values of base shear, V. For this frame, the column flexural capacities were computed with axial loads consistent with the combined action of gravity plus lateral forces. Consequently, the right-hand column capacities are larger than the left-hand column capacities. Although this axial load variation modified the flexural capacity of the first-story columns by up to 10 percent, its effect on the frame's lateral capacity was small.

Figure 4.9 indicates that the flexural demands at the bases of the columns are likely to be large. This location is particularly vulnerable because the lap splices are short. As expected (Sec. 4.2), the computed bending moments slightly exceeded the capacities because the average curvature in each segment was used to define the segment's stiffness. The figure also shows that the upper-level columns are unlikely to yield.

Figure 4.10 provides an overview of the extent of yielding in the interior frame at a base shear of 360 kips. For the columns and beams, Part (a) of this figure shows the ratios of the flexural strength to the moment demand at the maximum base shear (M_u/M_{360}). Part (b) shows the ratio of the yield moment to the moment demand at the maximum base shear (M_y/M_{360}). Finally Part (c) shows the ratio of the yield curvature to the average curvature at the maximum base shear $(\phi_y/(\phi_{avg})_{360})$. None of these ratios reflect the influence of anchorage slip, splice deterioration, and joint deterioration. Yielding at the base of the first-story column bases occurred first, and ductility demands were large at this location. Yielding in the beams was limited to one location; however, yielding was imminent at two other locations. The maximum base shear was defined as the point at which the curvature demands at the column bases exceeded their curvature capacities.

Column Bending Moments
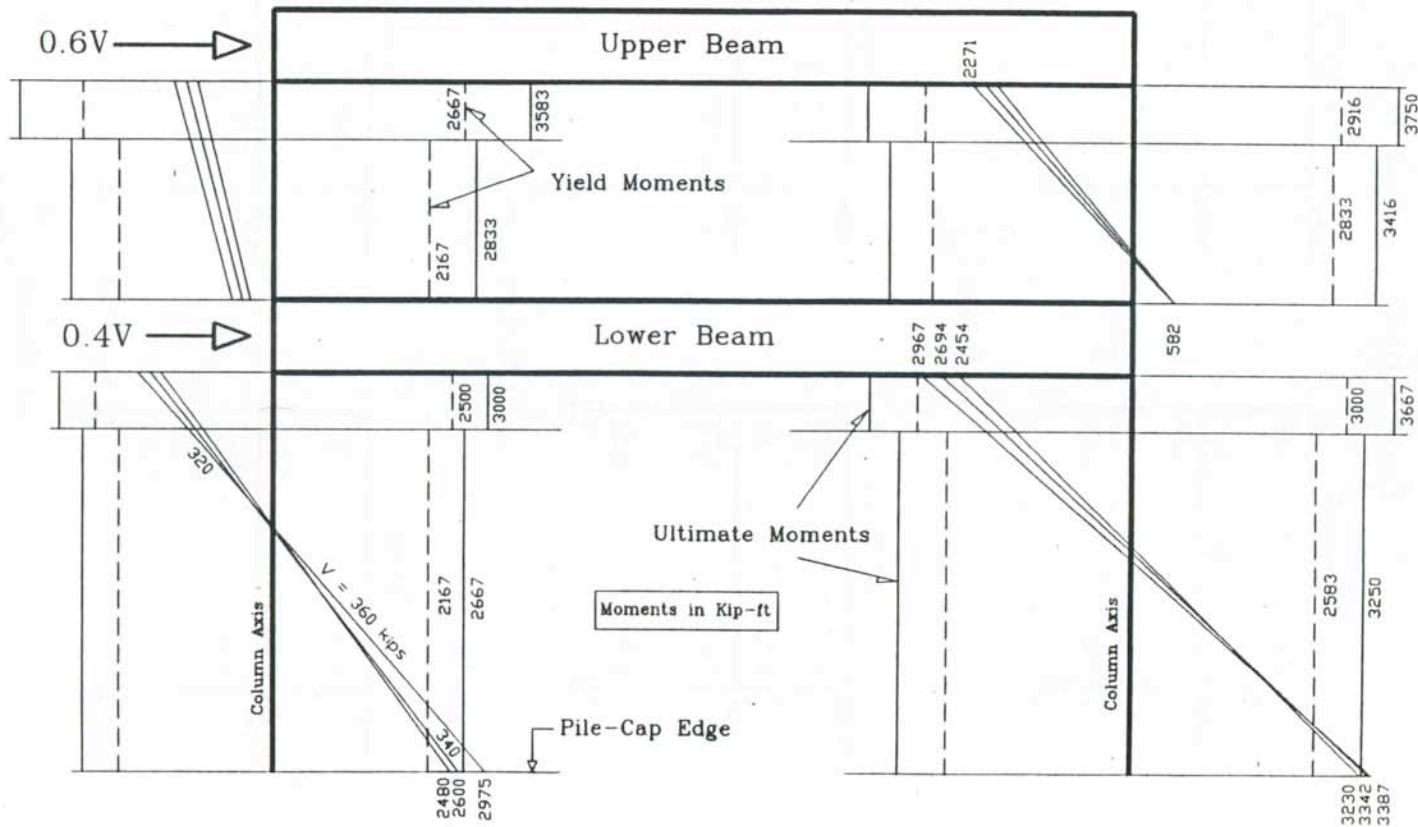
Figure 4.9. Moments in Interior-Frame Columns (Fixed Bases)

Interior Bent – Fixed Base
Base Shear = 360 kips

Columns

2.55		1.65
4.85		5.87
1.57		1.24
0.98		0.96

(+) Beams (−)

1.41		1.61
1.18		1.12

a) Ratios $\dfrac{M_u}{M_{360}}$

Columns

1.90		1.28
3.71		4.87
1.31		1.01
0.80		0.76

(+) Beams (−)

1.02		1.47
0.84		1.02

b) Ratios $\dfrac{M_y}{M_{360}}$

Columns

1.94		1.33
3.53		5.66
1.36		1.05
0.26		0.18
$\mu_\varphi = 3.9$		$\mu_\varphi = 5.6$

(+) Beams (−)

1.02		1.50
0.10		1.05
$\mu_\varphi = 10.0$		
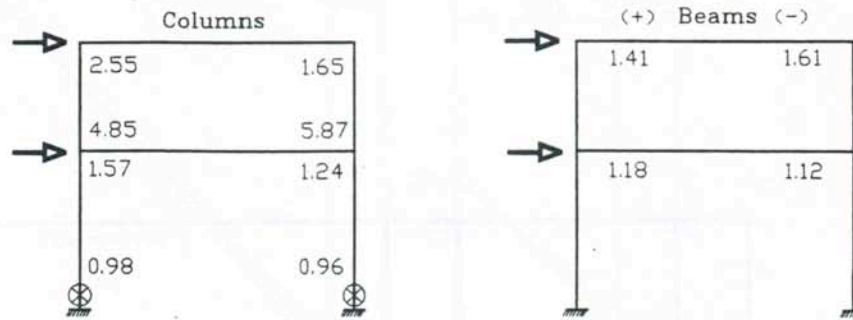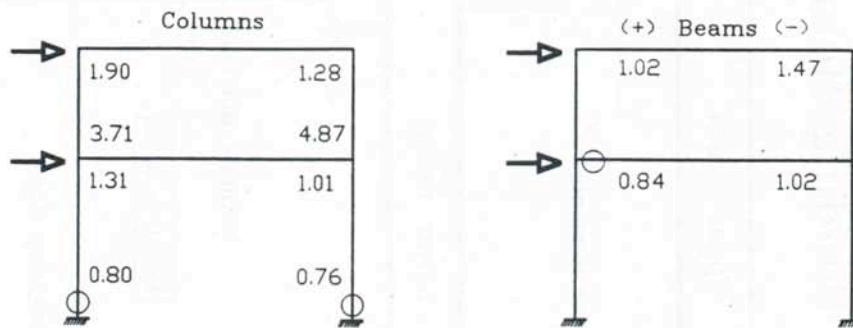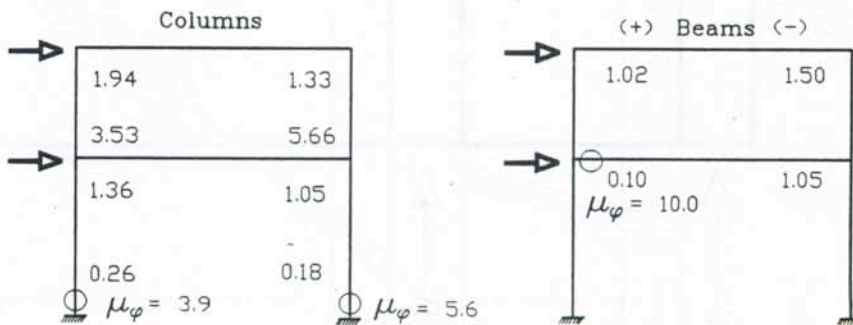
c) Ratios $\dfrac{\varphi_y}{(\varphi_{avg})_{360}}$

μ_φ = Computed Curvature Ductility

Figure 4.10. Flexural Capacity/Demand Ratios for Interior Frames (Fixed Bases)

b) Exterior frame

Results for the exterior frames are described below for the fixed-support condition. The behavior of the exterior bottom-deck beam was similar to that of the corresponding interior beam. Positive moment near the joint was critical because the inadequate development length may limit the beam's flexural capacity.

Bending-moment diagrams and capacities for the exterior frame's columns are depicted in Figure 4.11. For the exterior frames, column capacities were computed considering axial loads caused by gravity loads only. The variation in column capacities with seismic axial load would be expected to have little influence of the frame's overall force-displacement relationship. However, this variation would be expected to affect the distribution of yielding between the columns and beams.

Flexural capacity-to-demand ratios for the columns and beams are shown in Figure 4.12. Although the capacity of the exterior bents is significantly lower than that of the interior bents (200 kips versus 360 kips), the computed C/D ratios are similar (Figs. 4.10 and 4.12). Again, the capacity of the frame was defined by the point at which the curvature demand exceeded the capacity at the column bases.

Pinned-Base Condition

Transverse force-displacement relationships for the pinned-base condition are shown in Figure 4.13. The lateral-force capacities of the interior (220 kips) and exterior bents (118 kips) were approximately 60 percent of the computed capacities for the fixed-base condition. For both frames, the displacement at the maximum base shear corresponded to a drift ratio of 1.2 percent. This ratio was approximately 75 percent larger than the ratio computed for the fixed-base condition.

Bending-moment demands and capacities for the columns are shown in Figures 4.14 and 4.15 for the interior and exterior frames, respectively. In both cases the critical zones are located at the tops of the first-level columns. The second-story moment demands were much smaller than their capacities.

57

Column Bending Moments
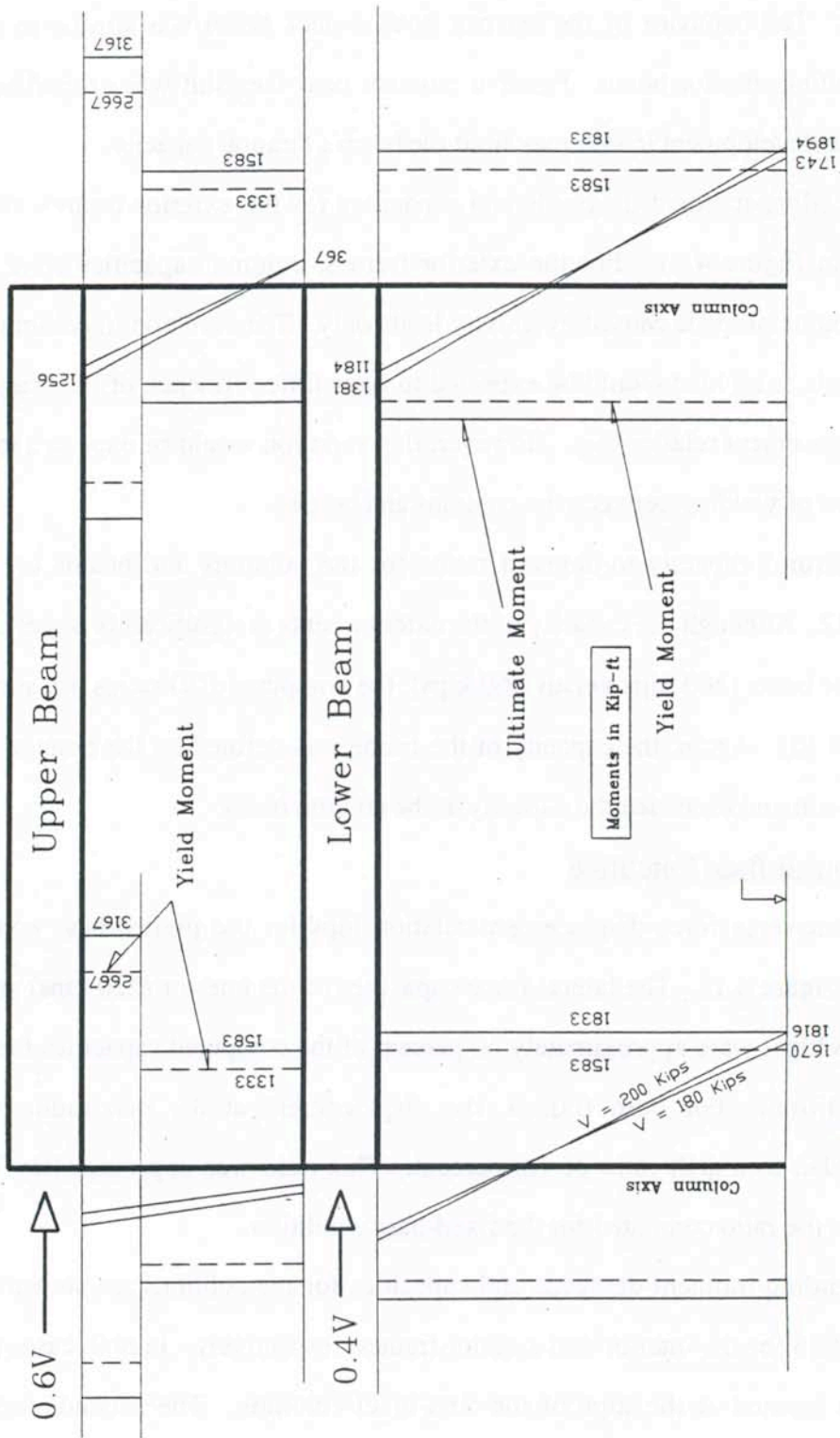
Figure 4.11. Moments in Exterior-Frame Columns (Fixed-Bases)

58

Exterior Bent — Fixed Base
Base Shear = 200 Kips

Columns				(+) Beams (−)		
4.10	2.52			1.13		1.65
4.45	4.31					
1.82	1.33			1.03		1.19
1.01	0.97					

a) Ratios $\dfrac{M_u}{M_{200}}$

Columns				(+) Beams (−)		
3.45	2.12			1.02		1.39
3.70	3.63					
1.57	1.15			0.94		0.98
0.87	0.84					

b) Ratios $\dfrac{M_y}{M_{200}}$

Columns				(+) Beams (−)		
3.57	2.21			1.03		1.45
3.53	4.29					
1.67	1.20			0.07		1.00
				$\mu_\varphi = 14.6$		
0.43	0.33					
$\mu_\varphi = 2.3$	$\mu_\varphi = 3.0$					
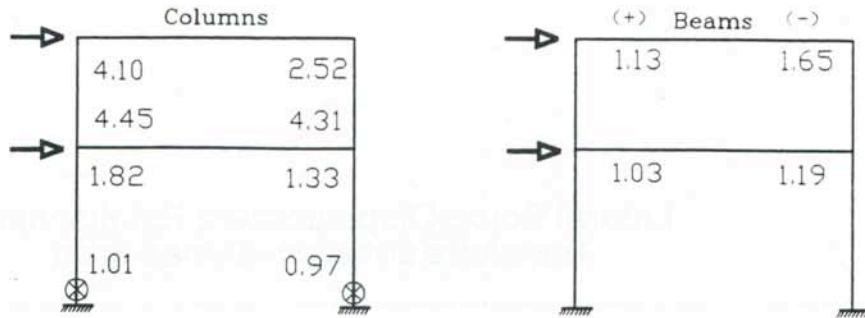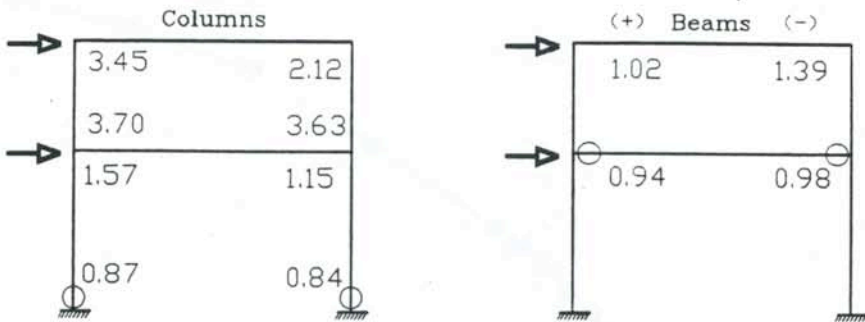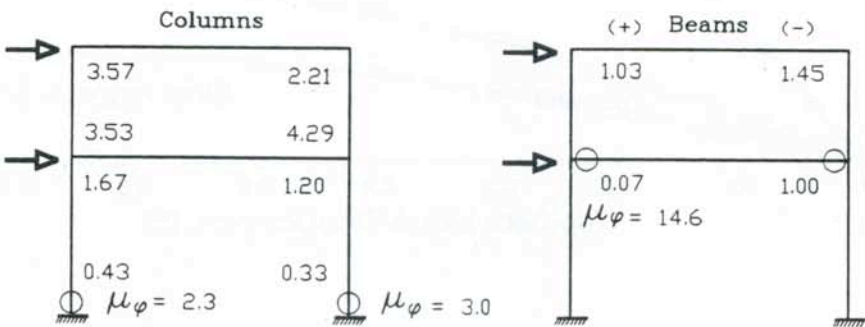
c) Ratios $\dfrac{\varphi_y}{(\varphi_{avg})_{200}}$

μ_φ = Computed Curvature Ductility

Figure 4.12. Flexural Capacity/Demand Ratios for Exterior Frames (Fixed Bases)

Lateral Force-Displacement Relationship
Transverse Direction - Pinned Base
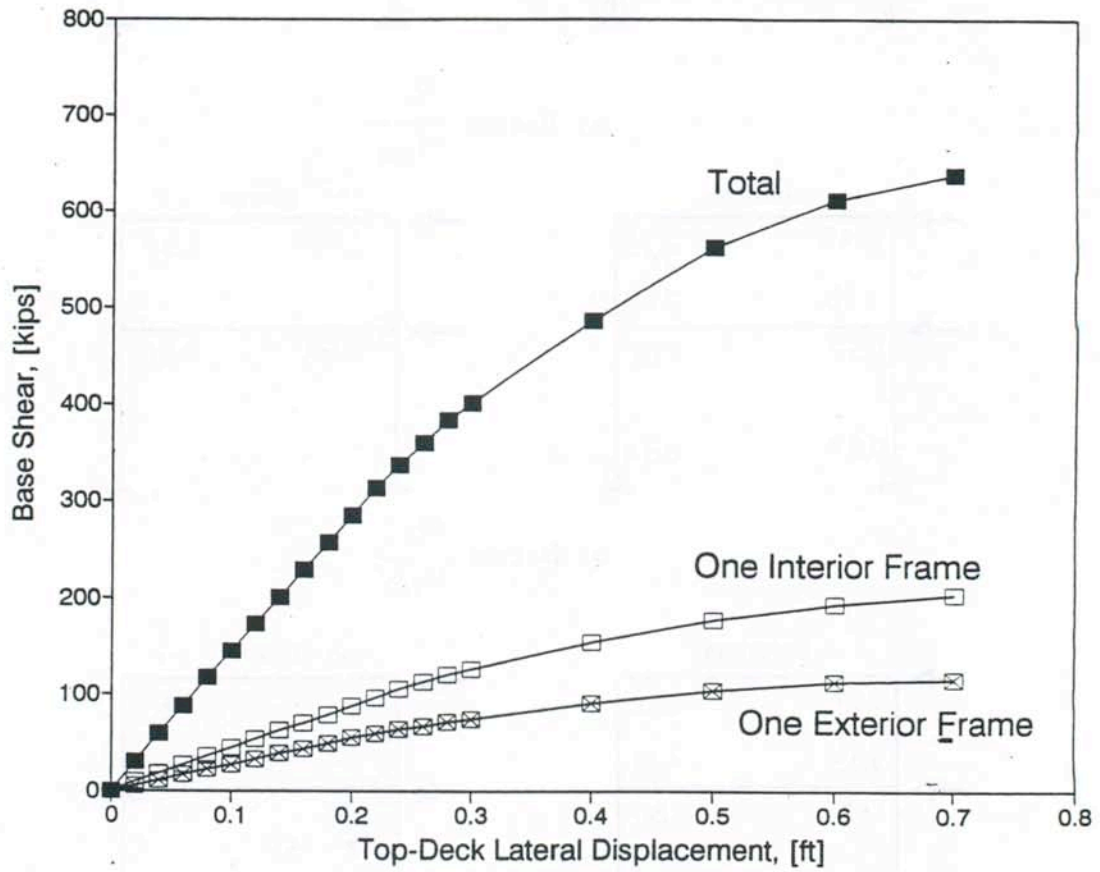
Figure 4.13. Transverse Force-Displacement Relationships (Pinned Bases)

60

Column Bending Moments
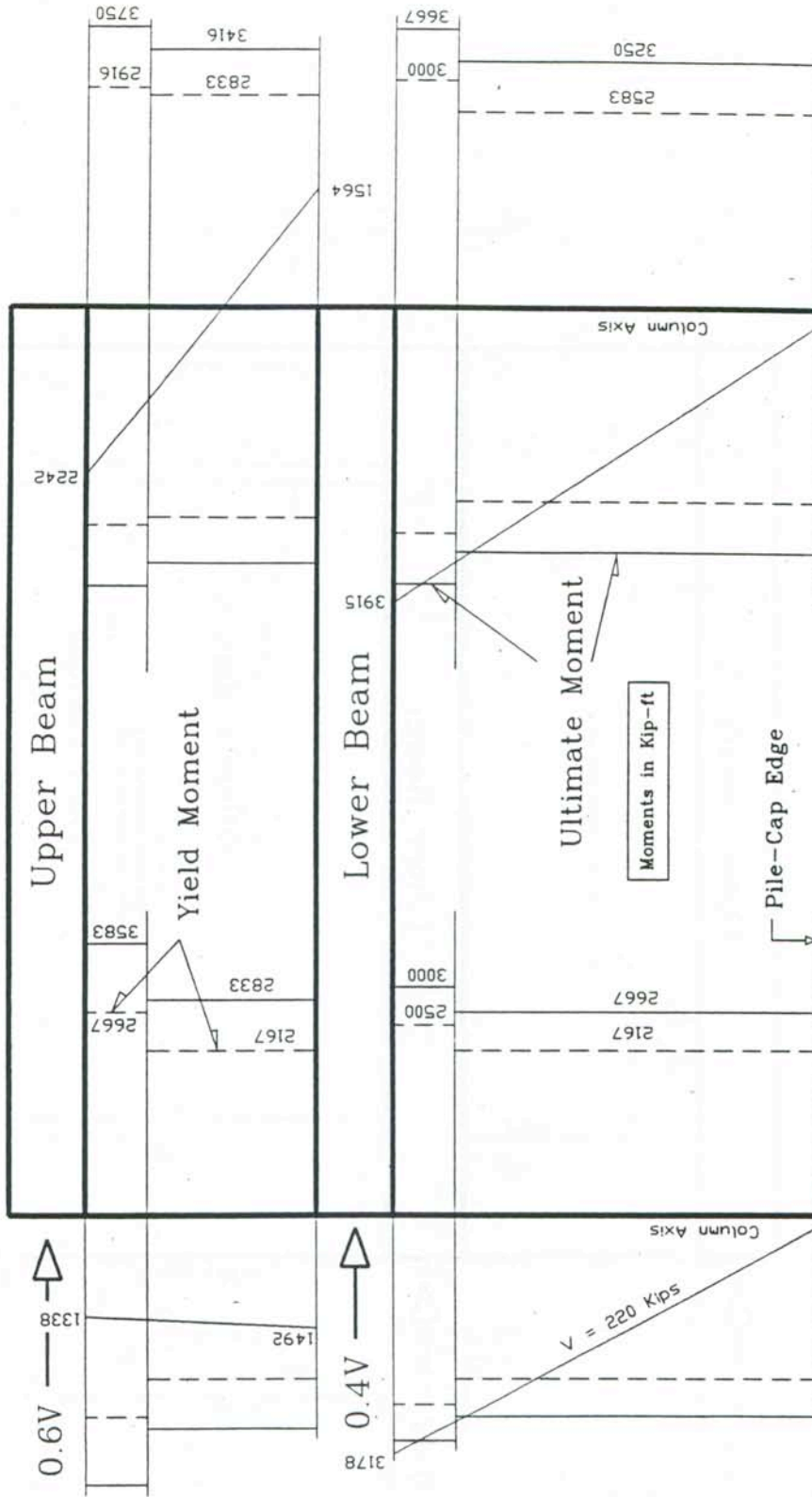
Figure 4.14. Moments in Interior-Frame Columns (Pinned Bases)

61

Column Bending Moments
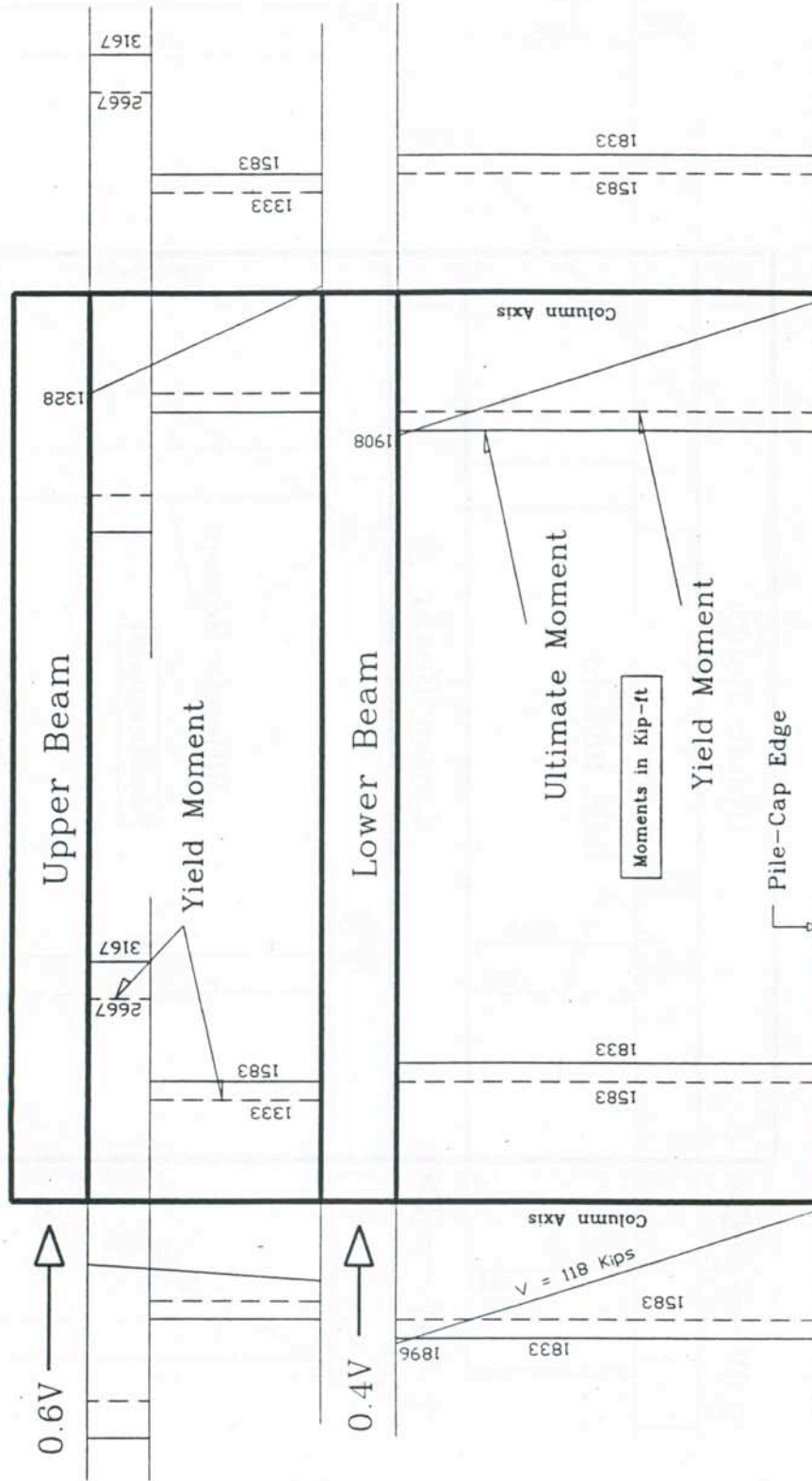
Figure 4.15. Moments in Exterior-Frame Columns (Pinned Bases)

62

Flexural capacity-to-demand ratios for the beams and columns for the interior and exterior frames are shown in Figures 4.16 and 4.17. For this support condition, the displacement capacity of both frames was limited by the curvature capacity at the tops of the first-story columns. In a manner similar to that of the fixed-support case, hinges formed in the first-deck beams. However, it is difficult to predict the locations of yielding with certainty because the first-story columns and beams had similar flexural capacity-to-demand ratios. This uncertainty is further increased by the uncertainty in the effective slab width.

4.4 LONGITUDINAL-DIRECTION RESPONSE

In the longitudinal direction, two identical frames (Fig. 4.2) provide the unit's lateral-force resistance.

Fixed-Base Condition

Figure 4.18 shows the relationship between the top-deck lateral displacement and the base shear. The unit's capacity in the longitudinal direction (1080 kips) was negligibly smaller than its capacity in the transverse direction (1120 kips). The maximum top-deck displacement was 0.33 ft, corresponding to a drift ratio of 0.6 percent. This is slightly smaller than the value computed for the transverse direction. The maximum base shear was defined by a first-story mechanism, and again, the maximum displacement was limited by the curvature limit for the first-story columns.

For convenience, bending moments and shears for the longitudinal girders are presented separately for the exterior and interior spans. Figure 4.19 shows the bending-moment diagrams for the bottom-deck girder of the exterior span. The exterior column is located at the left-hand side of the figure. The demands are shown for both positive and negative lateral loads. As in Section 4.3, demands were computed without consideration of splices and anchorages, whereas capacities were computed assuming a development

Interior Bent – Pinned Base

Base Shear = 220 Kips

	Columns	
2.68		1.67
1.90		6.71
0.94		0.94

	(+) Beams (−)	
1.63		1.67
1.14		1.06

a) Ratios $\dfrac{M_u}{M_{220}}$

	Columns	
1.99		1.30
1.45		5.57
0.79		0.77

	(+) Beams (−)	
1.17		1.52
0.81		0.97

b) Ratios $\dfrac{M_y}{M_{220}}$

	Columns	
2.00		1.33
1.46		33.33
0.22		0.14

$\mu_\varphi = 7.0$
$\mu_\varphi = 4.6$

	(+) Beams (−)	
1.18		1.58
		$\mu_\varphi = 6.6$
0.08		0.15
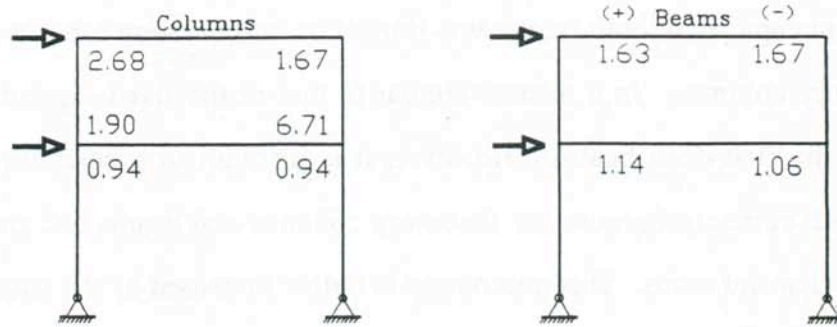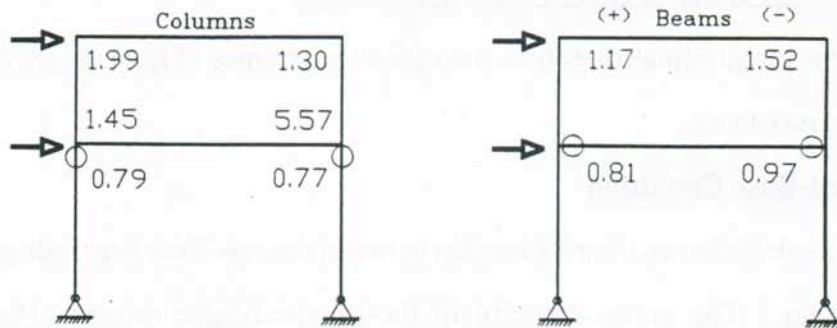
$\mu_\varphi = 12.0$
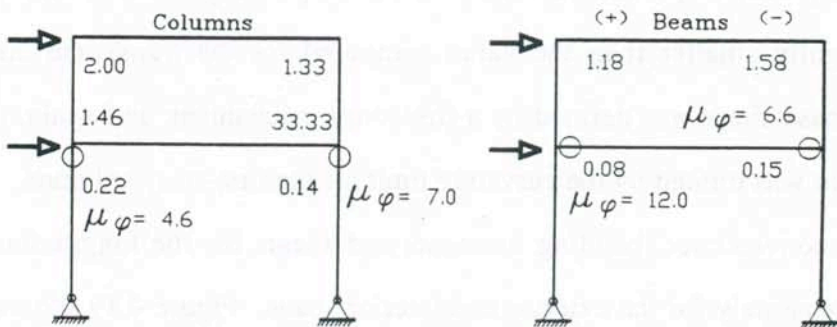
c) Ratios $\dfrac{\varphi_y}{(\varphi_{avg})_{220}}$

μ_φ = Computed Curvature Ductility

Figure 4.16. Flexural Capacity/Demand Ratios for Interior-Frames (Pinned Bases)

Exterior Bent – Pinned Base

Base Shear = 118 Kips
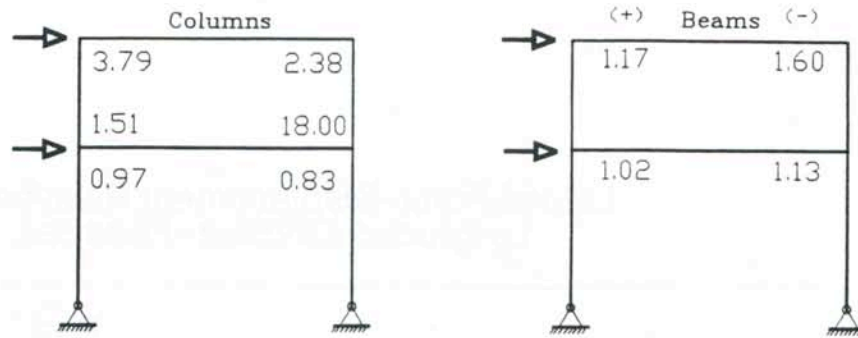
a) Ratios $\dfrac{M_u}{M_{118}}$
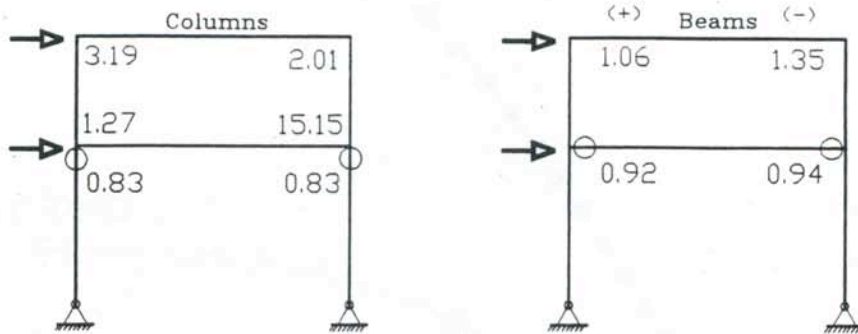
b) Ratios $\dfrac{M_y}{M_{118}}$
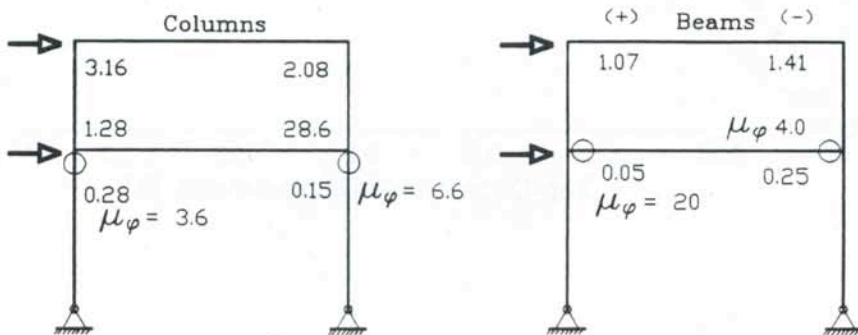
c) Ratios $\dfrac{\varphi_y}{(\varphi_{avg})_{118}}$

μ_φ = Computed Curvature Ductility

Figure 4.17. Flexural Capacity/Demand Ratios for Exterior Frames (Pinned Bases)

65
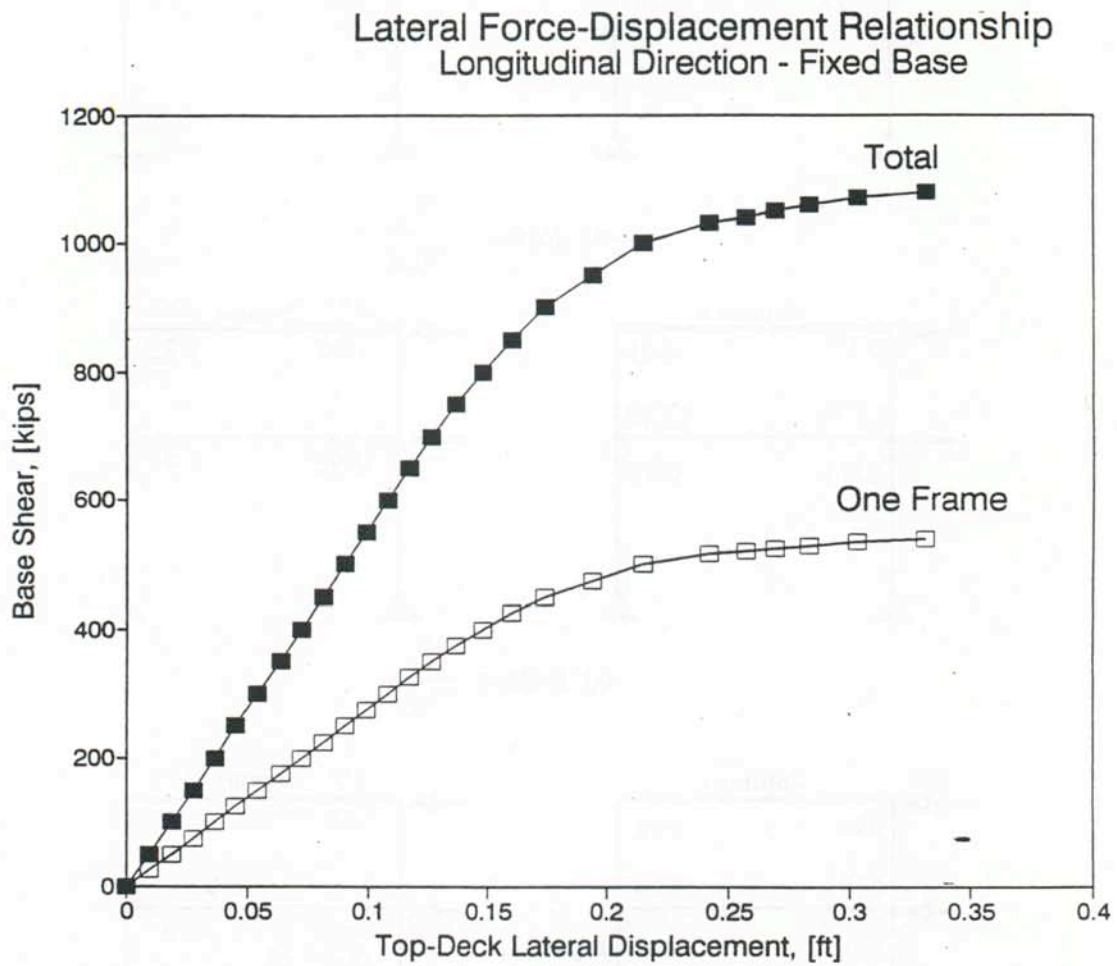
Figure 4.18. Longitudinal Force-Displacement Relationships (Fixed-Bases)

Bending Moment Diagrams
Bottom Girder - Ext. Spans
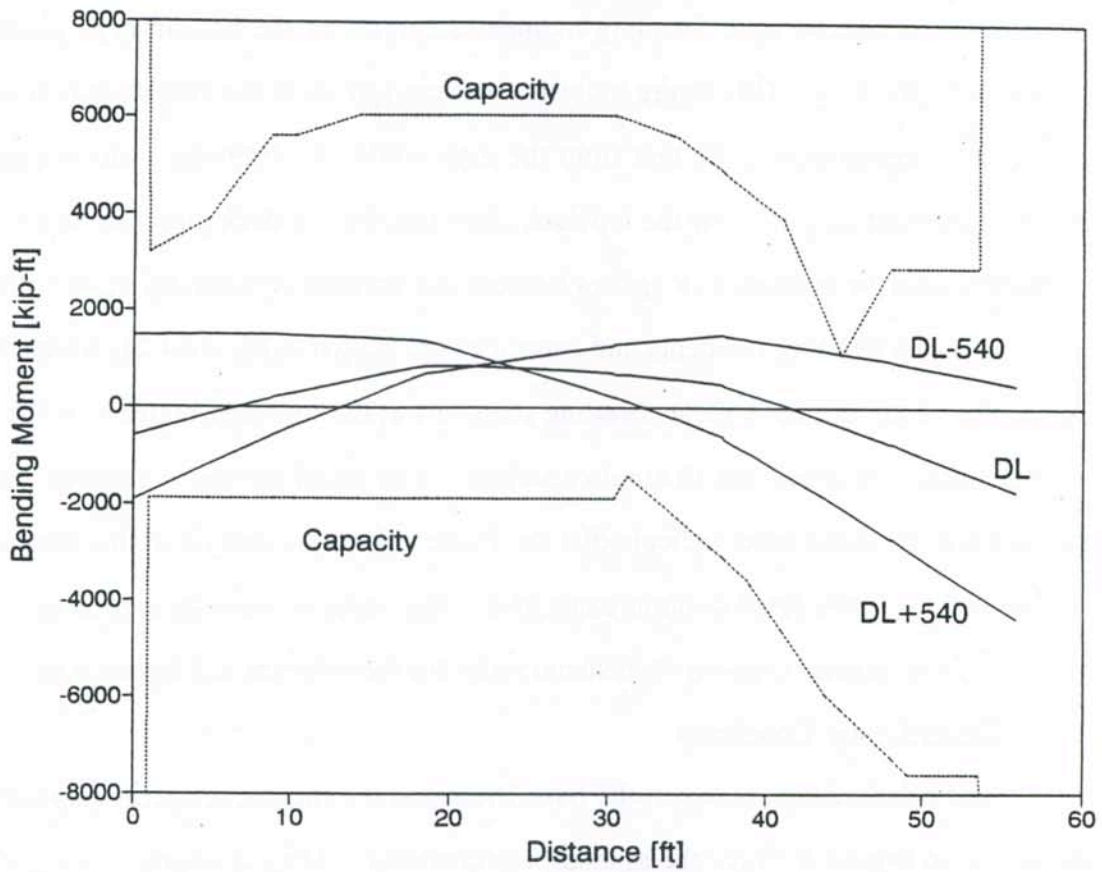
Figure 4.19. Moments in Exterior Span of Bottom Girder (Fixed-Bases)

67

length equal to 30-bar diameters. Figure 4.19 shows that failure of the lap splice located at about 45 feet from the exterior column may limit the frame's lateral-force capacity. The second hinge would be likely to form in the negative moment region near the exterior column. Both of these capacities are sensitive to the assumed development length and to the assumed effective slab width.

For the central span, bending-moment diagrams of the bottom-deck girder are shown in Figure 4.20. This figure indicates that lap splices of the bottom bars (positive moment) at approximately 12 feet from the ends could also limit the frame's capacity. Bending-moment diagrams for the top deck show that the top-deck girder splices are less vulnerable than the bottom-deck splices because the moment demands there are smaller.

Column bending moments and capacities are shown in Figure 4.21, which shows that at the maximum base shear, bending moments at the tops and bottoms of the first-level columns exceeded the flexural capacities. The small values of column bending moments in the upper level indicate that the frame's flexural capacity in this direction is limited by the lower-level column capacities. The same conclusion can be drawn by comparing the flexural capacity-to-demand ratios for the columns and beams (Fig. 4.22).

Pinned-Base Condition

The relationships between the base shear and the top-deck, lateral displacement are shown in Figure 4.23 for the pinned-base condition. The maximum capacity of the frame was again limited by the formation of a mechanism at the first-story level. As expected for this mechanism, the frame's lateral capacity for the pinned-base case (260 kips) was about half of the capacity for the fixed-base case (540 kips). Figures 4.24 and 4.25 show that, at the maximum base shear, the column bending moments slightly exceeded the flexural capacity at the column ends. Again, this phenomenon is an artifact of the solution procedure.

68

Bending Moment Diagrams
Bottom Girder - Central Span
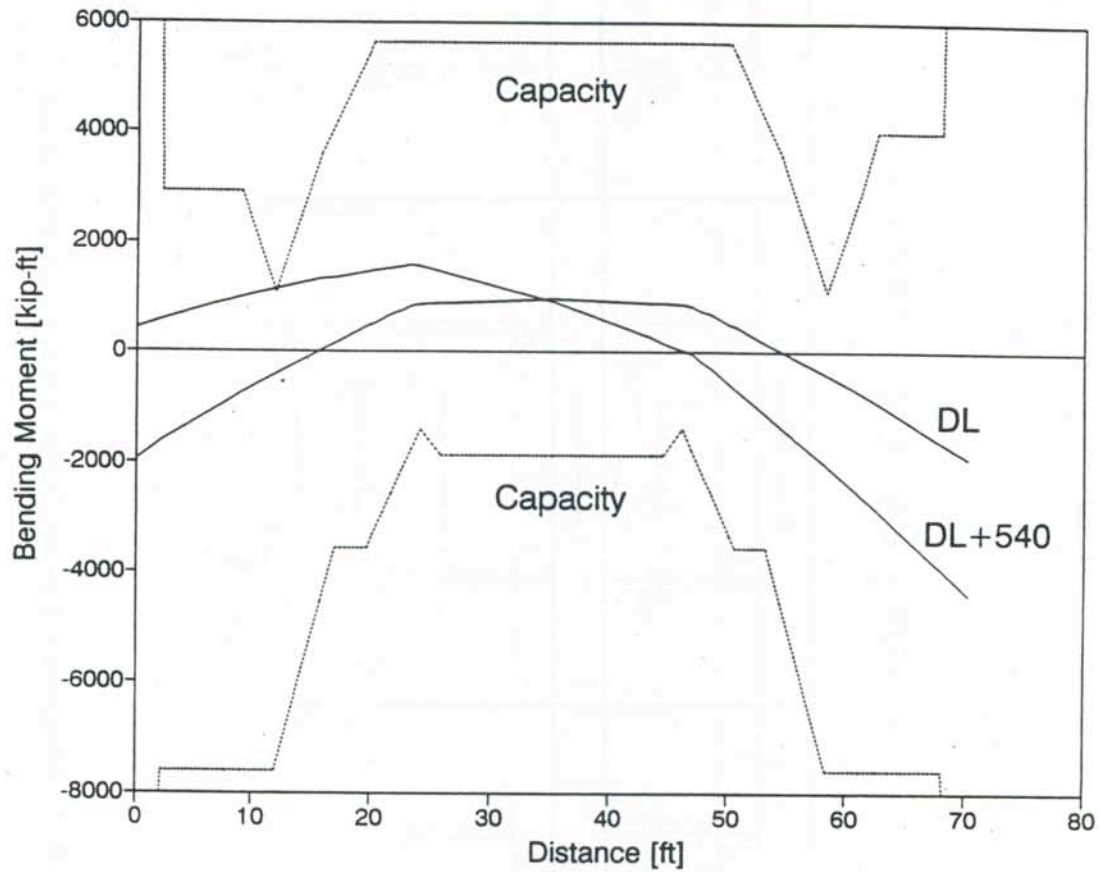
Figure 4.20. Moments in Central Span of Bottom-Girder (Fixed-Bases)

Column Bending Moments
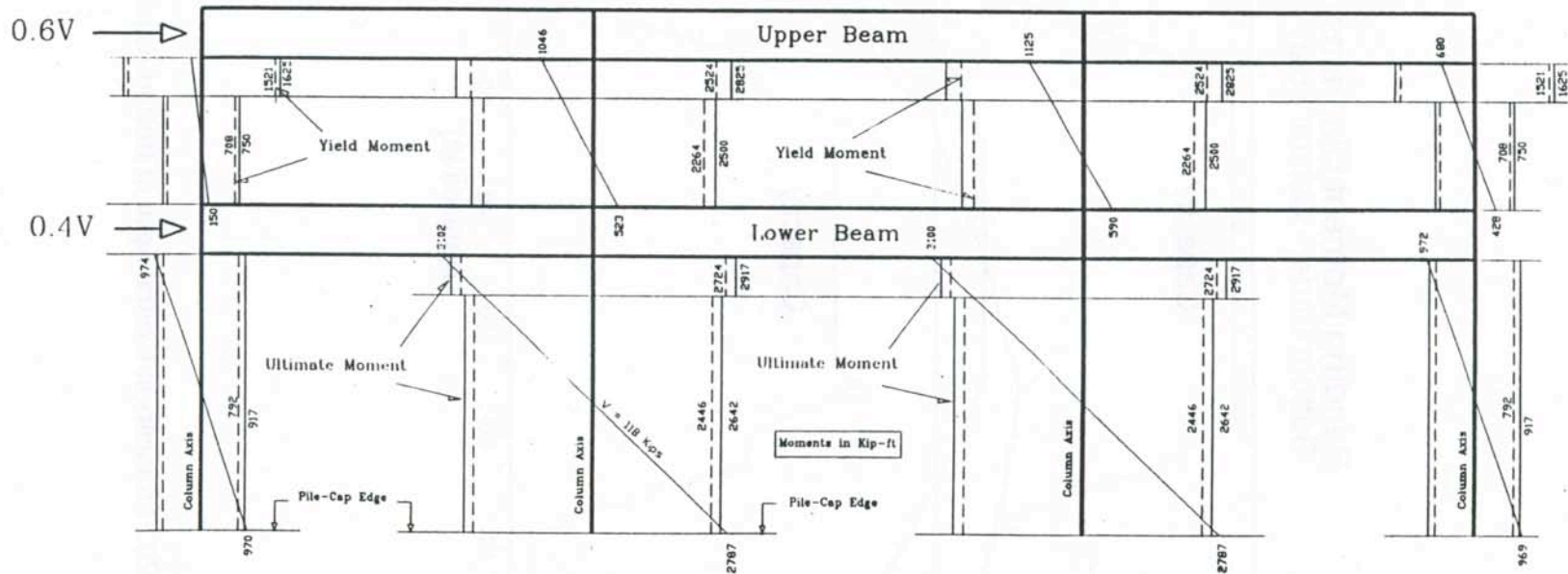
Figure 4.21. Moments in Longitudinal-Frame Columns (Fixed Bases)

Longitudinal Frame – Fixed Base

Base Shear = 540 Kips

Columns

7.39	2.70	2.51	2.39	
5.00	4.78	4.24	1.75	
0.94	0.94	0.94	0.94	
0.95	0.95	0.95	0.95	

(+)	(-)	(+)	(-)	Beams	(-)	(+)	(-)
10.64	3.08	5.47	3.07		5.02	2.21	
2.68	1.91		1.87		1.06		

a) Ratios $\dfrac{M_u}{M_{540}}$

Columns

6.91	2.41	2.24	2.24	
4.72	4.33	3.84	1.65	
0.81	0.88	0.88	0.81	
0.82	0.88	0.88	0.82	

(+)	(-)	(+)	(-)	Beams	(-)	(+)	(-)
8.40	2.88	4.30	2.87		3.94	1.96	
2.12	1.78		1.75		0.94		

b) Ratios $\dfrac{M_y}{M_{540}}$
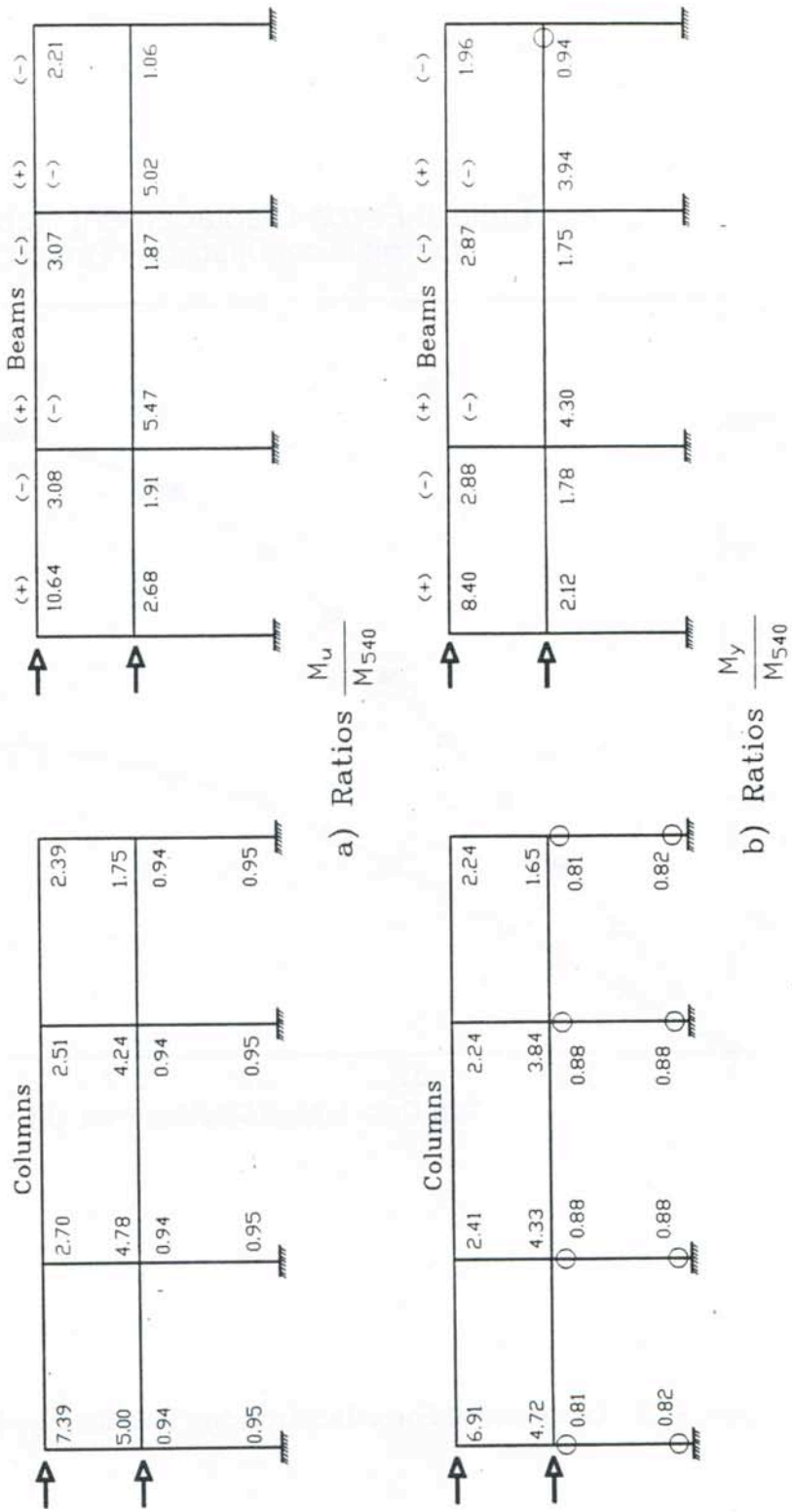
Figure 4.22. Flexural Capacity/Demand Ratios Longitudinal Frames (Fixed Bases)

71
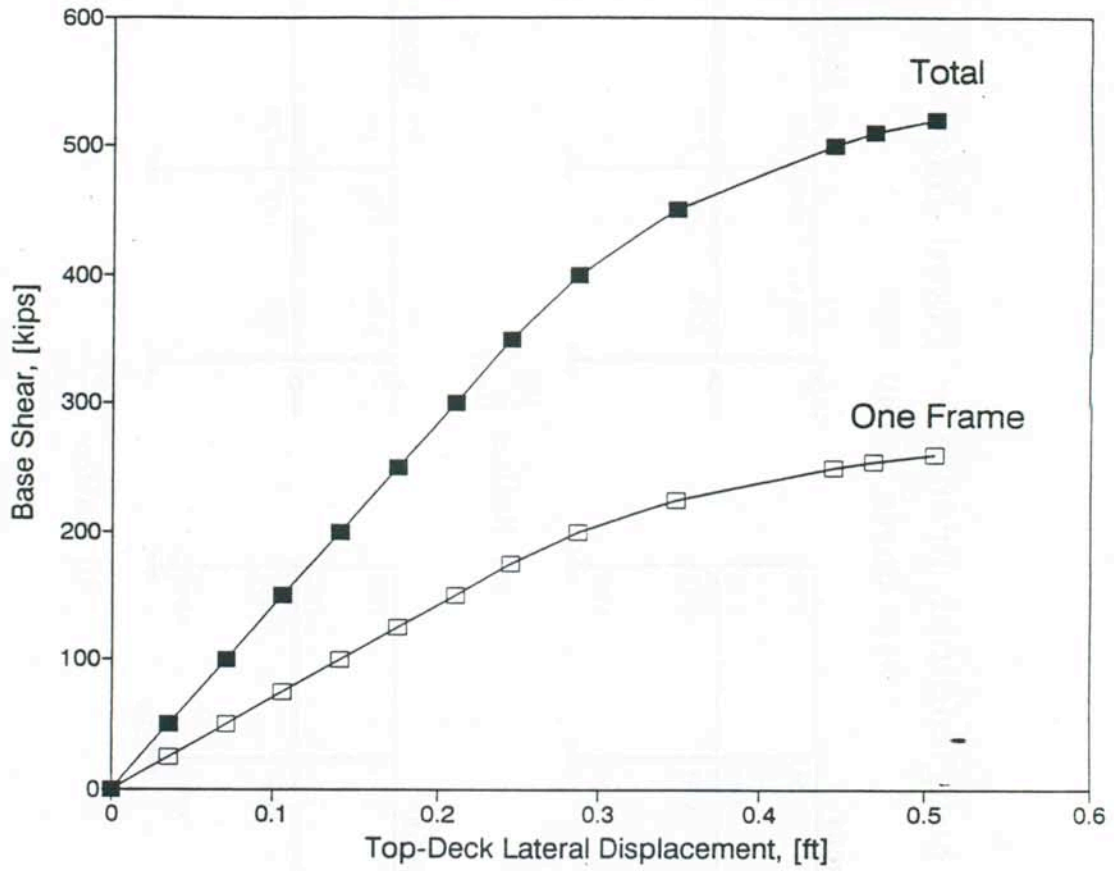
Figure 4.23. Longitudinal Force-Displacement Relationships (Pinned-Bases)

Column Bending Moments
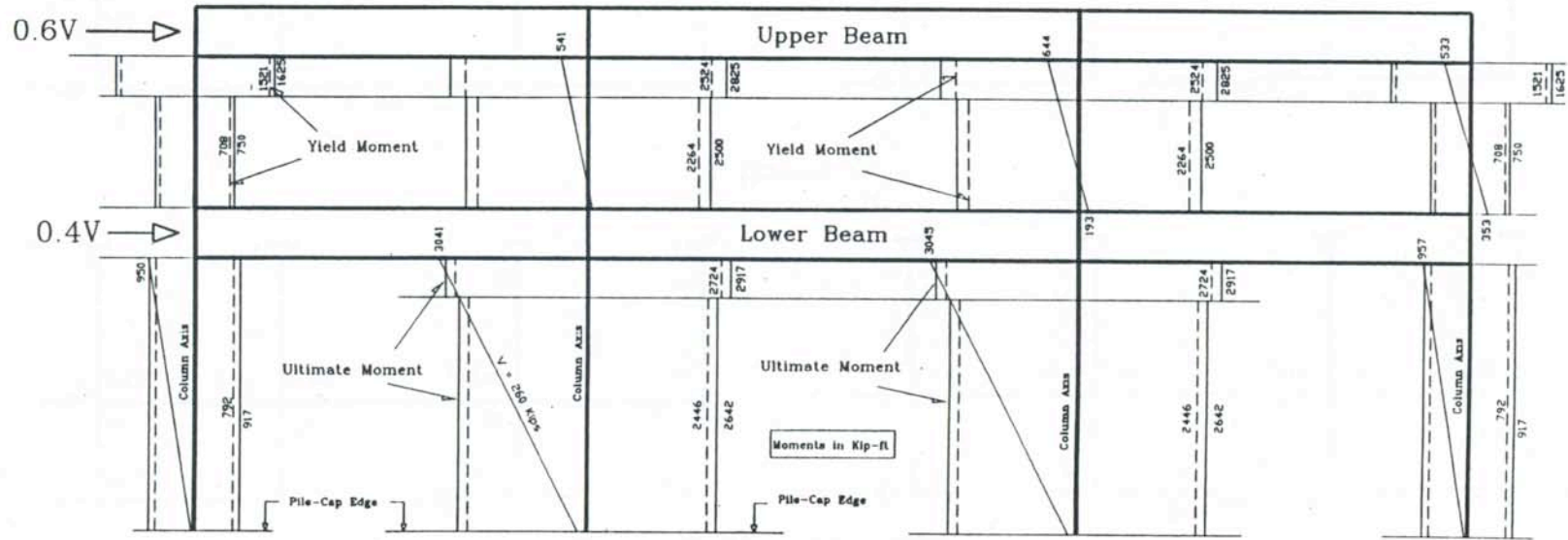
Figure 4.24. Moments in Longitudinal-Frame Columns (Pinned Bases)

Longitudinal Frame – Pinned Base

Base Shear = 260 Kips

Columns			
95.6	5.22	4.39	3.05
14.7	26.0	13.0	2.12
0.97	0.96	0.96	0.96

(+)	(−)	(+) Beams (−)		(+)	(−)
101	3.61	(−)	3.55	(−)	2.86
3.86	2.20	153	2.15	31.0	1.24

a) Ratios $\dfrac{M_u}{M_{260}}$

Columns			
89.5	4.67	3.92	2.85
13.9	23.6	11.7	2.01
0.83	0.90	0.89	0.83

(+)	(−)	(+) Beams (−)		(+)	(−)
80.1	3.36	(−)	3.31	(−)	2.54
3.05	2.05	120	2.01	24.4	1.11
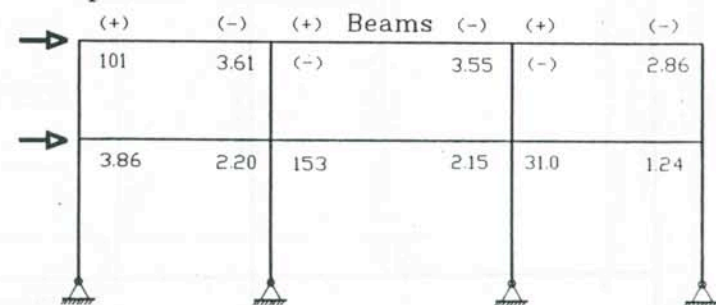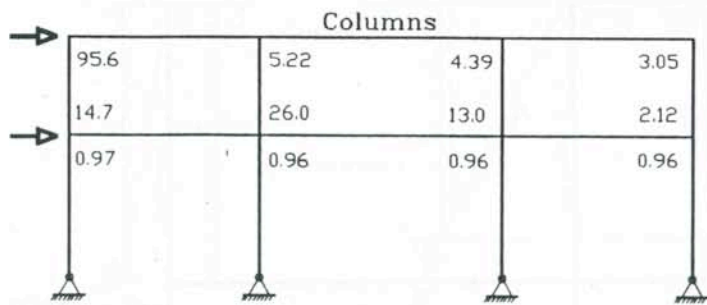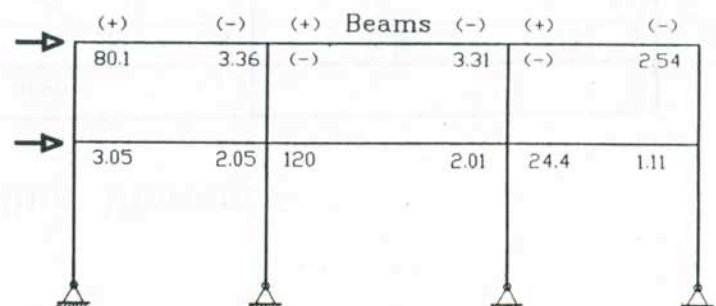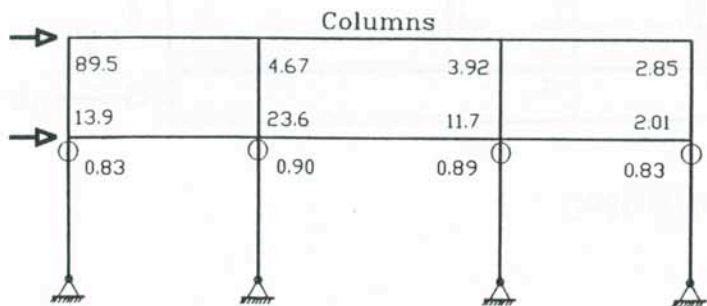
b) Ratios $\dfrac{M_y}{M_{260}}$

Figure 4.25. Flexural Capacity/Demand Ratios for Longitudinal Frames (Pinned Bases)

74

4.5 DISCUSSION

For the reader's convenience, Table 4.6 summarizes the computed force and displacement capacities. Comparison of the various capacities demonstrates the importance of foundation stiffness. For both the transverse and longitudinal directions, the unit's fixed-base capacity was equal to approximately 25 percent its weight. For the pinned-base condition, the lateral-force capacities decreased to only 40 to 50 percent of fixed-base values.

The computed drift capacities also changed markedly. For the fixed-base condition, the overall maximum drift ratios were equal to 0.7 percent for the transverse direction and 0.6 percent for the longitudinal direction. For the pinned-base condition, the top-deck drift ratios increased by approximately 75 percent.

It is important to emphasize the uncertainties inherent in the computed drift capacities. In all cases, the maximum drift was limited by the curvature capacity of the lower-level columns. The consequences of exceeding this limit vary greatly according to column geometry, axial load, and reinforcement details. It is also important to emphasize that these results do not include the effect of brittle failure modes. The lateral strengths

Table 4.6. Computed Lateral Capacities of the WSDOT Unit

Support Condition	Direction	Base Shear		Top-Deck Lateral Displacement	
		[kips]	[% of Weight]	[ft]	[% of Height]
Fixed	Transverse	1120	24	0.40	0.7
	Longitudinal	1080	23	0.33	0.6
Pinned	Transverse	676	14	0.70	1.2
	Longitudinal	520	11	0.50	0.9

and displacements would vary from those reported in Table 4.6 if flexural capacities are reduced by anchorage slip or splice deterioration. For example, the influence of limited anchorage length was already identified in the lower-deck end beams (Fig. 4.7). The influence of limited girder lap-splice lengths was identified in Figures 4.19 and 4.20. Moreover, brittle failure modes, such as shear failure or joint failure, could render these calculations moot. The influence of the details is considered in subsequent chapters.

CHAPTER 5

FLEXURAL DUCTILITY

If the transverse confinement is inadequate, large rotational demands can lead to crushing of the concrete, buckling of the longitudinal reinforcement, and strength reduction. Both the ATC-6-2 and Priestley, Seible, and Chai (1992) procedures address the adequacy of the confinement reinforcement, but their approaches differ greatly. The ATC-6-2 procedure expresses the adequacy of the confinement in terms of a confinement capacity-to-demand (C/D) ratio at each location, r_{cc}. The computed confinement C/D ratios depend directly on the flexural C/D ratios reported in Sections 3.6 and 3.7. In contrast, the Priestley et al. (1992) procedure expresses adequacy of the confinement in terms of a single capacity-to-demand ratio for the entire structure. For convenience, the procedure proposed by University of California, San Diego, (UCSD) researchers Priestley et al. (1992) will be referred to as UCSD. This procedure considers nonlinear response explicitly.

The researchers computed confinement capacity-to-demand ratios for four sets of conditions. For each foundation condition (fixed-base and pinned-base), two sets of response spectra were considered. The first spectrum was the soft-soil spectrum (Soil Type III) recommended by the "Seismic Design Guidelines for Highway Bridges, ATC-6, (1981) (Fig. 3.6). This spectrum was anchored by an effective acceleration of 0.25g. The researchers repeated the evaluations with the largest ordinates of four response spectra obtained from the seismological and geotechnical study (Kramer et al. 1995) (Fig. 3.10).

5.1 ATC-6-2 EVALUATION

Procedure

According to the ATC-6-2 procedure, the confinement C/D ratio, r_{cc}, is a measure of the adequacy of the transverse confinement. A ratio below 1.0 indicates that the confinement is inadequate. This ratio is computed as the product of the flexural C/D ratio, r_{ec}, and the ductility indicator, μ:

77

$$r_{cc} = \mu r_{ec} \tag{5.1}$$

The ductility indicator varies according to the axial stress and to the reinforcement details:

$$\mu = 2 + 4 \left(\frac{k_1 + k_2}{2} \right) k_3 \tag{5.2}$$

where, k_1 = $\dfrac{A_{sh}(c)}{A_{sh}(d)\left(0.5 + \dfrac{1.25P}{f_c A_g} \right)} \geq 1$

k_2 =   the minimum of $\dfrac{6}{s/db} \leq 1$ and $\dfrac{0.2}{s/b\ min} \leq 1$

k_3 =   effectiveness of transverse bar anchorage

P =   column's axial force, as determined with linear analysis

A_g =   column's cross-sectional area

b_{min} =   minimum width of column cross section

$A_{sh}(c)$ =   cross-sectional area of provided transverse confinement

$A_{sh}(d)$ =   maximum of $30\ a\ h\ f_c/f_y\ [A_g/A_c - 1]$ and $0.12\ a\ h\ f_c/f_y$

h =   core dimension of column in direction of shear

a =   vertical spacing of hoops

A_c =   area of column core

If the transverse reinforcement is poorly anchored, as in the case of the typical WSDOT unit (Figs. 2.2 and 2.3), k_3 varies as shown in Figure 5.1. Although the procedure can be expressed in a non-iterative form (Ryter, 1994), the ductility indicator is usually determined by iteration. For poorly-anchored reinforcement, μ varies from 2.0 to 3.0.

Confinement C/D Ratios r_{cc}

The details of the confinement calculations are reported in Appendix D, and the results are summarized in Table 5.1. Each table entry corresponds to the range of computed values for a particular response spectrum, foundation condition, and location
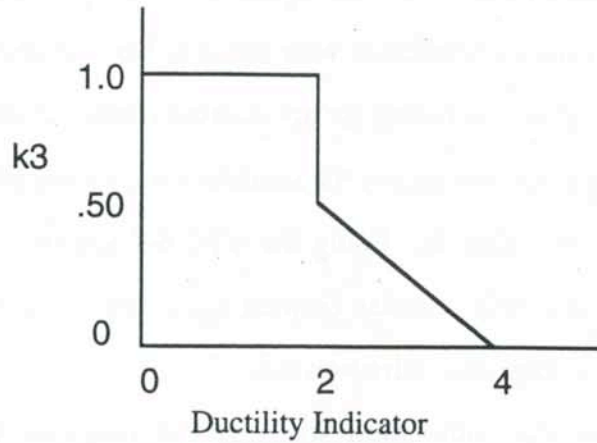
Figure 5.1. Effectiveness of Poorly-Anchored, Transverse Reinforcement

Table 5.1. Ranges of Confinement C/D Ratios, r_{cc}

Location	Fixed-Base Condition		Pinned-Base Condition	
	ATC-6	Site-Specific	ATC-6	Site-Specific
1	1.1-1.7	0.6-1.1	7.2-10.7	5.0-7.8
2	1.3-1.8	0.7-1.3	0.8-1.3	0.6-0.9
3	1.3-25.5	1.5-4.3	2.6-∞	2.0-∞
4	3.0-8.9	2.4-5.5	3.5-11.7	2.4-7.0

(defined in Fig. 3.7). Each tabulated range encompasses the results for the transverse and longitudinal directions, as well as for the interior and exterior columns. The ductility indicator (Eq. 5.2) was nearly constant for all of the analyses; it ranged from 2.39 to 2.59. Consequently, the values of r_{cc} (Eq. 5.1) were approximately equal to 2.5 times the values of r_{ec} (Appendix C).

In the first story, the values varied according to the foundation condition and to the response spectrum. For the fixed-base condition, the lowest values of r_{cc} occurred at

the tops and bottoms of the first-story columns (Locations 1 and 2). For the ATC spectrum, all of the values exceeded or were equal to 1.0. For the site-specific spectrum, the lowest value of r_{cc} (0.6) occurred for longitudinal motion of the interior column.

For the pinned-base condition, the smallest values were obtained at the top of the first-story columns (Location 2). Using the ATC-6-2 spectrum, the confinement was found to be marginal at this location (lowest $r_{cc} = 0.8$). Using the worst-case, site-specific spectrum, the minimum value was 0.6.

Regardless of the foundation stiffness and response spectrum, the column confinement C/D ratios in the second story (Locations 3 and 4) consistently exceeded 1.5. For some of the pinned-base analyses, the seismic moments at Location 3 were too small to overcome the gravity-load moments ($r_{cc} = \infty$).

5.2 PRIESTLEY, SEIBLE, AND UANG (1992) EVALUATION (UCSD)

The flexural vulnerability of the WSDOT-designed, typical unit may be expressed as the ratio of the equivalent elastic strength, V_E, to the seismic demand, V_D. V_E is computed from the lateral force-displacement relationship, and V_D is obtained from linear response spectra and the structure's mass. The ratios were computed for both the fixed- and pinned-base conditions.

Equivalent Elastic Strength, V_E

As illustrated in Figure 5.2, the equivalent elastic strength was computed as the product of unit's stiffness and ultimate displacement. The lateral stiffness was evaluated on the basis of the displacements computed at the height of the seismic force's resultant (49 feet above the top of the footings). Specifically, lateral stiffness was defined by the line in the force-displacement plane that joins the origin and the point corresponding to 75 percent of the computed capacity, V_U (Priestley et al. 1992).

It is difficult to estimate the magnitude of the maximum lateral displacement that the structure can safely sustain. The maximum displacements computed in Chapter 4

Base Shear-Displacement Curves
Transverse Direction - Fixed Base
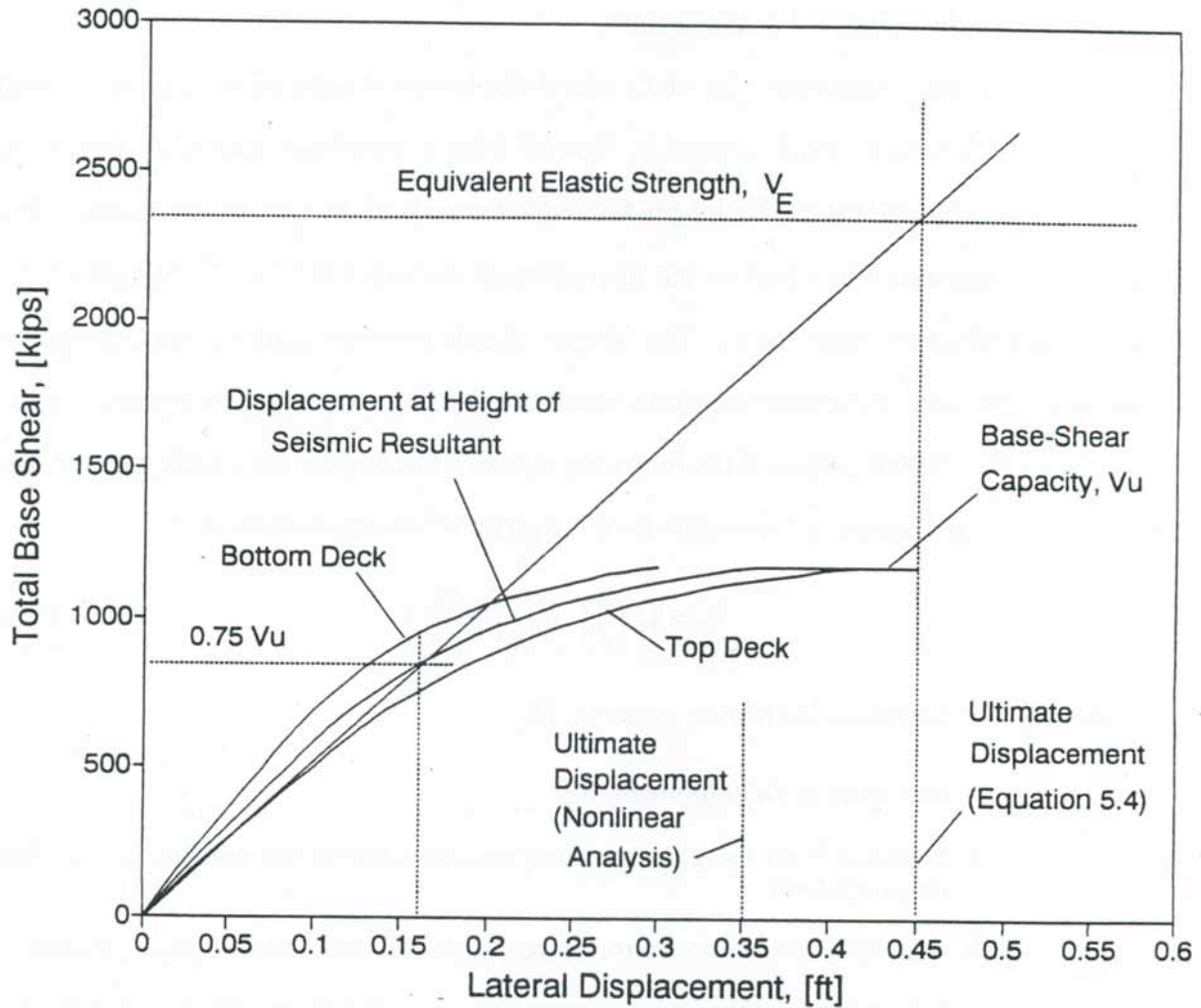
Figure 5.2. Definition of Equivalent Elastic Strength, V_E

provide one estimate of the frame's displacement capacity, but these capacities vary according to the length of the model's prismatic segments. This relationship is illustrated in Figure 5.3 for an interior, transverse frame with a fixed base. The figure shows that the magnitude of the top-deck, lateral displacement increases with the length of the lower-level, column-end segments. Moreover, the computed displacements did not take into account the slip of reinforcement relative to the concrete, which would increase the magnitude of the computed displacements.

Additional estimates of the unit's lateral-displacement capacity were obtained with plastic-hinge analysis. As illustrated in Figure 5.4 for a fixed-base, transverse frame, the researchers assumed that plastic hinges formed at the ends of the first-story columns. The yield displacement was taken as the displacement corresponding to 75 percent of the structure's ultimate base shear. The hinge's plastic-rotation capacity was computed following two sets of recommendations, which are described in the following paragraphs.

Corley (1966) proposed the following equation to compute the plastic rotation, θ_p, that occurs at a distance d/2 to each side of the point of maximum moment.

$$\theta_p = \phi_u \left(\frac{d}{2}\right) - \phi_y \left(\frac{d}{2}\right)\left(\frac{M_u}{M_y}\right) \tag{5.3}$$

where, ϕ_u = curvature at ultimate moment, M_u

ϕ_y = curvature at yield moment, M_y

d = distance from the extreme compression fiber to the centroid of tension reinforcement

On the basis of experiments on reinforced concrete, cantilever columns, Priestley and Park (1987) proposed another set of expressions to compute the plastic rotation, θ_p, and to compute the length of the plastic hinge, l_p. According to these authors, the effects of reinforcement slip and "shear spread of plasticity" are implicit in the following formulas:

82
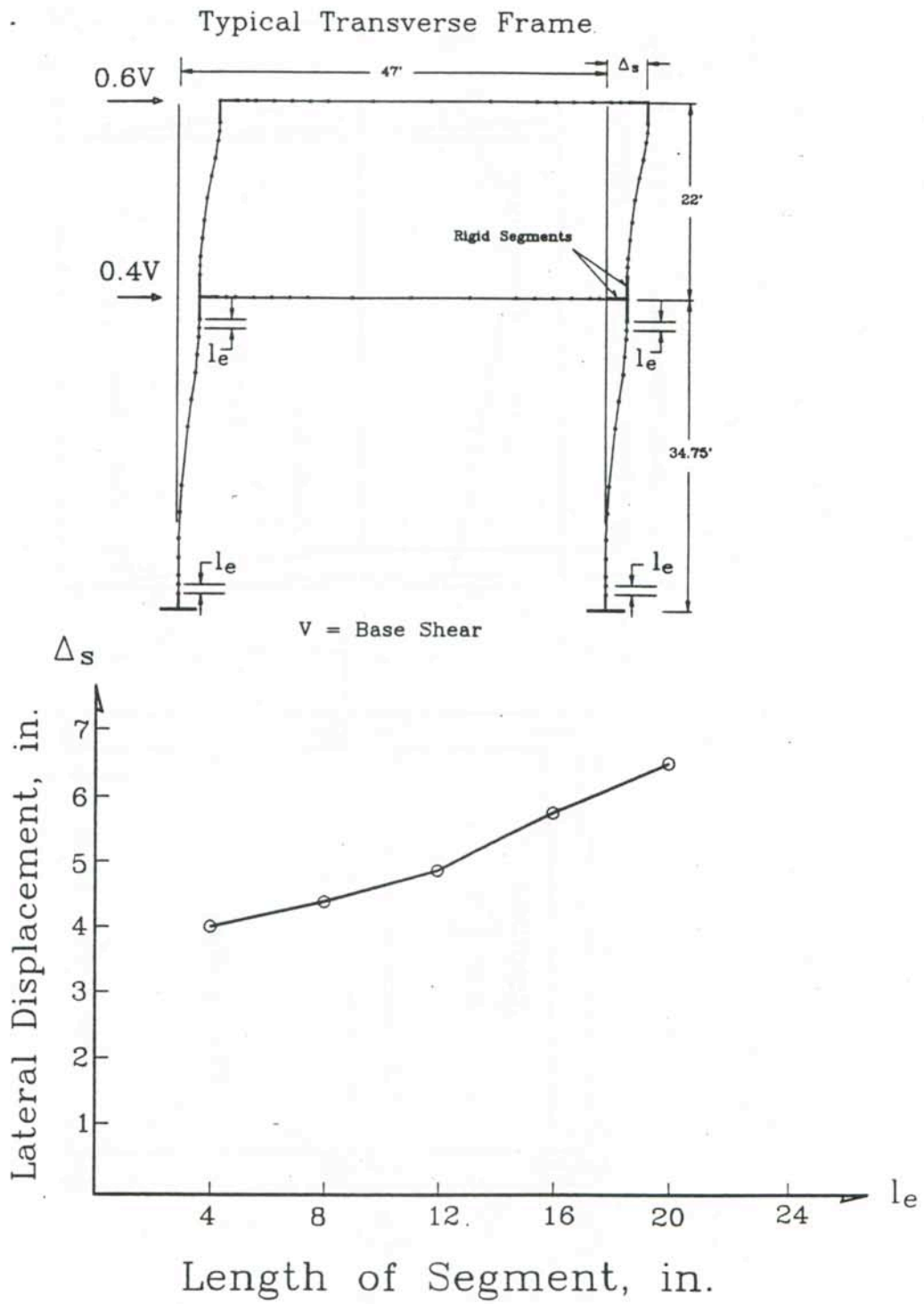
Figure 5.3. Variation of Computed Ultimate Displacement with Segment Length

V_{top}

V_{bottom}

Resultant

Plastic Hinges

Plastic–Hinge Length $= l_p$

L

Δ_y = Elastic Displacement

Δ_p = Plastic Displacement

Ultimate Displacement
$= \Delta_y + \Delta_p$

Elastic Frame

Plastic Frame

$\Delta_p = \Theta_p \cdot l'$

Θ_p = Plastic Rotation

$l' = L - l_p$
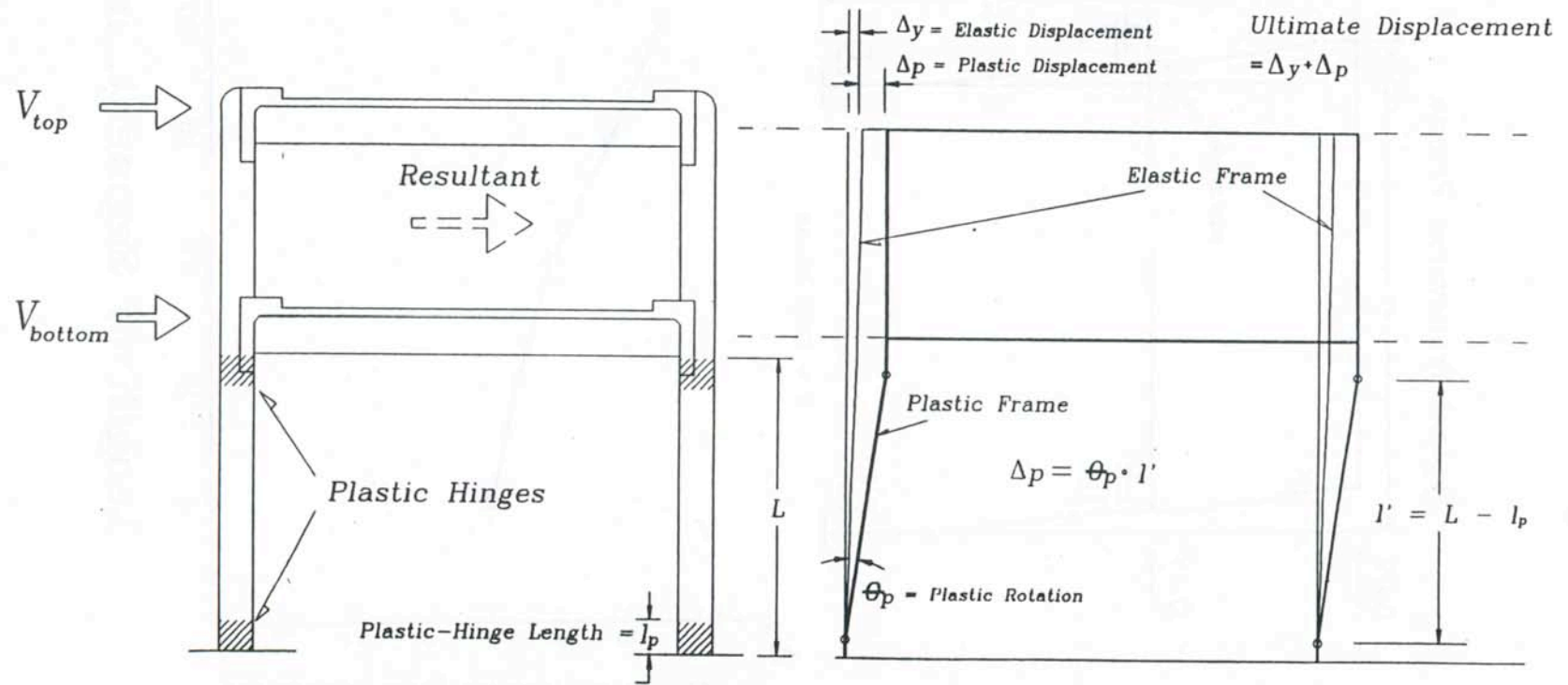
Figure 5.4. Computation of Ultimate Lateral Displacement

$$\theta_p = (\phi_u - \phi_y)\, l_p \qquad\qquad (5.4)$$

where, l_p = $0.08(L/2) + 0.15d_b f_y$

$\quad\quad$ L = member length (Fig. 5.4)

$\quad\quad$ d_b = diameter of column bars

$\quad\quad$ f_y = yield stress of the reinforcement (in ksi)

Table 5.2 provides a comparison between the displacements computed with Equation 5.3, with Equation 5.4, and with the nonlinear analyses for the fixed-base frames. In computing the displacements, the researchers assumed that the ultimate curvature corresponded to the curvature at which the maximum concrete compressive strain was 0.005 or at which the steel tensile strain was 0.05. Priestley et al. (1992) recommended these strain limits for columns with little confinement.

In the transverse direction, the ultimate displacements computed with the Priestley and Park equation (Eq. 5.4) were approximately 20 to 30 percent larger than the displacements computed with nonlinear analysis (Table 5.2). In the longitudinal direction, the displacements computed with the Priestley and Park equations exceeded the displacements computed with nonlinear analysis by 80 percent. The displacements computed with the Corley equation (Eq. 5.3) were approximately equal to the average of the displacements computed with the two other methods.

To be consistent with the evaluation procedure proposed by Priestley et al. (1992), the plastic displacements were computed with the formulas proposed by Priestley and Park (1987). The computed ultimate displacements are summarized in Table 5.3 for the fixed- and pinned-base conditions. Although the yield displacements for the pinned-base frames were approximately 60 to 80 percent higher than those computed for the fixed-base frames, the plastic displacements were nearly identical. Consequently, the ultimate displacements of the pinned- and fixed-base frames differed less than their yield displacements.

Table 5.2. Computed Displacements for Fixed-Base Frames[1]

	Parameter	Nonlinear Analysis	Corley[2]	Priestley and Park[2]
Transverse, Interior Frame	Yield Displacement, Δ_y [in.]	2.2	-	-
	Plastic-Hinge Length, l_p [in.]	-	20.5	23.7
	Plastic-Hinge Rotation, θ_p [rad]	-	0.008	0.0095
	Plastic Displacement, Δ_p [in.]	-	2.7	3.2
	Ultimate Displacement, Δ_R [in.]	4.2	4.9	5.4
Transverse, Exterior Frame	Yield Displacement, Δ_y [in.]	1.9	-	-
	Plastic-Hinge Length, l_p [in.]	-	20.5	25.2
	Plastic-Hinge Rotation, θ_p [rad]	-	0.009	0.011
	Plastic Displacement, Δ_p [in.]	-	3.0	3.7
	Ultimate Displacement, Δ_R [in.]	4.5	4.9	5.6
Longitudinal Frame	Yield Displacement, Δ_y [in.]	1.7	-	-
	Plastic-Hinge Length, l_p [in.]	-	17.9	23.7
	Plastic-Hinge Rotation, θ_p [rad]	-	0.011	0.015
	Plastic Displacement, Δ_p [in.]	-	3.6	5.0
	Ultimate Displacement [in.]	3.7	5.3	6.7

[1] Displacements computed at the height of the seismic force's resultant (height = 48 ft).

[2] The value of ϕ_u was defined by either $\varepsilon_{cu} = 0.005$ or $\varepsilon_{su} = 0.05$.

[3] Computed with properties of lower-level columns with the largest axial load.

[4] Eqs. (5.3) and (5.4) were evaluated using the properties of the interior column.

Table 5.3. Equivalent Elastic Base-Shear Strengths[1]

Support Condition	Direction	Lateral Stiffness	Yield Displ.	Ultimate Displ.	Base Shear V_E	$S_a(C)$ = V_E/Mass
		[kip/in.]	[in.]	[in.]	[kip]	[g]
Fixed	Transv.	430	1.9	5.4	2322	0.48
Base	Long.	480	1.7	6.7	3216	0.67
Pinned	Transv.	100	5.0	9.8	980	0.21
Base	Long.	120	3.2	10.8	1296	0.28

[1] Computed at the height of the resultant of seismic forces.

Table 5.3 lists the equivalent elastic strengths, V_E, as well as the accelerations $S_a(C)$ that result from dividing V_E by the structure's mass. The values of $S_a(C)$, which varied from 0.21g to 0.67g, provided a normalized measure of the unit's equivalent elastic strength. The magnitude of $S_a(C)$ varied greatly with the assumed foundation condition and, to a lesser extent, with the direction of motion. The factor of 2.3 between $S_a(C)$ for the fixed and pinned conditions was due primarily to the larger stiffness of the fixed-base unit. The equivalent base-shear strength in the longitudinal direction was approximately one third larger than the strength in the transverse direction. This difference was due to the longitudinal direction's higher stiffness and larger ultimate displacement.

Base-Shear Demand, V_D

The structural periods were computed with the stiffnesses listed in Table 5.3 and with the structure's mass. As shown in Table 5.4, the effective period in both directions was approximately 1.0 seconds for the fixed-base condition and 2.1 seconds for the pinned-base condition. These periods were slightly larger than those computed with the three-dimensional, linear model (Sec. 3.3).

Table 5.4. Global Capacity-to-Demand Ratios[1]

Base Condition	Direction	Period [sec]	ATC Spectrum		Site-Specific Spectrum	
			$Sa(D)_{ATC}$ [g]	$\dfrac{Sa(C)}{Sa(D)_{ATC}}$	$Sa(D)_{SITE}$ [g]	$\dfrac{Sa(C)}{Sa(D)_{SITE}}$
Fixed	Transv.	1.06	0.45	1.07	0.75	0.64
	Long.	1.00	0.47	1.43	0.75	0.89
Pinned	Transv.	2.17	0.28	0.75	0.40	0.53
	Long.	2.03	0.29	0.97	0.40	0.70

[1] Ratios were computed using the frame displacement at the resultant of the seismic forces.

The base shear demand V_D can be expressed as the product of the spectral acceleration, $S_a(D)$, and the structure's mass. Spectral demands varied from a low of 0.28g (pinned base, ATC Spectrum) to a high of 0.75g (fixed base, site-specific spectrum). The demands in the longitudinal and transverse directions were similar.

Global Capacity-to-Demand Ratios

For convenience, the base-shear, capacity-to-demand ratio V_E/V_D, can be expressed as a quotient of accelerations $S_a(C)/S_a(D)$. The normalized base-shear strength, $S_a(C)$, and the spectral acceleration, $S_a(D)$, are equal to V_E and V_D, respectively, divided by the structure's weight (4800 kips). These ratios are summarized in Table 5.4.

For the ATC spectrum, the capacity-to-demand ratios for the fixed-base condition were approximately 50 percent higher than they were for the pinned condition. This difference is largely due to the fact that the fixed-base structure is approximately four times stiffer than the pinned-base structure (Table 5.3). For the site-specific spectra, the capacity-to-demand ratios for the fixed-base condition were 25 percent larger than were the ratios for the pinned-base condition.

For a given foundation condition, the typical unit's flexural vulnerability is somewhat larger in the transverse direction than in the longitudinal direction. For example, for the fixed-base condition, the ratios $S_a(C)/S_a(D)$ were approximately 25 to 35 percent higher in the longitudinal direction than in the transverse direction.

The typical unit was found to be much more vulnerable when the spectral accelerations were computed with the worst-case, site-specific spectra than when they were computed with the ATC-6 spectrum. The site-specific ratios were 30 to 40 percent smaller than the ATC-6 ratios, depending on the direction of analysis and support condition.

5.3 GLOBAL DUCTILITY DEMANDS

The ratio of the base-shear demand to the nominal shear at yield gives a non dimensional measure of the ductility demands that will be imposed on the unit. For the purposes of this report, the nominal base shear at yield, V_Y, was defined as 75 percent of the base-shear capacity V_U. The base-shear demand was obtained from linear analysis (Table 5.4).

As shown in Table 5.5, the displacement ductility demands did not depend strongly on the direction of motion or the foundation condition. The ductility demand for the ATC-6 spectrum ranged from 2.6 to 3.6. For the worst-case, site-specific spectra, the ductility demand ranged from 3.8 to 4.9. If the displacement ductility demands are defined as V_D/V_U, they decrease by 25 percent.

5.4 COMBINED ASSESSMENT

Evaluations of flexural vulnerability are always inexact because there are uncertainties inherent in the estimates of the ground motions, structural response, and capacities. Nevertheless, despite the variations between the ATC-6-2 and Priestley et al. (1992) methodologies, the results were remarkably similar.

1. The typical unit's vulnerability to flexural failure appears to be low if the foundation rotation is negligible, and if the ground motion is well represented by the ATC-6 spectrum (Fig. 3.6).

2. Vulnerability increases significantly if the rotational resistance at the base of the column (such a low resistance would result from splice failure), or if the motion is well represented by the worst-condition, site-specific spectrum (Fig. 3.10).

3. If the rotational resistance is low AND if the worst-condition, ground-motion materializes, the flexural demands may significantly exceed the capacities.

Table 5.5. Global Ductility Demands[1]

Base Condition	Direction	Yield Shear $V_Y = 0.75 V_U$ [kips]	ATC Spectrum		Site-Specific Spectra	
			V_D [kips]	V_D/V_Y	V_D [kips]	V_D/V_Y
Fixed	Transv.	840	2160	2.6	3600	4.3
	Long.	810	2260	2.8	3600	4.4
Pinned	Transv.	507	1340	2.6	1920	3.8
	Long.	390	1390	3.6	1920	4.9

[1] Ratios were computed using the frame displacement at the resultant of the seismic forces.

CHAPTER 6

SHEAR

6.1 INTRODUCTION

This chapter presents three assessments of the shear vulnerability of the typical WSDOT unit. The evaluation team implemented the procedures proposed by the Applied Technology Council (ATC-6-2, 1983); by Priestley, Seible, and Uang (1994); and by Ascheim and Moehle (1992). All of these procedures share the same general form. The nominal capacity (V_n) is computed as the sum of three terms that reflect the concrete's contribution to shear strength (V_c), the resistance provided by the transverse reinforcement (V_s), and the effect of axial force (V_p).

$$V_n = V_c + V_s + V_p \qquad (6.1)$$

As shown in Figure 6.1, the initial shear capacity (V_i) is maintained until the member ductility demand μ_i, at which point the capacity decreases linearly with ductility demand until it reaches a final shear capacity (V_f).

Three scenarios are possible. If the initial shear capacity is insufficient to resist the maximum shear demand (V_d), the column will fail in a brittle manner (Case A). If the initial capacity exceeds the maximum shear demand, but the final capacity is less than the demand (i.e., $V_i > V_d > V_f$), a flexural/shear failure will occur if the ductility demand is sufficiently large (Case B). Finally, if the final shear capacity exceeds the maximum shear demand, the column will not fail in shear (Case C).

Table 6.1 and Figure 6.2 summarize the shear-strength equations proposed by the Applied Technology Council (ATC-6-2), by Priestley et al. (1994) and by Ascheim and Moehle (1992).
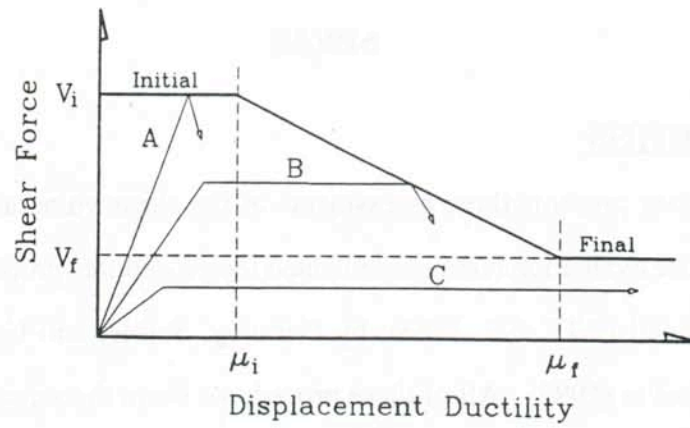
Figure 6.1. Variation of Shear Resistance with Ductility
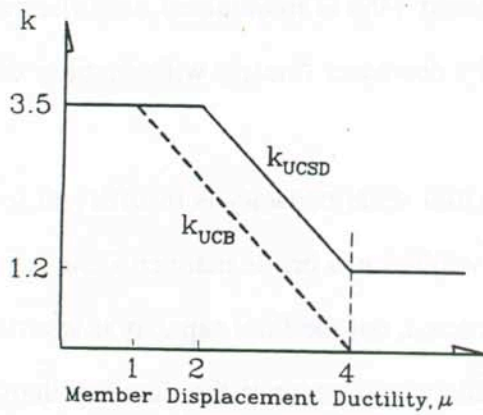
a) Variation of k
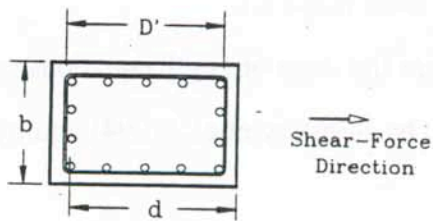
b) Column Cross Section
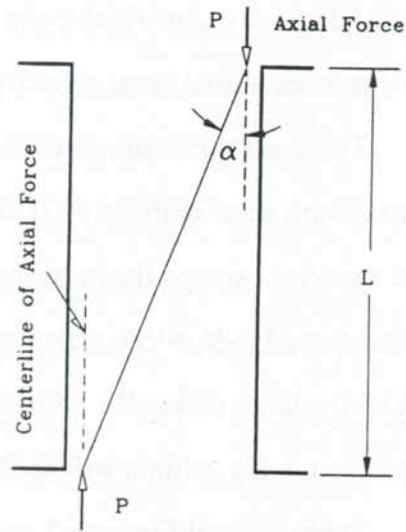
c) Column Elevation

Figure 6.2. Shear-Evaluation Parameters

Table 6.1. Equations to Compute Shear Capacity

	V_c	V_s	V_p
ATC-6	$2\sqrt{f_c}\,bd$	$(A_v\,f_y\,d)/s$	$(P/1000A_g)\,\sqrt{f_c}\,bd$
Priestley et al. (1994)	$k_{UCSD}\sqrt{f_c}\,(0.8A_g)$	$(A_v\,f_y\,D')/(s\tan 30^\circ)$	$P\tan\alpha$
Ascheim and Moehle (1992)	$k_{UCB}\sqrt{f_c}\,(0.8A_g)$	$(A_v\,f_y\,d)/(s\tan 30^\circ)$	$P\sqrt{f_c}/714$

Notes: k_{UCSD}, k_{UCB}, b, d, D', and α are defined in Fig. 6.2

f_y = yield stress of transverse reinforcement

s   = hoop spacing

A_g = column's gross area

A_v = transverse area of hoops

Axial load P and shear capacities are expressed in lbs., f_c, is expressed in psi.

6.2 ATC-6-2 EVALUATION OF COLUMNS

Standard Procedure

To compute the shear capacity-to-demand ratio, r_{cv}, it is convenient to define the following terms.

$V_u(d)$ =   shear demand that would occur if the columns develop their flexural capacities. According to ATC-6, the shear demand is computed as $1.3(M_{u1}+M_{u2})/L$, where M_{u1} and M_{u2} are the ultimate moments at the ends of a column, and L is the clear span length. The axial loads used in computing M_{u1} and M_{u2} are obtained from limit analysis, and strain hardening of the steel is not considered.

$V_e(d)$ =   the shear demand that was computed with linear analysis (Ch. 3).

$V_i(c)$ =   the column's initial shear capacity, which includes all three components of resistance (Eq. 6.1).

$V_f(c)$ = the final column capacity (Eq. 6.1). This resistance of the transverse reinforcement is considered only if it is properly anchored. If the axial stress exceeds 10 percent of the concrete's compressive strength, $V_f(c)$ includes the contribution of the column core concrete as well. Otherwise, the concrete's contribution to resistance is neglected.

If the column does not yield, the shear C/D ratio, r_{cv}, is equal to the ratio of the initial shear capacity $V_i(c)$ and the elastic shear demand $V_e(d)$. If the column yields, the equation for r_{cv} varies according to the three cases (A, B, and C), which are defined in Figure 6.1.

For Case A ($V_i(c) < V_u(d)$):

$$r_{cv} = V_i(c)/V_e(d) < r_{ec} \qquad (6.2)$$

For Case B ($V_i(c) > V_u(d) > V_f(c)$):

$$r_{cv} = \mu r_{ec} \qquad (6.3)$$

where, $\qquad \mu = 2 + \left(0.75 \dfrac{L_c}{b_c} \right) \dfrac{V_i(c) - V_u(d)}{V_i(c) - V_f(c)}$

$\qquad L_c \quad = \quad$ height of column

$\qquad b_c \quad = \quad$ width of column in the direction of shear

$\qquad L_c/b_c$ should always be less than or equal to 4

For Case C ($V_f(c) > V_u(d)$):

$$r_{cv} = (2 + 0.75\, L_c/b_c)\, r_{ec} \qquad (6.4)$$

Implementation

The details of the ATC-6-2 shear calculations for both the fixed- and pinned-base conditions are reported in Tables D.5 through D.8. With a couple of exceptions, the

researchers implemented the ATC-6-2 procedure with one significant modification. The deviations from the standard procedure follow:

1.　.The axial forces were not determined by limit analysis. Instead, the researchers obtained the axial forces from the nonlinear analyses described in Chapter 4. This assumption affected the computation of axial-force component of shear resistance, V_p, as well as the computation of M_{u1} and M_{u2}.

2.　The flexural capacities, M_{u1} and M_{u2}, were computed based on the estimated properties listed in Table 4.1 and accounting for some strain hardening. To compensate for this deviation from the standard procedure, the researchers did not include a factor of 1.3 in computing the upper bound on shear demand, $V_u(d)$. Therefore, because the steel strength estimate (55 ksi) was low, the estimate of $V_u(d)$ may not be conservative.

Shear C/D Ratios, r_{cv}

The results for the first-story columns differed greatly from the second-story results. The first-story columns were classified as Case B for all of the analyses. In the first story, r_{cv} ranged from 1.5 to 2.7 for the ATC-6 spectrum (Table 6.2), and r_{cv} ranged from 0.9 to 1.6 for the site-specific spectrum (Table 6.3). The value of 0.9 was obtained at Location 1 for longitudinal motion of the interior column.

If the second-story columns had yielded, all but one them would have been classified as Case A, the most brittle failure mode. The exception was longitudinal motion of the exterior column. In most of the analyses, the flexural demands were well below the flexural capacities, and the shear capacities were adequate. The site-specific analysis indicated that shear failure was possible at location 4 (r_{cv}=0.9), but this result can be dismissed because the first story will yield before the elastic forces reach the member's shear capacity.

95

Table 6.2. Shear C/D Ratios, r_{cv}: ATC-6 Spectrum (Fixed Bases)

Location	Seismic Axial Force	Exterior Transverse	Exterior Longitudinal	Interior Transverse	Interior Longitudinal
1	Compression	1.7	2.7	1.6	1.5
	Tension	1.6	2.5	1.5	1.5
2	Compression	2.1	2.8	2.1	1.7
	Tension	2.0	2.7	2.0	1.7
3	Compression	1.5	2.1	1.7	1.9
	Tension	1.5	2.1	1.6	1.9
4	Compression	1.5	2.1	1.7	1.9
	Tension	1.5	2.1	1.6	1.9

Table 6.3. Shear C/D Ratios, r_{cv}: Site-Specific Spectrum (Fixed Bases)

Location	Seismic Axial Force	Exterior Transverse	Exterior Longitudinal	Interior Transverse	Interior Longitudinal
1	Compression	1.3	1.6	1.3	0.9
	Tension	1.2	1.4	1.2	0.9
2	Compression	1.6	1.7	1.6	1.0
	Tension	1.5	1.5	1.5	1.0
3	Compression	1.2	1.4	1.3	1.1
	Tension	1.2	1.9	1.2	1.1
4	Compression	1.2	1.2	0.9	0.9
	Tension	1.2	1.2	1.2	1.0

Despite the fact that the release of the foundation moment reduced the shear demand by approximately one half, some of the values of r_{cv} were below 1.0. At Location 1, where r_{cv} was 0.9, the results are an artifact of the ATC-6-2 procedure. At Location 2, the low values of r_{cv} (0.9) are due to low values of r_{ec} (0.2).

6.3 EVALUATION OF BEAMS

In this section, the shear vulnerability of the WSDOT unit is again quantified in terms of capacity-to-demand ratios. The shear capacities, V_n, were computed with Equation 6.1, the ATC-6-2 equations listed in Table 6.1, and the material properties listed in Table 4.1. No axial forces were considered in computing the beam and girder shear capacities. The shear demands were obtained from the nonlinear analyses (Ch. 4). Because member shears were larger for the fixed-base condition than for the pinned-base condition, this section considers only the shears corresponding to the fixed-base condition.

Shear diagrams for a bottom-deck beam are shown in Figure 6.3 for several levels of base shear near the interior frame's lateral-force capacity (360 kips). For comparison, the figure also shows the computed shear capacities. The reduction of capacity toward the center of the beam is a result of the increased stirrup spacing. Shear failure is unlikely (even if the shear demand were to increase by a factor of 1.3) because the capacities greatly exceed the demands at all cross sections. The top-deck beam (Fig. 6.4) and the exterior-frame beams are even less likely to fail in shear.

The shear diagrams along the bottom-deck girder are shown in Figure 6.5 for the exterior span, and the diagrams for the central spans are shown in Figure 6.6. Again, the capacities greatly exceeded the demands. Similar analyses indicate that the top-deck girders are similarly unlikely to fail in shear.
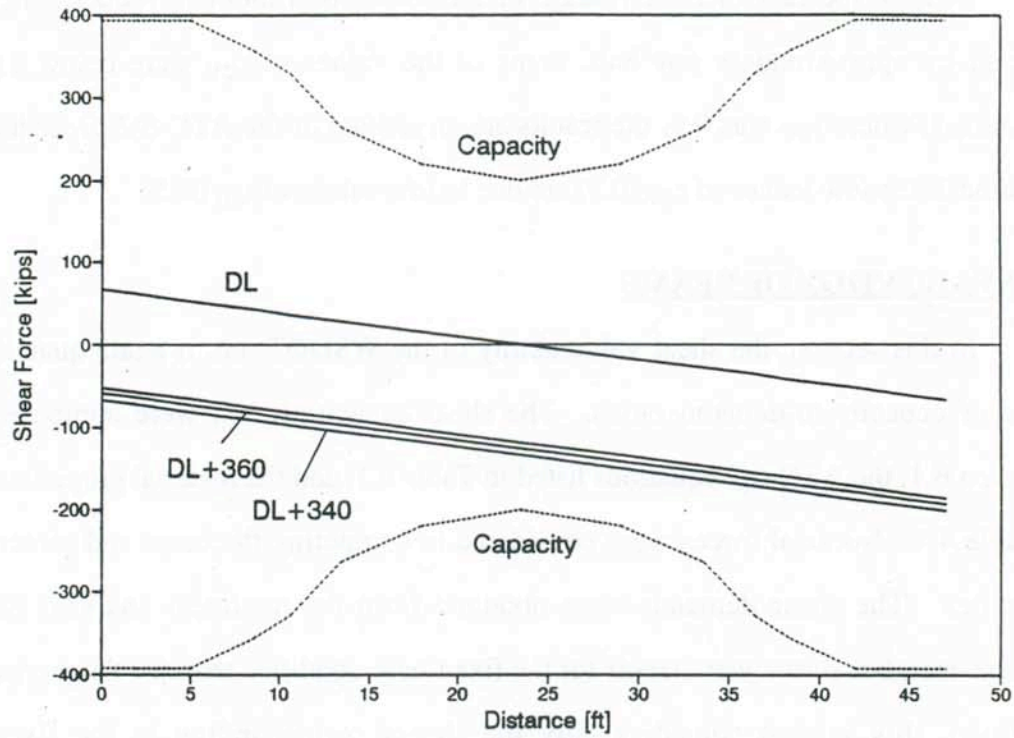
Figure 6.3. Shear Diagrams for Interior-Frame, Bottom-Deck Beam (Fixed Base)
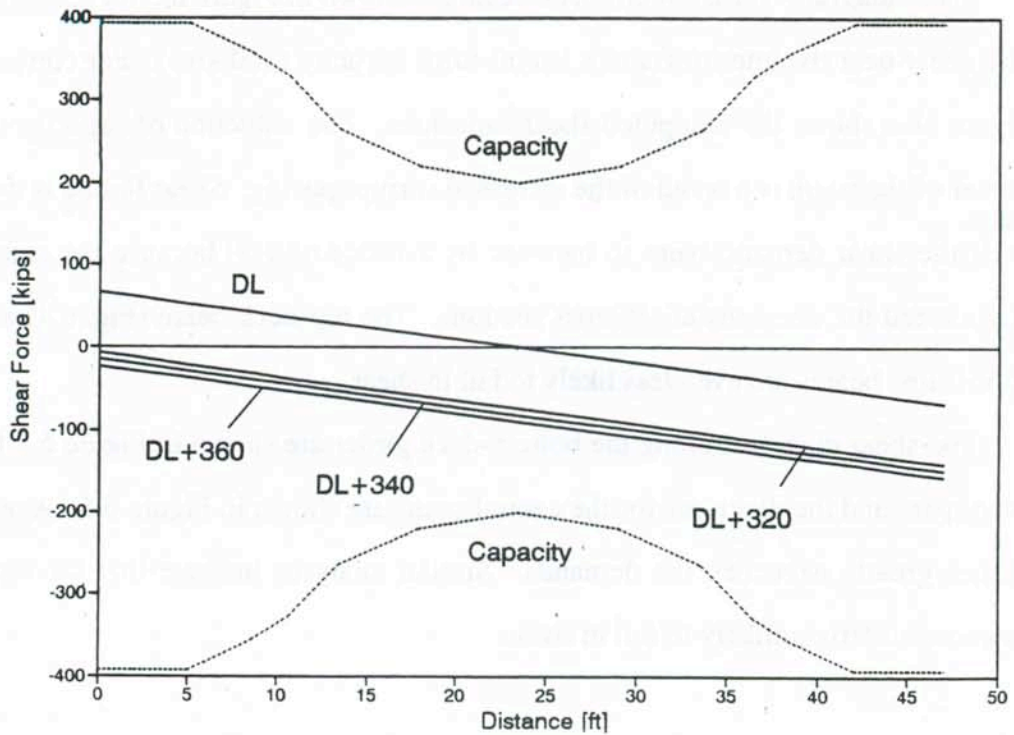

Figure 6.4. Shear Diagrams for Interior-Frame, Top-Deck Beam (Fixed Base)
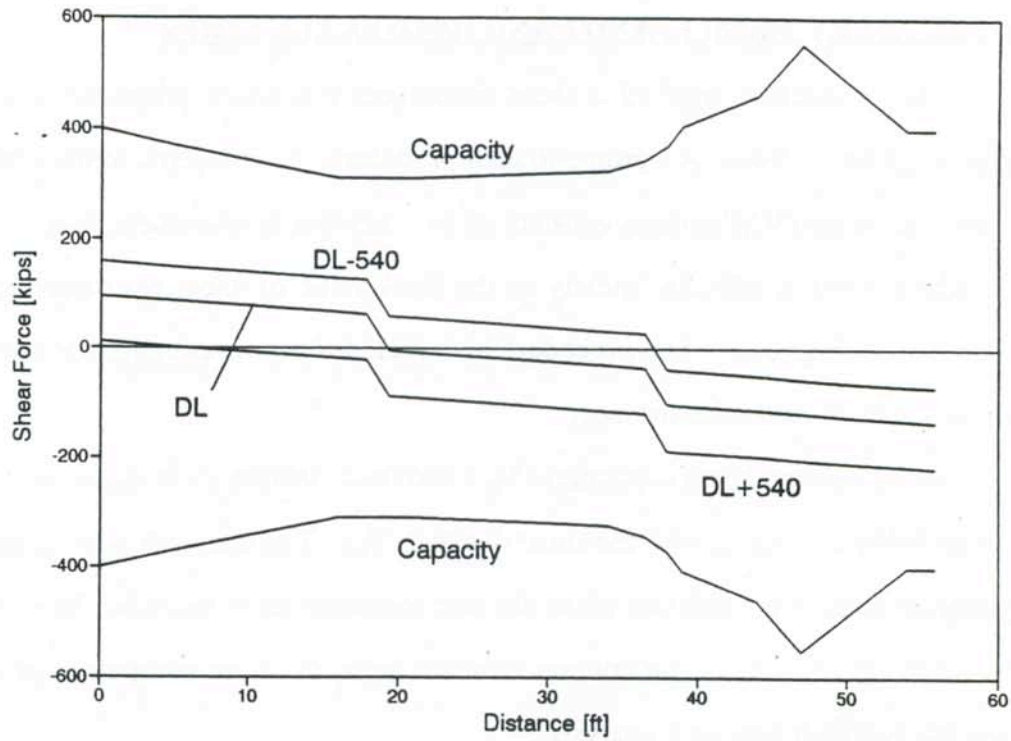
Figure 6.5. Shear Diagrams for Bottom-Deck Girder: Exterior Span (Fixed Base)
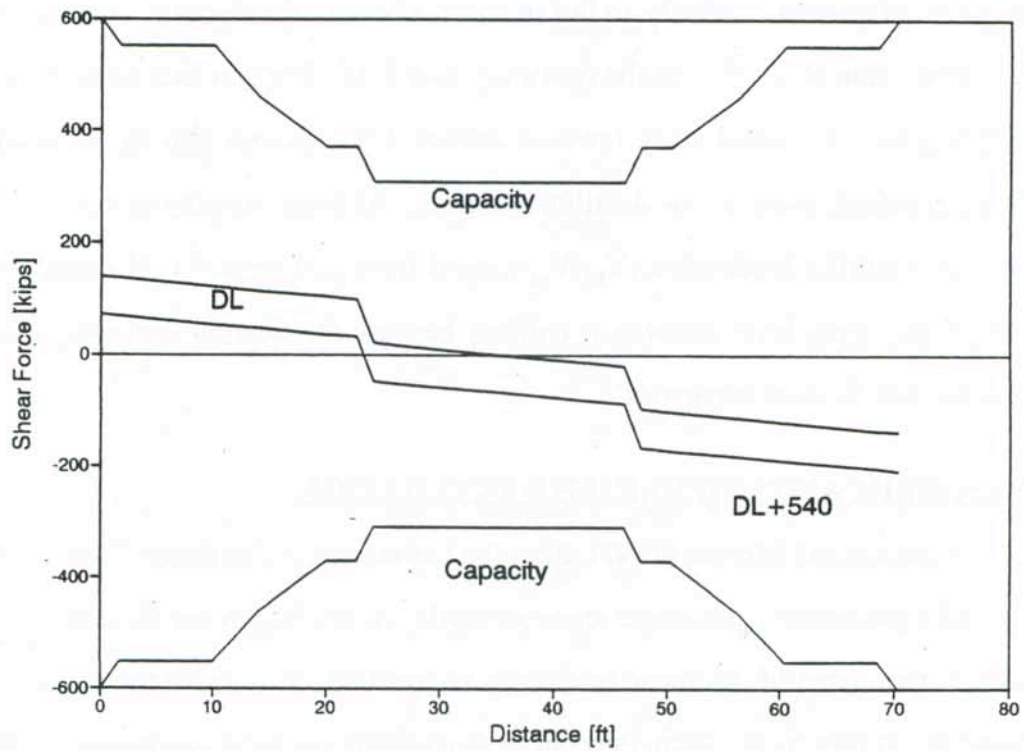
Figure 6.6. Shear Diagrams for Bottom-Deck Girder: Central Span (Fixed Base)

99

6.4 PRIESTLEY, SEIBLE, AND UANG (1994) EVALUATION

The researchers applied a shear-assessment procedure proposed by Priestley, Seible, and Uang (1994). According to their procedure, the concrete's initial contribution to shear resistance (V_{ci}) remains constant up to a member displacement ductility equal to 2, at which point it reduces linearly to the final value of shear resistance (V_{cf}) at a ductility of 4 (Fig. 6.2). The procedure also includes a new equation to compute the influence of axial load on resistance.

Initial column shear capacities (V_{ni}) and final column shear capacities (V_{nf}) are listed in Table 6.4, along with the shear demand, V_{uf}. The demands were computed by considering column equilibrium when ultimate moments act at its ends. As in the ATC-6-2 evaluation (Sec. 6.2), the column ultimate moments were computed for the axial loads obtained with nonlinear analysis.

The initial and final capacity-to-demand ratios (V_{ni}/V_{uf}, V_{nf}/V_{uf}) indicate that the first-story columns are unlikely to fail in shear, even at high ductility demands ($\mu \geq 4$). The lowest value of V_{nf}/V_{uf} in the first story was 1.23. The fact that most of the values of V_{ni}/V_{uf} in the second story hovered around 1.0 indicates that these columns are potentially brittle, even at low ductility demands. At large ductility demands, the shear capacities would be inadequate (V_{nf}/V_{uf} ranged from 0.51 to 0.74). Nonetheless, shear failure of the upper-level columns is unlikely because the flexural demands are unlikely to exceed their flexural capacities.

6.5 ASCHEIM AND MOEHLE (1992) EVALUATION

Ascheim and Moehle (1992), from the University of California, Berkeley (UCB), proposed a procedure to compute shear strength. According to the their procedure, the concrete's contribution to shear resistance is constant up to a displacement ductility demand of 1.0 (Fig. 6.2). Then, the concrete's contribution decreases linearly with ductility demand until a ductility demand of 4.0, at which point its contribution is equal to 0.0.

Table 6.4. Priestley et al. (1994) Shear Evaluation for Columns

Frame	Level	Seismic Axial Force	Column Dimensions				Bottom Moment	Top Moment	Axial Load
			Length	c1	c2	D'			
			[ft]	[ft]	[ft]	[in.]	[kip-ft]	[kip-ft]	[kips]
Exterior	Bottom	comp	29	4	2	43	2022	2022	510
Frame		tens	29	4	2	43	1722	1723	274
Transverse	Top	comp	14.7	4	2	43	1683	3259	242
Direction		tens	14.7	4	2	43	1557	3151	143
Exterior	Bottom	comp	29	2	4	19	957	957	430
Columns		tens	29	2	4	19	801	801	232
Longitudinal	Top	comp	14.7	2	4	19	766	1619	188
Direction		tens	14.7	2	4	19	726	1578	137
Interior	Bottom	comp	29	4	3.5	43	3250	3667	1009
Frame		tens	29	4	3.5	43	2667	3000	560
Transverse	Top	comp	14.7	4	3.5	43	3416	3750	475
Direction		tens	14.7	4	3.5	43	2833	3583	296
Interior	Bottom	comp	29	3.5	4	37	2642	2917	851
Columns		tens	29	3.5	4	37	2642	2917	831
Longitudinal	Top	comp	14.7	3.5	4	37	2500	2825	418
Direction		tens	14.7	3.5	4	37	2500	2825	407

Initial Concrete Capacity V_{ci} [kips]	Final Concrete Capacity V_{cf} [kips]	Steel Contrib. V_s [kips]	Compressi Block Depth c [in.]	Tangent of Angle Alpha	Axial-Load Contrib. V_p [kips]	Total Initial Capacity V_{ni} [kips]	Total Final Capacity V_{nf} [kips]	Shear at Flexural Capacity V_{uf} [kips]	Initial C/D Ratio (mu=2)	Final C/D Ratio (mu=4)
216	74	60	12	0.10	53	329	187	139	2.36	1.34
216	74	60	12	0.10	28	305	163	119	2.57	1.37
216	74	60	12	0.20	49	326	184	336	0.97	0.55
216	74	60	12	0.20	29	306	163	320	0.95	0.51
216	74	27	6	0.05	22	265	123	66	4.02	1.86
216	74	27	6	0.05	12	255	113	55	4.62	2.04
216	74	27	6	0.10	19	262	120	162	1.62	0.74
216	74	27	6	0.10	14	257	115	157	1.64	0.73
379	130	60	12	0.10	104	543	294	239	2.28	1.23
379	130	60	12	0.10	58	497	248	195	2.54	1.27
379	130	60	12	0.20	97	536	287	487	1.10	0.59
379	130	60	12	0.20	60	499	250	436	1.14	0.57
379	130	52	10.5	0.09	77	507	259	192	2.65	1.35
379	130	52	10.5	0.09	75	506	257	192	2.64	1.34
379	130	52	10.5	0.18	75	505	256	362	1.39	0.71
379	130	52	10.5	0.18	73	503	254	362	1.39	0.70

Notes: $f'c$ = 4500 psi a_s = 0.11 in.2   Cover = 2.5
         f_{yt} = 44000 psi A_v = 0.22 in.2   Spacing = 12

The researchers applied this procedure to the first-story columns of a typical interior frame. For a first-story mechanism, the overall ductility demands and the first-story column ductility demands are equal. At a displacement ductility of 2.0, which is consistent with the ATC-6 spectrum, the computed capacity-to-demand ratios were approximately equal to 2.0 in the first story. However, at a ductility of 4.0, which is consistent with the worst-case, site-specific spectra (Table 5.5, fixed base), the procedure indicates that the concrete's contribution to shear strength drops to zero. Since the contributions of the axial load and transverse reinforcement are small (120 to 160 kips), the column shear resistance is inadequate.

6.6 COMBINED ASSESSMENT

Despite variations among the procedures, a number of conclusions can be drawn:

1. Beam shear failure is unlikely.

2. Shear failure of the second-story columns is unlikely, unless the splices significantly reduce the columns' shear capacity.

3. Shear failure of the first-story columns would be unlikely if the ground motion is well represented by the ATC-6 spectrum.

4. If the worst-case site-specific spectra represent the actual ground-motions well, the factor of safety against shear failure of the first-story columns would be small. Following the ATC-6-2, the researchers obtained values of r_{cv} as low as 0.9. The Priestley, Seible, and Uang (1994) assessment was more optimistic than the ATC-6-2 assessment, but the factor of safety was only 1.2. According to the Ascheim and Moehle (1992) assessment procedure, the column shear strength is inadequate at large ductility demands.

CHAPTER 7

ANCHORAGE

Inadequate anchorage of the longitudinal reinforcement can decrease flexural and shear capacities. To gain insight into the adequacy of the anchorage conditions, the researchers implemented the evaluation procedures proposed by ATC-6-2 (1983) and by Priestley, Seible, and Chai (1992).

7.1 ATC-6-2 EVALUATION

The ATC-6-2 guidelines provide a procedure for evaluating the adequacy of the column confinement conditions. In this section, this procedure is applied to the columns of the WSDOT typical unit. In addition, the ATC-6-2 development-length expressions are used to characterize the anchorage conditions at the ends of the beams and girders.

Procedure

For straight bars, the required anchorage length, $\ell_a(d)$, is defined as follows:

$$\ell_a(d) = \frac{k_s d_b}{\sqrt{f'c}\left(1 + \frac{2.5c}{d_b} + k_{tr}\right)} \geq 30\,d_b \tag{7.1}$$

where, k_s = reinforcing steel constant = $\dfrac{f_y - 11000}{4.8}$

d_b = bar diameter

$f'c$ = concrete compressive strength (psi)

f_y = yield stress of steel (psi)

c = lesser of clear cover or one half clear spacing between bars

k_{tr} = factor that accounts for effect of transverse confinement

For anchorage with hooked ends, ATC-6-2 provides another expression to define $\ell_a(d)$:

$$\ell_a(d) = \frac{k_m\,1200\,d_b\,f_y}{60000\,\sqrt{f'c}} \geq 15\,d_b \tag{7.2}$$

where, k_m =   0.7 for #11 bars or smaller, adequate side cover, and adequate end cover

k_m =   1.0 for all other cases

The anchorage capacity, $\ell_a(c)$, for straight bars is defined as the actual embedment length. For hooked bars, ATC-6-2 defines $\ell_a(c)$ as the portion of the embedment length preceding the hook. If the anchorage length is insufficient ($\ell_a(c)\ell_a(d)$), then the anchorage C/D ratio, r_{ca}, is a function of the column flexural C/D ratio, r_{ec}.

$$r_{ca} = \frac{\ell_a(c)}{\ell_a(d)} \ r_{ec} \tag{7.3}$$

On the other hand, if the anchorage length is sufficient ($\ell_a(c)\ell_a(d)$), then the anchorage C/D ratio depends on the anchorage details and the footing flexural C/D ratio, r_{ef}. The viaduct's footings have no top reinforcement, and the column starter bars terminate with a 90° hook pointing away from the column centerline. For this detail, r_{ca} is given as follows:

$$r_{ca}=1.3 \ r_{ef} \tag{7.4}$$

Implementation

Table 7.1 lists the computed values of the anchorage demands, $\ell_a(d)$, for the typical unit. In computing these demands, c was assumed as 2.0 inches, and k_{tr} was conservatively assumed as zero. The concrete compressive strength was assumed as 3300 psi in the footings (#11 hooked and #13 hooked), and the compressive strength was assumed as 4500 psi everywhere else. For all bar sizes, the straight-bar anchorage length was approximately equal to 30 bar diameters, and the hooked-bar anchorage length was approximately equal to 15 bar diameters.

Table 7.1. Required Embedment Lengths

| Bar Size | ATC-6-2 $l_a(d)$ | | UCSD |
	straight bars [in.]	hooked bars [in.]	ls_{min} [in.]
#9	NA	17	16
#11	42	21^1	19
#13	49	25^1	22
#17	65	33	29

Note 1: $f'_c = 3300$ psi

The footing flexural C/D ratio, r_{ef}, is equal to the flexural capacity of the footing divided by the moment demand. The flexural strength of the footings was calculated by means of the same procedure that was used to compute column strengths (Chapter 3). The researchers neglected the contribution to resistance provided by the concrete's tensile strength.

The footing moment demands were assumed to be the same as those computed at the base of the columns with linear analysis (Table C.1). As discussed in Chapter 10, this assumption may be overly conservative because the column moment exceeds the footing moment at the column face. For the exterior footings, which support two columns from adjacent units, the moment demand was computed for two conditions. First, the moment demand was computed for one column only. Then, the moment demand was set equal to twice the moment from one exterior column.

Anchorage C/D Ratios

For all of the footings, the anchorage length of the starter bars appears to be adequate; i.e., $\ell_a(c)$ exceeds the required anchorage length, $\ell_a(d)$ (Table 7.2). However, if the footings experience large flexural ductility demands, the anchorages may still be

Table 7.2. Anchorage C/D Ratios at Base of Columns, rca

Location		Footing Capacity Kip-ft	Moment Kip-ft	Ref	Bar Size	la(c) in.	la(d) in.	la(c)/la(d)	Rec	Rca
Ext Trans	1 Col.	1925	3620	0.53	#13	27	24.9	1.08	0.56	0.69
	2 Col.	1925	7240	0.27	#13	27	24.9	1.08	0.56	0.35
Ext Long	1 Col.	2263	1395	1.62	#13	27	24.9	1.08	0.61	2.11
	2 Col.	2263	2790	0.81	#13	27	24.9	1.08	0.61	1.05
Int Trans	1 Col.	2150	6138	0.35	#11	33	21.2	1.56	0.53	0.46
Int Long	1 Col.	2263	6386	0.35	#11	33	21.2	1.56	0.43	0.46
Notes:	$f'c=$ 3300		$fy=$ 44000		$c=$ 2.0					

Table 7.3. Anchorage Conditions for Beams, Girders, and Top of Columns

Location			Bar Size	la(c) in.	la(d) in.	la(c)/la(d)	Rmem (worst case)
Beams	Exterior	+ Mom	#13 str	34	48.8	0.70	0.50
		- Mom	#13 hook	42	24.9	1.69	0.98
	Interior	+ Mom	#17 str	40	65.0	0.62	0.94
		- Mom	#17 hook	42	32.6	1.29	1.46
Girder	at Exterior Column	+ Mom	#17 str	21	65.0	0.32	2.77
			#17 hook	21	32.6	0.65	2.77
		- Mom	#9 hook	21	16.9	1.24	0.80
Columns	Ext Col	Top	#13 str	46	48.8	0.94	1.89
	Int Col	Top	#11 str	62	42.3	1.47	1.96
Notes:	$f'c=$ 4500		$fy=$ 44000		$c=$ 2.0		

vulnerable because the footings do not have top reinforcement. According to Equation 7.4, the anchorage conditions are inadequate for locations that yield and at which r_{ef} is less than $1/1.3 = 0.8$.

According to the results summarized in Table 7.2, the exterior footings are likely to reach their flexural strengths if the exterior columns from adjacent frames develop their capacities at the same time ($r_{ef} < r_{ec}$). However, the exterior footings are unlikely to yield as a result of longitudinal motion of the typical unit. The interior footings are likely to develop their capacities for both transverse and longitudinal motion. Consequently, according to ATC-6-2, the anchorage of the starter bars is inadequate ($r_{ca} < 1$). Moreover, these ratios would decrease if the ground-motion intensity were well characterized by the worst-case, site-specific spectrum. On the other hand, the computed anchorage C/D ratios would increase if foundation flexibility were included in the model.

To gain additional insight into the vulnerability of the anchorages, the evaluation team considered the beams, girders, and tops of columns. At each location, the researchers computed the ratio $l_a(c)/l_a(d)$ and the flexural C/D ratio (Table 7.3). The results can be summarized as follows:

- As is typical in many older bridges, the beam reinforcement is adequately anchored to resist negative moments (all bars terminate with hooks), but the anchorage is inadequate to resist large, positive moments.

- The girder anchorages appear to be much less vulnerable than the beam anchorages. Two-thirds of the positive moment reinforcement terminates with a hook, and the moment demands are likely to be small ($r_{ec} = 2.77$).

- Anchorage at the tops of the columns is adequate because the provided anchorage lengths approach or are equal to the required lengths. Moreover, the moment demands are small in the second story.

107

7.3 PRIESTLEY, SEIBLE, AND CHAI (1992) EVALUATION

Procedure

.Priestley et al. (1992) also recommend procedures to evaluate bar anchorages. According to their report (and other references), the type of failure depends on whether sufficient confining stress is provided by transverse reinforcement, by longitudinal reinforcement, or by member forces.

If enough confinement is provided and maintained, it is assumed that the average bond stress can reach a maximum intensity, μ_u. An example of a confined condition is the beam reinforcement passing through a beam-column joint in which the column's longitudinal reinforcement and compressive axial load provide large confinement. For this condition, the anchorage evaluation consists of comparing the anchorage length of a bar with the length required to limit the average bond stress, μ_u, to $18\sqrt{f'c}$ (psi)   . Assuming that the bar's ultimate strength is equal to 1.5 times its yield stress, it can be shown that the minimum anchorage length, ls_{min}, is given by the following equation:

$$ls_{min} = \frac{1.5 \cdot A_b \cdot f_y}{\pi \cdot d_b \cdot \mu_u} = 0.021 \frac{d_b \cdot f_y}{\sqrt{f'_c}} \qquad (7.5)$$

where, A_b = area of the reinforcing bar [in.^{2}]

d_b = diameter of the reinforcing bar [in.]

f_y = yield stress of the steel [psi]

. f'_c = compressive strength of the concrete [psi]

μ_u = maximum average bond stress between concrete and steel [psi]

For f_y = 44 ksi and f'_c = 4500 psi, Table 7.1 lists the minimum lengths computed for the bar sizes used in the beams, girders, and columns of the WSDOT-designed section.

A second type of failure is likely when insufficient confinement is pesent. An example of this condition is a column's exterior reinforcement that is anchored in a beam-

108
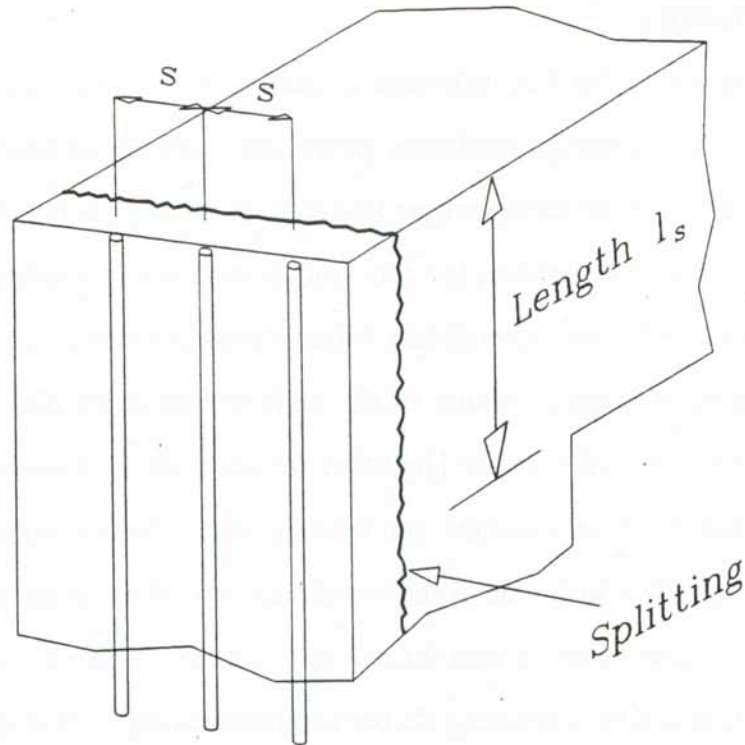
Figure 7.1. Cracking Pattern Associated with Unconfined Anchorage Failure

column knee joint with little transverse reinforcement. This type of failure, illustrated in Figure 7.1, is characterized by splitting cracks parallel to the anchored bars. In this example, the column's interior-face reinforcement can also be in the unconfined condition if the beam reinforcement yields. Anchorage evaluation for this condition is based on the concrete's resistance to splitting in the plane defined by the anchored bars. If no transverse reinforcement is placed in the joint, the maximum force, T_s, that can be developed by each bar is as follows:

$$T_s = f_t \cdot l_s \cdot s \qquad (7.6)$$

where, f_t = concrete resistance, assumed equal to $4\sqrt{f'_c}$ [psi]

l_s = anchorage length [in.]

s = bar spacing [in.] (Fig. 7.1)

Vulnerability

A summary of the bar anchorage evaluation is presented in Table 7.4 for the exterior joints. Bar anchorage conditions for the transverse-frame beams are summarized in the upper portion of the table, and the longitudinal-frame girders are considered in the lower portion. For each frame, the top- and bottom-level members are considered separately. Because the condition of bars within a joint can vary with the direction of the bending moments, the third column of the table indicates the direction of moments considered. Four sets of bars are identified for each joint. Letters a and b refer to exterior and interior bars of columns, and letters c and d identify top and bottom bars of beams and girders. The anchorage condition of each type of bar is discussed below.

Type-a column bars of top-level joints are not confined, and consequently, anchorage is evaluated by comparing the bar's splitting force, T_s, with its tensile strength, T_u. Based on this comparison, it appears that the top-deck type-a bars cannot develop their ultimate strength because concrete splitting would limit the tensile force to approximately 80 to 90 percent of T_u. Although the ratios of T_s to T_u for these bars indicate that anchorage failure can occur, such a failure is unlikely because flexural demands are small for the upper-story columns (see Chapters 3 and 4). Type-a bars of lower-level joints are adequately anchored because the anchorage length, l_s, is large. For these bars, the splitting force, T_s, is 40 percent higher than the bar's tensile strength, T_u.

The anchorage conditions for the type-b bars are the same as that of the type-a bars when the type-d bars yield and confinement is lost. If the type-b bars are assumed to be confined, the anchorage evaluation is reduced to a comparison of the l_s with ls_{min}. This comparison is equivalent to verifying that the average bond stress does not exceed $\mu_u = 18 \sqrt{f'_c}$ (psi) . Anchorage failure for these confined cases is unlikely because l_s/ls_{min} exceeds 2.0 at all locations.

The anchorage condition of the type-c bars appears to be adequate. These bars extend to the outside face of the column, and the bars end with a hook.

Table 7.4. Priestley et al. (1992) Anchorage Evaluation

TRANSVERSE DIRECTION

Frame	Deck Level	Moment	Bar ID	Bar #	Location	Condition	s [in.]	Length, ls [in.]	Ts [kips]	Tu [kips]	Ts/Tu Ratio	ls/lsmin
Exterior	Top Level	(-)	a	13	Column/Ext	-	7.3	48.5	91.1	114.1	0.80	-
		(+)	b	13	Column/Int	d yields	7.3	48.5	91.1	114.1	0.80	-
						d doesn't yield						2.1
		(-)	c	13	Beam/Top	-		Hooked Bar				-
		(+)	d	13	Beam/Bot	b yields	16	34	146.0	114.1	1.28	-
						b doesn't yield						1.5
	Bottom Level	(-)	a	13	Column/Ext	-	7.3	82.5	161.6	114.1	1.42	-
		(+)	b	13	Column/Int	c and d yield	7.3	82.5	161.6	114.1	1.42	-
						no yield						3.7
		(-)	c	13	Beam/Top	-		Hooked Bar				-
		(+)	d	13	Beam/Bot	b yields	16	34	146.0	114.1	1.28	-
						b doesn't yield						1.5
Interior	Top Level	(-)	a	11	Column/Ext	-	5.7	48.5	71.1	81.7	0.87	-
		(+)	b	11	Column/Int	d yields	5.7	48.5	71.1	81.7	0.87	-
						d doesn't yield						2.4
		(-)	c	17	Beam/Top	-		Hooked Bar				-
		(+)	d	17	Beam/Bot	b yields	16	40	171.7	195.1	0.88	-
						b doesn't yield						1.4
	Bottom Level	(-)	a	11	Column/Ext	-	5.7	74.5	113.9	81.7	1.40	-
		(+)	b	11	Column/Int	c and d yield	5.7	74.5	113.9	81.7	1.40	-
						no yield						3.8
		(-)	c	17	Beam/Top	-		Hooked Bar				-
		(+)	d	17	Beam/Bot	b yields	16	40	171.7	195.1	0.88	-
						b doesn't yield						1.4

LONGITUDINAL DIRECTION

Frame	Deck Level	Moment	Bar ID	Bar #	Location	Condition	s [in.]	Length, ls [in.]	Ts [kips]	Tu [kips]	Ts/Tu Ratio	ls/lsmin Ratio
(Exterior)	Top Level	(-)	a	13	Column/Ext	-	7.5	46.5	93.6	114.1	0.82	-
		(+)	b	13	Column/Int	d yields	7.5	46.5	93.6	114.1	0.82	-
						d doesn't yield						2.1
		(-)	c	9	Girder/Top	-		Hooked Bar				-
		(+)	d/hook	17	Girder/Bot	-		2 of 3 bars end in a hook				-
	Bottom Level	(-)	a	13	Column/Ext	-	7.5	82.5	166.0	114.1	1.46	-
		(+)	b	13	Column/Int	c and d yield	7.5	82.5	166.0	114.1	1.46	-
						no yield						3.7
		(-)	c	9	Girder/Top	-		Hooked Bar				-
		(+)	d	17	Girder/Bot	-		2 of 3 bars end in a hook				

f'c = 4500 psi   fy = 44000 psi   fsu = 55000 psi

l_s for bars a and b

l_s for bar d

l_s for bars a and b

l_s for bar d
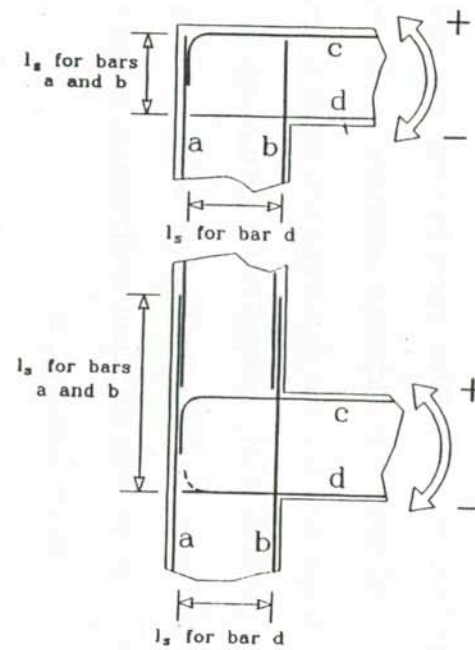
In the girders, two of the three type-*d* bars end in a hook, so anchorage failure of these bars is also unlikely. The anchorage conditions for the beam's type-*d* bars are less favorable. If one assumes that the anchorage evaluation is determined by the splitting resistance of the concrete, T_s/T_u is equal to 1.3 for the exterior beams, and it is equal to 0.9 for the interior beams. On the other hand, if the bars are assumed to be confined (i.e., bar *b* and the axial load provide sufficient confinement), the anchorage is sufficient for all the type-*d* bars. The ratio of l_s to ls_{min} is 1.4.

7.4 COMBINED ASSESSMENT

Despite the large differences between the ATC-6-2 and UCSD procedures, the results of the anchorage evaluations were consistent.

The anchorage conditions appear to be adequate at the following locations: ends of girders, ends of top-story beams, and tops of columns.

The anchorage conditions of the first-story beam's bottom bars is marginal, particularly for the interior frame. During intense ground motions that reduce the column's axial load (Table C.1), and which lead to large beam-moment demands, (Table C.2 and Fig. 4.10) anchorage failure is possible.

The anchorage lengths of the column starter bars appear to be adequate. However, the adequacy of the anchorage conditions cannot be determined without considering the behavior of the pile-supported footings, which is discussed in Chapter 10.

CHAPTER 8

SPLICES

. All of the column longitudinal bars are spliced at the column bases and in the second story, just above the lower deck. In this chapter, the effect of these splices on the behavior of the WSDOT-designed, typical unit is investigated. The splices' vulnerability is related to splice length, to the amount of confining steel, and to force and deformation demands. Splice failure can decrease a member's flexural and shear resistances to moments and to shears, especially if a splice experiences displacement reversals.

8.1 ATC-6-2 EVALUATION

Procedure

According to ATC-6-2, the area of transverse steel, $A_{tr}(d)$, required to prevent splice failure is computed as follows:

$$A_{tr}(d) = \frac{s\, f_y\, A_b}{l_s\, f_{yt}} \tag{8.1}$$

where, s = spacing of ties or hoops (in.)

A_b = area of spliced bar (in^2.)

l_s = splice length (in.)

f_{yt} = yield strength of transverse reinforcement (ksi)

The cross-sectional area of the transverse reinforcement is $A_{tr}(c)$. If the splice length is too short, ($l_s < 1860 d_b\sqrt{f_c}$), if the amount of transverse reinforcement inadequate ($A_{tr}(c) < A_{tr}(d)$), or if the tie spacing is too large ($s > 6$ in.), then the column splice C/D ratio, r_{cs}, is equal to the product of four non-dimensional factors:

$$r_{cs} = \frac{A_{tr}(c)}{A_{tr}(d)} * \frac{6}{s} * \frac{l_s}{\frac{1860}{\sqrt{f'_c}} d_b} r_{ec} < \frac{A_{tr}(c)}{A_{tr}(d)} r_{ec} \tag{8.2}$$

In Equation 8.2, the factor 6/s should not be taken as larger than 1.0, and $1860d_b/\sqrt{f_c}$ should not be taken as less than 30. If the minimum splice length was provided, then r_{cs} should not be less than $0.75r_{ec}$.

Column Splice C/D Ratios, r_{cs}

The ATC-6-2 splice evaluation calculations are summarized in Table 8.1. The splices were found to be deficient in three ways: (1) the area of transverse reinforcement is only 16 percent of that required; (2) the hoop spacing is twice that permitted; and (3) the splice length is only 66 to 74 percent of that required. Given Equation 8.2, r_{cs} for these splice details would be less than 1.0 for any location at which r_{ec} is less than 18.0. All the unit's splices were found to be deficient. The column splice C/D ratio ranged from 0.02 to 0.04 at the base of the columns, and it ranged from 0.05 to 0.12 at Location 3.

Table 8.1. Column Splice C/D Ratios, r_{cs}

			Bar Size	db in.	Ab in.^2	ls in.	s in.	Atr(c) in.^2
Exterior Column	Location 1	Trans.	#13	1.63	2.07	36	12	0.11
		Long.	#13	1.63	2.07	36	12	0.11
	Location 3	Trans.	#13	1.63	2.07	36	12	0.11
		Long.	#13	1.63	2.07	36	12	0.11
Interior Column	Location 1	Trans.	#11	1.41	1.56	28	12	0.11
		Long.	#11	1.41	1.56	28	12	0.11
	Location 3	Trans.	#11	1.41	1.56	28	12	0.11
		Long.	#11	1.41	1.56	28	12	0.11

			A(c)/Atr(d)	6/s	ls/lsmin	Rec	Rcs
Exterior Column	Location 1	Trans.	0.159	0.50	0.74	0.49	0.03
		Long.	0.159	0.50	0.74	0.61	0.04
	Location 3	Trans.	0.159	0.50	0.74	1.96	0.12
		Long.	0.159	0.50	0.74	0.92	0.05
Interior Column	Location 1	Trans.	0.165	0.50	0.66	0.46	0.02
		Long.	0.165	0.50	0.66	0.43	0.02
	Location 3	Trans.	0.165	0.50	0.66	1.88	0.10
		Long.	0.165	0.50	0.66	2.72	0.15

Notes: ATC Spectrum, Fixed-Base Condition;   f'c= 4500 psi

114

8.2 PRIESTLEY, SEIBLE, AND CHAI (1992) EVALUATION

Procedure

Splice failure is associated with the development of longitudinal cracks between bars and along the inner plane (Fig. 8.1). Priestley et al. (1992) provide recommendations to predict the flexural behavior of columns if all bars are spliced at the same location. The expected behavior varies according to the relative values of the maximum force that can be developed between lapped bars T_b, the bar yield force T_y, and the bar strength, T_u. According to Priestley et al. (1992), the magnitude of the axial force that can be transmitted between lapped bars depends on the splice length (l_s), the bar separation (s), the bar cover (c), and the concrete's compressive strength (f_c). For a rectangular column, T_b (in lb.) can be estimated by means of the following equation:

$$T_b = f_t \cdot p \cdot l_s \tag{8.3}$$

where, f_t = concrete resistance, assumed equal to $4\sqrt{f_c}$ (psi)

   p = length of concrete failure surface [in.] (see Figure 8.1b)

   l_s = splice length [in.]

As illustrated in Figure 8.1c, three ranges of T_b define the flexural response of column sections with spliced bars. First, if T_b is smaller than the bar yield force (i.e., $T_b < T_y$), the column splice will fail at a moment smaller than its yield moment M_y. Second, if T_b is larger than the bar yield force, but T_b is less than the bar strength (i.e., $T_y < T_b < T_u$), the column will reach the yield moment, M_y, but it will have limited ductility. The flexural capacity of such splices attains its maximum value at the curvature $\phi_{0.002}$, the curvature at which the maximum concrete compressive strain, ε_c, is 0.002. Finally, if T_b exceeds the bar strength, T_u, the column splice will not fail even at high ductilities.

115

a) Elevation

b) Cross Section A-A

$p = 2(c + d_b) + s/2$

c) Moment-Curvature Relationship
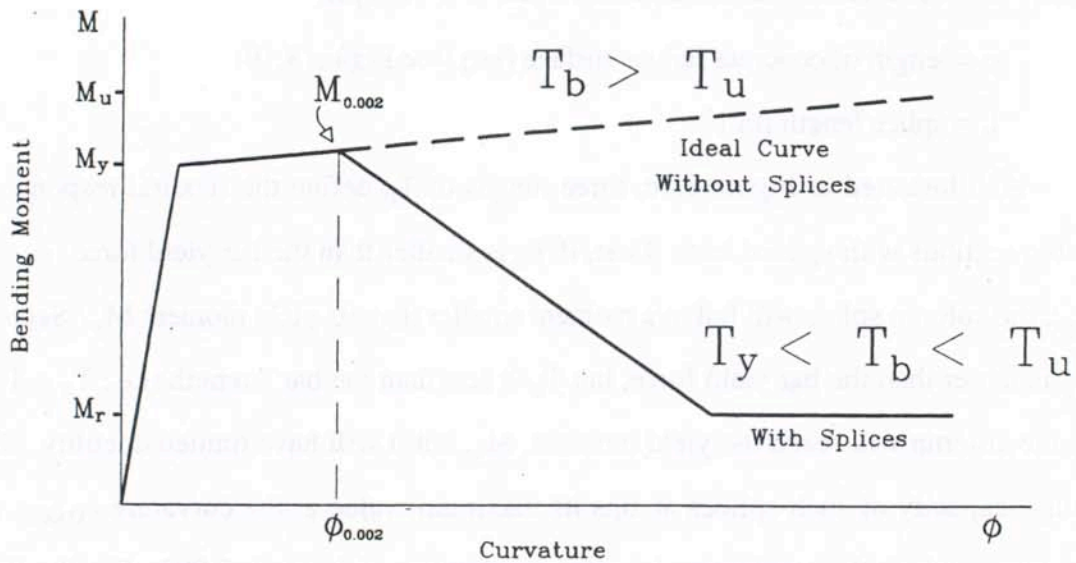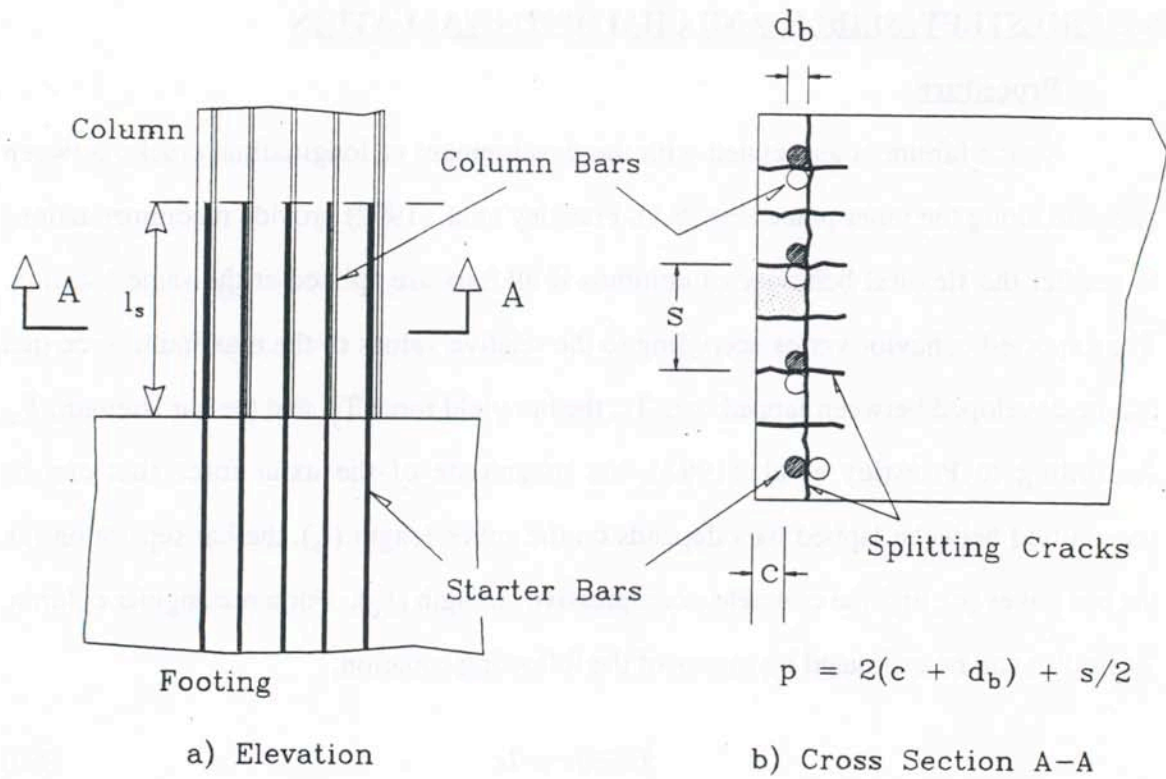
Figure 8.1. Priestley, Seible, and Chai (1992) Evaluation

116

Table 8.2. Splice Capacities

Direction	Column	$s^{(1)}$ [in.]	$p^{(2)}$ [in.]	l_s [in.]	T_b [kips]	T_y [kips]	T_u [kips]	T_b/T_y	T_b/T_u
Trans.	Interior	13	11.3	28	85	68.6	85.8	1.24	0.99
	Exterior	12	11.3	36	108.8	91.1	113.9	1.19	0.96
Long.	Interior	12	10.8	28	81.3	68.6	85.8	1.19	0.95
	Exterior	15	12.8	36	123.2	91.1	113.9	1.35	1.08

[1] see Figure 8.1b

[2] using conservatively $c = 1.0$ in.

Vulnerability

Values of T_b, T_y, and T_u are listed in Table 8.2 for the lower-level splices. Because $T_b > T_y$, it is expected that the splices could develop the bar's yield force. However, because the values of T_b are nearly equal to those of T_u (i.e. $T_b \approx T_u$), it is questionable whether the splices could repeatedly develop the column's ultimate moment, M_u. The results of the assessment would be more pessimistic if the steel's ultimate strength were assumed to exceed 55 ksi.

To estimate the effect of the splices on the frame's force-deflection response, a new set of nonlinear structural analyses was performed with updated moment-curvature relationships. Because the force T_b does not exceed T_u for splices where plastic hinges can occur, modified moment-curvature (M-ϕ) relationships were constructed with the shape shown in Figure 8.1c. The lateral response of the frames before a cross-section reaches $\phi_{0.002}$ is equal to the response without splices computed in Chapter 5. Because the frame's capacity is limited by the capacity of the sections with splices, the ultimate base-shear was attained when the splice curvature reached $\phi_{0.002}$. The unit's response beyond this point was not computed, and the displacement at which the cross-section reached $\phi_{0.002}$ was assumed to be the ultimate displacement. Table 8.3 lists the ultimate base shears and displacements. According to these results, the splice's main effect is to reduce the frame's displacement capacity by approximately 30 percent.

117

Table 8.3. WSDOT Unit Capacities Computed with Nonlinear Analysis

Direction of Analysis	Splice Failure?	Ultimate Base Shear[2] [kips]	Ultimate Displacement[1] [in.]	Base-Shear Reduction	Displacement Reduction
Transverse	No	1120	4.2		
	Yes	1060	3.1	5%	26%
Longitudinal	No	1080	3.7		
	Yes	1030	2.6	5%	30%

[1] Computed at the height of the resultant of seismic forces

[2] Computed as the sum of the ultimate base shear of both (ext. and int.) frames

Table 8.4. Displacement Capacities Calculated with Plastic-Hinge Analysis

Direction of Analysis	Column	Axial Load [kips]	$\phi_{0.002}$ [1/in.]	ϕ_u [1/in.]	Δ_y [in.]	Δ_p [in.]
Transverse	Interior	1000	0.00019	0.00045	2.2	1.1
	Exterior	390	0.00021	0.00048	1.9	1.3
Longitudinal	Interior	785	0.00026	0.00067	1.7	1.7

Table 8.5. Global Capacity-to-Demand Ratios[1]

Direction	Splice Failure?	Ultimate Displacement [in.]	V_E [kips]	$S_a(C)$ [g]	$\frac{Sa(C)}{Sa(D)_{ATC}}$	$\frac{Sa(C)}{Sa(D)_{SITE}}$
Trans.	No	5.4	2320	0.48	1.07	0.64
	Yes	3.2	1380	0.29	0.64	0.38
Long.	No	6.7	3220	0.67	1.43	0.89
	Yes	3.4	1630	0.34	0.72	0.45

[1] Ratios were computed using the displacements at the resultant of the seismic forces.

To account for the splice's effect on the unit's global capacity-to-demand ratios, the plastic-hinge analyses (Tables 5.2 and 5.3) were repeated with one modification: the ultimate curvature ϕ_u was replaced by $\phi_{0.002}$. The reduced displacement capacities are listed in Table 8.4. As illustrated in Table 8.5, a new set of capacities V_E were computed (based on stiffnesses listed in Table 5.3), and these capacities were compared with the acceleration demands for the ATC-6 and the site-specific spectra (Chapter 5). For comparison, Table 8.5 repeats the calculations for the structure without considering splices. According to the results of the analyses, splice failure greatly increases the unit's vulnerability. The capacity-to-demand ratios computed considering splice failure are approximately one-half the capacity-to-demand ratios computed without considering splice failure. The lowest capacity-to-demand ratio was 0.64 for the ATC-6 spectrum and 0.39 for the worst-case, site-specific spectrum.

Residual Moment

As illustrated in Figure 8.1c, Priestley et al. (1992) indicate that flexural capacity does not decrease to zero at $\phi_{0.002}$. Instead, the capacity decreases to a residual bending moment, M_r, which is the resistance provided solely by the column compression force. M_r is computed with the following expression (Fig. 8.2 and Table 8.6).

$$M_r = P\left(\frac{h'}{2} - \frac{a}{2}\right) \tag{8.2}$$

where, $a = P/(0.85f'_cb')$

P = axial load in the column

b' = width of the compression zone shown in Figure 8.2

h' = depth of the compression zone

Values of residual moments, M_r, as well as those of M_y and M_u, are listed in Table 8.6. The value of the residual moment, M_r, ranges between 35 and 60 percent of M_y, or equivalently, between 30 and 45 percent of M_u.

119

CHAPTER 9

JOINTS

9.1 INTRODUCTION

Current U.S. codes do not provide guidance on assessing the seismic vulnerability of joints that have little joint reinforcement. In fact, the "Seismic Retrofitting Guidelines for Highway Bridges" (ATC-6-2, 1983) do not address joints at all. The American Concrete Institute's Building Code (ACI, 1989) provides limits on the allowable joint-shear stress, but these limits are relevant only when the joints have a prescribed amount of joint reinforcement and proportions are such that the columns remain essentially elastic. No such reinforcement was placed in the viaduct's joints.

The joints were assessed on the basis of the nominal shear stress and the maximum tensile stress. The nominal shear stress has been used extensively to design joints (Meinheit and Jirsa, 1981). For structures with little or no joint reinforcement, Thewalt and Stojadinovic (1992) proposed limiting the nominal joint shear stress to $3.5 \sqrt{f_c}$ (psi). Priestley et al. (1992) proposed that joint vulnerability be assessed on the basis of the maximum tensile stress, f_{tmax}. They found that diagonal cracking in a joint begins when the nominal tensile stress exceeds $3.5 \sqrt{f_c}$ (psi).

9.2 EFFECTIVE JOINT AREAS

Before estimating the nominal joint stresses, one must first estimate the joints' effective area. For the typical unit, the joint areas are not uniquely defined by the beam and column dimensions. For example, the interior beams are much narrower than the interior columns. To estimate stresses resulting from transverse motion, the full column area was assumed to be effective (Fig. 9.1). This assumption is reasonable because the longitudinal girders will transfer horizontal forces to the columns through torsion. Furthermore, the longitudinal girders provide some joint confinement.

123
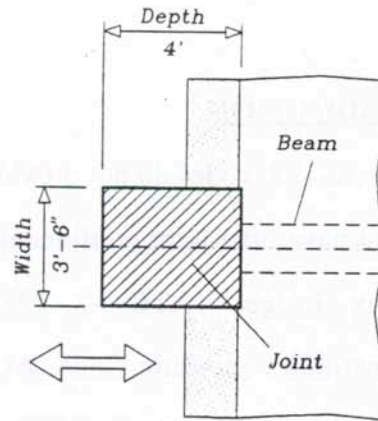
a) Interior Joints

b) Exterior Joints
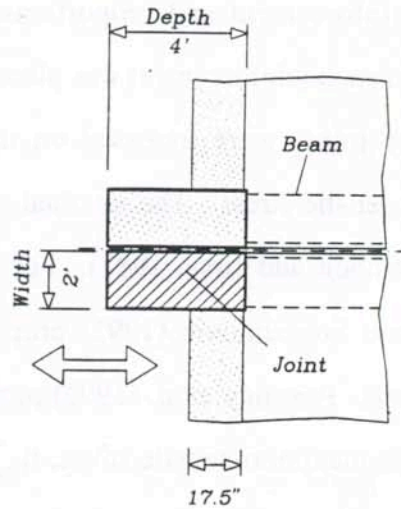
c) Joint Designations
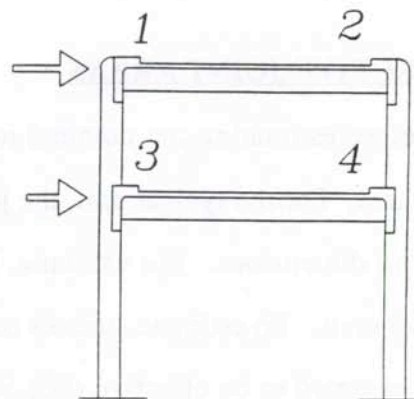
Figure 9.1. Joint Designations and Effective Areas for Transverse Response

In the longitudinal direction (Fig. 9.2), it was more difficult to estimate the effective joint areas. It would be unconservative to consider the full column width as the joint's effective width. On the other hand, it would be overly conservative to assume that the joint width is equal to the girder width. As a compromise between these extremes, the evaluation team used a simple approximation to estimate the area influenced by the longitudinal girder.

The width for the exterior joint was obtained by defining an area bounded by the girder face, the column faces, and a line starting at the girder's exterior edge and extending into the joint at a 45° angle to the girder centerline. This approximation was equivalent to assuming an interior joint width of 33 inches. For the interior joints, the 45° line does not intersect the column's back face. Therefore, half of the protruding column dimension was used to conservatively define the joint's effective width as 30 inches (Fig. 9.2).

9.3 EVALUATION BASED ON SHEAR STRESS

Estimates of the ultimate shear stresses, v_{ult}, were computed with the following expression:

$$v_{ult} = V_{ult} / (b_j d_j) \qquad (9.1)$$

where, V_{ult} = $(M_{ult}{}^L + M_{ult}{}^R)/z$

$M_{ult}{}^L$ = beam's or girder's ultimate moment (M_{ult}) at left of joint

$M_{ult}{}^R$ = beam's or girder's ultimate moment (M_{ult}) at right of joint acting in the same direction of $M_{ult}{}^L$

z = effective lever arm of the beams (51.4 in.) or girders (80 in.)

b_j = the effective width of the joint (see Section 9.2)

d_j = the effective joint depth

a) Interior
   Joints
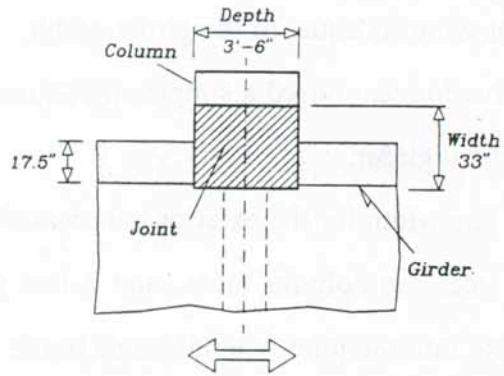
b) Exterior
   Joints
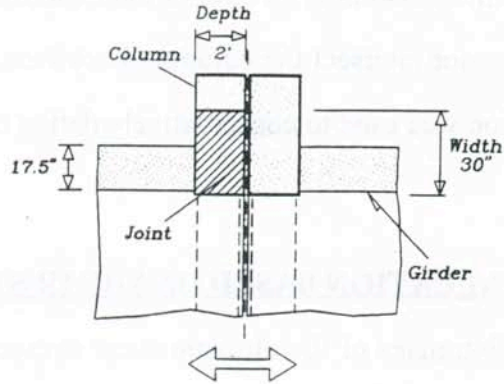
c) Joint
   Designations
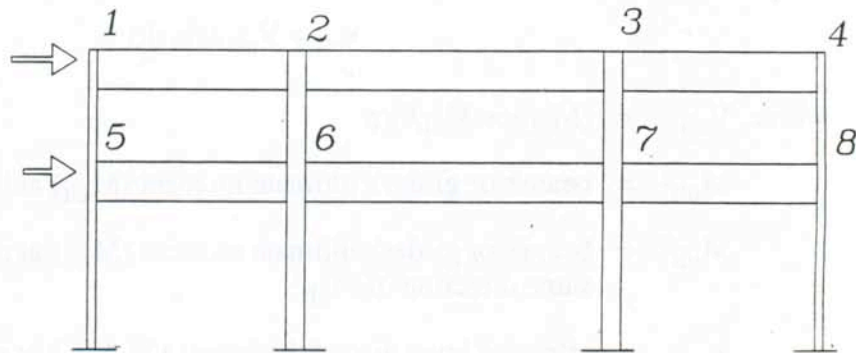
Figure 9.2. Joint Designations and Effective Areas for Longitudinal Response

126

In computing v_{ult}, the following assumptions were made:

- The beam and girder moment capacities were computed as 1.3 times the yield moments M_y, where M_y was computed for $f_y = 40$ ksi.

- For negative bending, it was assumed that the reinforcement within the slab's effective width (ACI, 1989) would be mobilized.

- The beam and girder moments were limited by the moments that the column capacities, M_{ult}, could equilibrate.

- Because it is difficult to estimate higher-mode effects, the researchers neglected the effect of the upper-story column shear on the lower-joint shear stress.

The normalized computed shear stresses, $v_{ult}/\sqrt{f_c}$, are listed in the second column of Table 9.1. Joint numbers are defined in Figure 9.1, and the results are discussed in Sections 9.5 and 9.6. A less conservative estimate of shear stresses, denoted by v_{nonl}, was made based on the bending moments computed with the nonlinear analyses (Chapter 4).

9.4 EVALUATION BASED ON MAXIMUM TENSILE STRESS

To compute the maximum tensile stress, f_{tmax}, each joint was assumed to be in a state of planar stress. As illustrated in Figure 9.3 for an exterior joint, the stress state depends not only on the beam moment, but also on the following: the column axial force (P), the column shear forces, the beam shear forces (V_g is due to gravity loads and V_s is due to seismic action), and the beam's axial force (T). Because it is difficult to estimate the beam axial forces and upper-column shear forces, these forces were neglected.

The other assumptions made in evaluating each joint type are consistent with the recommendations of Priestley et al. (1992). In the transverse direction (Fig. 9.1), the beam's seismic shear force, V_s, at joints 1 and 3 acts upwards when transverse forces act from left to right. Consequently, an upward force equal to $V_s - V_g - P$ was assumed to act on these joints (the seismic shear force, V_s, was computed by considering beam equilibrium when the ultimate moments ($1.3M_y$) act at its ends). The normal stress, p, is

Table 9.1. Nominal Joint Stresses[1]

| Joint Location | Slab Reinforcement Included | | | No Slab Reinf. |
	$v_{ult}/\sqrt{f_c}$	$v_{nonl}/\sqrt{f_c}$	$f_{tmax}/\sqrt{f_c}$	$v_{ult}/\sqrt{f_c}$
1-Transv/Int.	**2.7**	**2.5**	**2.9**	**2.7**
2-Transv/Int.	**6.5**	**4.1**	**6.5**	**3.1**
3-Transv/Int.	2.7	2.9	1.8	2.7
4-Transv/Int.	8.3	7.1	7.0	4.5
1-Transv/Ext.	**2.8**	**2.5**	**3.0**	**2.8**
2-Transv/Ext.	**6.5**	**4.0**	**6.5**	**3.4**
3-Transv/Ext.	2.8	2.7	1.9	2.8
4-Transv/Ext.	7.2	6.2	6.0	4.1
1-Longitudinal	**5.0**	**1.2**	**5.0**	**5.0**
2-Longitudinal	**4.6**	**2.3**	**4.6**	**4.6**
3-Longitudinal	**4.6**	**2.5**	**4.6**	**4.6**
4-Longitudinal	**5.0**	**2.6**	**5.0**	**3.2**
5-Longitudinal	5.2	4.6	3.8	5.2
6-Longitudinal	8.7	7.7	7.0	8.7
7-Longitudinal	8.7	7.9	6.9	8.7
8-Longitudinal	5.0	5.5	3.3	3.2

[1] See Figure 9.1 for joint designations. Upper-deck joints are typed in boldface.

128
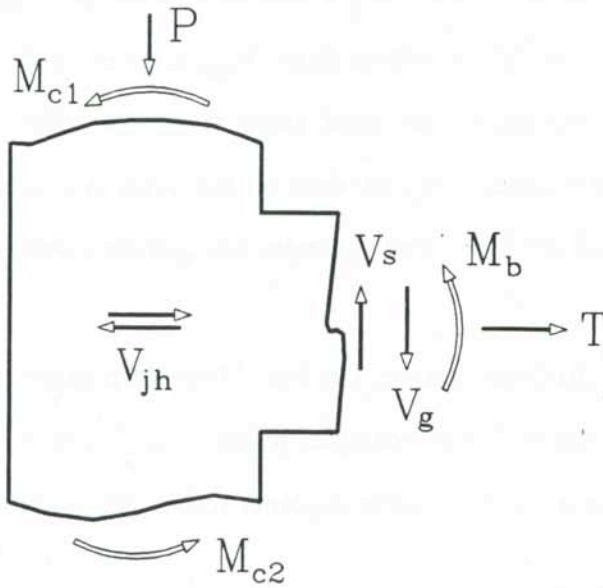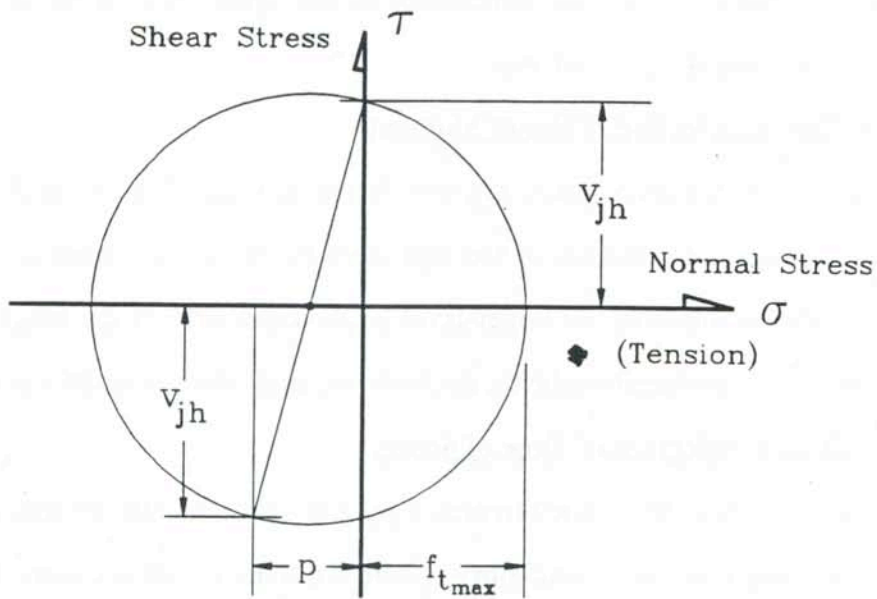
a) Joint Forces

b) Stress State

Figure 9.3. Idealized Joint Forces and Stress State

equal to the vertical force (V_s-V_g-P) divided by the joint area, and the horizontal shear stress, v_{ult}, is equal the joint shear force, V_{ult}, divided by the joint area. In the transverse direction, the seismically-induced shear force for joints 2 and 4 acts downwards. Nonetheless, the added compression on the joint was assumed ineffective (p=P/bd) because the resultant of V_g and V_s enters through the lower portion of the joint (Priestley et al. 1992).

For longitudinal motion, the evaluation team made assumptions similar to those for transverse motion. For example, joints 1, 4, 5, and 8 in the longitudinal direction were modeled in a similar manner to joints 1, 2, 3, and 4 in the transverse direction.

9.5 DISCUSSION

This section discusses the computed nominal joint stresses (v_{ult}, v_{nonl}, and f_{tmax}). In Table 9.1, these stresses are normalized by the square root of the assumed concrete compressive strength, f'_c (4500 psi).

Effect of Selection of Beam Moments

In all the first-level joints, v_{ult} was similar to v_{nonl}. This result is consistent with the fact that flexural demands in the first-story beams and columns are large. Larger differences were found in the upper-level joints, especially in the longitudinal frames. According to the nonlinear analyses, the force demands were small in these locations.

Effect of Selection of Type of Stress

The values of the shear stresses, v_{ult}, and of the maximum tensile stresses f_{tmax} were most similar in the second story, where the axial forces are low. This result had been expected because both stresses were computed with the same beam moment, $1.3M_y$. For the upper-deck joints, the stresses are nearly equal because there are no column axial forces. The slightly larger value of f_{tmax} in joint 1 of transverse frames is due to the tension induced by the shear forces (V_s - V_g). For the lower-deck joints, the values of f_{tmax} were consistently smaller than those of v_{ult} because of the effect of column

compression. Nonetheless, this effect was small for the highly-stressed joints. For example the normalized shear stress was 8.3 for transverse motion of interior joint 4, while the maximum normalized tensile stress was 7.0.

Effect of Beam Reinforcement

The effect of varying amounts of reinforcement in the top and in the bottom of the members is noticeable when one compares the stresses of joints on either side of the frames. For example, the stresses in the transverse-frame, left-hand joints (1 and 3) are smaller than the corresponding stresses in the right-hand joints (2 and 4). This difference is due to the fact that the amount of reinforcement in the bottom of beams is less than that in the top, particularly if the slab steel is considered.

Effect of Column Moment Capacity

The column flexural capacities greatly affect the joint stresses. For example, consider the longitudinal-frame interior joints (2, 3, 6, and 7). In these joints, the flexural capacity of both adjacent beams (one under positive moment and one under negative moment) were added to obtain the joint shear. However, in the upper deck, only one column resists the girder moments, whereas there are two columns in the lower deck. Consequently, the upper-deck values of v_{ult} were smaller than those of the lower-deck.

Effect of Slab Reinforcement

The effect of slab reinforcement was studied to determine the sensitivity of the results to the assumed effective slab width. The fifth column in Table 9.1 lists the ultimate shear stress, v_{ult}, in which the moment was assumed to equal 1.3 times the beam moment, but in which the slab steel was neglected. Because slab reinforcement contributes significantly to the flexural capacity under negative moments only, the stresses tabulated in columns 2 and 5 differ for the right-hand joints only (transverse joints 2 and 4, and longitudinal joints 4 and 8). The reduction ranged from 40 to 50 percent for transverse frames, and it was equal to approximately 35 percent for longitudinal frames.

131

9.6 **VULNERABILITY**

On the basis of a stress limit of $3.5\sqrt{f_c}$ (psi), it appears that the transverse-frame joints are likely to be damaged when subjected to negative moments (joints 2 and 4). This vulnerability is especially great if the slab reinforcement is mobilized. For this condition, the capacity-to-demand ratios ranged from 0.4 to 0.9. The joints were found to be less vulnerable when the beams are subjected to positive moment (joints 1 and 3) with capacity-to-demand ratios ranging from 1.2 to 1.9.

The results also indicate that the lower-level joints are vulnerable during longitudinal motion. In the lower level, the capacity-to-demand ratios ranged from 0.4 to 1.1, whereas in the second level, they ranged from 0.7 to 2.9. The vulnerability may be increased by interaction between the short second-story splice and the nearby joint.

CHAPTER 10

PILE-SUPPORTED FOOTINGS

The evaluation team considered the vulnerability of the pile-supported footings to flexural yielding, shear failure, joint-shear failure, and to anchorage failure of the starter bars (Figure 10.1). In assessing vulnerability, the concrete's compressive strength was assumed equal to 1.5 times the specified strength (i.e., $f'c = 1.5 * 2200 = 3300$ psi). The reinforcement was assumed to have the properties listed in Table 4.1.

10.1 **PILE FORCES**

Before estimating the likelihood of failure, it was necessary to estimate the pile axial forces. These forces were estimated on the basis of the following assumptions:

- The footings were assumed to be rigid.

- The soil resistance beneath the footings was neglected.

- The piles were assumed to have a linear force-displacement relationship in compression.

- The piles' tension resistance was neglected because their connection to the footing may be weak.

- The pile-supported footings were assumed to be subjected to a moment, M. For the interior footings (Fig. 10.2), M was taken as the interior column's flexural capacity. For transverse motion of the exterior frames (Fig. 10.3), M was taken as twice the exterior column's flexural capacity. For longitudinal motion of the exterior frames, M also included the effect of variations in the column's seismic axial load.

- The footings were assumed to be subjected to an axial load, P, induced by the gravity and earthquake actions. The weight of the footing and the soil were included in the axial load estimate.

Consistent with these assumptions, the vertical and rotational equilibrium equations of each footing were expressed in terms of the footing's vertical displacement, y, and its rotation, θ. These displacements are illustrated in Figures 10.2 and 10.3 for transverse motion. Table 10.1 lists the values of P and M, as well as the computed pile forces, F_i. In each case, one row of piles went into tension.

133

a) Flexure

b) Shear

c) Anchorage

d) Joint Shear
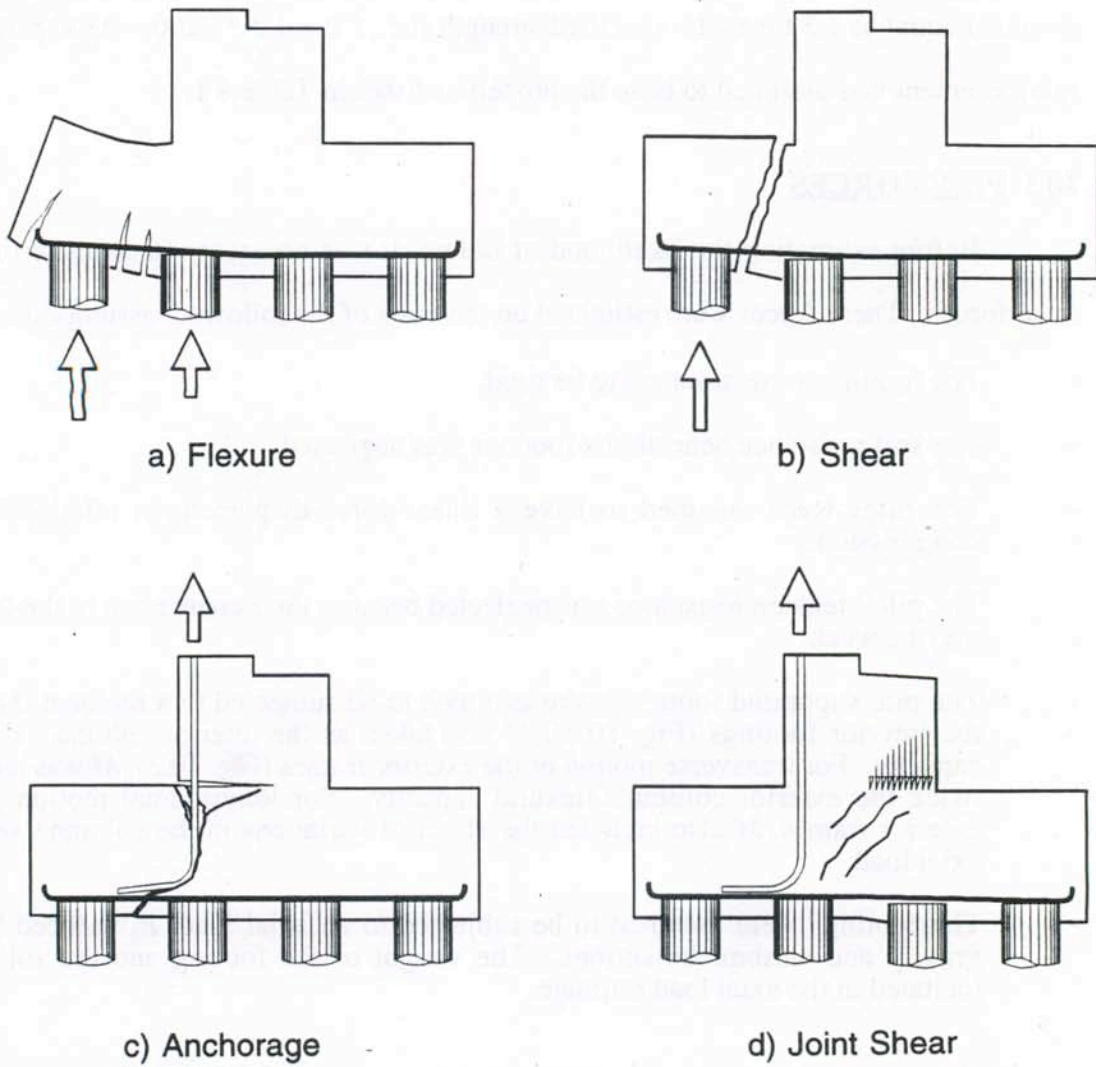
Figure 10.1. Failure Modes for Pile-Supported Footings

Figure 10.2. Geometry of Interior Pile-Supported Footings

b) Elevation

4 Piles per Row

d_i

u_i

3.5'

γ

θ

$u_i = \gamma + \theta d_i$

Initial Position

P

M

a) Plan View

3'

Concrete Piles Diameter = 1.5'

12'

Interior Column Size: 4' x 3.5'

1.5'

6'

6'

A

a) Plan View

$$u_i = y + \theta d_i$$

b) Longitudinal Elevation
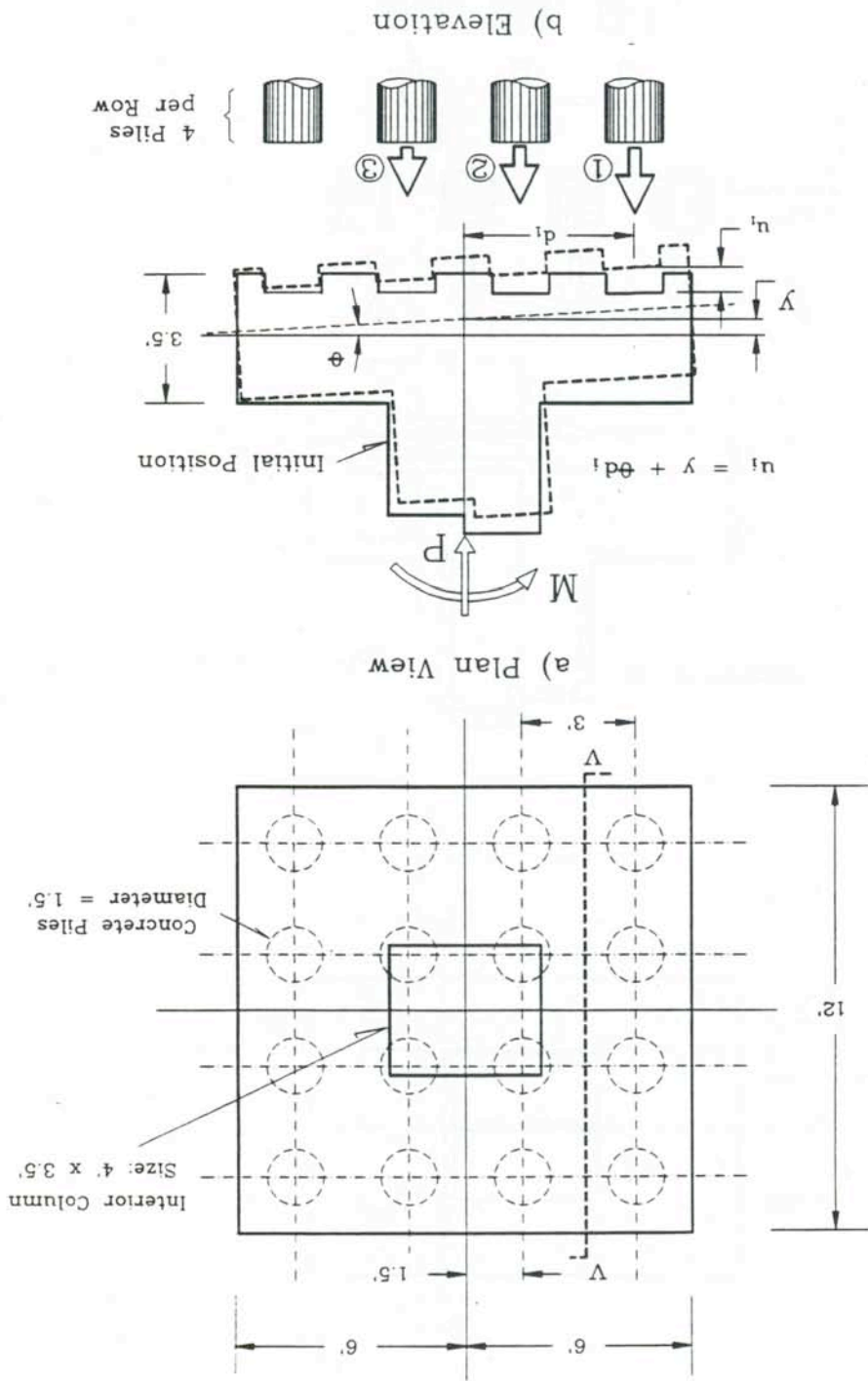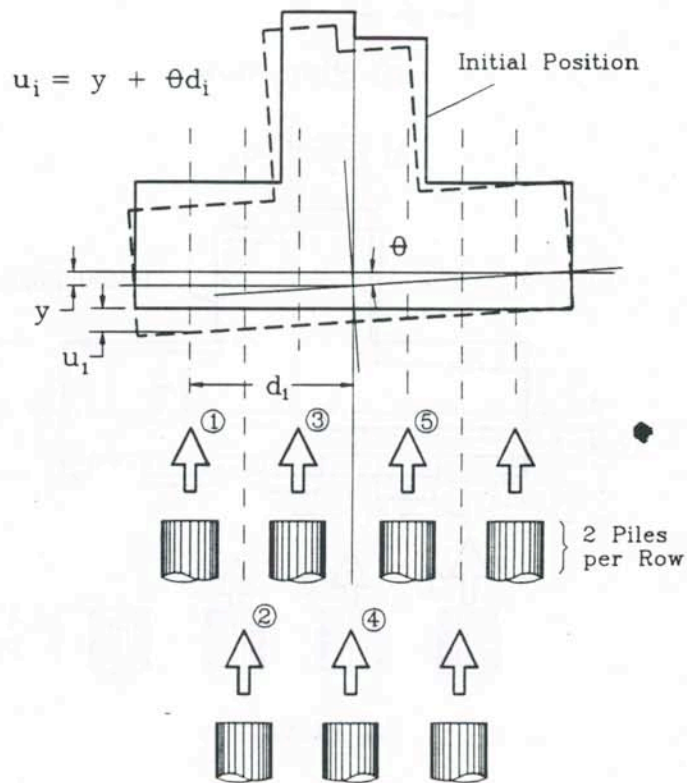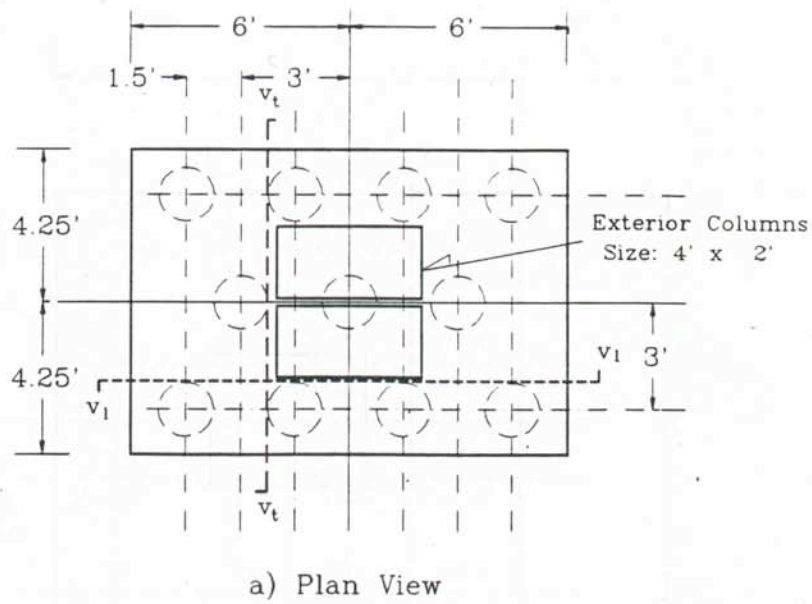
Figure 10.3. Geometry of Exterior Pile-Supported Footings

Table 10.1. Pile Forces

Direction	Location	M [kip-ft]	P [4] [kip]	F_1 [kip]	F_2 [kip]	F_3 [kip]	F_4 [kip]	F_5 [kip]
Transverse	Interior	3250[1]	1134	636	378	120	(-)	
	Exterior	3666[2]	1110	586	212	262	50	(-)
Longitudinal	Interior	2642[1]	956	520	319	117	(-)	
	Exterior	1666[3]	782	555	227	(-)		

[1] Equal to interior column's ultimate moment

[2] Equal to two times exterior column's ultimate moment

[3] Computed for two exterior columns with varying axial loads

[4] Includes weight of soil and footing: 125 kips for interior footing and 90 kips for exterior footing

10.2 FLEXURE

Flexural demands were computed based the pile forces listed in Table 10.1. The critical moment demand M_d, reported in Table 10.2, was computed at the column faces. To evaluate flexural capacities of footings, Priestley et al. (1992) recommend using an effective width, b_e, equal to the width of the column, c, plus twice the footing's effective depth, d. The footing's capacity, which was computed considering strain hardening of the reinforcement, was limited by the ultimate curvature in the concrete, $\varepsilon_c = 0.005$, (Section 4.2). Anchorage failure of the footing bars was not considered. The resulting flexural capacity-to-demand ratios for the footings are listed in Table 10.2.

Computed capacity-to-demand ratios, M_u/M_d, indicate that the interior pile-supported footings are unlikely to reach their flexural capacity. For these footings, the flexural capacities exceed moment demands by 35 percent in the transverse direction and by 60 percent in the longitudinal direction. Nonetheless, since the capacity-to-demand ratio for yielding in the transverse motion is only 1.1, yielding may occur.

137

Table 10.2. Flexural Capacity-to-Demand Ratios

Direction	Location	M_d	b_e	M_y	M_u	M_y/M_d	M_u/M_d
		[kip-ft]	[ft]	[kip-ft]	[kip-ft]	[kip-ft]	[kip-ft]
Transverse	Interior	1591	9.5	1750	2150	1.1	1.3
	Exterior	1677	8.5	1565	1925	0.9	1.1
Longitudinal	Interior	1430	10.0	1840	2260	1.3	1.6
	Exterior	509	10.0	1840	2260	3.6	4.4

For the exterior footings, the transverse and longitudinal direction moment capacities differ by only 15 percent. Nonetheless, the transverse direction is critical because the pile forces' moment arm in this direction is larger than the moment arm in the longitudinal direction (Figure 10.3a). As a result, it is likely that the footings would yield in the transverse direction (M_y/M_d= 0.9), and yielding in the longitudinal direction (M_y/M_d= 3.6) would be unlikely.

10.3 SHEAR

Shear demands were computed with the pile forces listed in Table 10.1. Table 10.3 reports the magnitudes of the shear demand, V_d, at the column face and at a one-half the footing depth from the column face. As for flexure, Priestley et al. (1992) recommend using the effective width, b_e (Table 10.2), to compute the shear capacity, V_c. Because the flexural reinforcement ratio, p_ω, is only 0.35 percent, the shear capacity was computed with the following expression (ACI-ASCE Committee 426, 1974):

$$V_c = (0.85 + 120p_\omega) \sqrt{f_c} \, (b_e \, d) \quad \leq 2.4 \sqrt{f_c} \, (b_e \, d) \tag{10.1}$$

where d is the effective depth of the footing (33.5 in.). The shear capacity, V_c, and the capacity-to-demand ratios, V_c/V_d, are listed in Table 10.3. These ratios indicate that the

138

Table 10.3. Shear Capacity-to-Demand Ratios

Direction	Location	V_c [kips]	Face of Column		d/2 from Column	
			V_d [kips]	V_c/V_d	V_d [kips]	V_c/V_d
Transverse	Interior	279	636	0.44	636	0.44
	Exterior	249	798	0.31	586	0.42
Longitudinal	Interior	293	520	0.56	520	0.56
	Exterior	293	555	0.53	0	∞

footing's shear capacity ranges between one-half and two-thirds of the shear demand. Even if the total width of the footings were assumed to be effective (instead of b_e), one would still conclude that shear failure is likely.

On the one hand, Equation 10.1 is conservative because the shear spans are short. In all cases, the distance between the pile centerlines and column face is shorter than the footing depth. On the other hand, the anchorage conditions for the bottom flexural reinforcement are marginal. This reinforcement extends 16 inches beyond the centerline of the exterior piles. According to Equation 7.5, the minimum anchorage length for a #9 bar is 18 inches.

10.4 ANCHORAGE OF STARTER BARS

Anchorage failure of the starter bars is illustrated in Figure 10.1c. Anchorage failures can occur when the tensile force in the bars exceeds the force that the surrounding concrete within the footing can sustain before spalling. Anchorage is particularly a concern if flexural cracks develop in the top of the footing because the footing has no confinement reinforcement, nor does it have top steel. Cracking reduces

10.5 COLUMN-TO-FOOTING JOINTS

Joint failure in the footing is illustrated in Figure 10.1d. This type of failure, also known as diagonal-tension failure, occurs when a joint experiences large vertical shear forces. As was done in Chapter 9, joint failure was evaluated by comparing the maximum tensile stress, f_t, with a limiting stress value of $3.5\sqrt{f_c}$ (psi) . The shear-stress approach was not used to evaluate the column-to-footing joints because the column axial loads are large.

Table 10.5 summarizes the calculations to estimate the joint's vertical compressive stress. The maximum tensile stress in the joints, f_{tmax}, occurs when the column axial load is low (gravity loads reduced by seismic action). The area used to compute the compressive stress was evaluated by taking into account the spreading of stresses in both directions.

In Table 10.6, the vertical shear stress is computed and combined with the compressive stress to estimate the maximum tensile stress, f_{tmax}. The maximum shear force in each joint was computed by dividing each column's ultimate moment by its effective depth. The joint area resisting the shear force (Fig. 10.5) was defined to be consistent with the recommendations of Priestley et al. (1992). The effective depth of the joint was considered equal to that of the footings (d = 33.5 in.). To account for the spreading of stresses within the footings, the effective width of the joint, w_e, was assumed equal to the column's width, c, plus the footing's depth (i.e., $w_e = c + d$).

Using a stress of $3.5\sqrt{f_c}$ (psi) as the limiting stress at which joint distress begins, it appears that joint-shear failure is likely. In a recent study, Xiao et al. (1994) report that stresses of up to $5\sqrt{f_c}$ can be sustained if the column and footing remain elastic. Nonetheless, even if the higher limit is adopted, the joint stresses are still unacceptable.

Table 10.5. Calculation of Vertical Compressive Stresses

Direction	Location	No. of Columns	Axial Load [kips]	Area [in. x in.]	Compressive Stress [psi]
Transverse	Interior	1	1009	75.5 x 81.5	164
	Exterior	2	1020	81.5 x 83.5	150
Longitudinal	Interior	1	831	75.5 x 81.5	135
	Exterior	1	346	75.5 x 41.0	112

Table 10.6. Calculation of Maximum Tensile Stresses

Direction	Loc.	Column Effective Depth [in.]	Shear Force [kips]	Joint Width w_e [in.]	Vertical Shear Stress [psi]	Max. Shear Stress [psi]	Max. Tensile Stress [psi]	$f_{tmax}/\sqrt{f'_c}$
Trans.	Int.	38.4	1016	75.5	402	410	328	5.7
	Ext.	38.4	1146	83.5	410	418	337	5.9
Long.	Int.	33.6	944	81.5	346	352	285	5.0
	Ext.	19.2	573	81.5	210	217	161	2.8
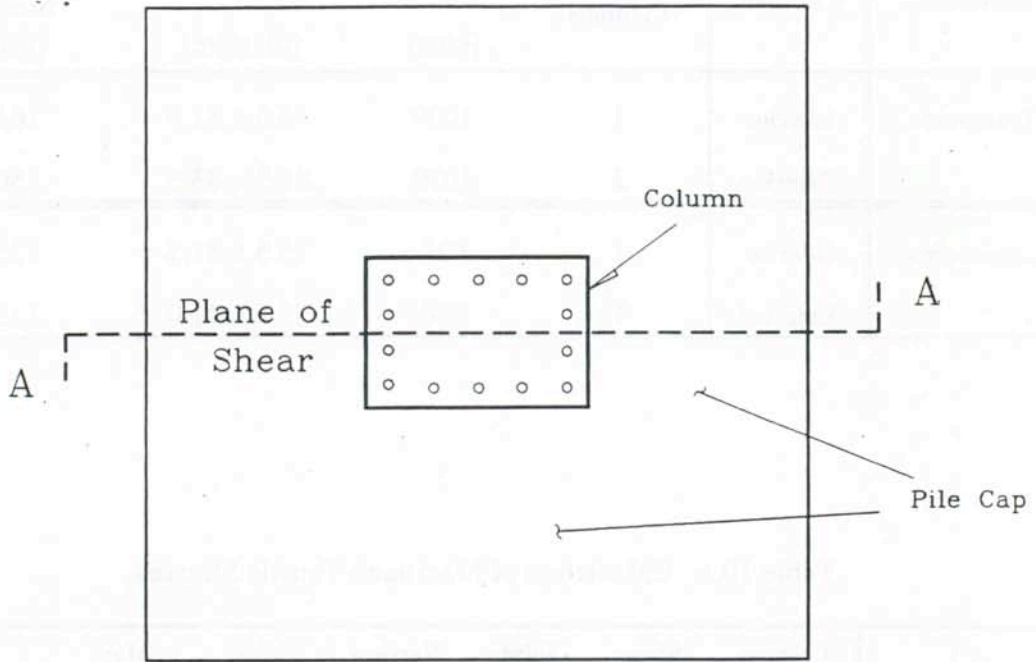
a) Plan View
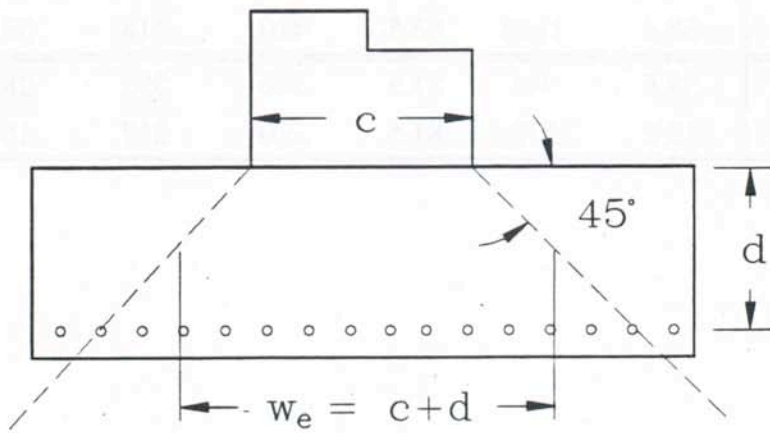
b) Section A–A

Figure 10.5. Parameters to Estimate Joint Area

144

10.6 DISCUSSION

If the columns develop their flexural capacities, it appears that the pile-supported footings are vulnerable to several modes of brittle failure. Although the bottom reinforcement is light ($p_\omega = 0.0035$), the footings are unlikely to reach their flexural capacity. Instead, the footing capacities are likely to be limited by shear failure (capacity-to-demand ratios, V_c/V_u, ranged between 0.3 and 0.6), anchorage failure, or joint failure ($f_{tmax}/3.5\sqrt{f_c}$) ranged varied between 0.6 and 1.2).

These assessments were based on conservative criteria. However, even if one makes minor changes to the assessment procedure, it is likely that the footings will be found to be vulnerable.

CHAPTER 11

DISCUSSION

.The findings of the University of Washington study indicate that the Alaskan Way Viaduct does not meet current seismic design standards and that it might collapse during the design earthquake. Two factors combine to make the viaduct vulnerable: (1) the site-specific motion would strongly excite the viaduct (Fig. 3.10); and (2) the viaduct's details lack the ductility required by current standards. The inadequate ductility also makes the viaduct vulnerable to differential support displacements caused by liquefaction of the underlying loose, saturated soils (Kramer et al. 1995).

11.1 UNCERTAINTIES

The researchers evaluated the Alaskan Way Viaduct WSDOT-designed unit by following the most up-to-date evaluation procedures that are available. Nevertheless, in interpreting the results of this study, it is important to consider the uncertainties that are present in the estimates of seismic vulnerability.

The estimates of structural vulnerability depend strongly on the estimated site-specific ground motion (Kramer et al. 1995). The researchers used a design motion that was estimated to have a 10 percent probability of being exceeded during the next 50 years. However, such an estimate is difficult to make, and even if the estimate is accurate, the intensity of ground shaking during the next earthquake could be considerably more or less intense than the design motion. In addition, the motion would vary along the length of the viaduct.

The estimates of structural response depend on the modeling assumptions. The evaluation team modeled the response of a typical three-span unit standing alone. In reality, longitudinal motion of the unit would likely cause it to collide with adjacent units. Variations in foundation stiffness, joint stiffness, and cracked moment of inertias would further affect the calculated response.

Uncertainties in the member capacities are also large. The calculated capacities depend on the assumed material properties, which are likely to vary from those the researchers assumed. Most importantly, many of the evaluation procedures have been calibrated against only a limited number of tests.

11.2 RETROFIT PRIORITIES

Despite these uncertainties, there is no doubt that the Alaskan Way Viaduct is vulnerable to a strong ground motion and to differential support displacements. To aid decision makers in selecting retrofit measures, this section discusses the importance of addressing each of the viaduct's deficiencies. The decision to address a particular deficiency should be based on the following considerations:

- likelihood of failure
- consequence of failure
- cost of retrofit.

Table 11.1 organizes these considerations into a simple matrix. The highest priority is assigned to failure modes that are most likely to occur, that would place the public at the greatest risk, and that are relatively inexpensive to suppress. Such failure modes are assigned a rating of "1" in columns three through six. The lowest priority is assigned to failure modes that are least likely to occur, that are the least likely to cause collapse, and that are expensive to suppress. Such failure modes are assigned a rating of "4."

Splices

The splices at the bottom of the columns are vulnerable and relatively easy to repair. Steel elliptical jackets could be placed around the first-story column bases to improve the splice's performance (Priestley et al. 1992). These splices are accessible from ground level, and retrofit construction would not disrupt traffic on the viaduct. For the exterior columns, a single jacket could be placed around two columns without

148

Table 11.1. Priority List for Retrofit Measures

Location	Failure Mode	Likelihood	Consequence	Cost	Priority
Lower-Level Splices	Flexure	1	2	1	1
	Shear	?	1	1	
Joints	Diagonal Tension	2	1	3	1
	Anchorage	3	3	3	
Columns	Flexure	2-3	4	2	1-2
	Shear	2-3	1	2	
Footings	Shear	3	2	3	2
	Joint Shear	3	2	3	
	Anchorage	2	3	3	
Top-Level Splices	Flexure	4	2	2	2
	Shear	4	1	2	

" 1 " indicates high likelihood, important consequence, or low cost

" 4 " indicates low likelihood, minor consequence, or high cost

affecting the viaduct's ability to accommodate thermal movements. However, if a single jacket is used to confine two exterior columns, the shear strength of the columns and footings must be checked for the new conditions.

The upper-level splices are also inadequate by current standards, but they are likely to experience low demands. A reduction in splice flexural strength in this location would not be catastrophic, as long as the shear strength of the sections was preserved. Retrofitting of the split columns at the ends of each unit will require special consideration to allow for thermal movements. Possible interaction between the second-story splices and the first-level joints will also be important to consider.

Joints

It is important to retrofit the viaduct's joints because failure in this area could be catastrophic. During the 1989 Loma Prieta earthquake, a number of double-deck viaducts experienced severe joint distress, even though they did not experience intense ground shaking. While several options are available to improve the joint's resistance, a cursory review indicates that prestressing the joints may be both economical and effective.

Columns

The first-story shear capacity of the columns is marginal; if the worst-case ground motion materialized, the safety margin against shear failure would be low. Column shear failure would likely lead to collapse of the unit. Shear failure of the second-story columns is unlikely because the shear demands are low. To maintain the present margin of safety, it is important that retrofit measures not substantially increase the second-story forces by strengthening the first story. The columns are shear critical. In other words, they would fail in shear before they developed their flexural capacity in an earthquake.

Pile-Supported Footings

Retrofit of the lower-level column reinforcement splices may necessitate improvements to the footing's resistance. Although footing failures are rare, failure is possible. The possibility of liquefaction-induced lateral spread and settlement (Kramer et al. 1995) makes it especially difficult to assess the consequences of footing failure. Unfortunately, such retrofit measures are likely to be expensive. An alternative would be to preserve the splice's shear resistance and some of its moment resistance without allowing it to develop its full flexural capacity. The consequences and details of such a retrofit would have to be studied.

150

11.3 AREAS FOR FURTHER INVESTIGATION

Before retrofit measures are designed, it would be prudent to extract concrete cores and samples of longitudinal reinforcement. Testing of these materials would reduce the uncertainty associated with the evaluation of the structural vulnerability.

Retrofit measures for the Alaskan Way Viaduct are likely to be expensive. Therefore, the behavior of the modified components should be confirmed by tests, particularly if the retrofit measures are unique to the Alaskan Way Viaduct. Such tests would be cost-effective because typical units are repeated many times in the 2.2-mile long structure. The viaduct has approximately 180 bents. Tests may also be warranted to estimate the vulnerability of some existing components. For example, current analytical assessment procedures are inadequate to evaluate the effect of the interaction between the second-story splices and the first-level joints.

In addition, a preliminary evaluation indicated that many of the atypical bents have outrigger columns that are potentially vulnerable. A field inspection found that the outrigger columns near Bents 50 through 60 already have shear cracks that are visible from street level. Further investigation and experiments would be needed to assess the vulnerability and to design retrofit measures for these bents and other atypical frames of the Alaskan Way Viaduct.

ACKNOWLEDGMENTS

REFERENCES

ACI-ASCE Committee 426. (1973, June). "The Shear Strength of Reinforced Concrete Members," *Journal of the Structural Division*, American Society of Civil Engineers, Vol. 99, No. ST6, pp. 1091-1187.

American Concrete Institute. (1989). *Building Code Requirements for Reinforced Concrete (ACI-319-89)*. American Concrete Institute. Detroit.

ANSYS 5.0 Owner's Manual. (1993). Swanson Analysis Systems Inc., Houston, PA.

Applied Technology Council. (1981, October). "Seismic Design Guidelines For Highway Bridges(ATC-6)." Redwood City, California.

Applied Technology Council. (1983, August). "Seismic Retrofitting Guidelines for Highway Bridges (ATC-6-2)." Redwood City, California.

Ascheim, M., and Moehle, J. P. (1992, March). "Shear Strength and Deformability of RC Bridge Columns Subjected to Inelastic Cyclic Displacements." Report No. UCB/EERC - 92/04. University of California, Berkeley.

Brown, C. B., Eberhard, M. O., Kramer, S. L., Roeder, C. W., and Stanton, J. F. (1992, April). "Preliminary Investigation of the Seismic Vulnerability of the Alaskan Way Viaduct." WA-RD 265.1. Washington State Department of Transportation.

Corley, W. G. (1966, October). "Rotational Capacity of Reinforced Concrete Beams." *Journal of the Structural Division*, ASCE. pp. 121-146.

Dodson, J., Rochelle, S. G., and Stoddard, R.B. (1990, May). "Earthquake Analyses of the Alaskan Way Viaduct." Executive Summary. Washington State Department of Transportation.

Knaebel, P., Eberhard, M. O., and De la Colina, J. (1995, July). "Seismic Vulnerability of the Alaskan Way Viaduct: SED Typical Unit," WA-RD 363.3. Washington State Department of Transportation.

Kramer, S. L., and Eberhard, M. O. (1995, July). "Seismic Vulnerability of the Alaskan Way Viaduct: Final Summary Report." WA-RD 363.4. Washington State Department of Transportation.

Kramer, S. L., Sivaneswaran, N., and Tucker, K. N. (1995, July). "Seismic Vulnerability of the Alaskan Way Viaduct: Geotechnical Engineering Aspects," WA-RD 363.2. Washington State Department of Transportation.

Lukose, K., Gergely P., and White, R. N. (1982, Sept-Oct). "Behavior of Reinforced Concrete Lapped Splices for Inelastic Cyclic Loading." *ACI Structural Journal.*, pp. 355-365.

McLean, D. I. (1994, Forthcoming). "Seismic Retrofitting of Bridge Substructures." Washington State Department of Transportation.

Meinheit, D. F. and Jirsa, J. O. (1981, November). "Shear Strength of R/C Beam-Column Connections." *Journal of the Structural Division*, ASCE, pp. 2227-2244.

Moehle J. P., Thewalt, C. R., Mahin, S. A., and Lowes, L. N. (1994, January). "Evaluation and Upgrading of Multi-Column Bridges." *Proceedings*, 2nd U.S.-Japan Workshop on Seismic Retrofit of Bridges, Berkeley, California.

Park, R., Priestley, M. J. N. , and Gill, W.J. (1992, April). "Ductility of Square-Confined Concrete Columns." *Journal of the Structural Division*. ASCE. April. pp. 929-950.

Priestley, M. J. N. and Park, R. (1987, January-February). "Strength and Ductility of Concrete Bridge Columns Under Seismic Loading." *ACI Structural Journal.*, pp.61-76.

Priestley, M. J. N., Seible, F., and Chai, Y. H. (1992, August). "Design Guidelines for Assessment Retrofit and Repair of Bridges for Seismic Performance," Report No. SSRP-92/01. Department of Applied Mechanics and Engineering Sciences. University of California, San Diego.

Priestley, M. J. N., Seible, F., and Uang, C.-M. (1994, February).."The Northridge Earthquake of January 17, 1994," Report No. SSRP-94/06. Department of Applied Mechanics and Engineering Sciences. University of California, San Diego.

Ryter, S. (1994, March). "Seismic Vulnerability of the Alaskan Way Viaduct." thesis submitted in partial fulfillment of the requirements for the degree of Master of Science in Civil Engineering. University of Washington, Seattle.

Standard Specifications for Road and Bridges Construction. (1948, April). State of Washington, Department of Highways.

Thewalt, C., and Stojadinvic, B. (1992, July). "Behavior and Retrofit of Bridge Outrigger Beams." *Proceedings,* 10th World Conference on Earthquake Engineering. Madrid, Spain.

Wilson, E. L., Der Kiureghian, A. (1981). "A Replacement For the SRSS Method in Seismic Analysis," *Earthquake Engineering and Structural Dynamics*, Vol. 9 pp. 187-194.

Wilson, E. L., and Habibullah, A. (1988). *Sap90 5.04 Owner's Manual*. Computers and Structures, Inc., Berkeley, California.

Xiao, Y., Priestley, M. J. N., Seible, F., and Hamada, N. (1994, May). "Seismic Assessment and Retrofit of Bridge Footings," Report No. SSRP-94/11. Department of Applied Mechanics and Engineering Sciences. University of California, San Diego.

APPENDIX A
STRUCTURAL DRAWINGS OF TYPICAL UNIT

ALASKAN W

TYPICAL WSD

TABLE OF
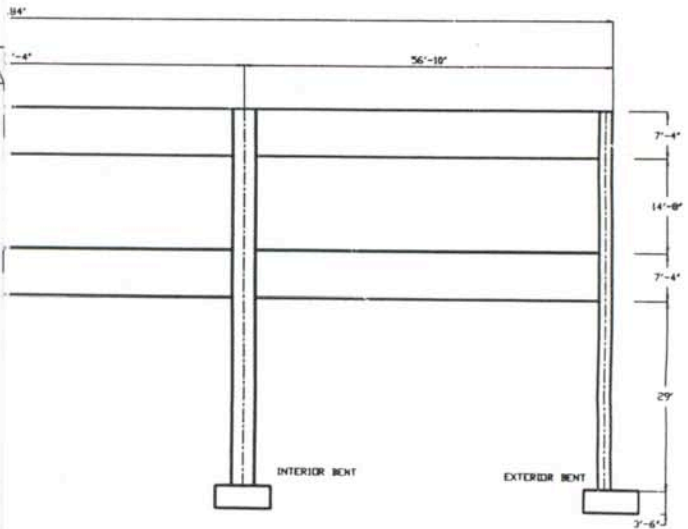
3 BAY 184' UNIT
₵ OF EXPANSION JOINTS

NOTE: THES
184' UNIT.
FROM PLAN
DEPARTMEN
MODIFICATI
SUPERELEV
FOOTING HI

#13 (911)

€ COL

47

4' 3'-2' 20'

EL. 61' #13 (202)

#13 (202)

#17

7'-4'

'A' 'A'

"A-A"
TOP-BEAM JOINT

16 SPACES @ 1'-0" = 16'-0"

4'

2 #13 (201)

2 #13 (200)

2 #13 (202)

14'-8"

2 #13 (199)

2 #13 (248)

4'-6"

20'

€ STR. € STR.

EL 39'

2'-9" SPLICE

7'-4'

0 0 0 0 0 0

10'-0 3/4" 8'-11 1/2" 8'-11

2' = 10'-0" 1' 2 1/4'
RS

2 1/4'

4'-0"

2'

8-11 1/2'

29'

58 #3 HOOPS (685) & 116 #3 TIES (686)

39 SPACES @ 1'-0" = 39'-0"

8 #13 (247)

13 SPC @ 7 1/2' = 8'-11 1/2'
#9 BARS

(150)

2 1/4' 1'-6' = 9' 1'-6'

2 1/4'

'B' 3'SPL 'B'

8 #13 DOWELS

(178)

3'-6' 6' EL 0.0

"B-B"
ELEVATION OF NT PILE CAP

TYPICAL EXTER

OCTOBER 11, 1993
STANLEY RYTER
SHEET 2 OF 9

A-2

SECTION "D-D"
INTERIOR COLUMN-BOTTOM BEAM JOINT

ELEVATION OF
TYPICAL INTERIOR

"E-E"
PILE CAP

OCTOBER 11, 1993
STANLEY RYTER
SHEET 3 OF 9

A-3

"G" Г 4'

"J" TOP
"K" BOT

Г 1'-5 1/2'
GIRDER

35'-2'

31'

8'

10'-2'

2 (471)

"I"

2'-0'
SPLICE

(474) #9

"G"

3'-2'

CURB EDGE

#9 (476)

6'-6 3/4'

3 #5 @ 6 (1876)

1 3/4'

2 1/4'

€ STGR

2'

31 SPCS @ 6 1/2' = 16'-9 1/2'
#5 TOP   #5 BOT
(1800)   (1801)

20 SPCS @ 6 1/2' = 10'-10'
#5 TOP   #5 BOT

"F"

"F"

23'-6'

1'-0'
INTERMEDIATE BEAM   SPLICE

20'

8'-11 1/2'

#4 @ 1
AND 1

(185

2 (1707)

6 BARS #9 EACH STRINGER

2'MIN SPLICE

€ STGR

2'MIN SPLICE

4'-5 3/4'

8'-3 1/2'

3'-3 1/2'

3'

2'-6'

5'

5'

2'-6'

3'-3'

1'

2 (1709)

2 (1702) 2 (1701)

2 (1706) 2 (1705)

2 (1705)

2 (1706)

2 (1707)

€ RDWY

1'-1'

€
FLOOR
BEAMS
& COLUMNS

"J" TOP
"K" BOT

END BEAM
EXTERIOR BAY

18'-7'

11'-9'

"I"

INTERMEDIATE BEAM
CENTER BAY

€ UNIT

OCTOBER 11, 1993
STANLEY RYTER
SHEET 4 OF 9

2 #9 (1709)
2 #4 (1722)
"N"

1'-1" 2@9" 2@1'-0" 4 @ 1'-6" = 6'-0" 2@1' 2@10' 2@8' 4@6' 1' 1'-1" 2@7' @6' 3@5" 11.5' 1' 3@5" 4@6' 2@9" 3 @ 1' 2@1'-6" #4 STIRRUPS
1'-6" 2'-0" 2'-0" SPLICE =2'-0" =1'-8" 1'-4" =2'-0" 1'-2'-0" 1'-3" 1'-3" 2'-0" 1'-6" = 3'-0" = 3'-0" (1783)

1'-6" SPL
2'-4 1/2'
5'-0 1/2'

5 #9 EACH STRINGER
1'-3" SPL
5 #9 EACH STRINGER

2 #9
(1711)
3
2 #9
(1718)
2 #9
(1714)
3 #9

16'-10' 1'-9' 3'- 2'-8 1/2' 3'-3' 8'-6'

"N"

(652)
#5 STIRRUPS
1'-3' 3 @ 1' 2 @ 1'3' 19 @ 1'- 3 @ 1'-3' 7 @ 1'-6' = 10'-6'
= 3'-0' = 2'-6' 2 (473) & 1 (472) = 3'-9' 2 (474) 9'

1 #9
(472)
2 #9
(473)

1 #17
(480)

2 #4 (486)

2 #4 (486)
1'-6' SPLICE

2 #17
(481)
2 #13 (479) 1 #13 (478) 3 BARS #17 & 3 BARS #17 & 2 BARS #13 EACH GIRDER

4'-10' 5'-6' 19'

#5 @ 6-1/2' 6 1/2'
#5 @ 6-1/2'
UP

(1705) #9 (1707) #9 (1706) #9
(1852) #4
(1722) #4
3' FILLET
1'-10'
#4 STIRRUPS (1783)
(1718) #9
1'-1 1/2'

SECTION "N-N"
STRINGER, CENTER BAY
NEAR INTERMEDIATE BEAM

A-5

3'-2"

7'-4"

2 # 17
(1630)

1 #17 (1630)

| 1'-5 1/2" | 5" | 7" | 3 @ 8" = 2' | 7" | 9" | 2@10"=1'-8" | 7" | 2@1'-0 = 2' | 1'-4 1/ |
| | 5" | 7" | 2 @ 9" | 7" | 2@8-1/2" | 7" | 2@8-1/2" | 7" | 10.5" | 2 @ 1'-0" |

SE(
INTE

3'-2"

7'-4"

2 #4 (1628)

1'-6'
SPLIC

2 # 17
(1630)

1 #17 (1632)

4'

2_
(6

| 1'-5 1/2" | 5" | 7" | 4@6" = 2'-0" | 7" | 3@7"=1'-9" | 8" | 7" | 6 @ 8" = 4'-0" |
| | 5" | 7" | 3@6=1'-6" | 7" | 5" | 2 @ 6" | 7" | 5" | 2 @ 6" | 7" | 6 @ 8" = 4' |

SEC
INTERME

A-6

€ COLUMN

12'-6"

2 #13 (248)

3 #5 (1875)

'R'

3 #5 (1876)

2 #13 (91

2'
SPL

2 #9 (914) BOT. (916) TOP
BEAM   BEAM

1'-0"

3 1/2"

CONSTRUCTION
JOINT

7'-4"

2 #6 (307)

3 1/2"

RUPS

4 #4 (908)

3'-9"

09

'R'

10

1'-5 1/2"

3 #13

CTION 'S-S'

BEAM, EXTERIOR BAY, MIDSPAN

1'-5 1/2"

NOTE: STIRF
REINFORCIN
BOTTOM BE

SEC
END BE

4'-6"

9'-6

3 #5 (1874)

1 #9 (912)

3 #5 (1876)

'T'

7'-4"

2 #13 (911)

1 #13 (910)

3'-6"

2 #13 (909)

1'-5 1/2"

5' 7' 2 @ 1' = 2' 7' 2@1'2-1/2"=2'5" 7' 1'-6" 1'-10 1/2

5' 7' 1'-6" 7' 1'-5" 7' 1'-5" 7' 1'-4 1/2" 1'-6

CONSTR. JOINT

'T'

SE
END B

A-7

Upper section (SECTION "V-V" area):

E COLUMN

19'-0"

2 #11 (236)   4 #5 (1875)   'U'

3 #5 (1876)

2 #9 (905) TOP BEAM

(903) BOTTOM BEAM

5'-0 1/2"

1 #4 (908)

3 #17

1'-5 1/2"

'U'

1'-5 1/2"

IION "V-V"

NOTE: STIRRUP CENTER BAY, MIDSPAN
REINFORCING
BOTTOM BEAM

SECT
END BEAM, C

Lower section (SECTION "W-W" area):

12'-0"

4 #5 (1874)   'W'

1 #17 (901)

3 #5 (1876)   3 #17

2 #4 (908)

2 #17 (906)

2'-2 1/2"   1 #17 (899)   6'-6"   2 #13

3 #17

1'-5 1/2" 5' 7' 4@6" = 2'-0" 7' 3@7"=1'-9" 8' 7' 3@8"=2'-0" 10.5'

5' 7' 3@6"=1'-6" 7' 5' 2@6" 7' 2@8.5' 7' 2 @ 1' = 2' 1'-4 1/
            1'-0"   1'-5"

'W'

SECT
END BEAM, C

OCTOBER 11, 1993
STANLEY RYTER
SHEET 8 OF 9

A-8

BAR LIST

MARK	LOCATION	SIZE	LENGTH		BENDING DIAGRAM
150	FOOTINGS – LONGITUDNAL AND TRANSVERSE	9	11'--10'		
157	FOOTINGS – LONGITUDNAL	9	8'-		
177	COLUMN DOWELS – INTERIOR BENT	11	5'--11'		
178	COLUMN DOWELS – EXTERIOR BENT	13	6'-9'-1'	STR.	
199	COLUMNS – EXTERIOR BENT	13	20'4'-9'	STR.	
			-6'	STR.	
200	COLUMNS – EXTERIOR BENT	13	11'-'-2'		
201	COLUMNS – EXTERIOR BENT	13	9'--6'	STR.	
202	COLUMNS – EXTERIOR BENT	13	13'-'-0'	STR.	
231	COLUMNS – INTERIOR BENT	11	13'-'-0'	STR.	
235	COLUMNS – INTERIOR BENT	11	20'5-0'	STR.	
236	COLUMNS – INTERIOR BENT	11	14'--10'	STR.	
237	COLUMNS – INTERIOR BENT	11	10'-		
241	COLUMNS – INTERIOR BENT	11	38'-'-0'	STR.	
247	COLUMNS – EXTERIOR BENT	13	39'--6'	STR.	
248	COLUMNS – EXTERIOR BENT	13	25'-'-3'	STR.	
			'-0'	STR.	
469	GIRDERS – TOP BARS	17	24'4-0'	STR.	
470	GIRDERS – TOP BARS	17	34'4-0'	STR.	
471	GIRDERS – TOP BARS	17	49'-'-5'	STR.	
472	GIRDERS – TOP BARS	9	50'4-6'	STR.	
473	GIRDERS – TOP BARS	9	38'4-5'	STR.	
474	GIRDERS – TOP BARS	9	24'2-0'	STR.	
476	GIRDERS – TOP BARS	9	50'4-6'	STR.	
478	GIRDERS – BOTTOM BARS	13	24'4-4'	STR.	
479	GIRDERS – BOTTOM BARS	13	36'4-4'	STR.	
480	GIRDERS – BOTTOM BARS	17	47'4-3'	STR.	
481	GIRDERS – BOTTOM BARS	17	48'4-8'	STR.	
482	GIRDERS – BOTTOM BARS	17	27'4-9'	STR.	
483	GIRDERS – BOTTOM BARS	17	49'4-2.5'		
485	GIRDERS – BOTTOM BARS	13	38'4		
486	GIRDERS – LONGITUDNAL BARS	4	31'--7'	STR.	
487	GIRDERS – LONGITUDNAL BARS	8	39'4	STR.	18'-4' OR 27'-3'
			-5'	STR.	
645	GIRDERS AT INTERMEDIATE BENT – LONG. WEB	8	20'?-1'		
652	GIRDER STIRRUPS	5	16'--11'		
677	COLUMN TIES	3	3'4-0'	STR.	
681	COLUMN HOOPS	3	14'-		
685	COLUMN HOOPS	3	11'-		
686	COLUMN TIES	3	2'-		
898	TOP & BOT END BEAM, CENTER BAY – BOT BARS	13	26'-		
899	TOP & BOT END BEAM, CENTER BAY – BOT BARS	17	39'-		
901	BOT END BEAM, CENTER BAY – TOP BARS	17	18'-		
902	BOT END BEAM, CENTER BAY – TOP BARS	17	26'-		
903	BOT END BEAM, CENTER BAY – TOP BARS	9	10'-		
904	TOP END BEAM, CENTER BAY – TOP BARS	17	25'-		
905	TOP END BEAM, CENTER BAY – TOP BARS	9	13'-		
906	TOP & BOT END BEAM, CENTER BAY – BOT BARS	17	49'-		
907	TOP & BOT END BEAM, CENTER BAY – TOP BARS	6	28'-		
908	TOP & BOT END BEAM, CTR BAY – LONG BARS	4	23'-		
909	TOP & BOT END BEAM, EX BAY – BOT BARS	13	33'-		
910	TOP & BOT END BEAM, EX BAY – BOT BARS	13	40'-		
911	TOP & BOT END BEAM, EX BAY – BOT BARS	13	48'-		
912	BOT END BEAM, EX BAY – TOP BARS	9	11'-		
913	BOT END BEAM, EX BAY – TOP BARS	13	21'-		
914	BOT END BEAM, EX BAY – TOP BARS	9	19'-		
915	TOP END BEAM, EX BAY – TOP BARS	13	17'-		
916	TOP END BEAM, EX BAY – TOP BARS	9	26'-		
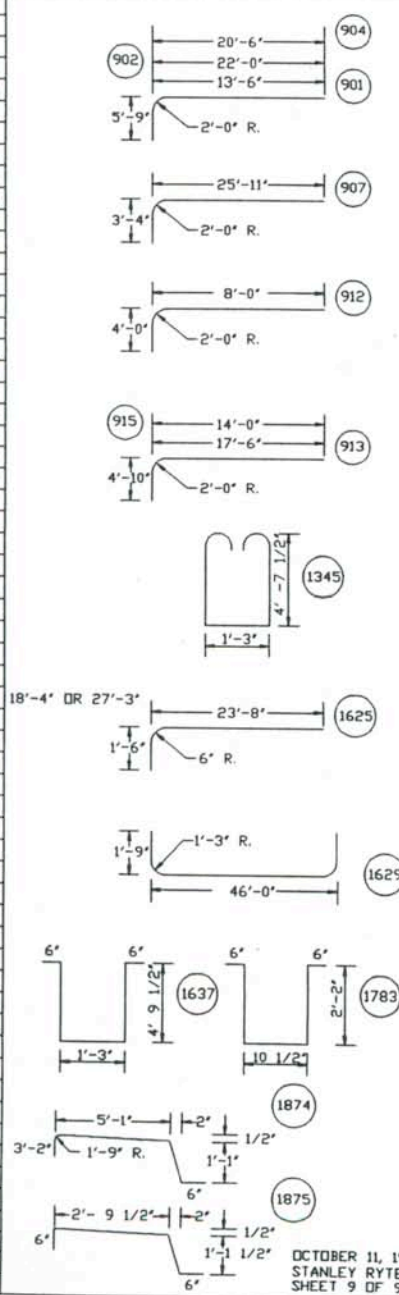
OCTOBER 11, 1993
STANLEY RYTER
SHEET 9 OF 9

A-9

APPENDIX B
MOMENT AND SHEAR DISTRIBUTIONS
COMPUTED WITH LINEAR ANALYSIS

INTERIOR FRAME, FIXED BASE
GRAVITY LOADS

379

569

566

201

397

126 K-FT

a) Moments

82

77

77

82

11

11 K
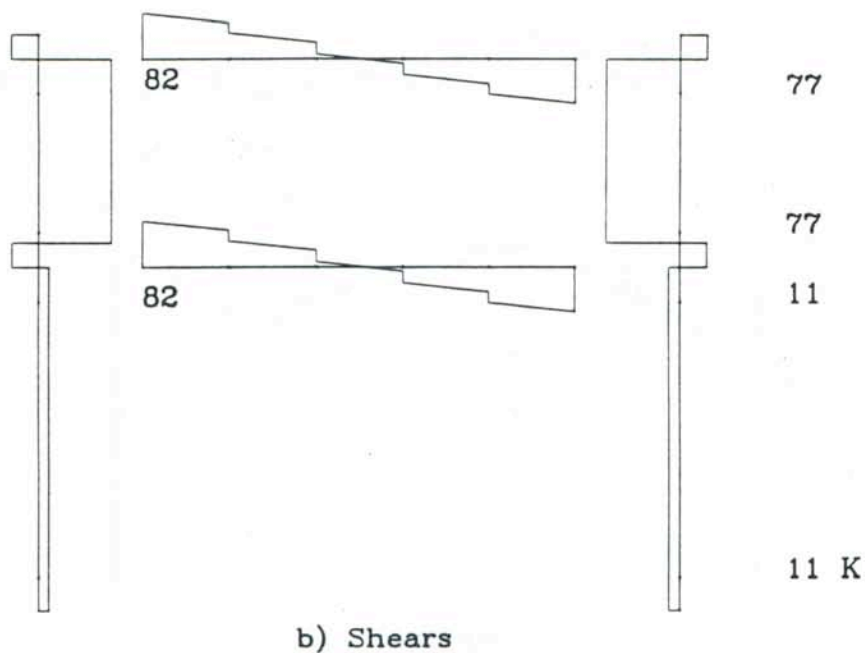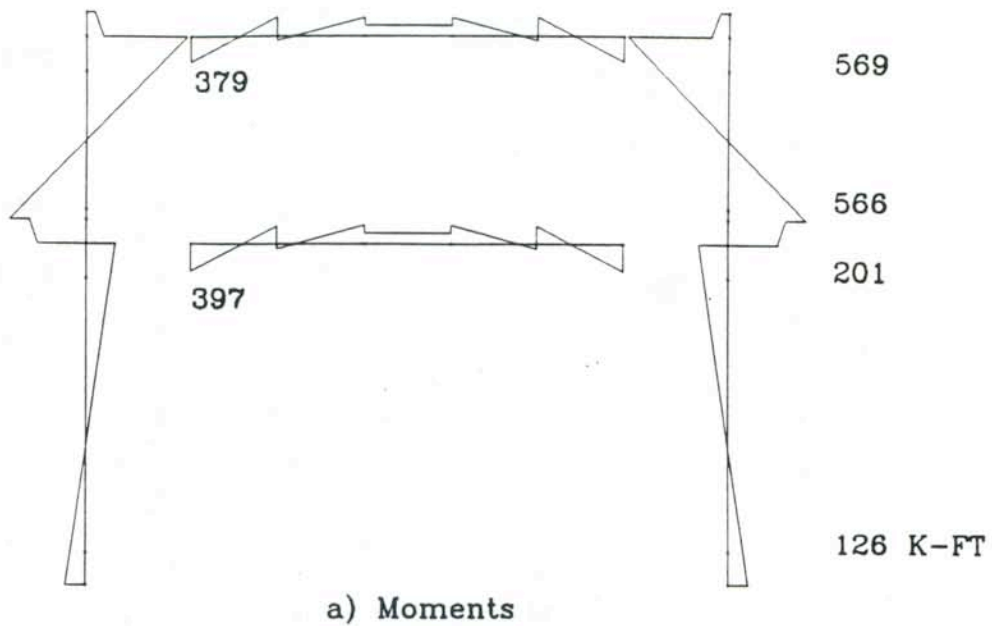
b) Shears

Figure B.1. Gravity Moment and Shear Diagrams: Interior Transverse Frame
(Fixed Bases)

EXTERIOR FRAME, PINNED BASE
GRAVITY LOADS
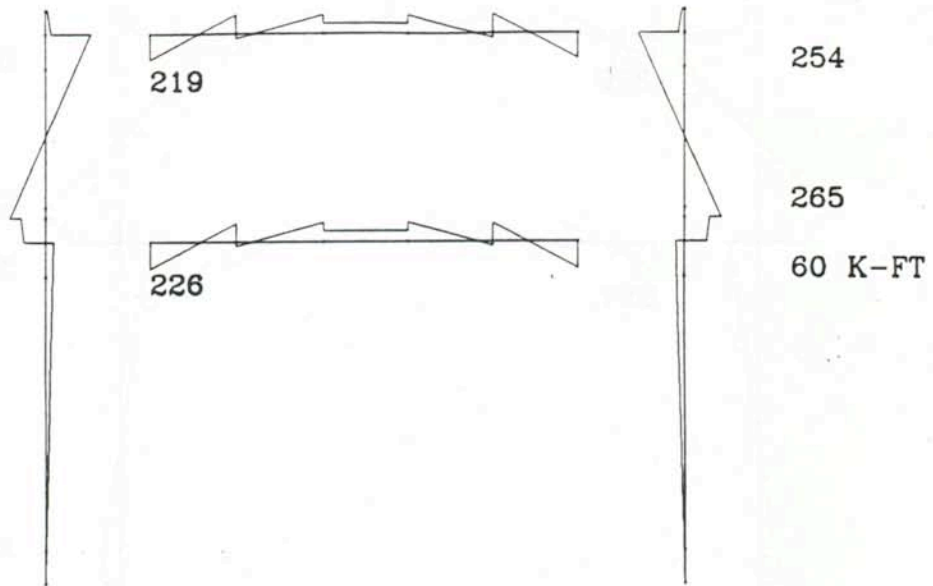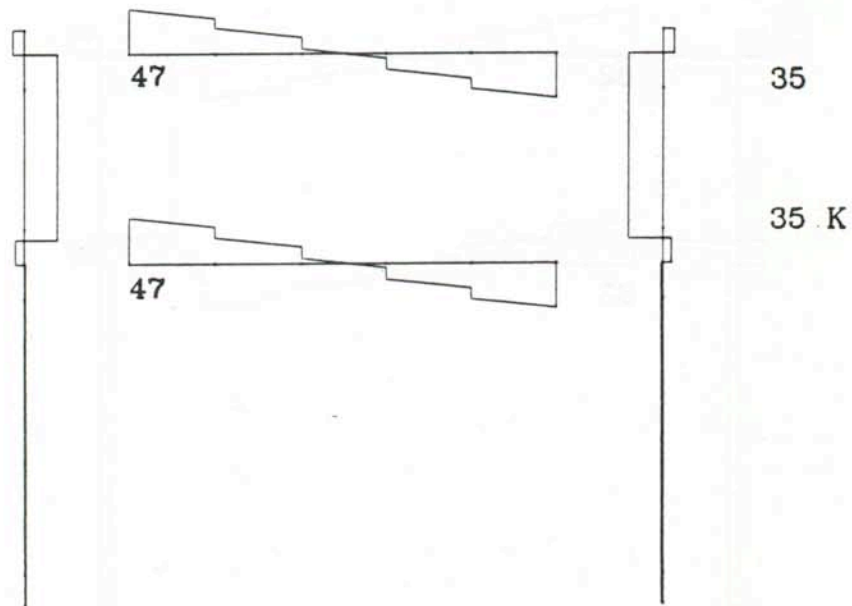
a) Moments

b) Shears

Figure B.2. Gravity Moment and Shear Diagrams: Exterior Transverse Frame
(Pinned Bases)

INTERIOR FRAME, PINNED BASE
GRAVITY LOADS

383   572

604

388   145 K-FT

a) Moments

82   80

80

82   4

4 K
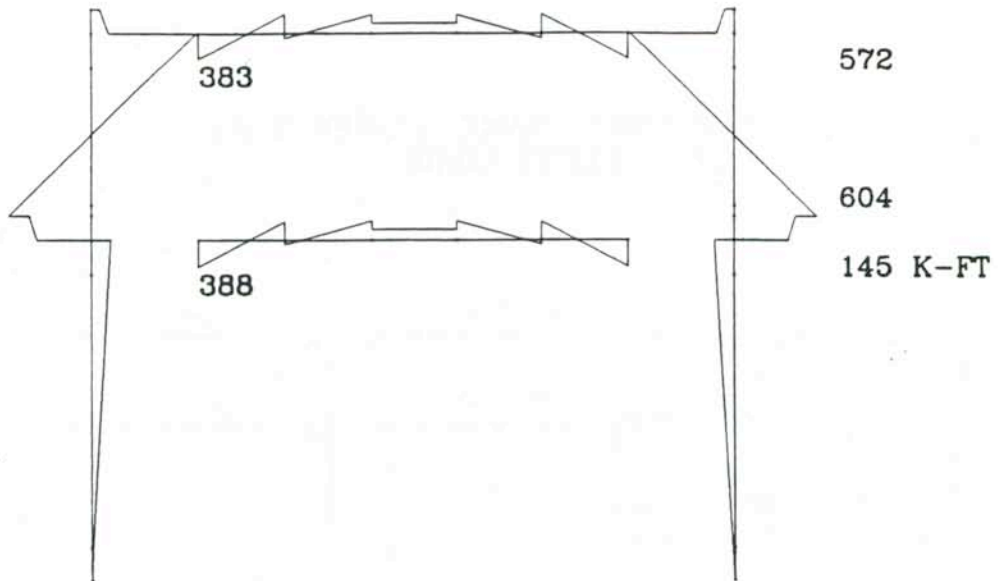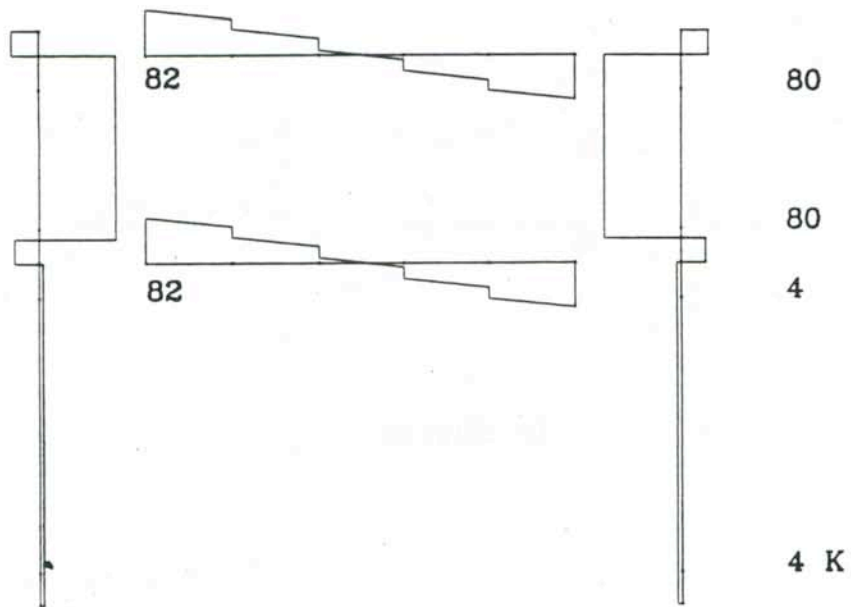
b) Shears

Figure B.3. Gravity Moment and Shear Diagrams: Interior Transverse Frame
(Pinned Bases)

LONGITUDINAL FRAME, PINNED BASE
GRAVITY LOADS
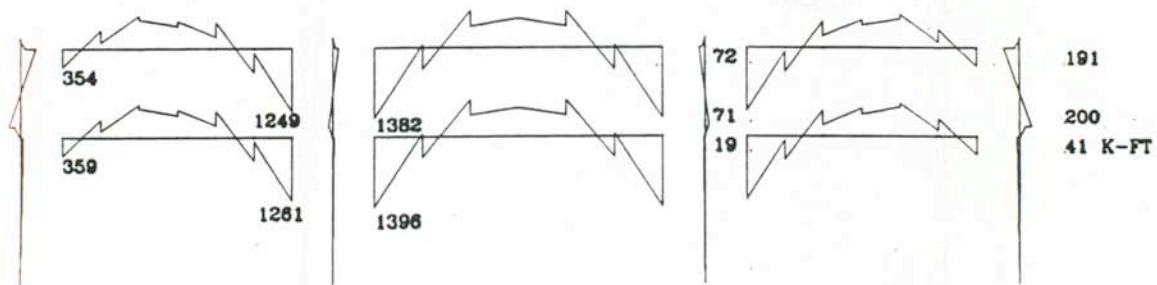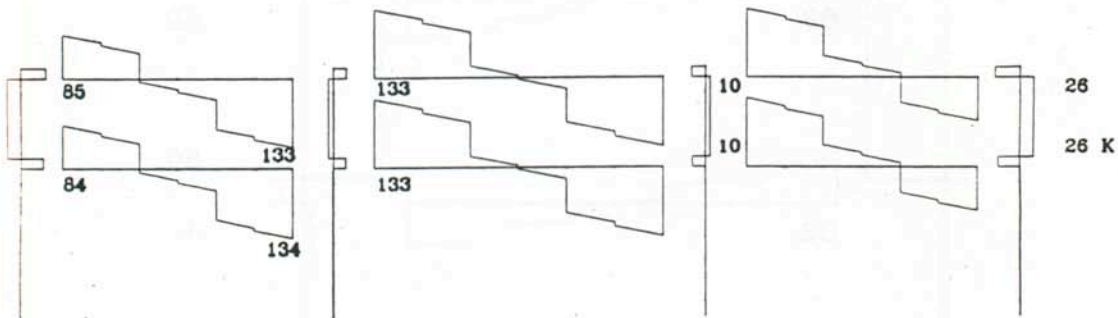
a) Moments

b) Shears

Figure B.4. Gravity Moment and Shear Diagrams: Longitudinal Frame (Pinned Bases)

INTERIOR FRAME, FIXED BASE
ATC-6 SPECTRUM, .25g

994

2058

802

2612

4699

6012 K-FT

a) Moments

108

194

194

275

369

369 K

b) Shears
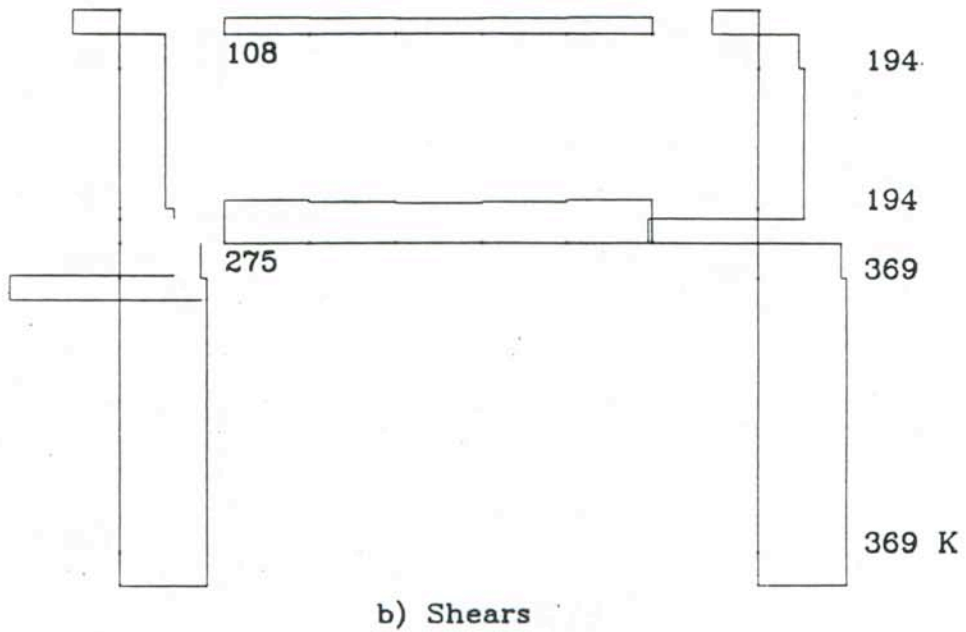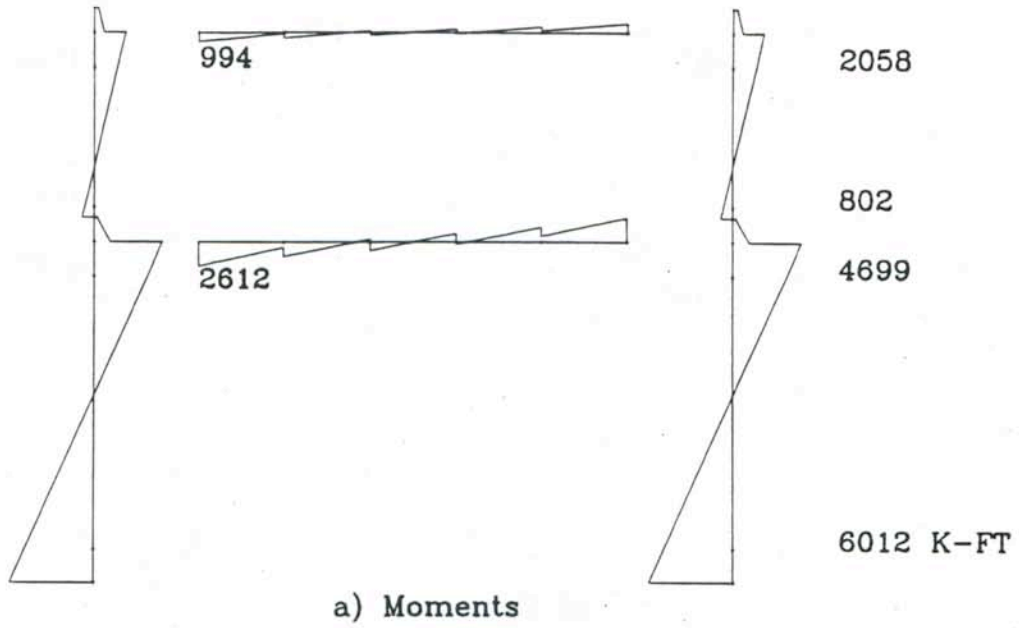
Figure B.5. Seismic Moment and Shear Diagrams: Interior Transverse Frame
(Fixed Bases)

EXTERIOR FRAME, PINNED BASE
ATC-6 SPECTRUM, .25g

609

1044

118

4567 K-FT

2447

a) Moments

53

78

78

204

139

139 K
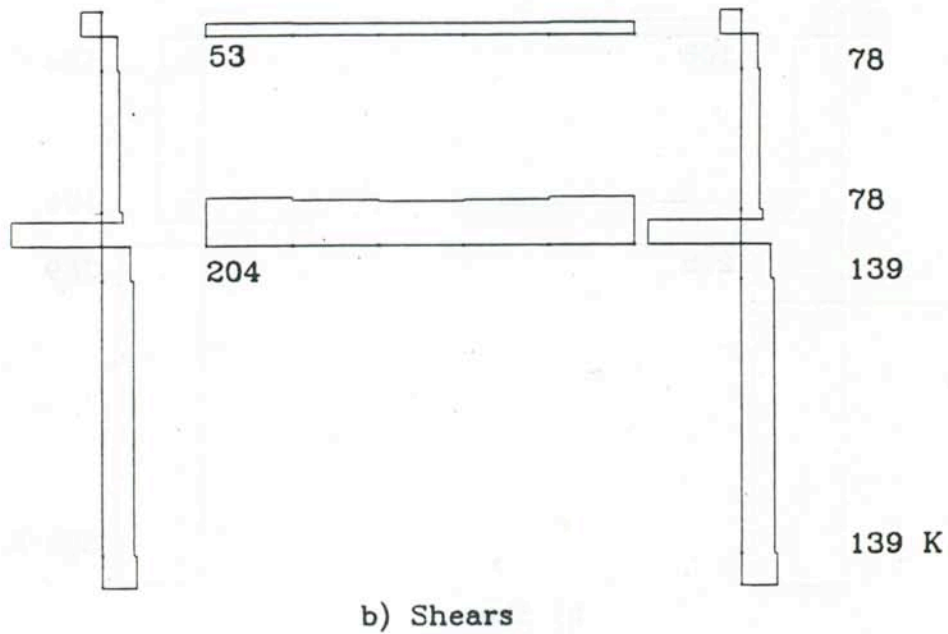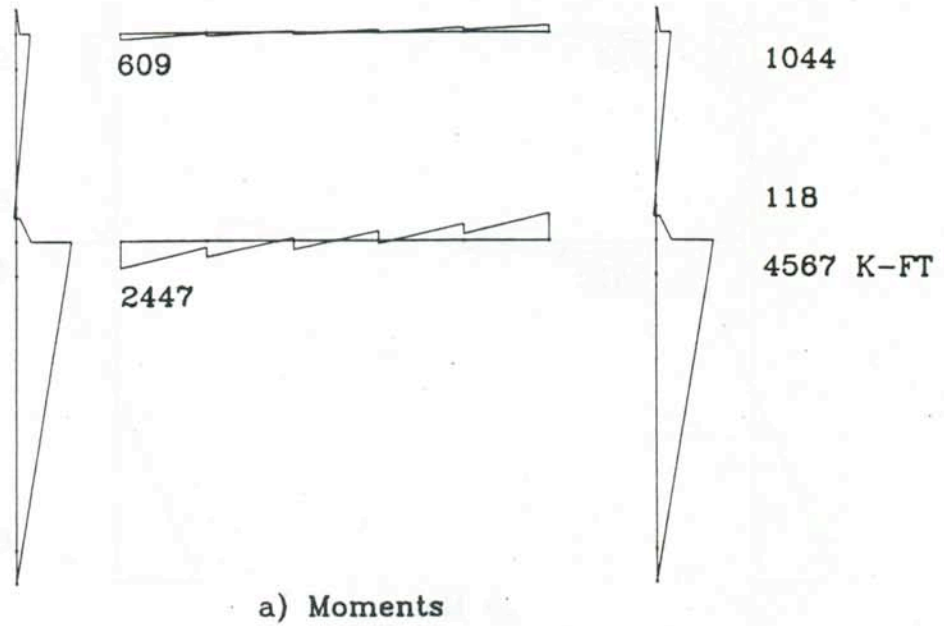
b) Shears

Figure B.6. Seismic Moment and Shear Diagrams: Exterior Transverse Frame
(Pinned Bases)

INTERIOR FRAME, PINNED BASE
ATC−6 SPECTRUM, .25g

1286

1720

136

3017

7665 K−FT

a) Moments

76

110

110

315

234

234 K
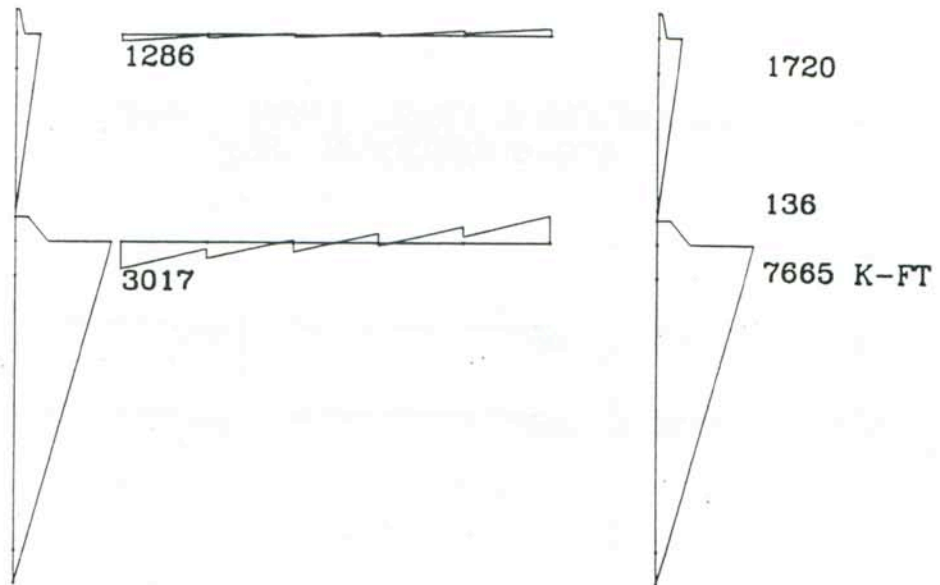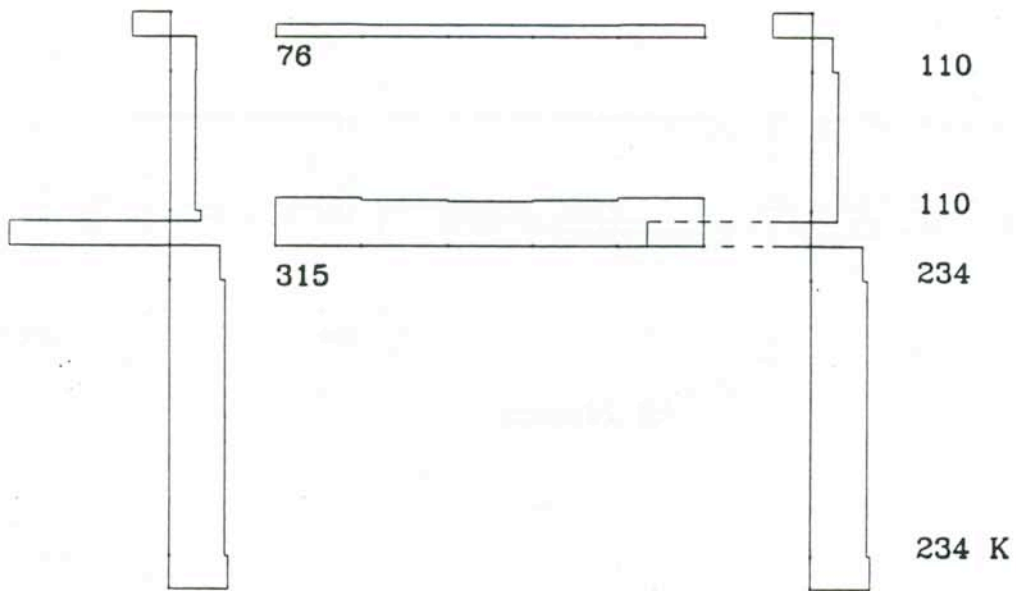
b) Shears

Figure B.7. Seismic Moment and Shear Diagrams: Interior Transverse Frame
(Pinned Bases)

LONGITUDINAL FRAME, PINNED BASE
ATC-6 SPECTRUM, .25g

559	576	490		1274	527
				15	531
2062	3385	3666		8750	1810 K-FT

a) Moments

30	30	20		87	72
				87	72
				267	54
135	143	153			
				280	62 K
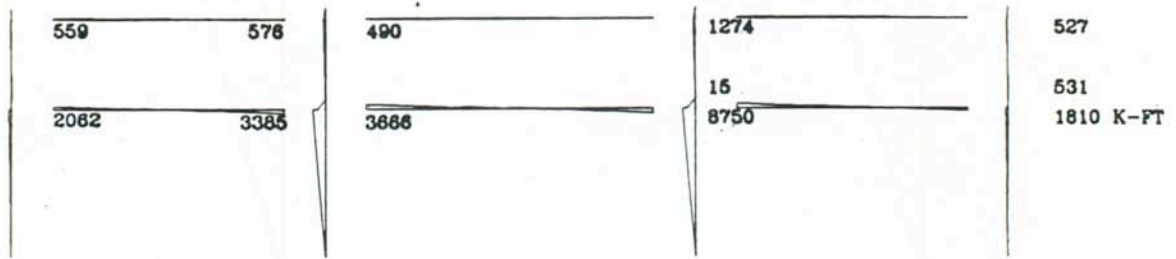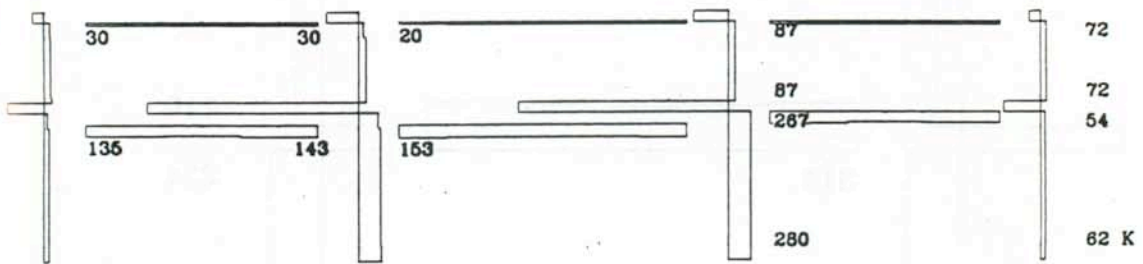
b) Shears

Figure B.8. Seismic Moment and Shear Diagrams: Longitudinal Frame (Pinned Bases)

APPENDIX C

CALCULATIONS OF ATC-6-2 FLEXURAL C/D RATIOS

Table C.1. Column Flexural C/D Ratios (Fixed Base, ATC-6 Spectrum)

	Location	Seismic Moment Kip-ft	Seismic Axial Force Kips	Gravity Moment Kip-ft	Gravity Axial Force Kips	Total Moment Kip-ft	Axial Force (nonlin.) Kips	Moment Capacity Kip-ft	Capacity/ Demand Ratio
Exterior Frame Transverse Direction	1	3563	280	57	339	3620	510	2022	0.56
						3506	274	1722	0.49
	2	2861	280	84	304	2945	510	2023	0.69
						2777	274	1723	0.62
	3	608	80	250	160	858	242	1683	1.96
						358	143	1557	4.35
	4	1264	80	253	142	1517	242	3259	2.15
						1011	143	3151	3.12
Exterior Columns Longitudinal Direction	1	1357	162	38	339	1395	430	957	0.69
						1319	232	801	0.61
	2	1280	162	63	304	1343	430	958	0.71
						1217	232	801	0.66
	3	637	37	198	160	835	188	766	0.92
						439	137	726	1.65
	4	632	37	190	142	822	188	1619	1.97
						442	137	1578	3.57
Interior Frame Transverse Direction	1	6012	451	126	830	6138	1009	3261	0.53
						5886	560	2679	0.46
	2	4699	451	201	770	4900	1009	3271	0.67
						4498	560	2678	0.60
	3	802	120	566	399	1368	475	2566	1.88
						236	296	2330	9.87
	4	2058	120	569	368	2627	475	3079	1.17
						1489	296	2842	1.91
Interior Columns Longitudinal Direction	1	6406	7	20	830	6426	851	2743	0.43
						6386	831	2723	0.43
	2	5545	7	30	770	5575	851	2774	0.50
						5515	831	2741	0.50
	3	867	5	70	399	937	418	2548	2.72
						797	407	2532	3.18
	4	1738	5	72	368	1810	418	2825	1.56
						1666	407	2825	1.70

Table C.2. Beam and Girder Flexural C/D Ratios (Fixed Base, ATC-6 Spectrum)

Member	Deck	Location		Seismic Moment Kip-ft	Gravity Moment Kip-ft	Total Moment Kip-ft	Capacity Kip-ft	Capacity/ Demand Ratio
Girder	Bottom	at Ext Col	+	1880	-377	1503	4167	2.77
			-			-2257	-1811	0.80
		at Int Col	+	3117	-1396	1721	2771	1.61
			-			-4513	-7373	1.63
	Top	at Ext Col	+	670	-377	293	4167	14.22
			-			-1047	-1811	1.73
		at Int Col	+	853	-1396	-543	2771	N/A
			-			-2249	-7373	3.28
Beam Ext Frame	Bottom	at Ext Col	+	2131	-231	1900	945	0.50
			-			-2362	-2312	0.98
	Top	at Ext Col	+	798	-217	581	1372	2.36
			-			-1015	-2127	2.10
Beam Int Frame	Bottom	at Int Col	+	2612	-397	2215	2089	0.94
			-			-3009	-4396	1.46
	Top	at Int Col	+	994	-379	615	2089	3.40
			-			-1373	-4396	3.20
Inter Beam Ext Bay	Bottom	at Girder	+	256	-230	26	3776	145.23
			-			-486	-2389	4.92
	Top	at Girder	+	280	-218	62	3776	60.90
			-			-498	-2389	4.80

Table C.3. Column Flexural C/D Ratios (Pinned Base, ATC-6 Spectrum)

	Location	Seismic Moment Kip-ft	Seismic Axial Force Kips	Gravity Moment Kip-ft	Gravity Axial Force Kips	Total Moment Kip-ft	Axial Force (nonlin.) Kips	Moment Capacity Kip-ft	Capacity/ Demand Ratio
Exterior Frame	1	521	288	6	338	527	510	2022	3.84
						515	274	1722	3.34
	2	4567	288	60	303	4627	510	2023	0.44
						4507	274	1723	0.38
Transverse Direction	3	118	61	265	160	383	242	1683	4.39
						-147	143	1557	N/A
	4	1044	61	254	142	1298	242	3259	2.51
						790	143	3151	3.99
Exterior Columns	1	219	166	4	338	223	430	957	4.29
						215	232	801	3.73
	2	1810	166	41	303	1851	430	958	0.52
						1769	232	801	0.45
Longitudinal Direction	3	531	28	200	160	731	188	766	1.05
						331	137	726	2.19
	4	527	28	191	142	718	188	1619	2.26
						336	137	1578	4.70
Interior Frame	1	870	474	16	832	886	1009	3261	3.68
						854	560	2679	3.14
	2	7665	474	145	771	7810	1009	3271	0.42
						7520	560	2678	0.36
Transverse Direction	3	136	85	604	399	740	475	2566	3.47
						-468	296	2330	N/A
	4	1720	85	572	368	2292	475	3079	1.34
						1148	296	2842	2.48
Interior Columns	1	981	9	2	832	983	851	2743	2.79
						979	831	2723	2.78
	2	8750	9	19	771	8769	851	2774	0.32
						8731	831	2741	0.31
Longitudinal Direction	3	15	9	71	399	86	418	2548	29.63
						-56	407	2532	N/A
	4	1274	9	72	368	1346	418	2825	2.10
						1202	407	2825	2.35

Table C.4. Beam and Girder Flexural C/D Ratios (Pinned Base, ATC-6 Spectrum)

Member	Deck	Location		Seismic Moment	Gravity Moment	Total Moment	Capacity	Capacity/ Demand Ratio
				Kip-ft	Kip-ft	Kip-ft	Kip-ft	
Girder	Bottom	at Ext Col	+	2063	-359	1704	4167	2.45
			-			-2422	-1811	0.75
		at Int Col	+	3666	-1396	2270	2771	1.22
			-			-5062	-7373	1.46
	Top	at Ext Col	+	559	-354	205	4167	20.33
			-			-913	-1811	1.98
		at Int Col	+	576	-1383	-807	2771	N/A
			-			-1959	-7373	3.76
Beam Ext Frame	Bottom	at Ext Col	+	2447	-226	2221	945	0.43
			-			-2673	-2312	0.86
	Top	at Ext Col	+	609	-219	390	1372	3.52
			-			-828	-2127	2.57
Beam Int Frame	Bottom	at Int Col	+	3017	-388	2629	2089	0.79
			-			-3405	-4396	1.29
	Top	at Int Col	+	722	-383	339	2089	6.16
			-			-1105	-4396	3.98
Inter Beam Ext Bay	Bottom	at Girder	+	313	-196	117	3776	32.27
			-			-509	-2389	4.69
	Top	at Girder	+	308	-216	92	3776	41.04
			-			-524	-2389	4.56

Table C.5. Column Flexural C/D Ratios (Fixed Base, Site-Specific Spectrum)

	Location	Seismic Moment Kip-ft	Seismic Axial Force Kips	Gravity Moment Kip-ft	Gravity Axial Force Kips	Total Moment Kip-ft	Axial Force (nonlin.) Kips	Moment Capacity Kip-ft	Capacity/ Demand Ratio
Exterior Frame Transverse Direction	1	4620	363	57	339	4677	510	2022	0.43
						4563	274	1722	0.38
	2	3710	363	84	304	3794	510	2023	0.53
						3626	274	1723	0.48
	3	787	103	250	160	1037	242	1683	1.62
						537	143	1557	2.90
	4	1639	103	253	142	1892	242	3259	1.72
						1386	143	3151	2.27
Exterior Columns Longitudinal Direction	1	2321	277	38	339	2359	430	957	0.41
						2283	232	801	0.35
	2	2188	277	63	304	2251	430	958	0.43
						2125	232	801	0.38
	3	1090	64	198	160	1288	188	766	0.59
						892	137	726	0.81
	4	1081	64	190	142	1271	188	1619	1.27
						891	137	1578	1.77
Interior Frame Transverse Direction	1	7797	585	126	830	7923	1009	3261	0.41
						7671	560	2679	0.35
	2	6094	585	201	770	6295	1009	3271	0.52
						5893	560	2678	0.45
	3	1035	156	566	399	1601	475	2566	1.60
						469	296	2330	4.97
	4	2667	156	569	368	3236	475	3079	0.95
						2098	296	2842	1.35
Interior Columns Longitudinal Direction	1	10959	12	20	830	10979	851	2743	0.25
						10939	831	2723	0.25
	2	9486	12	30	770	9516	851	2774	0.29
						9456	831	2741	0.29
	3	1478	7	70	399	1548	418	2548	1.65
						1408	407	2532	1.80
	4	2971	7	72	368	3043	418	2825	0.93
						2899	407	2825	0.97

Table C.6. Column Flexural C/D Ratios (Pinned Base, Site-Specific Spectrum)

	Location	Seismic Moment Kip-ft	Seismic Axial Force Kips	Gravity Moment Kip-ft	Gravity Axial Force Kips	Total Moment Kip-ft	Axial Force (nonlin.) Kips	Moment Capacity Kip-ft	Capacity/ Demand Ratio
Exterior Frame Transverse Direction	1	822	454	6	338	828	510	2022	2.44
						816	274	1722	2.11
	2	7210	454	60	303	7270	510	2023	0.28
						7150	274	1723	0.24
	3	172	96	265	160	437	242	1683	3.85
						-93	143	1557	N/A
	4	1648	96	254	142	1902	242	3259	1.71
						1394	143	3151	2.26

	Location	Seismic Moment Kip-ft	Seismic Axial Force Kips	Gravity Moment Kip-ft	Gravity Axial Force Kips	Total Moment Kip-ft	Axial Force (nonlin.) Kips	Moment Capacity Kip-ft	Capacity/ Demand Ratio
Exterior Columns Longitudinal Direction	1	315	239	4	338	319	430	957	3.00
						311	232	801	2.58
	2	2597	239	41	303	2638	430	958	0.36
						2556	232	801	0.31
	3	762	41	200	160	962	188	766	0.80
						562	137	726	1.29
	4	757	41	191	142	948	188	1619	1.71
						566	137	1578	2.79

	Location	Seismic Moment Kip-ft	Seismic Axial Force Kips	Gravity Moment Kip-ft	Gravity Axial Force Kips	Total Moment Kip-ft	Axial Force (nonlin.) Kips	Moment Capacity Kip-ft	Capacity/ Demand Ratio
Interior Frame Transverse Direction	1	1375	749	16	832	1391	1009	3261	2.34
						1359	560	2679	1.97
	2	12111	749	145	771	12256	1009	3271	0.27
						11966	560	2678	0.22
	3	169	134	604	399	773	475	2566	3.32
						-435	296	2330	N/A
	4	2715	134	572	368	3287	475	3079	0.94
						2143	296	2842	1.33

	Location	Seismic Moment Kip-ft	Seismic Axial Force Kips	Gravity Moment Kip-ft	Gravity Axial Force Kips	Total Moment Kip-ft	Axial Force (nonlin.) Kips	Moment Capacity Kip-ft	Capacity/ Demand Ratio
Interior Columns Longitudinal Direction	1	1408	12	2	832	1410	851	2743	1.95
						1406	831	2723	1.94
	2	12564	12	19	771	12583	851	2774	0.22
						12545	831	2741	0.22
	3	21	12	71	399	92	418	2548	27.70
						-50	407	2532	N/A
	4	1830	12	72	368	1902	418	2825	1.49
						1758	407	2825	1.61

APPENDIX D

CALCULATIONS OF ATC-6-2 C/D RATIOS

FOR ALL FAILURE MODES

Table D.1. Column Confinement C/D Ratios (Fixed Base, ATC-6 Spectrum)

Transverse Confinement
Fixed Base, ATC Spectrum

rc = 4500 fy = 44000

Exterior Frame Transverse Direction

Location		s (in)	hc (in)	bc (in)	Ac (in^2)	Ag (in^2)	Ash(c) (in^2)	Ash(d) (in^2)	Axial Load (Kips)	k1	bmin (in)	db (in)	k2	k3 (int)	u(int)	k3 (final)	u	Iterator	Rec	Acc
1	Comp	12	45	21	945	1152	0.44	6.63	510	0.11	24	1.625	0.40	1	3.01	0.40	2.40	0.40	0.56	1.34
1	Tension	12	45	21	945	1152	0.44	6.63	274	0.12	24	1.625	0.40	1	3.03	0.40	2.41	0.40	0.49	1.18
2	Comp	12	45	21	945	1152	0.44	6.63	510	0.11	24	1.625	0.40	1	3.01	0.40	2.40	0.40	0.69	1.66
2	Tension	12	45	21	945	1152	0.44	6.63	274	0.12	24	1.625	0.40	1	3.03	0.40	2.41	0.40	0.62	1.49
3	Comp	12	45	21	945	1152	0.44	6.63	242	0.12	24	1.625	0.40	1	3.04	0.40	2.41	0.40	1.96	4.73
3	Tension	12	45	21	945	1152	0.44	6.63	143	0.12	24	1.625	0.40	1	3.06	0.40	2.41	0.40	4.35	10.50
4	Comp	12	45	21	945	1152	0.44	6.63	242	0.12	24	1.625	0.40	1	3.04	0.40	2.41	0.40	2.15	5.18
4	Tension	12	45	21	945	1152	0.44	6.63	143	0.12	24	1.625	0.40	1	3.06	0.40	2.41	0.40	3.12	7.52

Exterior Columns Longitudinal Direction

Location		s (in)	hc (in)	bc (in)	Ac (in^2)	Ag (in^2)	Ash(c) (in^2)	Ash(d) (in^2)	Axial Load (Kips)	k1	bmin (in)	db (in)	k2	k3 (int)	u(int)	k3 (final)	u	Iterator	Rec	Acc
1	Comp	12	21	45	945	1152	0.44	3.09	430	0.24	24	1.625	0.40	1	3.27	0.38	2.48	0.38	0.60	1.70
1	Tension	12	21	45	945	1152	0.44	3.09	232	0.26	24	1.625	0.40	1	3.31	0.38	2.49	0.38	0.61	1.51
2	Comp	12	21	45	945	1152	0.44	3.09	430	0.24	24	1.625	0.40	1	3.27	0.38	2.48	0.38	0.71	1.77
2	Tension	12	21	45	945	1152	0.44	3.09	232	0.26	24	1.625	0.40	1	3.31	0.38	2.49	0.38	0.66	1.64
3	Comp	12	21	45	945	1152	0.44	3.09	188	0.26	24	1.625	0.40	1	3.32	0.38	2.50	0.38	0.92	2.29
3	Tension	12	21	45	945	1152	0.44	3.09	137	0.27	24	1.625	0.40	1	3.33	0.38	2.50	0.37	1.65	4.13
4	Comp	12	21	45	945	1152	0.44	3.09	188	0.26	24	1.625	0.40	1	3.32	0.38	2.50	0.38	1.97	4.92
4	Tension	12	21	45	945	1152	0.44	3.09	137	0.27	24	1.625	0.40	1	3.33	0.38	2.50	0.37	3.57	8.93

Interior Frame Transverse Direction

Location		s (in)	hc (in)	bc (in)	Ac (in^2)	Ag (in^2)	Ash(c) (in^2)	Ash(d) (in^2)	Axial Load (Kips)	k1	bmin (in)	db (in)	k2	k3 (int)	u(int)	k3 (final)	u	Iterator	Rec	Acc
1	Comp	12	45	30	1755	2016	0.44	6.63	1009	0.10	42	1.41	0.70	1	3.61	0.36	2.57	0.36	0.53	1.37
1	Tension	12	45	30	1755	2016	0.44	6.63	560	0.12	42	1.41	0.70	1	3.63	0.36	2.58	0.36	0.46	1.17
2	Comp	12	45	30	1755	2016	0.44	6.63	1009	0.10	42	1.41	0.70	1	3.61	0.36	2.57	0.36	0.67	1.72
2	Tension	12	45	30	1755	2016	0.44	6.63	560	0.12	42	1.41	0.70	1	3.63	0.36	2.58	0.36	0.60	1.53
3	Comp	12	45	30	1755	2016	0.44	6.63	475	0.12	42	1.41	0.70	1	3.63	0.36	2.58	0.36	1.88	4.84
3	Tension	12	45	30	1755	2016	0.44	6.63	296	0.12	42	1.41	0.70	1	3.66	0.36	2.58	0.36	9.87	25.49
4	Comp	12	45	30	1755	2016	0.44	6.63	475	0.12	42	1.41	0.70	1	3.63	0.36	2.58	0.36	1.17	3.02
4	Tension	12	45	30	1755	2016	0.44	6.63	296	0.12	42	1.41	0.70	1	3.66	0.36	2.58	0.36	1.91	4.93

Interior Columns Longitudinal Direction

Location		s (in)	hc (in)	bc (in)	Ac (in^2)	Ag (in^2)	Ash(c) (in^2)	Ash(d) (in^2)	Axial Load (Kips)	k1	bmin (in)	db (in)	k2	k3 (int)	u(int)	k3 (final)	u	Iterator	Rec	Acc
1	Comp	12	30	45	1755	2016	0.44	5.74	851	0.12	42	1.41	0.70	1	3.65	0.36	2.58	0.35	0.43	1.10
1	Tension	12	30	45	1755	2016	0.44	5.74	631	0.12	42	1.41	0.70	1	3.66	0.36	2.58	0.35	0.43	1.10
2	Comp	12	30	45	1755	2016	0.44	5.74	851	0.12	42	1.41	0.70	1	3.66	0.36	2.58	0.35	0.50	1.29
2	Tension	12	30	45	1755	2016	0.44	5.74	631	0.12	42	1.41	0.70	1	3.66	0.36	2.58	0.35	0.50	1.28
3	Comp	12	30	45	1755	2016	0.44	5.74	418	0.14	42	1.41	0.70	1	3.67	0.36	2.59	0.35	2.72	7.06
3	Tension	12	30	45	1755	2016	0.44	5.74	407	0.14	42	1.41	0.70	1	3.68	0.36	2.59	0.35	3.18	8.24
4	Comp	12	30	45	1755	2016	0.44	5.74	418	0.14	42	1.41	0.70	1	3.67	0.36	2.59	0.35	1.56	4.06
4	Tension	12	30	45	1755	2016	0.44	5.74	407	0.14	42	1.41	0.70	1	3.68	0.36	2.59	0.35	1.70	4.40

Transverse Confinement
Pinned-Base, ATC Spectrum

Table D.2. Column Confinement C/D Ratios (Pinned Base, ATC-6 Spectrum)

r'c = 4500 fy = 44000

Exterior Frame / Transverse Direction

Location		s in	hc in	bc in	Ac in^2	Ag in^2	Ash(c) in^2	Ash(d) in^2	Axial Load Kips	k1	bmin in	db in	k2	k3 (int)	u(int)	k3 (final)	u	Iterator	Rec	Rcc
1	Comp	12	45	21	945	1152	0.44	0.63	510	0.11	24	1.625	0.40	1	3.01	0.40	2.40	0.40	3.84	9.21
	Tension	12	45	21	945	1152	0.44	0.63	274	0.12	24	1.625	0.40	1	3.03	0.40	2.41	0.40	3.34	8.05
2	Comp	12	45	21	945	1152	0.44	0.63	510	0.11	24	1.625	0.40	1	3.01	0.40	2.40	0.40	0.44	1.05
	Tension	12	45	21	945	1152	0.44	0.63	274	0.12	24	1.625	0.40	1	3.03	0.40	2.41	0.40	0.38	0.92
3	Comp	12	45	21	945	1152	0.44	0.63	242	0.12	24	1.625	0.40	1	3.04	0.40	2.41	0.40	4.39	10.59
	Tension	12	45	21	945	1152	0.44	0.63	143	0.12	24	1.625	0.40	1	3.05	0.40	2.41	0.40	N/A	
4	Comp	12	45	21	945	1152	0.44	0.63	242	0.12	24	1.625	0.40	1	3.04	0.40	2.41	0.40	2.51	6.05
	Tension	12	45	21	945	1152	0.44	0.63	143	0.12	24	1.625	0.40	1	3.05	0.40	2.41	0.40	3.60	9.63

Exterior Columns / Longitudinal Direction

Location		s in	hc in	bc in	Ac in^2	Ag in^2	Ash(c) in^2	Ash(d) in^2	Axial Load Kips	k1	bmin in	db in	k2	k3 (int)	u(int)	k3 (final)	u	Iterator	Rec	Rcc
1	Comp	12	21	45	945	1152	0.44	3.09	430	0.24	24	1.625	0.40	1	3.27	0.38	2.48	0.38	4.29	10.66
	Tension	12	21	45	945	1152	0.44	3.09	232	0.28	24	1.625	0.40	1	3.31	0.38	2.49	0.38	3.73	9.29
2	Comp	12	21	45	945	1152	0.44	3.09	430	0.24	24	1.625	0.40	1	3.27	0.38	2.48	0.38	0.52	1.28
	Tension	12	21	45	945	1152	0.44	3.09	232	0.28	24	1.625	0.40	1	3.31	0.38	2.49	0.38	0.45	1.13
3	Comp	12	21	45	945	1152	0.44	3.09	188	0.26	24	1.625	0.40	1	3.32	0.38	2.50	0.38	1.06	2.62
	Tension	12	21	45	945	1152	0.44	3.09	137	0.27	24	1.625	0.40	1	3.33	0.38	2.50	0.37	2.19	5.48
4	Comp	12	21	45	945	1152	0.44	3.09	188	0.26	24	1.625	0.40	1	3.32	0.38	2.50	0.38	2.28	5.63
	Tension	12	21	45	945	1152	0.44	3.09	137	0.27	24	1.625	0.40	1	3.33	0.38	2.50	0.37	4.70	11.74

Interior Frame / Transverse Direction

Location		s in	hc in	bc in	Ac in^2	Ag in^2	Ash(c) in^2	Ash(d) in^2	Axial Load Kips	k1	bmin in	db in	k2	k3 (int)	u(int)	k3 (final)	u	Iterator	Rec	Rcc
1	Comp	12	45	30	1755	2016	0.44	0.63	1009	0.10	42	1.41	0.70	1	3.61	0.36	2.57	0.36	3.68	9.46
	Tension	12	45	30	1755	2016	0.44	0.63	560	0.12	42	1.41	0.70	1	3.63	0.36	2.58	0.36	3.14	8.08
2	Comp	12	45	30	1755	2016	0.44	0.63	1009	0.10	42	1.41	0.70	1	3.61	0.36	2.57	0.36	0.42	1.08
	Tension	12	45	30	1755	2016	0.44	0.63	560	0.12	42	1.41	0.70	1	3.63	0.35	2.58	0.36	0.36	0.92
3	Comp	12	45	30	1755	2016	0.44	0.63	475	0.12	42	1.41	0.70	1	3.63	0.36	2.58	0.36	3.47	8.95
	Tension	12	45	30	1755	2016	0.44	0.63	296	0.12	42	1.41	0.70	1	3.66	0.35	2.58	0.36	N/A	
4	Comp	12	45	30	1755	2016	0.44	0.63	475	0.12	42	1.41	0.70	1	3.63	0.36	2.58	0.36	1.34	3.47
	Tension	12	45	30	1755	2016	0.44	0.63	296	0.12	42	1.41	0.70	1	3.66	0.36	2.58	0.36	2.48	6.39

Interior Columns / Longitudinal Direction

Location		s in	hc in	bc in	Ac in^2	Ag in^2	Ash(c) in^2	Ash(d) in^2	Axial Load Kips	k1	bmin in	db in	k2	k3 (int)	u(int)	k3 (final)	u	Iterator	Rec	Rcc
1	Comp	12	30	45	1755	2016	0.44	5.74	851	0.12	42	1.41	0.70	1	3.66	0.35	2.58	0.35	2.79	7.21
	Tension	12	30	45	1755	2016	0.44	5.74	831	0.12	42	1.41	0.70	1	3.66	0.35	2.58	0.35	2.78	7.19
2	Comp	12	30	45	1755	2016	0.44	5.74	851	0.12	42	1.41	0.70	1	3.66	0.35	2.58	0.35	0.32	0.82
	Tension	12	30	45	1755	2016	0.44	5.74	831	0.12	42	1.41	0.70	1	3.66	0.35	2.58	0.35	0.31	0.81
3	Comp	12	30	45	1755	2016	0.44	5.74	418	0.14	42	1.41	0.70	1	3.67	0.35	2.59	0.35	29.63	76.82
	Tension	12	30	45	1755	2016	0.44	5.74	407	0.14	42	1.41	0.70	1	3.68	0.35	2.59	0.36	N/A	
4	Comp	12	30	45	1755	2016	0.44	5.74	418	0.14	42	1.41	0.70	1	3.67	0.35	2.59	0.35	2.10	5.44
	Tension	12	30	45	1755	2016	0.44	5.74	407	0.14	42	1.41	0.70	1	3.68	0.35	2.59	0.35	2.35	6.09

Table D.3. Column Confinement C/D Ratios (Fixed Base, Site-Specific Spectrum)

Transverse Confinement
Fixed Base, 20' Fill, 20' Tidal Soil

f'c = 4500 fy = 44000

Exterior Frame, Transverse Direction

Location		s (in)	hc (in)	bc (in)	Ac (in^2)	Ag (in^2)	Ash(c) (in^2)	Ash(d) (in^2)	Axial Load (Kips)	k1	bmin (in)	db (in)	k2	k3(int)	u(int)	k3(final)	u	Iteration	Rac	Rcc
1	Comp	12	45	21	945	1152	0.44	0.83	510	0.11	24	1.625	0.40	1	3.01	0.40	2.40	0.40	0.43	1.04
	Tension	12	45	21	945	1152	0.44	0.83	274	0.12	24	1.625	0.40	1	3.03	0.40	2.41	0.40	0.38	0.91
2	Comp	12	45	21	945	1152	0.44	0.83	510	0.11	24	1.625	0.40	1	3.01	0.40	2.40	0.40	0.53	1.28
	Tension	12	45	21	945	1152	0.44	0.83	274	0.12	24	1.625	0.40	1	3.03	0.40	2.41	0.40	0.48	1.14
3	Comp	12	45	21	945	1152	0.44	0.83	242	0.12	24	1.625	0.40	1	3.04	0.40	2.41	0.40	1.62	3.91
	Tension	12	45	21	945	1152	0.44	0.83	143	0.12	24	1.625	0.40	1	3.06	0.40	2.41	0.40	2.90	7.00
4	Comp	12	45	21	945	1152	0.44	0.83	242	0.12	24	1.625	0.40	1	3.04	0.40	2.41	0.40	1.72	4.16
	Tension	12	45	21	945	1152	0.44	0.83	143	0.12	24	1.625	0.40	1	3.06	0.40	2.41	0.40	2.27	5.49

Exterior Columns, Longitudinal Direction

Location		s (in)	hc (in)	bc (in)	Ac (in^2)	Ag (in^2)	Ash(c) (in^2)	Ash(d) (in^2)	Axial Load (Kips)	k1	bmin (in)	db (in)	k2	k3(int)	u(int)	k3(final)	u	Iteration	Rac	Rcc
1	Comp	12	21	45	945	1152	0.44	3.09	430	0.24	24	1.625	0.40	1	3.27	0.38	2.48	0.38	0.41	1.01
	Tension	12	21	45	945	1152	0.44	3.09	232	0.26	24	1.625	0.40	1	3.31	0.38	2.49	0.38	0.36	0.87
2	Comp	12	21	45	945	1152	0.44	3.09	430	0.24	24	1.625	0.40	1	3.27	0.38	2.48	0.38	0.43	1.06
	Tension	12	21	45	945	1152	0.44	3.09	232	0.26	24	1.625	0.40	1	3.31	0.38	2.49	0.38	0.38	0.94
3	Comp	12	21	45	945	1152	0.44	3.09	188	0.26	24	1.625	0.40	1	3.32	0.38	2.50	0.38	0.59	1.48
	Tension	12	21	45	945	1152	0.44	3.09	137	0.27	24	1.625	0.40	1	3.33	0.38	2.50	0.37	0.81	2.04
4	Comp	12	21	45	945	1152	0.44	3.09	188	0.26	24	1.625	0.40	1	3.32	0.38	2.50	0.38	1.27	3.18
	Tension	12	21	45	945	1152	0.44	3.09	137	0.27	24	1.625	0.40	1	3.33	0.38	2.50	0.37	1.77	4.43

Interior Frame, Transverse Direction

Location		s (in)	hc (in)	bc (in)	Ac (in^2)	Ag (in^2)	Ash(c) (in^2)	Ash(d) (in^2)	Axial Load (Kips)	k1	bmin (in)	db (in)	k2	k3(int)	u(int)	k3(final)	u	Iteration	Rac	Rcc
1	Comp	12	45	30	1755	2016	0.44	0.83	1009	0.10	42	1.41	0.70	1	3.61	0.36	2.67	0.36	0.41	1.06
	Tension	12	45	30	1755	2016	0.44	0.83	560	0.12	42	1.41	0.70	1	3.63	0.36	2.68	0.36	0.36	0.90
2	Comp	12	45	30	1755	2016	0.44	0.83	1009	0.10	42	1.41	0.70	1	3.61	0.36	2.67	0.36	0.52	1.34
	Tension	12	45	30	1755	2016	0.44	0.83	560	0.12	42	1.41	0.70	1	3.63	0.36	2.68	0.36	0.45	1.17
3	Comp	12	45	30	1755	2016	0.44	0.83	475	0.12	42	1.41	0.70	1	3.63	0.36	2.68	0.36	1.60	4.14
	Tension	12	45	30	1755	2016	0.44	0.83	298	0.12	42	1.41	0.70	1	3.66	0.36	2.68	0.36	4.97	12.63
4	Comp	12	45	30	1755	2016	0.44	0.83	475	0.12	42	1.41	0.70	1	3.63	0.36	2.68	0.36	0.96	2.48
	Tension	12	45	30	1755	2016	0.44	0.83	298	0.12	42	1.41	0.70	1	3.65	0.36	2.68	0.36	1.36	3.50

Interior Columns, Longitudinal Direction

Location		s (in)	hc (in)	bc (in)	Ac (in^2)	Ag (in^2)	Ash(c) (in^2)	Ash(d) (in^2)	Axial Load (Kips)	k1	bmin (in)	db (in)	k2	k3(int)	u(int)	k3(final)	u	Iteration	Rac	Rcc
1	Comp	12	30	45	1755	2016	0.44	5.74	851	0.12	42	1.41	0.70	1	3.66	0.35	2.58	0.35	0.25	0.65
	Tension	12	30	45	1755	2016	0.44	5.74	831	0.12	42	1.41	0.70	1	3.66	0.35	2.58	0.35	0.25	0.64
2	Comp	12	30	45	1755	2016	0.44	5.74	851	0.12	42	1.41	0.70	1	3.66	0.35	2.58	0.35	0.29	0.75
	Tension	12	30	45	1755	2016	0.44	5.74	831	0.12	42	1.41	0.70	1	3.66	0.35	2.58	0.35	0.29	0.76
3	Comp	12	30	45	1755	2016	0.44	5.74	418	0.14	42	1.41	0.70	1	3.67	0.35	2.59	0.35	1.66	4.27
	Tension	12	30	45	1755	2016	0.44	5.74	407	0.14	42	1.41	0.70	1	3.68	0.35	2.59	0.35	1.80	4.66
4	Comp	12	30	45	1755	2016	0.44	5.74	418	0.14	42	1.41	0.70	1	3.67	0.35	2.59	0.35	0.93	2.41
	Tension	12	30	45	1755	2016	0.44	5.74	407	0.14	42	1.41	0.70	1	3.68	0.35	2.59	0.35	0.97	2.53

Table D.4. Column Confinement C/D Ratios (Pinned Base, Site-Specific Spectrum)

Transverse Confinement
Pinned Base, 30' Ftg, 30' Total Soil

f'c = 4600 fy = 44000

Exterior Frame — Transverse Direction

Location		s in	hc in	bc in	Ac in^2	Ag in^2	Ash(c) in^2	Ash(d) in^2	Axial Load Kips	k1	bmin in	db in	k2	k3(int)	u(int)	k3(final)	u	Iterator	Rsc	Rcc
1	Comp	12	45	21	945	1152	0.44	6.63	510	0.11	24	1.625	0.40	1	3.01	0.40	2.40	0.40	2.44	5.66
1	Tension	12	45	21	945	1152	0.44	6.63	274	0.12	24	1.625	0.40	1	3.03	0.40	2.41	0.40	2.11	6.08
2	Comp	12	45	21	945	1152	0.44	6.63	510	0.11	24	1.625	0.40	1	3.01	0.40	2.40	0.40	0.26	0.67
2	Tension	12	45	21	945	1152	0.44	6.63	274	0.12	24	1.625	0.40	1	3.03	0.40	2.41	0.40	0.24	0.58
3	Comp	12	45	21	945	1152	0.44	6.63	242	0.12	24	1.625	0.40	1	3.04	0.40	2.41	0.40	3.65	9.28
3	Tension	12	45	21	945	1152	0.44	6.63	143	0.12	24	1.625	0.40	1	3.05	0.40	2.41	0.40	N/A	
4	Comp	12	45	21	945	1152	0.44	6.63	242	0.12	24	1.625	0.40	1	3.04	0.40	2.41	0.40	1.71	4.13
4	Tension	12	45	21	945	1152	0.44	6.63	143	0.12	24	1.625	0.40	1	3.06	0.40	2.41	0.40	2.26	6.44

Exterior Columns — Longitudinal Direction

Location		s in	hc in	bc in	Ac in^2	Ag in^2	Ash(c) in^2	Ash(d) in^2	Axial Load Kips	k1	bmin in	db in	k2	k3(int)	u(int)	k3(final)	u	Iterator	Rsc	Rcc
1	Comp	12	21	45	945	1152	0.44	3.09	430	0.24	24	1.625	0.40	1	3.27	0.38	2.49	0.38	3.00	7.45
1	Tension	12	21	45	945	1152	0.44	3.09	232	0.26	24	1.625	0.40	1	3.31	0.38	2.49	0.38	2.58	6.42
2	Comp	12	21	45	945	1152	0.44	3.09	430	0.24	24	1.625	0.40	1	3.27	0.38	2.49	0.38	0.36	0.90
2	Tension	12	21	45	945	1152	0.44	3.09	232	0.26	24	1.625	0.40	1	3.31	0.38	2.49	0.38	0.31	0.78
3	Comp	12	21	45	945	1152	0.44	3.09	188	0.26	24	1.625	0.40	1	3.32	0.38	2.50	0.38	0.80	1.99
3	Tension	12	21	45	945	1152	0.44	3.09	137	0.27	24	1.625	0.40	1	3.33	0.38	2.50	0.38	1.29	3.23
4	Comp	12	21	45	945	1152	0.44	3.09	188	0.26	24	1.625	0.40	1	3.32	0.38	2.50	0.38	1.71	4.26
4	Tension	12	21	45	945	1152	0.44	3.09	137	0.27	24	1.625	0.40	1	3.33	0.38	2.50	0.38	2.79	6.97

Interior Frame — Transverse Direction

Location		s in	hc in	bc in	Ac in^2	Ag in^2	Ash(c) in^2	Ash(d) in^2	Axial Load Kips	k1	bmin in	db in	k2	k3(int)	u(int)	k3(final)	u	Iterator	Rsc	Rcc
1	Comp	12	45	30	1755	2016	0.44	6.63	1009	0.10	42	1.41	0.70	1	3.61	0.35	2.57	0.36	2.34	6.03
1	Tension	12	45	30	1756	2016	0.44	6.63	560	0.12	42	1.41	0.70	1	3.63	0.35	2.56	0.36	1.97	5.06
2	Comp	12	45	30	1756	2016	0.44	6.63	1009	0.10	42	1.41	0.70	1	3.61	0.35	2.57	0.36	0.27	0.69
2	Tension	12	45	30	1756	2016	0.44	6.63	560	0.12	42	1.41	0.70	1	3.63	0.35	2.56	0.36	0.22	0.58
3	Comp	12	45	30	1756	2016	0.44	6.63	475	0.12	42	1.41	0.70	1	3.63	0.35	2.56	0.36	3.32	8.57
3	Tension	12	45	30	1756	2016	0.44	6.63	296	0.12	42	1.41	0.70	1	3.65	0.35	2.56	0.36	N/A	
4	Comp	12	45	30	1756	2016	0.44	6.63	476	0.12	42	1.41	0.70	1	3.63	0.35	2.56	0.36	0.94	2.42
4	Tension	12	45	30	1756	2016	0.44	6.63	296	0.12	42	1.41	0.70	1	3.65	0.35	2.56	0.36	1.33	3.43

Interior Columns — Longitudinal Direction

Location		s in	hc in	bc in	Ac in^2	Ag in^2	Ash(c) in^2	Ash(d) in^2	Axial Load Kips	k1	bmin in	db in	k2	k3(int)	u(int)	k3(final)	u	Iterator	Rsc	Rcc
1	Comp	12	30	45	1756	2016	0.44	5.74	851	0.12	42	1.41	0.70	1	3.66	0.35	2.58	0.35	1.96	5.03
1	Tension	12	30	45	1756	2016	0.44	5.74	831	0.12	42	1.41	0.70	1	3.66	0.35	2.58	0.35	1.94	5.00
2	Comp	12	30	45	1756	2016	0.44	5.74	851	0.12	42	1.41	0.70	1	3.66	0.35	2.58	0.35	0.22	0.57
2	Tension	12	30	45	1756	2016	0.44	5.74	831	0.12	42	1.41	0.70	1	3.66	0.35	2.58	0.35	0.22	0.56
3	Comp	12	30	45	1756	2016	0.44	5.74	418	0.14	42	1.41	0.70	1	3.67	0.35	2.59	0.35	27.70	71.81
3	Tension	12	30	45	1756	2016	0.44	5.74	407	0.14	42	1.41	0.70	1	3.68	0.35	2.59	0.35	N/A	
4	Comp	12	30	45	1756	2016	0.44	5.74	418	0.14	42	1.41	0.70	1	3.67	0.35	2.59	0.35	1.49	3.85
4	Tension	12	30	45	1756	2016	0.44	5.74	407	0.14	42	1.41	0.70	1	3.68	0.35	2.59	0.35	1.61	4.17

Table D.5. Column Shear C/D Ratios (Fixed Base, ATC-6 Spectrum)

Column Shear
Fixed Base, ATC Spectrum

r'c 4500
fy 44000

Frame	Location		Mu1 Kip-ft	Mu2 Kip-ft	L ft	Vu(d) Kips	Ve(d) Kips	b in	d in	Ag in^2	Av in^2	Axial Load	s in	Vi Kips	Ac in^2	Vf Kips	Status	bc ft	Lc/bc	Result	Key	Rec	Rcv
Exterior Frame Transverse Direction	1	Comp	2022	2023	29	139.5	221	24	45	1080	0	510	12	215.4	945	0.00	Case B	4	4	3.06	u	0.56	1.71
	1	Tension	1722	1723	29	118.8	221	24	45	1080	0	274	12	199.6	945	0.00	Case B	4	4	3.21	u	0.49	1.58
	2	Comp	2023	2022	29	139.5	221	24	45	1080	0	510	12	215.4	945	0.00	Case B	4	4	3.06	u	0.69	2.10
	2	Tension	1723	1722	29	118.8	221	24	45	1080	0	274	12	199.6	945	0.00	Case B	4	4	3.21	u	0.62	1.99
	3	Comp	1683	3259	14.7	336.2	127	24	45	1080	0	242	12	197.4	945	0.00	No Yield	4	3.675	1.56	Rcv	1.96	1.56
	3	Tension	1557	3151	14.7	320.3	127	24	45	1080	0	143	12	190.6	945	0.00	No Yield	4	3.675	1.50	Rcv	4.35	1.60
	4	Comp	3259	1683	14.7	336.2	127	24	45	1080	0	242	12	197.4	945	0.00	No Yield	4	3.675	1.66	Rcv	2.16	1.66
	4	Tension	3151	1557	14.7	320.3	127	24	45	1080	0	143	12	190.6	945	0.00	No Yield	4	3.675	1.50	Rcv	3.12	1.50
Exterior Columns Longitudinal Direction	1	Comp	957	958	29	66.0	91	48	21	1008	0	430	12	198.0	945	0.00	Case B	2	4	4.00	u	0.69	2.74
	1	Tension	801	801	29	55.3	91	48	21	1008	0	232	12	184.7	945	0.00	Case B	2	4	4.10	u	0.61	2.49
	2	Comp	958	957	29	66.0	91	48	21	1008	0	430	12	198.0	945	0.00	Case B	2	4	4.00	u	0.71	2.85
	2	Tension	801	801	29	55.3	91	48	21	1008	0	232	12	184.7	945	0.00	Case B	2	4	4.10	u	0.66	2.70
	3	Comp	766	1619	14.7	162.3	86	48	21	1008	0	188	12	181.7	945	0.00	Case B	2	4	2.32	u	0.82	2.13
	3	Tension	728	1578	14.7	156.7	86	48	21	1008	0	137	12	178.3	945	0.00	No Yield	2	4	2.07	Rcv	1.66	2.07
	4	Comp	1619	766	14.7	162.3	86	48	21	1008	0	188	12	181.7	945	0.00	No Yield	2	4	2.11	Rcv	1.97	2.11
	4	Tension	1578	728	14.7	166.7	86	48	21	1008	0	137	12	178.3	945	0.00	No Yield	2	4	2.07	Rcv	3.57	2.07
Interior Frame Transverse Direction	1	Comp	3261	3271	29	225.3	369	42	45	1860	0	1009	12	357.6	1755	0.00	Case B	4	4	3.11	u	0.53	1.65
	1	Tension	2679	2678	29	184.7	369	42	45	1860	0	560	12	327.4	1755	0.00	Case B	4	4	3.31	u	0.45	-1.51
	2	Comp	3271	3261	29	225.3	369	42	45	1860	0	1009	12	357.6	1755	0.00	Case B	4	4	3.11	u	0.67	2.08
	2	Tension	2678	2679	29	184.7	369	42	45	1860	0	560	12	327.4	1755	0.00	Case B	4	4	3.31	u	0.80	1.97
	3	Comp	2566	3079	14.7	384.0	194	42	45	1860	0	475	12	321.7	1755	0.00	No Yield	4	3.675	1.66	Rcv	1.66	1.66
	3	Tension	2330	2842	14.7	361.8	194	42	45	1860	0	296	12	309.7	1755	0.00	No Yield	4	3.675	1.60	Rcv	9.87	1.60
	4	Comp	3079	2566	14.7	384.0	194	42	45	1860	0	475	12	321.7	1755	0.00	No Yield	4	3.675	1.66	Rcv	1.17	1.66
	4	Tension	2842	2330	14.7	361.8	194	42	45	1860	0	296	12	309.7	1755	0.00	No Yield	4	3.675	1.60	Rcv	1.91	1.60
Interior Columns Longitudinal Direction	1	Comp	2743	2774	29	190.2	412	48	39	1872	0	851	12	371.2	1755	0.00	Case B	3.5	4	3.46	u	0.43	1.48
	1	Tension	2723	2741	29	188.4	412	48	39	1872	0	831	12	369.8	1755	0.00	Case B	3.5	4	3.47	u	0.43	1.48
	2	Comp	2774	2743	29	190.2	412	48	39	1872	0	851	12	371.2	1755	0.00	Case B	3.5	4	3.46	u	0.50	1.72
	2	Tension	2741	2723	29	188.4	412	48	39	1872	0	831	12	369.8	1755	0.00	Case B	3.5	4	3.47	u	0.50	1.73
	3	Comp	2548	2625	14.7	366.5	177	48	39	1872	0	418	12	342.1	1755	0.00	No Yield	3.5	4	1.93	Rcv	2.72	1.93
	3	Tension	2532	2625	14.7	364.4	177	48	39	1872	0	407	12	341.4	1755	0.00	No Yield	3.5	4	1.93	Rcv	3.18	1.93
	4	Comp	2625	2548	14.7	366.5	177	48	39	1872	0	418	12	342.1	1755	0.00	No Yield	3.5	4	1.93	Rcv	1.56	1.93
	4	Tension	2625	2532	14.7	364.4	177	48	39	1872	0	407	12	341.4	1755	0.00	No Yield	3.5	4	1.93	Rcv	1.70	1.93

Column Shear
Fixed Base, 20' Fill, 20' Tidal Soil

r'c 4500
fy   44000

Table D.7. Column Shear C/D Ratios (Fixed Base, Site-Specific Spectrum)

	Location		Mu1 Kip-ft	Mu2 Kip-ft	L ft	Vu(d) Kips	Vs(d) Kips	b in	d in	Ag in^2	Av in^2	Axial Load	s in	Vi Kips	Ac in^2	Vf Kips	Status	bc ft	Lc/bc	Result	Key	Rec	Rcv
Exterior Frame Transverse Direction	1	Comp	2022	2023	29	139.5	287	24	45	1080	0.22	510	12	215.4	945	0.00	Case B	4	-	3.06	u	0.43	1.32
		Tension	1722	1723	29	118.8	287	24	45	1080	0.22	274	12	199.6	945	0.00	Case B	4	-	3.21	u	0.38	1.21
	2	Comp	2023	2022	29	139.5	287	24	45	1080	0.22	510	12	215.4	945	0.00	Case B	4	-	3.06	u	0.53	1.63
		Tension	1723	1722	29	118.8	287	24	45	1080	0.22	274	12	199.6	945	0.00	Case B	4	-	3.21	u	0.48	1.53
	3	Comp	1683	3259	14.7	336.2	165	24	45	1080	0.22	242	12	197.4	945	0.00	No Yield	4	3.675	1.20	Rcv	1.82	1.20
		Tension	1557	3151	14.7	320.3	165	24	45	1080	0.22	143	12	190.8	945	0.00	No Yield	4	3.675	1.16	Rcv	2.90	1.16
	4	Comp	3259	1683	14.7	336.2	165	24	45	1080	0.22	242	12	197.4	945	0.00	No Yield	4	3.675	1.20	Rcv	1.72	1.20
		Tension	3151	1557	14.7	320.3	165	24	45	1080	0.22	143	12	190.8	945	0.00	No Yield	4	3.675	1.16	Rcv	2.27	1.16
Exterior Columns Longitudinal Direction	1	Comp	957	956	29	66.0	155	48	21	1008	0.44	430	12	196.0	945	0.00	Case B	2	-	4.00	u	0.41	1.62
		Tension	601	601	29	66.3	155	48	21	1008	0.44	232	12	184.7	945	0.00	Case B	2	-	4.10	u	0.36	1.44
	2	Comp	956	957	29	66.0	155	48	21	1008	0.44	430	12	196.0	945	0.00	Case B	2	-	4.00	u	0.43	1.70
		Tension	601	601	29	66.3	155	48	21	1008	0.44	232	12	184.7	945	0.00	Case B	2	-	4.10	u	0.38	1.56
	3	Comp	766	1619	14.7	182.3	148	48	21	1008	0.44	188	12	181.7	945	0.00	Case B	2	-	2.32	u	0.59	1.36
		Tension	728	1578	14.7	156.7	148	48	21	1008	0.44	137	12	178.3	945	0.00	Case B	2	-	2.38	u	0.81	1.62
	4	Comp	1619	766	14.7	182.3	148	48	21	1008	0.44	188	12	181.7	945	0.00	No Yield	2	-	1.23	Rcv	1.27	1.23
		Tension	1578	728	14.7	156.7	148	48	21	1008	0.44	137	12	178.3	945	0.00	No Yield	2	-	1.21	Rcv	1.77	1.21
Interior Frame Transverse Direction	1	Comp	3261	3271	29	225.3	479	42	45	1890	0.22	1009	12	357.6	1755	0.00	Case B	4	-	3.11	u	0.41	1.28
		Tension	2679	2679	29	184.7	479	42	45	1890	0.22	560	12	327.4	1755	0.00	Case B	4	-	3.31	u	0.35	1.16
	2	Comp	3271	3261	29	225.3	479	42	45	1890	0.22	1009	12	357.6	1755	0.00	Case B	4	-	3.11	u	0.52	1.62
		Tension	2678	2679	29	184.7	479	42	45	1890	0.22	560	12	327.4	1755	0.00	Case B	4	-	3.31	u	0.45	1.50
	3	Comp	2566	3079	14.7	384.0	252	42	45	1890	0.22	475	12	321.7	1755	0.00	No Yield	4	3.675	1.28	Rcv	1.80	1.28
		Tension	2330	2842	14.7	351.8	252	42	45	1890	0.22	296	12	309.7	1755	0.00	No Yield	4	3.675	1.23	Rcv	4.97	1.23
	4	Comp	3079	2566	14.7	384.0	252	42	45	1890	0.22	475	12	321.7	1755	0.00	Case A	4	3.675	1.28	Rcv<Rec	0.95	0.95
		Tension	2842	2566	14.7	351.8	252	42	45	1890	0.22	296	12	309.7	1755	0.00	No Yield	4	3.675	1.23	Rcv	1.36	1.23
Interior Columns Longitudinal Direction	1	Comp	2743	2774	29	190.2	705	48	30	1872	0.44	851	12	371.2	1755	0.00	Case B	3.5	-	3.46	u	0.25	0.87
		Tension	2723	2741	29	188.4	706	48	30	1872	0.44	831	12	369.8	1755	0.00	Case B	3.5	-	3.47	u	0.25	0.86
	2	Comp	2774	2743	29	190.2	705	48	30	1872	0.44	851	12	371.2	1755	0.00	Case B	3.5	-	3.46	u	0.29	1.01
		Tension	2741	2723	29	188.4	705	48	30	1872	0.44	831	12	369.8	1755	0.00	Case B	3.5	-	3.47	u	0.29	1.01
	3	Comp	2548	2625	14.7	365.5	303	48	30	1872	0.44	418	12	342.1	1755	0.00	No Yield	3.5	-	1.13	Rcv	1.66	1.13
		Tension	2532	2625	14.7	364.4	303	48	30	1872	0.44	407	12	341.4	1755	0.00	No Yield	3.5	-	1.13	Rcv	1.80	1.13
	4	Comp	2625	2548	14.7	365.5	303	48	30	1872	0.44	418	12	342.1	1755	0.00	Case A	3.5	-	1.13	Rcv<Rec	0.93	0.93
		Tension	2625	2532	14.7	364.4	303	48	30	1872	0.44	407	12	341.4	1755	0.00	Case A	3.5	-	1.13	Rcv<Rec	0.97	0.97

Table D.6. Column Shear C/D Ratios (Pinned Base, ATC-6 Spectrum)

Column Shear
Pinned-Base, ATC Spectrum

r'c = 4500
f'y = 44000

Exterior Frame — Transverse Direction

Location		Mu1 Kip-ft	Mu2 Kip-ft	L ft	Wu(d) Kips	Ve(d) Kips	b in	d in	Ag in^2	Av in^2	Axial Load	s in	V Kips	Ac in^2	Vt Kips	Status	bc ft	Lc/bc	Result	Key	Rec	Rcv
1	Comp	0	2023	29	66.8	130	24	45	1080	0.22	510	12	215.4	945	0.00	No Yield	4	4	1.56	Rcv	3.84	1.56
	Tension	0	1723	29	66.8	130	24	45	1080	0.22	274	12	199.6	945	0.00	No Yield	4	4	1.44	Rcv	3.34	1.44
2	Comp	2023	0	29	66.8	130	24	45	1080	0.22	510	12	216.4	945	0.00	Case B	4	4	4.03	u	0.44	1.78
	Tension	1723	0	29	66.4	130	24	45	1080	0.22	274	12	199.6	945	0.00	Case B	4	4	4.11	u	0.38	1.67
3	Comp	1683	3259	14.7	336.2	78	24	45	1080	0.22	242	12	197.4	945	0.00	No Yield	4	3.675	2.53	Rcv	4.30	2.53
	Tension	1567	3161	14.7	320.3	78	24	45	1080	0.22	143	12	190.8	945	0.00	No Yield	4	3.675	2.45	Rcv	100	2.45
4	Comp	3259	1683	14.7	336.2	78	24	45	1080	0.22	242	12	197.4	945	0.00	No Yield	4	3.675	2.53	Rcv	2.51	2.53
	Tension	3161	1567	14.7	320.3	78	24	45	1080	0.22	143	12	190.8	945	0.00	No Yield	4	3.675	2.45	Rcv	3.90	2.45

Exterior Columns — Longitudinal Direction

Location		Mu1 Kip-ft	Mu2 Kip-ft	L ft	Wu(d) Kips	Ve(d) Kips	b in	d in	Ag in^2	Av in^2	Axial Load	s in	V Kips	Ac in^2	Vt Kips	Status	bc ft	Lc/bc	Result	Key	Rec	Rcv
1	Comp	0	956	29	33.0	54	48	21	1008	0.44	430	12	198.0	945	0.00	No Yield	2	4	3.67	Rcv	4.29	3.67
	Tension	0	801	29	27.6	54	48	21	1008	0.44	232	12	184.7	945	0.00	No Yield	2	4	3.42	Rcv	3.73	3.42
2	Comp	956	0	29	33.0	54	48	21	1008	0.44	430	12	198.0	945	0.00	Case B	2	4	4.50	u	0.62	2.33
	Tension	801	0	29	27.6	54	48	21	1008	0.44	232	12	184.7	945	0.00	Case B	2	4	4.56	u	0.45	2.08
3	Comp	786	1619	14.7	162.3	72	48	21	1008	0.44	186	12	181.7	945	0.00	No Yield	2	4	2.52	Rcv	1.06	2.52
	Tension	728	1578	14.7	156.7	72	48	21	1008	0.44	137	12	178.3	945	0.00	No Yield	2	4	2.48	Rcv	2.19	2.48
4	Comp	1619	786	14.7	162.3	72	48	21	1008	0.44	186	12	181.7	945	0.00	No Yield	2	4	2.52	Rcv	2.28	2.52
	Tension	1578	728	14.7	156.7	72	48	21	1008	0.44	137	12	178.3	945	0.00	No Yield	2	4	2.48	Rcv	4.70	2.48

Interior Frame — Transverse Direction

Location		Mu1 Kip-ft	Mu2 Kip-ft	L ft	Wu(d) Kips	Ve(d) Kips	b in	d in	Ag in^2	Av in^2	Axial Load	s in	V Kips	Ac in^2	Vt Kips	Status	bc ft	Lc/bc	Result	Key	Rec	Rcv
1	Comp	0	3271	29	112.8	234	42	45	1890	0.22	1009	12	357.6	1755	0.00	No Yield	4	4	1.53	Rcv	3.66	1.53
	Tension	0	2878	29	92.4	234	42	45	1890	0.22	560	12	327.4	1755	0.00	No Yield	4	4	1.40	Rcv	3.14	1.40
2	Comp	3271	0	29	112.8	234	42	45	1890	0.22	1009	12	357.6	1755	0.00	Case B	4	4	4.06	u	0.42	1.70
	Tension	2878	0	29	92.4	234	42	45	1890	0.22	560	12	327.4	1755	0.00	Case B	4	4	4.15	u	0.36	1.44
3	Comp	2566	3079	14.7	384.0	110	42	45	1890	0.22	475	12	321.7	1755	0.00	No Yield	4	3.675	2.92	Rcv	3.47	2.92
	Tension	2330	2842	14.7	351.8	110	42	45	1890	0.22	290	12	309.7	1755	0.00	No Yield	4	3.675	2.82	Rcv	100	2.82
4	Comp	3079	2566	14.7	384.0	110	42	45	1890	0.22	475	12	321.7	1755	0.00	No Yield	4	3.675	2.92	Rcv	1.34	2.92
	Tension	2842	2330	14.7	351.8	110	42	45	1890	0.22	290	12	309.7	1755	0.00	No Yield	4	3.675	2.82	Rcv	2.44	2.82

Interior Columns — Longitudinal Direction

Location		Mu1 Kip-ft	Mu2 Kip-ft	L ft	Wu(d) Kips	Ve(d) Kips	b in	d in	Ag in^2	Av in^2	Axial Load	s in	V Kips	Ac in^2	Vt Kips	Status	bc ft	Lc/bc	Result	Key	Rec	Rcv
1	Comp	0	2774	29	96.6	267	48	30	1872	0.44	851	12	371.2	1755	0.00	No Yield	3.5	4	1.39	Rcv	2.70	1.39
	Tension	0	2741	29	94.6	267	48	30	1872	0.44	831	12	369.8	1755	0.00	No Yield	3.5	4	1.39	Rcv	2.78	1.39
2	Comp	2774	0	29	96.6	267	48	30	1872	0.44	851	12	371.2	1755	0.00	Case B	3.5	4	4.23	u	0.32	1.34
	Tension	2741	0	29	94.6	267	48	30	1872	0.44	831	12	369.8	1755	0.00	Case B	3.5	4	4.23	u	0.31	1.33
3	Comp	2548	2825	14.7	365.5	88	48	30	1872	0.44	418	12	342.1	1755	0.00	No Yield	3.5	4	3.89	Rcv	29.63	3.89
	Tension	2532	2825	14.7	364.4	88	48	30	1872	0.44	407	12	341.4	1755	0.00	No Yield	3.5	4	3.89	Rcv	100	3.89
4	Comp	2825	2548	14.7	365.5	88	48	30	1872	0.44	418	12	342.1	1755	0.00	No Yield	3.5	4	3.89	Rcv	2.10	3.89
	Tension	2825	2532	14.7	364.4	88	48	30	1872	0.44	407	12	341.4	1755	0.00	No Yield	3.5	4	3.89	Rcv	2.35	3.89

Table D.8. Column Shear C/D Ratios (Pinned Base, Site-Specific Spectrum)

Column Shear
Pinned Base, 30' Fill, 30' Tidal Soil

f'c = 4500
fy = 44000

	Location		Mu1 Kip-ft	Mu2 Kip-ft	L ft	Vu(d) Kips	Ve(d) Kips	b in	d in	Ag in^2	Av in^2	Axial Load	s in	V Kips	Ac in^2	Vt Kips	Status	bc ft	Lc/bc	Result	Key	Rec	Rcv
Exterior Frame	1	Comp	0	2023	29	70	220	24	45	1080	0.22	510	12	215.4	945	0.00	No Yield	4	4	0.98	Rcv	2.44	0.98
		Tension	0	1723	29	69	220	24	45	1080	0.22	274	12	190.6	945	0.00	No Yield	4	4	0.91	Rcv	2.11	0.91
	2	Comp	2023	0	29	70	220	24	45	1080	0.22	510	12	215.4	945	0.00	Case B	4	4	4.03	U	0.28	1.12
		Tension	1723	0	29	59	220	24	45	1080	0.22	274	12	190.6	945	0.00	Case B	4	4	4.11	U	0.24	0.99
Transverse Direction	3	Comp	1683	3259	14.7	336	123	24	45	1080	0.22	242	12	197.4	945	0.00	No Yield	4	3.675	1.60	Rcv	3.85	1.60
		Tension	1557	3151	14.7	320	123	24	45	1080	0.22	143	12	190.8	945	0.00	No Yield	4	3.675	1.66	Rcv	100	1.56
	4	Comp	3259	1683	14.7	336	123	24	45	1080	0.22	242	12	197.4	945	0.00	No Yield	4	3.675	1.60	Rcv	1.71	1.60
		Tension	3151	1557	14.7	320	123	24	45	1080	0.22	143	12	190.8	945	0.00	No Yield	4	3.675	1.66	Rcv	2.25	1.66
Exterior Columns	1	Comp	0	958	29	33	79	48	21	1008	0.44	430	12	198.0	945	0.00	No Yield	2	4	2.52	Rcv	3.00	2.52
		Tension	0	801	29	28	79	48	21	1008	0.44	232	12	184.7	945	0.00	No Yield	2	4	2.36	Rcv	2.58	2.36
	2	Comp	958	0	29	33	79	48	21	1008	0.44	430	12	198.0	945	0.00	Case B	2	4	4.50	U	0.36	1.63
		Tension	801	0	29	28	79	48	21	1008	0.44	232	12	184.7	945	0.00	Case B	2	4	4.55	U	0.31	1.43
Longitudinal Direction	3	Comp	766	1619	14.7	182	104	48	21	1008	0.44	198	12	181.7	945	0.00	Case B	2	4	2.32	Rcv	0.80	1.85
		Tension	728	1578	14.7	157	104	48	21	1008	0.44	137	12	178.3	945	0.00	No Yield	2	4	1.72	Rcv	1.29	1.72
	4	Comp	1619	766	14.7	182	104	48	21	1008	0.44	198	12	181.7	945	0.00	No Yield	2	4	1.76	Rcv	1.71	1.76
		Tension	1578	728	14.7	157	104	48	21	1008	0.44	137	12	178.3	945	0.00	No Yield	2	4	1.72	Rcv	2.79	1.72
Interior Frame	1	Comp	0	3271	29	113	370	42	45	1890	0.22	1009	12	367.6	1755	0.00	No Yield	4	4	0.97	Rcv	2.34	0.97
		Tension	0	2678	29	92	370	42	45	1890	0.22	560	12	327.4	1755	0.00	No Yield	4	4	0.88	Rcv	1.97	0.88
	2	Comp	3271	0	29	113	370	42	45	1890	0.22	1009	12	367.6	1755	0.00	Case B	4	4	4.06	U	0.27	1.08
		Tension	2678	0	29	92	370	42	45	1890	0.22	560	12	327.4	1755	0.00	Case B	4	4	4.15	U	0.22	0.93
Transverse Direction	3	Comp	2566	3079	14.7	384	174	42	45	1890	0.22	475	12	321.7	1756	0.00	No Yield	4	3.675	1.85	Rcv	3.32	1.85
		Tension	2330	2842	14.7	352	174	42	45	1890	0.22	298	12	309.7	1756	0.00	No Yield	4	3.675	1.78	Rcv	100	1.78
	4	Comp	3079	2566	14.7	384	174	42	45	1890	0.22	475	12	321.7	1756	0.00	Case A	4	3.675	1.85	Rcv<Rec	0.94	0.94
		Tension	2842	2330	14.7	352	174	42	45	1890	0.22	298	12	309.7	1756	0.00	No Yield	4	3.675	1.78	Rcv	1.33	1.78
Interior Columns	1	Comp	0	2774	29	98	365	48	39	1872	0.44	651	12	371.2	1756	0.00	No Yield	3.5	4	0.98	Rcv	1.95	0.98
		Tension	0	2741	29	96	365	48	39	1872	0.44	831	12	369.8	1756	0.00	No Yield	3.5	4	0.98	Rcv	1.94	0.98
	2	Comp	2774	0	29	98	365	48	39	1872	0.44	651	12	371.2	1756	0.00	Case B	3.5	4	4.23	U	0.22	0.93
		Tension	2741	0	29	96	365	48	39	1872	0.44	831	12	369.8	1756	0.00	Case B	3.5	4	4.23	U	0.22	0.92
Longitudinal Direction	3	Comp	2548	2825	14.7	356	127	48	39	1872	0.44	418	12	342.1	1756	0.00	No Yield	3.5	4	2.70	Rcv	2770	2.70
		Tension	2532	2825	14.7	354	127	48	39	1872	0.44	407	12	341.4	1756	0.00	No Yield	3.5	4	2.69	Rcv	100	2.69
	4	Comp	2825	2548	14.7	356	127	48	39	1872	0.44	418	12	342.1	1756	0.00	No Yield	3.5	4	2.70	Rcv	1.49	2.70
		Tension	2825	2532	14.7	354	127	48	39	1872	0.44	407	12	341.4	1756	0.00	No Yield	3.5	4	2.69	Rcv	1.61	2.69